Characterization of cationic conductances of human erythrocytes and their involvement in health and disease

David Monedero Alonso

Thèse

en vue de l'obtention du diplôme de docteur de Sorbonne Université

École Doctorale 515 : Complexité du Vivant

Discipline : Physiologie cellulaire

David MONEDERO ALONSO

Characterization of cationic conductances of human erythrocytes and their involvement in health and disease

En vue de la soutenance du 25 novembre 2019

Composition du jury

Dr. Hélène GUIZOUARN (Université de Nice)	**Rapportrice**
Professeur Mariano OSTUNI (Université de Paris)	**Rapporteur**
Professeur Paola BIANCHI (Hôpital polyclinique de Milan, Italie)	**Examinatrice**
Professeur Lars KAESTNER (Université de Saarland, Allemagne)	**Examinateur**
Professeur François LALLIER (Sorbonne Université)	**Examinateur**
Dr. Stéphane EGEE (Sorbonne Université)	**Directeur de thèse**

Équipe d'accueil:
Physiologie et destin cellulaire – UMR 8227 – Station Biologique de Roscoff – CNRS-SU

I admit that reason is a small and feeble flame, a flickering torch by stumblers carried in the starless night – blown and flared by passion's storm – and yet it is the only light. Extinguish that, and naught remains.

Robert G. Ingersoll

Contents

List of Figures

List of Tables

Terms and acronyms

2,3-DPG 2,3-diphosphoglycerate

A23187 A calcium ionophore. It is a compound which greatly increases the membrane permeability for Ca2+. Its use on RBCs leads to Gárdos activation.

Acanthocytes " Thorn cells". Erythrocytes with coarse, asymmetric membrane projections.

Additive Solutions (AS)
In the context of erythrocyte storage, cell media allowing long-term storage of erythrocytes.

ANT Adenosine Nucleotide Transporter

Antiporter Transporter exchanging ions or solutes across the plasma membrane in opposite directions.

ATP Adenosine triphosphate.

CCCP Protonophore used for membrane potential estimation experiments.

Channelopathy Hereditary anemia caused by mutations in genes coding for ion channels.

Chloride conductance inhibitor
Pharmacological blocker of the chloride conductance. Except for stilbene derivatives such as DIDS which target Band 3, their targets are unknown, possibly involving anion channels.

Chloride conductance It refers to the ease at which chloride and anions can cross the erythrocyte plasma membrane. It is constant at rest. It is conferred by anion channel activity and Band 3.

Citrate-Phosphate-Dextrose (CPD)
Anticoagulant solution added to whole blood prior to component processing and separation. Minute amounts remain in RBCCs.

Codocytes "Bell cells". Erythrocytes with a dense, hemoglobin rich center surrounded by a less dense pale ring-shape region.

Conductance Reciprocal of resistance. Ease with which charges or ions move across an insulator. It is measured in siemens, S. Ion channel openings increase the conductance of plasma membranes.

Conductive pathways Ionic transport which increases the conductance of plasma membranes. Typically synonymous with ion channel.

Current Number of ions (charges) per unit of time. It is measured in Ampere, A.

Dacryocytes "Tear cells". Erythrocytes that resemble a teardrop. They often appear in patients with splenic abnormalities or extramedullary hematopoiesis.

Depolarization Change towards membrane potentials greater than the resting membrane potential. In erythrocytes, change towards more positive membrane potential values, that is, greater than -10 mV.

Discocytes Normal biconcave shape of erythrocytes conferring great flexibility and a high surface to volume ratio. Also known as normocytes.

Elliptocytes "Elliptic cells" Erythrocytes resembling an ellipse or ovoid. Also known as ovalocyte.

Echinocytes "Hedgehog cells". Small round erythrocytes with evenly spaced membrane spikes which eventually come off as vesicles.

FDA Food and Drug Administration

Gárdos Gárdos channel, also known as Intermediate conductance calcium-activated potassium channel protein 4 and KCa3.1. It is encoded by gene KCNN4. It is assembled into a heterotetramer as it is constitutively associated to calmodulin. Four Gárdos monomers bind four calmodulin monomers.

Gárdos-HSt Gárdos-Hereditary Stomatocytosis. Hereditary Stomatocytosis caused by mutations in gene KCNN4 coding for the Gárdos channel.

Hereditary Elliptocytosis (HE)
Anemia of genetic origin caused by mutations in spectrin or protein 4.1R leading to loss of cytoskeletal interactions.

Hereditary Spherocytosis (HS)
Anemia of genetic origin caused by mutations in Band 3, Band 4.2, spectrin or Ankyrin leading to deficiency of these structural proteins.

Hereditary Stomatocytosis (HSt)
Anemia of genetic origin caused by mutations in many proteins including Band 3, RhAG, Gárdos and (sometimes classified as) Piezo1. It is characterized by cation imbalance and the occasional presence of stomatocytes in blood smears.

Hereditary Xerocytosis (HX)
Anemia of genetic origin caused by mutations in Piezo1. Erythrocytes are dehydrated to excessive salt efflux. (Gárdos mutations are sometimes also classified as hereditary Xerocytosis).

Hyperpolarization Change towards membrane potentials smaller than the resting membrane potential. In erythrocytes, change towards very negative membrane potential values, lower than -10 mV.

Ion channels Proteins containing generally multiple transmembrane α-helix domains and capable of opening an aqueous pathway upon activation through which ions can freely

pass according to the driving force. Their opening increases the membrane conductances of permeable ions. Activation can result from interaction with ligands, voltage changes or mechanical stimuli.

Ionic pores Proteins containing membrane-spanning β-barrel domains which interrupt the continuity of the lipid bilayer and allow passage of ions and solutes mostly according to size. Activation can result from interaction with ligands, oligomerization state or voltage changes.

Ionic strength Measure of the concentration of all ions in solution. A solution of $CaCl_2$ has a stronger ionic strength than a solution of NaCl, as $CaCl_2$ dissociates into three ions in aqueous solutions, whereas NaCl dissociates in only two ions.

Leak Cation permeability observed in RBCs coupled to the pumping activity of the Na+/K+ and Ca^{2+} ATPases and which increases as cells age. It normally refers to any cation movement across the lipid bilayer in resting conditions. It is consistent with Non Selective Cation channel activity.

Low Ionic Strength (LIS) solution

Solution of low ionic strength. In this thesis' context: medium for erythrocyte suspension where extracellular NaCl is replaced by sucrose, which leads to immediate depolarization of the erythrocyte membrane to very positive membrane potential values.

Maximum hyperpolarization

Smallest (most negative) membrane potential value recorded for an erythrocyte population following hyperpolarization, normally in the context of Gárdos activation.

Membrane potential Separation of ions (charges), across an insulator, the lipid bilayer and refers to the voltage between the extracellular medium and the cytosol. It is measured in milliVolt, mV.

Microcytes "Small cells". Erythrocytes with severely reduced volume. They often appear when there is cell dehydration.

Nernst equilibrium Membrane potential for a given ion at which the net ion movement across the plasma membrane is zero. $E_{ion} = -\frac{RT}{zF} \ln \frac{[ion]_i}{[ion]_o}$

Non Selective Cation channel (NSC)

Ion channels only permeable to cations due to charge exclusion at the channel pore, though nonspecific to cation species as long as they fit through the pore. They are permeable to Na+, K+, Ca2+ and Mg2+ and open as a result of interactions with ligands, voltage changes or mechanical stimuli.

Non-Selective Voltage-Dependent Cation Channel (NSVDC)

Channel of unknown molecular identity known to be active when erythrocytes are

resuspended in Low Ionic Strength solutions. It is active at a membrane potential of +40 mV in human erythrocytes. Its open probability depends on V_M.

NS309 Gárdos activator which lowers the calcium concentration threshold needed for channel opening.

NS3623 Efficient chloride conductance inhibitor. At high concentration it also enhances Non Selective Cation channel activity.

NSC (channel) Non Selective Cation (channel)

Osmolality Osmoles of a solute or solutes per kilogram of solvent in a solution. A mole of NaCl dissociates into 2 osmoles in aqueous solution. Units is Osm/kg.

Osmolarity Osmoles of a solute or solutes per liter of solvent in a solution. A mole of NaCl dissociates into 2 osmoles in aqueous solution. Unit is Osm/l.

Ovalocyte Another term for elliptocyte.

Peripheral type Benzodiazepine Receptor (PBR)
Protein complex including VDAC, TSPO and ANT. Benzodiazepines are ligands of this complex.

Piezo1 Mechanosensitive Non Selective Cation channel permeable to Na+, K+, Ca2+ and Mg2+. It assembles into a homotrimer. It is encoded by gene PIEZO1, previously termed FAM38A.

Piezo1-HX Piezo-Hereditary Xerocytosis. Hereditary Xerocytosis caused by mutations in PIEZO1 gene coding for Piezo1 channel.

Protonophore Compound which greatly increases the membrane permeability for H+.

Pump Protein anchored within the plasma membrane facilitating stoichiometric active transport of solutes or ions across the lipid bilayer against their gradients. It requires energy in the form of ATP to function.

RBCC Red Blood Cell Concentrate.

RBCs Red Blood Cells

Reactive Oxygen Species (ROS)
Highly oxidizing chemical species able to react with a wide variety of substances. Major reactive oxygen species are H_2O_2 and superoxide. Fe^{3+} is a potent oxidizer which can trigger an oxidation cascade in erythrocytes.

Repolarization Change towards the resting membrane potential either from a previous state of hyperpolarization or depolarization.

Resting membrane potential

Membrane potential of cells at rest. In unaltered healthy erythrocytes it is set by the high chloride conductance, as cationic conductance are tiny in these conditions. It largely corresponds to the Nernst equilibrium for chloride (−10 mV).

Saline-Adenine-Glucose-Mannitol

Additive solution widely used in Europe for the storage of erythrocyte intended for transfusion. It allows the storage of RBCs for six weeks.

SCD Sickle Cell Disease

Schistocytes "Split cells". Erythrocytes appearing fragmented and very irregularly shaped.

Sickle Cell Disease Hereditary recessive anemia cause by mutation E7V in hemoglobin β chain. Affected erythrocytes display a characteristic sickle shape upon deoxygenation. The disease is not restricted to hemolysis and has a complex pathophysiology.

Spherocytes "Spherical cells". Erythrocytes appearing spherical or round in blood smears, although they are rarely perfectly spherical. They appear in blood smears in connection to Hereditary Spherocytosis.

Spheroechinocytes Very small echinocytes whose membrane is full of evenly spaced tiny spikes. Terminal stage of the echinocytosis sequence.

Stomatocytes "Mouth cells". RBCs appearing more concave than discocytes.

Storage lesion Series of cellular alterations which appear during storage of erythrocytes intended for transfusion, which decrease efficacy and may be potentially deleterious.

Symporter Transporter moving two or more ions or solutes in the same direction, into or out of the cell.

Transporter Protein anchored within the plasma membrane facilitating stoichiometric movement of solutes or ions across the lipid bilayer.

TSPO Translocator Protein

Voltage-Dependent Anion Channel (VDAC)

β-barreled, ionic pore with high permeability to anions. It displays complex conductance modes where voltage-independent non selective cation activity is possible. Oligomerization alters gating.

Abstract

Erythrocytes possess many transport pathways at the plasma membrane. On one hand, anion permeability is very high and chloride can move freely. As a consequence, chloride is at equilibrium. On the other hand, cation permeability is very low, although it is not zero, a leak pathway exists, which is coupled to the operation of the Na^+/K^+ pump to ensure cation balance and homeostasis. However, red cell membranes are endowed with several ion channels. Normally silent, they will rapidly dissipate ionic gradients once activated. Albeit, the Gárdos channel, a Ca^{2+} -activated potassium channel and more recently Piezo1 a mechanosensitive cation channel permeable to Na^+, K^+, Ca^{2+} and Mg^{2+}, have been extensively described, the exact nature of the cation leak is not yet fully elucidated. Many observations in healthy mature RBCs and in pathophysiological conditions lead to the conclusion that such cation leak proceed through a non-selective cation channel (NSC).

The functional characterization of cation channels is rendered difficult in RBCs by the prevalence of a massive chloride conductance hindering the observation of cationic conductances. Although patch-clamp remains the golden standard for ion channel activity analysis, patch-clamping RBCs is challenging, laborious and imposes some constraints such as sustained pressure on the membrane. On the contrary, membrane potential estimation aided by proton ionophore CCCP allows the recording of membrane potential changes in RBC populations in real time and, thus, enables observation of ion channel activity as their opening alters the membrane potential.

Herein I present a pharmacological means (NS3623) for the enhancement of NSC channels in hyperpolarizing conditions with concomitant chloride conductance inhibition in freshly drawn healthy mature RBCs. This tool facilitates the study of NSC channels whose activities are small in comparison with the strong chloride conductance. The properties of such compound was subsequently used to describe dysfunctional cation homeostasis in hereditary anemia using patient cells affected by different mutations on Gárdos or Piezo1 channels. As the technique is fast, reliable and inexpensive it provides an alternative diagnostic tool with the added advantage of producing ion channel activity information as it may be different even in patients with the same mutation and thus explain the severity.

The last part of the thesis deals with the alteration of cation balance upon storage conditions for transfusion purposes which is part of the so-called “storage lesion”. To address this issue, ion channel activity was characterized throughout 42-day storage period of RBCs stored at 4 °C in CPD-SAGM according to French regulations. Experimental approaches were devised upon the knowledge gained from NSC channel studies in both fresh RBCs from healthy donors and from hereditary anemia patients. NSC activity was shown to increase over time during storage and dramatic ion channel activity was observed during the last week. Consequently, NSC activity may jeopardize cell volume and morphology upon reinfusion and account for erythrocyte removal observed within 24 hours of transfusion.

In conclusion, Non-Selective Cation channels play an important role in mature RBCs. They contribute or may constitute the origin of cation leak. They cause disease when malfunctioning and insight into their operation in these conditions may supply with therapeutic strategies. They are involved in the storage lesion, and may account for the RBCs demise once back in the circulation.

Résumé

Les érythrocytes possèdent de nombreuses voies de transport membranaire. La perméabilité aux anions est très élevée permettant aux chlorures d'être à l'équilibre. Ainsi le potentiel de membrane est proche de cet équilibre permettant aux anions de se déplacer librement. En revanche, la perméabilité aux cations est très faible, mais non nulle. En effet l'existence de voies de fuite couplée au fonctionnement de la pompe 3 $Na^+/2K^+$ assure l'équilibre des cations nécessaire à l'homéostasie cellulaire. La membrane des globules rouges est dotée de plusieurs canaux ioniques. Normalement silencieux, ils peuvent dissiper rapidement les gradients ioniques une fois activés. Bien que le canal Gárdos, un canal potassique activé par le Ca^{2+} et plus récemment le canal Piezo1, un canal mécanosensible, perméable au Na^+, au K^+, au Ca^{2+} et au Mg^{2+}, aient été abondamment décrits, la nature exacte de la fuite de cation n'est pas encore complètement élucidée. De nombreuses observations dans des globules rouges matures sains et dans des conditions physiopathologiques conduisent à la conclusion qu'une telle fuite de cations passe par un ou des canal (ux) cationique(s) non sélectif(s) (NSC).

L'objectif principal de la thèse a été d'apporter des éléments de compréhension sur la nature et le rôle des voies de conductances cationiques en conditions physiologiques ou physiopathologiques. La caractérisation fonctionnelle des voies de conductance cationique est rendue difficile du fait de la prédominance de la conductance anionique qui les masque. Bien que le patch-clamp reste la technique par excellence pour l'analyse de l'activité des canaux ioniques, elle reste néanmoins difficile et laborieuse à utiliser sur des populations des globules rouges hétérogènes. Au contraire, le suivi en temps réel du potentiel membranaire d'une population cellulaire facilité par le CCCP, un ionophore à proton, permet d'observer directement l'activité des canaux ioniques lorsque leur ouverture modifie le potentiel membranaire. Lors de cette étude, l'utilisation du NS3623 à des concentrations supérieures à celles requises pour l'inhibition des voies de conductances anioniques montre que ce composé active les canaux cationiques non sélectifs permettant ainsi leur étude y compris en conditions hyperpolarisantes.

Les propriétés de ce composé ont ensuite été utilisées pour décrire fonctionnellement les altérations de l'homéostasie cationique dans certains cas d'anémie héréditaire à l'aide de cellules de patients affectés par différentes mutations sur les canaux Gárdos ou Piezo1. Cette technique est rapide, fiable et peu coûteuse, elle pourrait constituer un outil de diagnostic alternatif avec l'avantage supplémentaire de donner des informations sur l'activité des canaux ioniques *in situ*, correlées à la sévérité qui peut varier pour des patients porteurs de la même mutation.

Enfin, la dernière partie de la thèse porte sur l'altération de l'équilibre des cations dans des conditions de stockage à des fins de transfusion. Pour répondre à cette question, l'activité des canaux ioniques a été caractérisée tout au long de la période de stockage réglementaire des globules rouges stockés à 4 ° C (42 jours). En utilisant les protocoles dédiés et mis au point lors de l'étude des patients porteurs de mutations héréditaires j'ai pu montrer que l'activité du/des NSC augmentait avec le temps, devenant spectaculaire la dernière semaine de stockage. Par conséquent, l'activité du NSC peut compromettre le volume et la morphologie des cellules lors de la transfusion et expliquer l'élimination des érythrocytes observée dans les 24 heures suivant la transfusion.

En conclusion, les canaux cationiques non sélectifs jouent un rôle dans l'homéostasie des globules rouges matures. Ils contribuent ou peuvent constituer l'origine de la fuite de cations. Ils sont à l'origine de maladies en cas de dysfonctionnement et la compréhension de leur fonctionnement dans ces conditions peut fournir des stratégies thérapeutiques. Enfin, ils sont clairement impliqués dans les lésions de stockage compromettant par leur activité l'efficacité transfusionnelle.

Resumen

Los eritrocitos poseen muchas vías de transporte en la membrana plasmática. Por un lado, su permeabilidad a los aniones es muy alta y los iones cloruro pueden moverse libremente. Por lo tanto, el cloro está en equilibrio. Por otro lado, la permeabilidad a los cationes es muy baja, aunque no es nula, una "filtración" existe y está, de hecho, acoplada al funcionamiento de la bomba de Na+/K+, que asegura un balance iónico y, con éste, la homeostasis. Sin embargo, la membrana de glóbulos rojos cuenta con varios canales iónicos. Si bien están normalmente inactivos, son capaces de disipar gradientes iónicos con rapidez en cuanto se activan. Dos canales se conocen en detalle: el canal Gárdos, un canal de potasio activado por calcio y Piezo1, un canal mecanosensible recientemente descubierto que es permeable a Na^+, K^+, Ca^{2+} y Mg^{2+}. A pesar de ello, la naturaleza de la filtración catiónica sigue siendo desconocida. Numerosas observaciones tanto en eritrocitos maduros de individuos sano como en condiciones fisiopatológicas llevan a la conclusión de que la llamada filtración catiónica proviene de la actividad de canales catiónicos no selectivos (NSC). La predominancia de la enorme conductancia de cloruro dificulta la observación y, por lo tanto, la caracterización funcional de los canales catiónicos. Aunque el patch-clamp sigue siendo la técnica por excelencia para analizar la actividad de los canales iónicos, realizar patch-clamp en glóbulos rojos humanos es complicado, laborioso y presenta una serie de restricciones como el hecho de aplicar presión continua sobre la membrana.

Por el contrario, estimaciones del potencial de membrana mediadas por el protonóforo CCCP permiten la medida de los cambios del potencial de membrana en tiempo real y, por tanto, la observación de la actividad de los canales iónicos ya que su apertura altera el potencial de membrana. En este trabajo, presento cómo potenciar la actividad de canales catiónicos no selectivos de eritrocitos maduros sanos en condiciones de hiperpolarización usando un compuesto (NS3623) que a la vez inhibe la conductancia de cloruro. Esta herramienta facilita el estudio de los canales catiónicos no selectivos cuya actividad es pequeña en comparación con la fuerte conductancia de cloruro. Se usó para describir la homeostasis catiónica disfuncional en anemias de origen genético usando eritrocitos de pacientes con mutaciones en los canales Gárdos y Piezo1. Este método es rápido, fiable y barato, proporcionando una herramienta de diagnóstico alternativa con la ventaja añadida de que genera información sobre la actividad de los canales iónicos.

La última parte de la tesis trata de la alteración del equilibrio catiónico durante las condiciones de almacenamiento de glóbulos rojos para trasfusión, lo que se denomina lesión por almacenamiento. Para abordar este problema, la actividad de canales iónicos se caracterizó a lo largo de 42 días de almacenamiento de dos unidades de concentrado de glóbulos rojos refrigerados a 4 °C. Las distintas estrategias experimentales se concibieron en función del conocimiento obtenido tanto de los estudios realizados en eritrocitos recién extraídos de donantes sanos, como de donantes que padecen anemia hereditaria. Se ha mostrado que la actividad de los canales catiónicos no selectivos aumenta con el tiempo durante el almacenamiento, particularmente durante la sexta y última semana de almacenamiento. Por lo tanto, la actividad de los canales catiónicos no selectivos puede poner en riesgo el volumen y la morfología celular cuando los glóbulos rojos se trasfunden al recipiente, pudiendo explicar así por qué los glóbulos rojos desaparecen de la circulación en las primeras 24 horas desde la trasfusión. En conclusión, los canales catiónicos no selectivos tienen un papel muy importante en los eritrocitos maduros. Contribuyen a la filtración catiónica y podrían constituir su origen. Causan enfermedades cuando no funcionan correctamente, por lo que es necesario conocer más sobre cómo funcionan en esas condiciones y así poder crear nuevas estrategias terapéuticas. Están involucrados en la lesión por almacenamiento y puede que sean responsables de la pérdida de eritrocitos cuando éstos vuelven a la circulación sanguínea.

Introduction

Chapter 1

Introduction

Main erythrocyte functions

Erythrocytes are the most abundant cells in humans, with an average human adult having 2.63×10^{13} total cells [1]. They are devoid of organelles and the nucleus is expelled before being released into the circulation as reticulocytes. Reticulocytes will degrade all remaining ribosomal proteins and RNA while maturing into erythrocytes. Red blood cells (RBCs) are the sole eukaryotic cells to be enucleated, a mammal innovation. Red blood cells have two main roles in physiology: i) carrying oxygen to tissues and ii) the reverse transport of carbon dioxide increasing, in this manner, the CO_2 carrying capacity of blood for it to be delivered and excreted in the lungs. Other functions include: i) increasing the buffering capacity of blood. ii) regulating vasodilation of blood vessels by releasing ATP, which stimulates NO signaling at the endothelium [2]. ii) aiding in coagulation through interactions with platelets iii) bacterial removal in blood by binding pathogens via triboelectric charges and killing them when oxygen is released [3, 4]. Dead pathogens are subsequently phagocytized at the liver or spleen by resident macrophages. In order to efficiently carry oxygen, RBCs contain a protein, hemoglobin (Hb), specialized in oxygen binding and release. The lack of internal organelles leaves much space to hemoglobin, which is highly concentrated in RBC cytoplasm, in the order of 5 mM, to the point it constitutes 97.5 % of the total protein by weight. Hemoglobin is a metalloprotein which emerged during evolution more than 500 million years ago as a widespread respiratory pigment. Its efficiency makes possible to satisfy very high metabolic needs. The oxygen-binding properties of hemoglobin are conferred by heme, where it lies a coordinated Fe atom. Iron-containing heme has been conserved for very long evolutionary times. Most vertebrates express hemoglobin in a tetrameric arrangement, comprising two alpha and two beta chains. Four oxygens can thus be bound to every hemoglobin molecule. Oxygen affinity is affected by red cell volume change (which impacts concentration), by intracellular pH changes and levels of 2,3-diphosphoglycerate (2,3-DPG) [5, 6]. 2,3-DPG is enzymatically converted from 1,3-dyphosphoglycerate (1,3-DPG), a glycolysis metabolite. 2,3-DPG is an allosteric regulator of hemoglobin which decreases the oxygen affinity of hemoglobin via molecular interactions and intracellular pH change thereby leading to O_2 release.

CO_2 is reversibly hydrated by the erythrocyte cytoplasmic enzyme carbonic anhydrase releasing H^+ when CO_2 is uptaken by erythrocytes.

$$CO_2 + H_2O \rightleftharpoons HCO_3^- + H^+$$

Whereas CO_2 can diffuse freely through the plasma membrane according to the gradient of partial pressure, HCO_3^- cannot. In order to shuttle bicarbonate in and out of the cell efficiently, at very high rates, and considering the almost instantaneous speed of the catalytic reaction, the RBC requires a dedicated transporter. Band 3 (also known as Anion Exchanger 1, AE1 or capnophorin, gene *SLC4A1*) is an abundant membrane protein (about 1 million copies per cell) whose primary functions are the exchange of bicarbonate (and more generally anions) and serving as a structural nexus for the binding of many accessory proteins facilitating their association to the erythrocyte plasma membrane. Key to the proper operation of the cycle, Band 3 presence results in H^+/HCO_3^- being passively distributed across the membrane. This system regulating CO_2 transport and pH, which is essential for efficient gas transport and respiration and which will reverse direction according

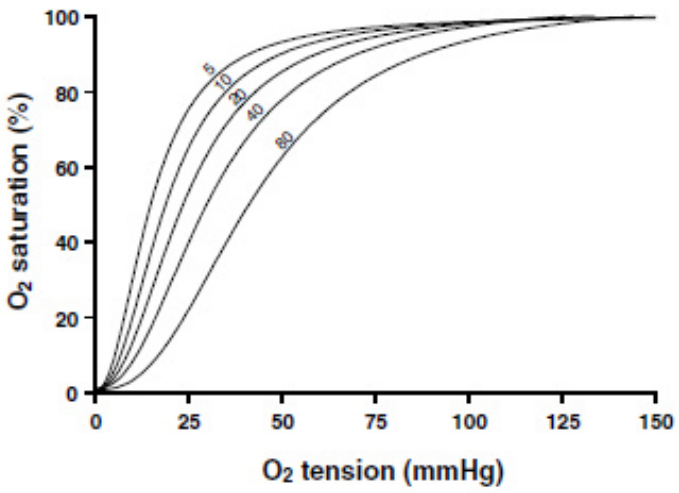

Figure 1.1: Bohr effect.
Effect of carbon dioxide on oxygen equilibrium of canine RBCs at 38 °C. CO_2 partial pressure is indicated in mmHg in each curve. Figure from [2], who used original data published by Bohr, Hasselbalch, and Krogh [11].

to erythrocytes being near tissues or near the lungs, is known as the Jacobs-Stewart cycle [7–9].

Protons (H^+) from the reaction are mainly buffered by hemoglobin. Hemoglobin has a very high buffering capacity, thanks to numerous histidine residues, which are the sole amino acid to display a wide range of pKa allowing to buffer H^+ at physiological pH [10]. CO_2 itself and its impact on pH via the above reaction cause the hemoglobin oxygen affinity to decrease, thus promoting O_2 release in the capillaries where the partial pressure of CO_2 is higher. In the lungs, the reduction of the partial pressure of CO_2 caused due to exhalation has the reverse effect; it increases the affinity of O_2 by hemoglobin [11]. Reciprocally, deoxygenated hemoglobin binds more CO_2 and H^+ than oxygenated hemoglobin, what is termed Haldane effect [12]. As the underlying molecular mechanisms are the same, this is often referred to as the Bohr-Haldane effect (**Fig. 1.1**). This phenomenon was discovered over a century ago and opened the way to red cell research throughout the twentieth century. The molecular explanation of this physiological adaptation stems from hemoglobin conformational changes that take place upon oxygen binding. When oxygen binds to hemoglobin, the tetramer shifts from a 'tense' (T) structure to a 'relaxed' (R) conformation changing the local environment of specific amino acids, lowering their pKa and releasing H^+.

$$H\text{-}Hb + O_2 \rightleftharpoons Hb^- - O_2 + H^+$$

In reverse, H^+ binding to these specific amino acids in the deoxygenated, T state stabilizes the structure by additional molecular interactions which delay the transition to the oxygenated, R state, where oxygen affinity is reduced. The specific amino acids involved are mainly the C-terminal histidines of beta-chains (responsible for half of the Bohr effect observed) and the N-terminal residues of alpha chains [2, 13, 14].

Figure 1.2 shows the elegant interplay between these processes allowing efficient delivery of O_2 to tissues and CO_2 disposal at the lungs. When CO_2 diffuses into erythrocytes, carbonic anhydrase will shift the reaction to production of bicarbonate and H^+, these protons will bind to hemoglobin, leading to O_2 release (Bohr effect). When O_2 diffusion is predominant (in the lungs), protons dissociate from hemoglobin and are available for the reaction catalyzed by carbonic anhydrase which makes CO_2 and water out of bicarbonate and H^+. The resulting CO_2 will diffuse out of the cell and eventually be exhaled.

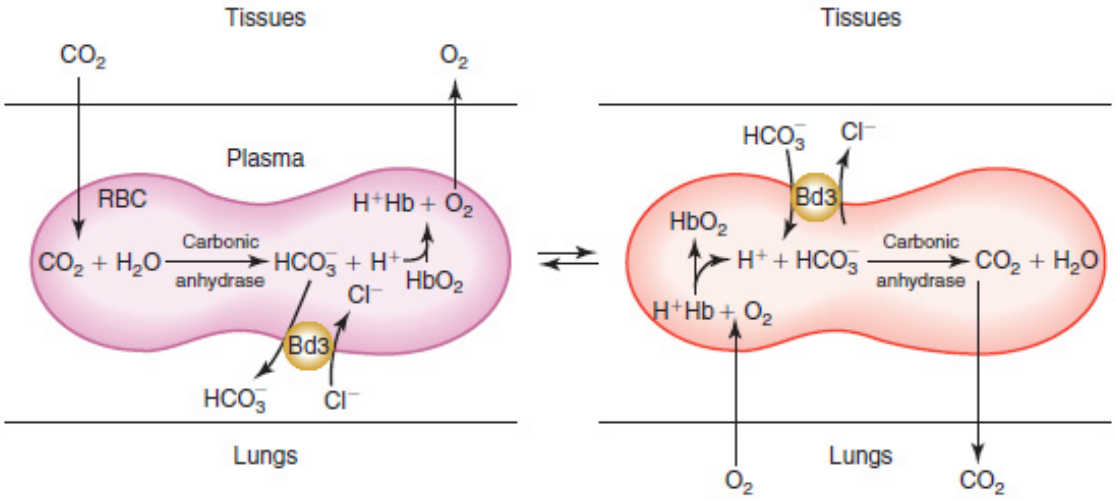

Figure 1.2: Jacobs-Stewart cycle and its interplay with the Bohr-Haldane effect.
Transport of O_2 and CO_2 within the RBC and its release according to the Bohr-Haldane effect and the Jacobs-Stewart cycle. Hb: hemoglobin. Bd3: Band 3/AE1. Scheme from [8, 15]

Red cells feature many other adaptations to assist them in circulation. RBCs have a biconcave disc shape with a diameter of 7.8 µm, which is 2.5 µm at the thickest part and about 1 µm in the center depression [16]. The volume of a typical, healthy RBC is 90-95 μm^3 or fl. It is a considerable reduction from 140 μm^3 or fl owing to membrane vesiculation during reticulocyte maturation [17]. The erythrocyte plasma membrane is roughly 1 % of the weight of a RBC and less than 0.1 % of its thickness, but with a total surface area of 140 μm^2. Thereby, RBCs have 1.5 times more membrane than volume to provide flexibility and elasticity. An erythrocyte membrane contains 2.5×10^8 phospholipids molecules, 1.95×10^8 cholesterol molecules, 1×10^7 glycolipid molecules and 6×10^6 proteins. The presence of abundant cholesterol and unique spectrin-heavy cytoskeleton give RBCs a remarkable flexibility and plasticity [18, 19]. These characteristics enable the cell to squeeze through capillaries and the spleen slits while having a lot of membrane surface in contact with the vascular wall, thereby easing gas exchange. Shape has thus a central role in proper RBC function within the bloodstream and it is often altered in disease [20].

Cell shape emerges by the passive and active interplay of lipids, which form the membrane bilayer, and proteins, which form the cytoskeleton with actin and spectrin being of prominence in the RBCs. Lipid-proteins interactions are abundant due to the presence of integral membrane proteins whose domains cross the plasma membrane. These proteins may affect membrane shape by the actual molecular arrangement within the lipid bilayer. Moreover, RBCs have large protein complexes which are anchored to the cytoskeleton, the most important being the Band 3 protein complex. Band 3 interacts with Band 4.2, CD47, RhAG and ankyrin, the latter interacting in turn with β-spectrin. Glyphorins and glycocalix-interacting integrins have also major structural roles. The resting shape of a RBCs is thus determined by a score of protein, lipid and possibly glucide interactions [6]. A biconcave shape is characteristic in conferring greater surface area than volume. This means that an increase in cell volume will increase the sphericity of the cell, whereas a loss of volume will wrinkle the membrane. Early observations of shape changes without water gain or loss lead to the description of stomatocytes (*"mouth cells"*) and echinocytes (*"hedgehog cells"*). They were induced by a wide range of experimental conditions, with the general finding that cationic amphiphiles induce stomatocyte formation whereas anionic amphiphiles induce echinocytes. Notably, both processes lead to highly spherocytic shapes

at late irreversible stages [21]. A curious shape change was reported in early literature: red blood cells turned spherocytic or echinocytic when in contact with glass, which could be prevented by low concentrations of albumin. Using high concentrations of this serum protein would have a stomatocytic effect instead [22–25].

The biconcave disk shape arises in part when early reticulocytes, which have an irregular nondiscocyte shape, remodel their cytoskeleton from a relaxed state to a shape resulting from the plasma membrane resistance to bending. Reticulocytes circulate about two days before fully maturing into RBCs, underscoring the importance of rheology on the final shape of the mature erythrocyte. Especially considering these reticulocytes have to traverse capillaries smaller than their own diameter as low as 4 µm in the splenic slits, which ensure RBC mechanical filtration [26, 27].

The average curvature of the cell increases in echinocytes and decreases in stomatocytes compared to biconcave cells [28]. Spontaneous curvature change comes from: i) adding or removing lipids from the bilayer. ii) asymmetrical exchange from one lipid monolayer to the other. iii) replacement of a lipid molecule in the outer monolayer by an exogenous molecule.

Discocytes are, thus, critical for proper hematological properties of blood, enabling efficient flow and adequate filtration at the spleen. Abnormal shapes have been used to diagnose a multitude of anemias and conditions since the early days of hematology, from characteristic sickle cells identifying underlying Sickle Cell Disease to target cells which are found in a variety of disorders, including, notably, thalassemia [29]. Furthermore, abnormally shaped erythrocyte are either unable or pass with difficulty the splenic slits of the red pulp, getting trapped and potentially giving rise to splenomegaly increasing the risk of infection and other complications. Spleen filtration is indeed the first quality control for removal of aged RBCs or those which do not fit the rheological requirements for free circulation in the narrowest capillaries [30].

Pump-leak concept

RBCs contain very large quantities of protein, hemoglobin, in the cytoplasm. As they are impermeant and charged (negatively on the whole at physiological pH) they generate a inward driving force for cations as well as an oncotic pressure. Thus, RBCs would swell and lyse if the membrane was permeant to cations. This concept that erythrocytes must have a membrane impermeant to cations to explain their constant volume in physiological conditions was shaken by the discovery of a Na^+ and K^+ leak through the membrane via radioisotope experiments. The fact that cation imbalance resulted from an inhibition of glycolysis revealed the presence of an active, ATP-consuming cation transport [31, 32]. A model in which a pump for Na^+/K^+ works against the leak of both cations so that the cation intracellular composition stays at equilibrium preventing water movements was proposed by Tosteson and Hoffman [33] in 1960 in a seminal paper. These fluxes are small, about 5×10^{-19} mmol $\cdot$ µm^{-2} $\cdot$ s^{-2} which corresponds roughly to 7×10^4 ions per µm^2 per second, a number easily compensated by the Na^+/K^+ pump at the steady-state. The intracellular levels of Na^+ and K^+ are kept within a 0.12 to 0.16 ratio. However, cation leak does not comprise only Na^+ and K^+ movements. Eukaryotic cell maintain very low levels of intracellular calcium. There is also a Ca^{2+} leak on the order of about 1×10^{-20} mmol $\cdot$ µm^{-2} $\cdot$ s^{-2} despite. As calcium is a secondary messenger involved in many processes within the RBCs, which lack calcium stores, a powerful pump is present in the membrane, the Plasma Membrane Calcium ATPase (PMCA), which is able to pump calcium ions out of the cells at a maximum rate 300 times faster than the leak brings ions in [34]. It matches the leak rate in resting, normal conditions [35]. These leaks have consis-

tently been measured, but their origin has not been elucidated. Ion diffusion, except for protons, through the lipid bilayer though not impossible is an extremely unlikely event, given ions are charged particles and the lipid bilayer core is apolar. Hence, the leak has come to mean the contribution of pathways known and unknown to the red cell cation movements.

Attempts to identify the leak pass through the inhibition of all known channels and transporters, even though the true leak will remain unknown through the contribution of unknown carriers. The membrane potential is at the Nernst equilibrium for Cl^- due to chloride movements being predominant in RBCs, due to the action of Band 3 and chloride conductive pathways. Chloride is at equilibrium in RBCs and, as a consequence, they have rather negative membrane potentials. In contrast, net movement of Na^+ and K^+ is two orders of magnitude lower than chloride. The membrane potential changes according to the Goldman-Hodgkin-Katz equation:

$$V_M = \frac{RT}{F} \ln \frac{G_{K^+} \cdot [K^+]_o + G_{Na^+} \cdot [Na^+]_o + G_{Cl^-} \cdot [Cl^-]_i}{G_{K^+} \cdot [K^+]_i + G_{Na^+} \cdot [Na^+]_i + G_{Cl^-} \cdot [Cl^-]_o} \qquad \text{(Eq. 1.1)}$$

At the resting state due to $G_{Cl^-} \gg G_{Na^+}$ or G_{K^+} the equilibrium (the membrane potential at rest) is:

$$E_M = \frac{RT}{F} \ln \frac{G_{Cl^-} \cdot [Cl^-]_i}{G_{Cl^-} \cdot [Cl^-]_o} = \frac{RT}{F} \ln \frac{G_{H^+} \cdot [H^+]_o}{G_{H^+} \cdot [H^+]_i} = -10 \text{ mV} \qquad \text{(Eq. 1.2)}$$

Symbols: R is the ideal gas constant, T the absolute temperature, F the Faraday constant, G_{ion} the respective ion conductance, [ion], the ion concentration, with *i* being inside or *o* being outside the cell. Therefore the pump-leak concept means the membrane potential is determined by chloride equilibrium.

In short, the maintenance of RBC volume relies on a balance between passive cation leak and active pumping of cations.

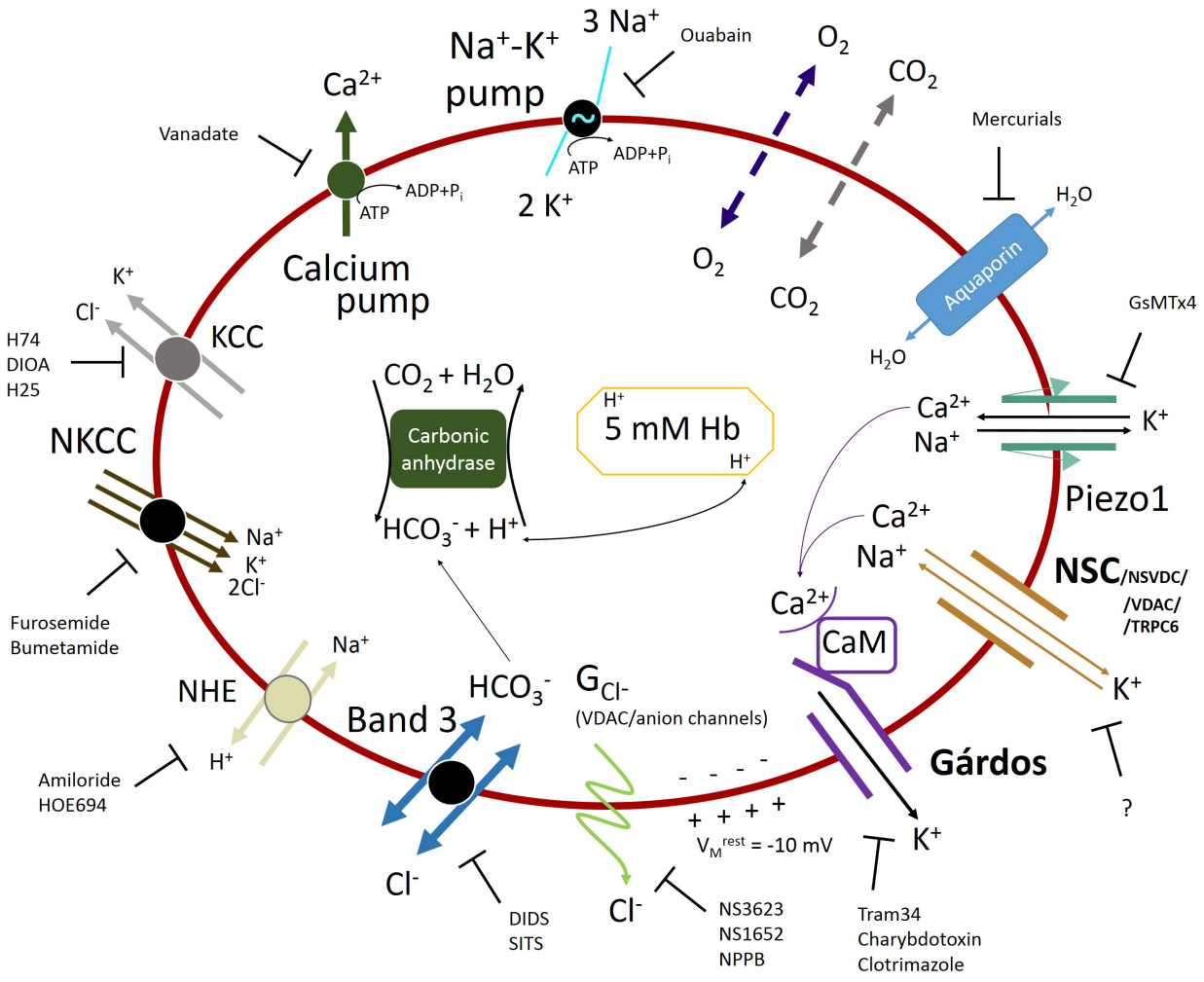

Figure 1.3: Major ion pathways and key actors in RBC physiology.
Gas permeabilities: O_2 and CO_2. Ion channels: Piezo1 (Page 40), NSVDC (Page 45), Gárdos (Page 38), G_{Cl^-} and Aquaporin (Page 36). Passive Transporters: Band3 (Page 33), NHE (Page 36), NKCC (Page 35) and KCC (Page 35). ATPases: Calcium Pump (Page 34) and Na^+-K^+ Pump (Page 33).

Clockwise: **O_2** can freely permeate the plasma membrane. **CO_2** can to some extent permeate the plasma membrane. **Aquaporin**: water channel. Water can move freely according to osmotic pressure. Constitutively open. **Piezo1**: mechanosensitive NSC. Once opened Na^+, K^+ and Ca^{2+} can move down their gradients. **NSC**: Non Selective Cation channel. A NSC exists in RBCs other than Piezo. It may be the NSVDC (perhaps not only at positive voltages), VDAC (under NSC configuration or TRPC6 (a member of ubiquitous TRPC family). **Gárdos**: Ca^{2+}-dependent K^+ channel. Calmodulin (CaM) is bound to the channel. Strong selective K^+ conductance once opened. **Chloride conductance** (G_{Cl^-}). Anionic channel activity, with VDAC as a major candidate. **Band 3** or Anion Exchanger 1: it shuttles anions, mainly bicarbonate and chloride ions. **NHE**: Na^+/H^+ exchanger. Minute activity in mature RBCs. Sensitive to a variety of stimuli. **NKCC**: Na^+-K^+-$2Cl^-$ cotransporter. Normally silent in mature RBCs at the resting state. **KCC**: K^+-Cl^- cotransporter. It plays a major role in Sickle Cell Disease. Activity is quickly lost when reticulocytes mature into RBCs. **Calcium pump** or Plasma Membrane Calcium ATPase (PMCA): it takes a calcium ion out of the cell for every ATP hydrolyzed. **Na^+-K^+ pump**: it takes 3 Na^+ out and 2 K^+ in for every ATP hydrolyzed. Cytoplasmic: **Carbonic Anhydrase**. Reversible reaction between bicarbonate and CO_2. Hb: **Hemoglobin**. Oxygen binding and release. Most abundant protein in RBCs.

Membrane transporters

Studies over the last 70 years identified several membrane transporters that may contribute to the ion and solute movements observed in physiological, pathophysiological or experimental conditions (**Fig. 1.3**).

Band 3

Band 3 is a major transporter in the red cell membrane with over one million copies per cell. It is the most abundant transporter in red cells and is found, as a truncated isoform, in type A intercalated cells in renal distal tubes. It exchanges anions, importantly Cl^- and bicarbonate, powering the Jacobs-Stewart cycle. In addition, it is an essential structural protein which associates with a myriad other RBC proteins, mainly as a way of relaying them to the plasma membrane as well as enabling close interactions. The cytoplasmic domain serves the structural, binding function, whereas the integral membrane domain crosses the lipid bilayer 14 times and is solely responsible of anion exchange. Key partners are deoxyhemoglobin, hemichromes, G3PD (glyceraldehyde-3-phosphate dehydrogenase), PGK (phosphoglycerate kinase), aldolase, ankyrin, glycophorin, protein 4.1, protein 4.2, adducin, Rh, RhAG and there is evidence carbonic anhydrase IV can bind to an extracellular loop [36]. Some evidence pointed to binding of carbonic anhydrase II to the C-terminal domain, though it was contested [37–39]. G3PD, PGK and aldolase are glycolysis enzymes, whereas ankyrin and adducin relay the membrane to the cytoskeleton via Band 3 (to spectrin and actin, respectively). The fact that so many essential factors of RBC physiology associate with Band 3 has lent weight to the notion that metabolism occurs mostly at the membrane, the rest of the cytoplasm left to hemoglobin. The presence of glycolytic enzymes close to the membrane and a physical enclosure by structural proteins provides an ATP pool to pumps [40]. The concerted interaction in close proximity of all these key actors in RBC metabolism has led to being termed a metabolon [41].

3 Na^+/2 K^+ pump

Since the discovery of cation leak in red cells and given the fact that the cytoplasm contains high levels of K^+ and low levels of Na^+, while they are low and high, respectively, in the surrounding plasma, the existence of a Na^+/K^+ pump was considered a necessity. Erythrocytes were widely used in the early characterization of the pump, due to ease of handling and lack of internal organelles facilitating measurements. RBCs were found to lose intracellular K^+ and gain Na^+ when stored in ice, but they restored the original cation distribution when stored at 37 °C in the presence of glucose [31, 32, 43, 44]. Radioisotope tracer experiments showed cation exchange in erythrocytes and other cell types [45, 46]. The notion that either Na^+ or K^+ was the ion species that was actively pumped, while the other followed according to the driving force persisted for a brief time [47]. It was shown that the coupling was stoichiometric, and a stoichiometry of 1:0.5 Na^+:K^+ was first proposed [48, 49]. The actual ratio is 3 Na^+ out for 2 K^+ for every ATP hydrolyzed, so it is electrogenic [50].

Although it is ubiquitous and central to general physiology, its role in RBC physiology is particularly essential, as it allows to keep the net cation movement very close to zero, and with it, the volume. It is estimated that 20-30 % of cell energy consumption comes from the ATPase activity of pumps. The Na^+/K^+ pump is inhibited by ouabain or low temperatures, and the latter plays an important role in cation imbalances during blood transport (shipping) and storage [51].

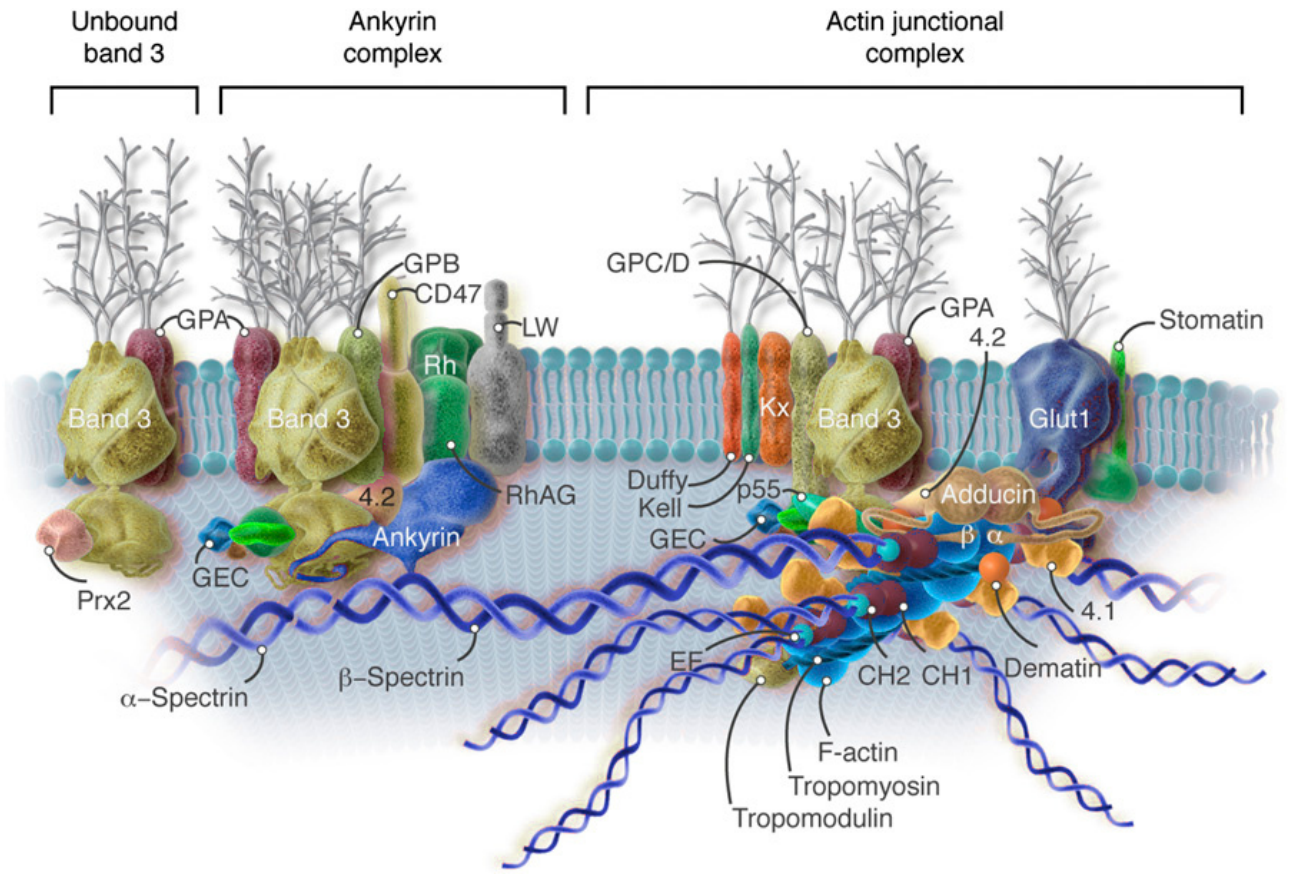

Figure 1.4: Major membrane-cytoskeleton complexes at the RBC membrane.
Schematic showing Band 3, ankyrin and adducin complexes and its interaction with the spectrin and actin cytoskeleton for which they provide a membrane anchor. Figure adapted from [42].

Ca^{2+} pump

The calcium pump, also known as the Plasma Membrane Calcium ATPase (PMCA), constitutes 0.1 % protein mass per gram of RBC mass and ensures intracellular calcium levels stay at the nanomolar range, at about 20-60 nM [34, 52–54]. Very low intracellular calcium concentration is a feature found ubiquitously in nature in both eukaryotes and prokaryotes. Many isoforms of PMCA exist and it is expressed in almost all cell types, especially in brain. As the surrounding plasma has a calcium concentration of 2 mM, there is a tremendous driving force arising from a 1000-fold difference in concentration on the two sides of the membrane, so the membrane must be very impermeable to Ca^{2+}. Indeed its permeability to calcium is very low, smaller than Na^+ or K^+ permeabilities as mentioned before. The pump can switch to from a low, *housekeeping* mode to a high activity mode via interactions with calmodulin. An ATP is consumed for every calcium ion pumped out. An interesting strategy used to determine the V_{max} of the Ca^{2+} pump employs $^{45}Ca^{2+}$, Co^{2+} and the calcium ionophore A23187. RBCs are placed in solution containing $^{45}Ca^{2+}$ and exposed to high concentrations of A23187. The ionophore-mediated influx will greatly surpass the V_{max} of the PMCA. In these conditions intracellular and extracellular calcium levels are largely equal. Addition of cobalt will immediately block A23187-induced calcium pores as it is a divalent cation of larger size than calcium. Pump activity will be thus revealed as calcium is pumped out against the artificial gradient [55]. Calcium leak was determined following inhibition of the PMCA. However, no specific inhibitors exist [56, 57]. In order to reach a satisfactory degree of inhibition three approaches can be employed: i) use of vanadate (with 99.7 % inhibition at 1 mM), ii) ATP depletion and iii) use of chelators to bring the intracellular calcium concentration below the threshold

of pump activity. The pump is subject to extensive regulation by: acidic long chain polyunsaturated fatty acids, phospholipids, protein G beta-gamma subunits, oligomerization, phosphorylation by protein kinases such as PKA and PKC and, importantly, by calpain in response to augmented calcium cytosolic levels [52].

Modeling of main erythrocyte gas transport function and ion homeostasis can be done with only Band 3 (and more generally the chloride conductance), Na^+/K^+ pump, the PMCA and constant cation leaks, underscoring the central role these play in erythrocyte physiology. These pathways are always working with the gradient like Band 3 and the leaks or against the gradient like the ATPases, but they are never *switched off* as their activity is necessary for the operation and survival of RBCs. Several other transporters and ion channels have been described and they are active only in response to stimuli or certain conditions, therefore presumably contributing to the background leak or as a failsafe to restore ion or water balance if homeostasis is disturbed. Nonetheless, their activation can entail an upheaval in ion distributions which would explain why they are normally silent.

NKCC

The $Na^+/K^+/2Cl^-$ cotransporter (NKCC) was discovered in 1974 when inward fluxes of sodium and potassium were detected in ouabain-containing solutions which were inhibitable by furosemide [58]. NKCC is an electroneutral ion transport protein expressed in many tissues, where it takes part in volume and chloride control. RBCs have isoform NKCC1. NKCC1 is a large protein with 12 transmembrane domains, at least three regulatory phosphosites, a phosphatase docking site and likely glycosylation extracellular sites, all predicted *in silico*. NKCC1 activity has typically been measured by looking at the decrease in cation influx in ouabain plus bumetanide, another NKCC1 inhibitor. $^{86}Rb^+$ is then used to analyze K^+ uptake. The bumetamide-K^+ sensitive influx is only 2 mmol $\cdot$ l_{cells}^{-1} $\cdot$ h^{-1}, however variations up to three times that value have been reported [59]. NKCC1 function in human erythrocytes is poorly understood. It is generally regarded as an actor in volume regulation sensing cell water and/or chloride loss. It is not yet clear, in human RBCs, up to what extent it is activated and regulable in response to stimuli or if it is simply maintaining an equilibrium, considering it is a passive transporter. Most cells display a significant inward driving force for chloride, whereas for RBCs intracellular chloride levels are high and at equilibrium, meaning there is little driving force to move salt through NKCC1 at the resting state. In a state of cationic imbalance, there may be an electromotive force to move salt into the cell, though likely dependable on the phosphorylation state, oxygen tension, macromolecular crowding and the concentration of chloride [60, 61].

KCC

The K^+/Cl^- cotransporter was first described in 1981 in an article reporting a passive chloride-dependent pathway specific for potassium which was sensitive to volume increase, inhibited by anti-L_1 antibody and unaffected by intracellular calcium levels [62]. A chloride dependent passive K^+ flux had been observed the year before in response to N-ethylmaleimide treatment of low-K^+ sheep RBCs [63]. KCC was identified at the molecular level in 1996 when looking for similar homologous sequences to NKCC, and hence it shares many characteristics with NKCC such as having over one thousand amino acids, 12 transmembrane domains as well as phosphorylation and glycosylation sites. Experiments with KCC1-overexpressing-cells showed a significant increase in $^{86}Rb^+$ uptake in the presence of N-ethylmaleimide as well as inhibition by bumetanide, furosemide and chloride

dependency [64]. Although the activity of the cotransporter greatly increases upon volume gain, a lag period is observed until the maximum transport rate is seen. The lag period is augmented by phosphatase inhibition or by sustained swelling, but can be considerably reduced by staurosporine or Mg^{2+} depletion. Nonetheless, no delay is observed in the decrease in activity that occurs upon shrinkage. KCC activity is raised by elevated P_{O_2}. The relationship between the cotransporter and P_{O_2} is similar to that of hemoglobin and P_{O_2} and fits a sigmoid curve [65]. Besides, low P_{O_2} renders KCC unresponsive to other influencing factors such as cell volume or moderate pH change [66]. In any case, KCC1 is inactive in mature RBCs, unresponsive to cell swelling and only amenable to N-ethylmaleimide stimulation or high hydrostatic pressures. Its importance in RBC physiology comes from its contribution to Sickle Cell Disease pathophysiology as it leads to major dehydration together with the Gárdos channel during cyclic deoxygenation [67]. Low P_{O_2} does not have an inhibiting effect on KCC1 in sickle cells and low pH and urea are still able to stimulate the symporter [65, 68]. KCC1 has been thus considered has a potential therapeutic target for SCD. Specific inhibitors, which act in the micromolar range, include H74, H25 and DIOA. H74 is rather specific and does not inhibit NKCC [69, 70].

Na^+/H^+ exchanger

The Na^+/H^+ exchanger 1 (NHE1) is a 100 kDa antiporter present in RBCs, with 12 transmembrane domains and a C-terminal cytosolic interacting domain. It is sensitive to cell hypoxia, shrinking, intracellular low pH and its activity can be modulated by catecholamines, kinases and phosphatases. Upon cell water loss, NHE1 activates bringing Na^+ into the cell, which together with Band 3 activity entails a net NaCl gain and, therefore, water by osmosis. Continued activity leads to high intracellular pH and the antiporter likely inactivates. In trout RBCs, NHE is stimulated by high cAMP levels which lead to PKA-mediated phosphorylation [71]. Use of calyculin A, a phosphatase inhibitor, induces a strong NHE activity in these cells by blocking the antiporter desensitization observed via PKA and PKC pathway [72]. A role of NHE1 may be volume regulation upon osmotic shrinkage happening during kidney transit [73]. Catecholamines are implicated in hypoxia signaling. Furthermore, it is thought NHE1 could affect RBC gas transport as its efficiency relies upon morphology, which is in turn impacted by osmolarity and pH [74]. NHE is inhibited by amiloride and derivatives as well as HOE694 [75, 76]. Amiloride binds domains IV and IX close to the site for Na^+ binding leading to competition in some circumstances [77]. HOE694 is a less potent but more selective blocker [78]. An involvement of NHE1 in disease has been reported for hypertension and SCD and ruled out for diabetes [79–81]. NHE1 activity for SCD was about 1.65-fold higher in HbS homozygotes than wild-type individuals. NHE1 activity is markedly diminished in mature healthy RBCs compared to reticulocytes, to the point it may not be sufficient to influence any considerable change in either pH or volume [81, 82].

Aquaporin

Erythrocytes have been noted to possess a high permeability to water since the earliest studies. Osmosis was largely defined by observing RBCs responses to hypo-, iso- and hypertonic solutions, so there has always been great interest on deepening our knowledge on water permeability. Especially considering that the lipid bilayer, though actually permeable to water, has a finite permeability and cannot account for almost instantaneous hemolysis occurring in strongly hypotonic solutions. Therefore, a protein pathway which would establish an aqueous *channel* through the membrane has long been suspected. Furthermore, treatment of RBCs with

sulphydryl-modifying mercurial compounds, which bind covalently to cysteines, reduces severely the water permeability of erythrocytes, although a residual permeability remains. Aquaporins were found by serendipity during attempts to isolate the 32 kDa subunit of the Rhesus antigen of red blood cells [83]. A putative protein, first thought to be a degradation product of Rh, consistently appear together with Rh. When it was cloned and sequenced it was found to match CHIP28, previously identified as member of the MIP (Major Intrinsic Protein) family [84]. Interestingly, proteins sharing very high homology with CHIP28 are found in bacteria, *Drosophila spp.*, bovine eye lens and plants. In humans it was discovered to be most abundant in RBCs and kidney tube cells, strongly pointing towards a water pathway function. Tests where CHIP28-expressing oocytes from *Xenopus laevis* burst within 5 minutes after osmotic shock compared to unaffected control confirmed CHIP28 as a water channel and was henceforth called aquaporin [85]. Aquaporin-1 is present in high numbers in the plasma membrane, up to 1.4×10^5 channels per cell. Another isoform, aquaporin-3 is interestingly refractory to the actions of mercurial agents. Aquaporin-3 is not determinant to water or glycerol permeability [86]. Aquaporin-3 is however permeable to urea which, together with other specific urea transporters, makes the RBC highly permeable to this molecule. The rationale behind these findings is that as RBCs have to pass through the renal medulla with extreme osmolarities over 1 M, high permeability to urea prevents most of the osmotic effects of its high concentration, while the high permeability to water allows fast water loading and unloading imposed by high levels of solutes. Nevertheless, individuals have been observed to present exon deletion or frameshift mutations in aquaporin-1 (synonymous with the Colton blood group) in a homozygous manner, and yet, lacking any phenotype despite a reduced water permeability. Even a completely nonfunctional aquaporin-1 observed in a subject does not bring any clinical consequence [87]. In spite of this, aquaporin-1 knock-out mice have a severe impairment in the production of concentrated urine [86]. The problem is compounded, rather than solved, by the finding that aquaporin-1 is permeable to CO_2, thereby increasing the permeability of this gas through the membrane [88]. Therefore, the sole explanation seem to be redundancy conferred by some other pathways, including RhAG which accounts for about 25% of red cell CO_2 transport [89].

Ion channels

Ion channels were discovered in the twentieth century in classical experiments in giant squid axons. Studies were focused on excitable membranes such as neurons and cardiac muscle. Definite proof of their electrical properties came in 1976 with the advent of patch-clamp from the work of Neher and Sakmann [90], developed in the following years [91–93]. Their work earned them the Nobel Prize in 1991. The method enables the recording of membrane current or potentials using a single pipette containing an electrode at single channel or cellular level. Hamill [94] made the first patch-clamp report in RBCs, hitherto considered unpatchable due to their small size. Nonetheless, the existence of ion channels in RBCs was proposed long before the adaptation of patch-clamp to erythrocytes. Ion movements through transporters are rate-limited as discrete ions must bind and protein conformation must change before release on the other side of the lipid bilayer. Hence, fast and sudden ion movements can only be accounted for by ion channel activity which provide aqueous passage to ions down their gradients according to ion selectivity and driving force. Because a channel opening increases the ion conductance, the membrane potential changes accordingly, as expressed in the equation for a potassium channel, for example:

$$G_{K^+} > G_{Cl^-} \gg G_{Na^+} \text{ then:}$$

$$V_M = \frac{RT}{F} \ln \frac{G_{K^+} \cdot [K^+]_o + G_{Cl^-} \cdot [Cl^-]_i}{G_{K^+} \cdot [K^+]_i + G_{Cl^-} \cdot [Cl^-]_o} \quad \text{(Eq. 1.3)}$$

And given that $I_{ion} = G_{ion}(V_M - E_{ion})$, from the resting state $I_{K^+} \approx 0$ will change to $I_{K^+} > 0$ on channel opening, with the ion flow direction dictated by V_M and itself by the relative concentrations of the ion in and out of the RBC.

Note that V_M depends not only on the conductance (G_{ion}) but on the ion concentrations inside and outside the cell, so that ion movement through the channel alters the ion concentration therefore the change in V_M decreases over time as the chemical gradient dissipates and an equilibrium is reached. Channels carry millions of ions per second and ion channels with large unitary conductances can shift the membrane potential extremely fast setting a new equilibrium. Return to the resting original state cannot occur until the channel closes and ion pumps restore ion distribution.

Cation channels

Gárdos channel

Discovery and characterization Gárdos reported in 1958 a curious effect by which an increase in K^+ permeability, which was known to be caused by glycolysis inhibition, could be abolished with calcium chelation, such as EDTA or sodium oxalate. Supplementation with $CaCl_2$ triggered also the increase in potassium permeability, demonstrating calcium was key to this effect [95]. The Ca^{2+}-dependent increase in K^+ permeability was termed the Gárdos effect. This effect could be reproduced consistently including in ghosts and membrane vesicles [34, 96, 97]. Pb^{2+} also triggers a K^+ permeability increase and the fact that oligomycin inhibited both not only Pb^{2+} but also Ca^{2+} lent support that they act on the same system [98]. Moreover, the calcium binding site was proven to be cytosolic [99]. This Ca^{2+}-dependent K^+ transport was demonstrated to be electrogenic in experiments with frog RBCs, which are so big that an intracellular electrode can be used to record currents. If these cells were impaled Ca^{2+} went inside before resealing and puncturing again the cells led to a transient hyperpolarization relative to the Nernst potassium equilibrium [100, 101]. In human RBCs, this was demonstrated by the use of fluorescent dye for the determination of the membrane potential [102]. Total absence of K^+ in the extracellular solution irreversibly inactivates the pathway only if Ca^{2+} was present [103, 104]. As lack of external K^+ is inhibitory, a binding site was suspected to be on the outer membrane. Quinine is inhibitory at low concentrations in K^+-free solutions and at increasing concentration if solutions contain more K^+, so it was concluded that quinine competes for the same inhibitory site as K^+ [105]. This started a controversy whether the pathway was a transporter or a channel. With the advent of gigaseal patching, which minimizes noise allowing patch-clamp recording of human RBCs (too small until then for patching), more evidence was gathering towards establishing the Gárdos effect as a channel. Cell-attached recordings revealed two K^+ channel types, with a 18 pS channel found in ATP-depleted cells. In whole-cell mode it was found that frog erythrocytes display outward rectified currents upon application of depolarizing voltage steps in the presence of at least 1 µM Ca^{2+} and high K^+ pipette concentrations. At pipette calcium levels of 1 to 10 nM, discrete outward currents could be discerned, though not at greater concentrations [106]. Using protonophore-mediated estimations of the membrane potential, addition of small concentrations of calcium ionophore A23187 was shown to lead to membrane potential oscillation due to K^+ exit, within a limited Ca^{2+} concentration range. However, closure

is an spontaneous process as it happens before the PMCA has time to pump the calcium out and both glycolysis and the PMCA were left uninhibited in these experiments. Furthermore, very low calcium concentration elicited no response under A23187 influence whereas if high calcium concentrations were used a permanent hyperpolarization was observed, as was the case if RBCs are depleted in ATP. Treating hyperpolarized cells with EGTA brought the membrane potential back to resting values, while K^+ loss and hyperpolarization was still seen in ATP-depleted erythrocytes [107]. The pathway displays single-file diffusion, typical of channel behavior [108]. Detailed characterization of the channel came from recordings in the inside-out configuration of patch-clamp. It confirmed all the properties previously reported such as activation by lead, or requirement of K^+ in the extracellular solution. The study established that the channel activity is inwardly rectified, that 50% maximum activity is reached at 2 μM intracellular calcium and that the selectivity ratio is 15:1 K^+:Na^+ [109]. The potassium selectivity of the channel has been confirmed by tracer studies and, since, $^{86}Rb^+$ has been widely employed to assess channel activity. The selectivity filter of the channel was lost if low concentrations of trypsin were applied to the internal side of the plasma membrane by using resealed ghosts showing that amino acid truncations on the cytosolic side affect the transmembrane pore [110]. The Gárdos channel (henceforth called simply henceforth called simply Gárdos) displays an increase in conductance proportional to temperature increase, whereas low temperatures significantly increase the open probability (P_o) of the channel, so that there is a 10 % probability of the channel being open at 35 °C while at 0 °C the probability rises to 80 % [111].

Channel pharmacology Many inhibitors exist for Gárdos, though those used during early characterization studies were largely unspecific such as quinine, oligomycin or cetiedil, though the latter was reported to irreversibly block the channel [105, 112, 113]. Three potent inhibitors are antifungal clotrimazole, deathstalker toxin charybdotoxin and designed triarylmethane Tram34, with IC_{50} of 50 nM, 5.4 nM and 25 nM, respectively. Even though Tram34 has a higher E_{50} than charybdotoxin, it is consider a better inhibitor as it was designed to be highly specific for Gárdos, therefore preventing off-target effects [114–117]. Gárdos activators include antihypertensive propranolol, 1-EBIO (1-ethyl-2-benzimidazolinone) and NS309 (6,7-dichloro-1H-indole-2,3-dione 3-oxime) [118–120]. Propranolol is a Gárdos activator up to 2 mM where it has inhibitory effects and it was thought to act by displacing membrane-bound calcium, thus raising the intracellular calcium concentration. However, an article pointing to its blocking effects on the calmodulin-activated PMCA, but not on the basal Ca^{2+}-pump, as an explanation for its ability to activate Gárdos [121]. Another study, found in patch-clamp recording of inside-out patches that propranolol augments the calcium sensitivity of Gárdos, whilst reducing its single-channel conductance and activity at the same time [122]. 1-EBIO and NS309 were also shown to increase the calcium sensitivity of the channel, but NS309 was 1000 times more potent than 1-EBIO and much more selective towards Gárdos compared to other K^+ channels, making the compound the best activator known to date [120, 123, 124].

Phosphorylation and molecular identity Gárdos could be labile to phosphorylation and experiments had been carried out with agonists of the cAMP pathway such as theophylline, among other methylxanthines, although PKA or PKG stimulation was ruled out upon use of specific inhibitors and after mutation of PKA phosphosite abrogated the effect [125, 126]. Methylxanthines are Gárdos agonists via other mechanisms. In addition, calpromotin, a protein with similarity with the Thiol-Specific Antioxidant protein (TSA), can bind Gárdos and activate it [127, 128]. Gárdos copy number has not unequivocally been established. It was first estimated at 100-200 copies through $^{86}Rb^+$ fluxes studies in inside-out vesicles [34]. A study employing ^{125}I-

charybdotoxin in basic, low ionic strength conditions offered 120 ± 36 binding sites per cell [129]. If 150 copy numbers per cell were used for calculation by feeding independent experimental data of a single channel conductance of 10 pS and considering the effect of temperature on the open probability, the channel has a conductance of 85 μS/cm^2, which largely corresponds with the K^+ conductance measured at saturating Ca^{2+} concentrations, 61 μS/cm^2 [111, 130–132]. A copy number of about 135 channel per cell is in agreement with an estimated 115 channels per ghost and 315 channels per RBC calculated from mass spectrometry data [133]. The molecular identity was revealed in the late nineties, when a small-conductance Ca^{2+}-activated channel was screened and cloned from a human library into Chinese Hamster Ovary cells [134]. Based on electrophysiology experiments on these cells the channel was termed hSK4 (human Small Conductance Potassium channel 4), which has led to some confusion as the channel turned out to be an intermediate conductance calcium-activated channel as reported by Ishii and coworkers soon after the first report [135]. The channel shows all the properties described for Gárdos channel, such as inhibition by clotrimazole or charybdotoxin, activation with 1-EBIO and a single channel conductance at zero current of 20 pS, as found in RBCs [135, 136]. Moreover, SK channel inhibitor apamin does not affect the cloned channel. Association of calmodulin to the channel was shown in Rb^+-loaded inside-out vesicles as well as by use of calmodulin blockers [97]. Nevertheless, a laboratory found no requirement of calmodulin to evoke Gárdos currents in patch-clamp experiments, sparking a search for direct binding of Ca^{2+} to Gárdos polypeptide chain, which was proven fruitless [137]. Calmodulin was found to co-precipitate with Gárdos using a yeast-two hybrid strategy [138]. Calmodulin is constitutively bound to Gárdos, hence the reason why inhibitors sometimes failed to block may stem from tight interactions. Four Gárdos monomers assemble with four calmodulins to form a homotetramer (**Fig. 1.5A**). When cytosolic calcium levels rise, calmodulin binds calcium and changes Gárdos conformation, opening the pore (**Fig. 1.5B**).

Piezo1

Discovery 2010 marked the discovery of mechanosensitive (MS) channels in humans beginning with the first molecular characterization of a nonselective cation channel in the neuroblastoma mouse cell line Neuro2A. Overexpression of the channel in different cell lines including Human Embryonic Kidney (HEK) cells elicited MS currents, i.e. in response to pressure on the membrane caused by a blunt pipette. Microarray analysis and a siRNA approach identified gene *FAM38A* as the soon-to-be-called Piezo1 [141]. Six years before the discovery, it was found to be present in senile astrocytes and induced by beta-amiloid treatment, though little else was known [142]. The channel was named Piezo for 'pressure' in Greek. Our laboratory described in 2010 pressure-induced Ca^{2+} entry in response to membrane deformations during cell-attach patch-clamp sealing, which is improved by applying negative pressure on the cell, leading to Gárdos activation [140] (**Fig. 1.5C**). In hindsight, it is likely Piezo was responsible for this activity. Whereas Piezo2 is expressed in the lung and dorsal root ganglion neurons, Piezo1 is present in the lung, skin, bladder, stomach, colon, kidney and erythroid cells [141]. Piezo1 systemic knockout was shown to be embryonic lethal in mice. An erythroid knockout leads to increased RBCs fragility and overhydration [143]. Piezo2 is critical for vascular and lung development. Two diseases have been linked to these channels. Distal Arthrogryposis type 5 is caused by mutations in Piezo2 and Hereditary Xerocytosis is caused by mutations in Piezo1, resulting in a form of hemolytic anemia in which cells are dehydrated.

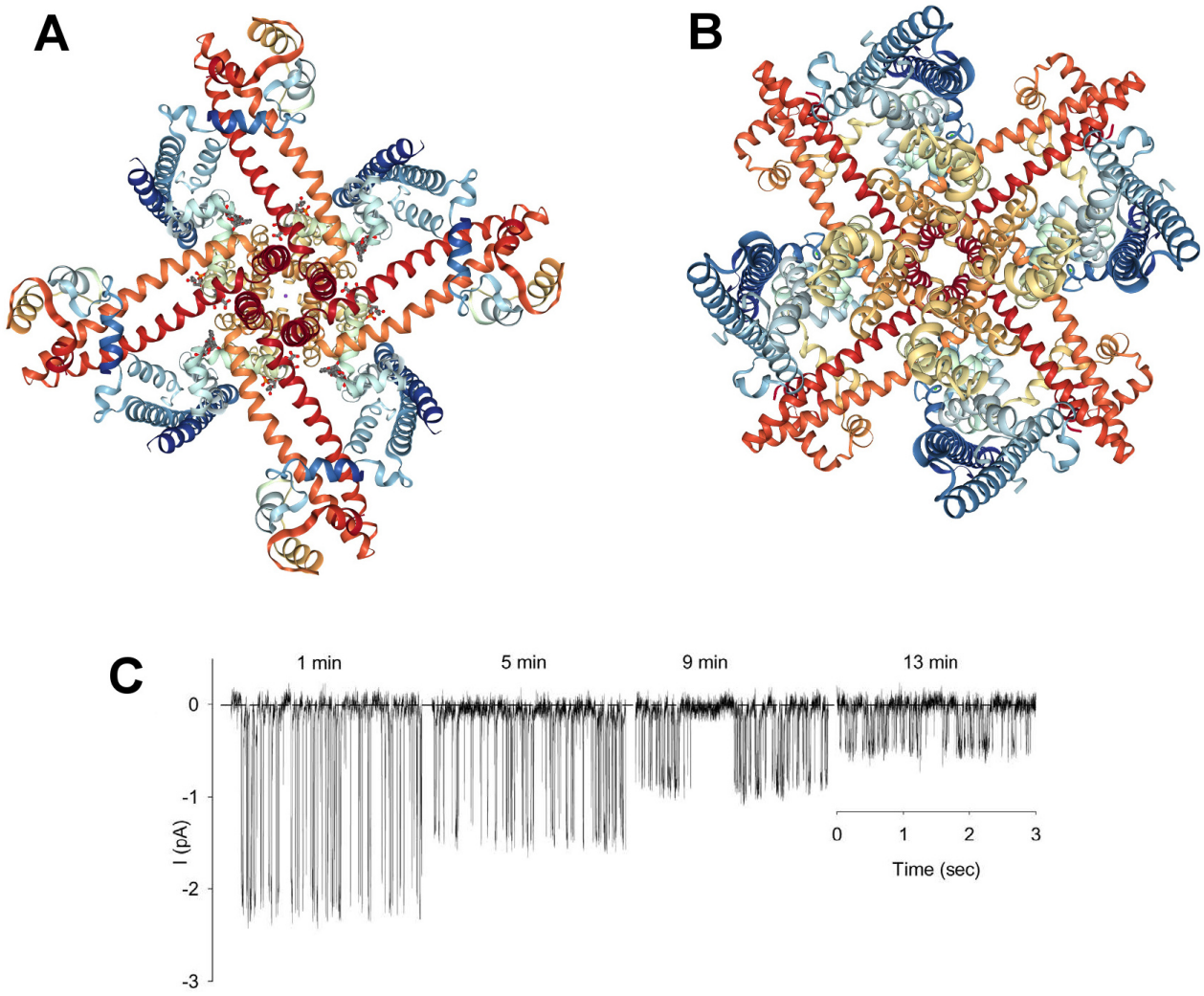

Figure 1.5: Gárdos homotetrameric structure and single-channel currents over time.
3D structure of human Gárdos channel. **A**: Cryo-EM structure of the Gárdos-calmodulin channel complex. **B**: Complex in the Ca^{2+} bound state II. Structures from the Protein Data Bank: 6cnn, 6cnno [139]. **C**: Representative example (out of 50 patches) of progressive decline of Gárdos activity recorded at different times after seal formation with solution B (150 mM KCl, pCa3) in the pipette solution and solution A (150 mM NaCl, pCa3) in bathing solution at 0 mV pipette potential. Patch-clamp traces from [140].

Mechanosensitivity Mechanosensors such as Piezo allow the transduction of mechanical stimuli exerted on plasma membranes into electrochemical signaling [144]. Mechanosensitivity seems to have been arrived at via convergent evolution, as known MS channels have widely differently structures. Descendants of the ancestral bacterial MS channel MscS can be found in eukaryotes, including importantly human parasites such as *Plasmodium*. Homologs of Piezo exist in animals, plants, algae and, notably, sponges and unicellular eukaryotes, which raises the question whether Piezo was required in the jump to multicellularity [145]. When a protein shows inherent mechanosensitivity it is said it operates under a 'force-from-lipids' paradigm, without relying in ancillary proteins or the cytoskeleton. Hard-tested approaches to elucidate lack of extraneous influence on MS channel come from experiment with bacterial MS channels. Amphipaths can activate mechanosensitive channels by altering the properties of the lipid bilayer, for instance, by inducing convexity in the lipid bilayer due the asymmetric distribution of the newly incorporating lipids [146]. Evidence suggests the size of the polar group is the determining factor in the ability of amphipaths in changing the lipid bilayer curvature, rather than

the charge. Definite proof of a 'force-from-lipids' mechanism is obtained by channel reconstitution in artificial lipid bilayers or liposomes and by observing recapitulation of original properties via patch-clamp recordings. This strategy demonstrated that a force-from-lipids paradigm is valid for eukaryotic mechanosensitive channels [145, 147]. Piezo seems to be gated via direct stretching of the membrane, i.e. in force-from-lipids manner. Piezo1 undergoes a dimension change of about 8 nm^2 which is similar as seen in inherent bacterial MS channels MscS and MscL, hence Piezo may sense membrane tension akin to bacterial MS channels. Half maximal activation (T_{50}) of Piezo1 is 2.7 mN/m either as positive or negative pressure as applied by a pipette [148, 149]. Some evidence points to an involving of scaffolding proteins in mechanotransduction fine tuning [150]. However, the fact that Piezo1 currents could be measured from Piezo-embedded reconstructed lipid bilayers and proteoliposomes demonstrate inherent mechanosensitivity in Piezo [149, 151]. Lipid solubility mismatch and membrane curvature contribute to membrane domain formation. Tension can induce a lipid mismatch and/or alter the curvature of the membrane. The thickness of the lipid bilayer can, in turn, be changed by the rearrangement of constitutive lipids and embedded proteins. Some of these altered configurations may promote mechanosensitive channel open states and trigger channel activation even without external stimulus, just by the intrinsic curvature of lipid domains which is conferred by the physicochemical properties of lipid molecules that form them [152–155].

Structure and permeation Piezo is a very large protein with barely any homology with other channels. It has a length of 2521 amino acids for Piezo1 and 2752 for Piezo2, both sharing only 47% identity, with 38 transmembrane domains spanning the plasma membrane. Three Piezo1 monomers assemble to form a homotrimer, a very large, 0.86 MDa structure that can be imaged by electron microscopy (**Fig. 1.6**). Human Piezo1 presence at the membrane was confirmed by immunofluorescence experiments [145]. The protein is a true pore-forming nonselective cation channel meaning there is only size and charge exclusion and mono- and divalent cations can freely traverse the membrane once opened. The pore, at around 8 Å of diameter, is at the C-terminal part of the protein [157, 158]. Permeability for K^+ and Na^+ follows a 1:0.82 ratio and the channel is permeable to divalent cations such as Mg^{2+} and, importantly, Ca^{2+}, as it is a key secondary messenger [159]. However permeability studies have been carried out in overexpressing HEK cells, so the actual permeabilities in RBCs may vary. Inactivation is dependent on membrane potential and is prolonged with any depolarizing voltage change [160].

Channel pharmacology Piezo1 is inhibited by nonspecific inhibitors Ruthenium Red (RR) and Gd^{3+} and more specifically by GsMTx4 a peptide from the Chilean fire tarantula (*Grammostola rosea*), though it was hitherto reported as a broad mechanosensitive channel blocker. GsMTx4 appears to stabilize the close state of the channel as its presence before applying pressure blocks channel activation [161]. On the other hand, increasing pressure is able to overcome GsMTx4 block. The toxin only works on the outer side of the membrane, but it directly binds the lipid bilayer, pointing towards Piezo having inherent mechanosensitivity and GsMTx4 disrupting the curvature of the lipid bilayer [145, 161, 162].
An agonist of Piezo1, Yoda1, was identified after screening a large collection of small molecule compounds using Fluo3, a calcium sensitive probe in a fluorescent assay. Yoda1 was found to be inactive against Piezo2. Yoda1 appears to not only increase the opening probability but it also slows the inactivation rate, a feature imposed by several Piezo1 mutations. Hence Yoda1-activated channels are opened about 4 times longer than those opened by mechanical stimulus [163]. Another high-throughput screening identified Jedi1 and Jedi2 as Piezo

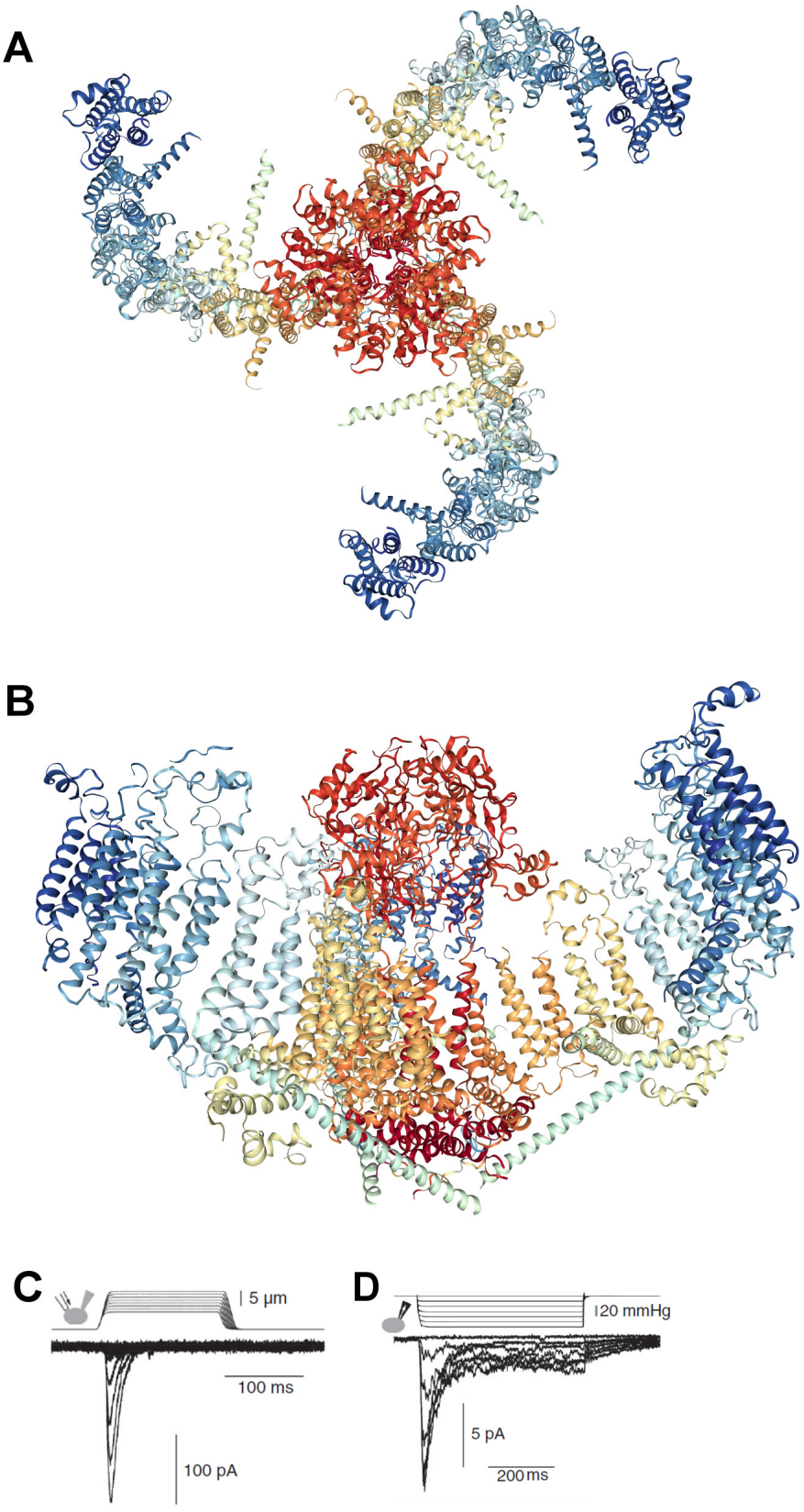

Figure 1.6: Piezo1 homotrimeric structure and mechanically activated currents.
Protein structure of a mouse Piezo1 homotrimer. (**A**) Top view. (**B**) Side view. (**C**) Representative traces of mechanically activated inward currents expressed in N2A cells. Cells were subjected to a series of mechanical steps of 1 µm movements of a stimulation pipette in the whole-cell patch configuration at a holding potential of –80 mV. (**D**) Representative currents (averaged traces) induced by means of negative pipette pressure (0 to –60 mmHg, Δ10 mmHg) in a N2A cell. **A** and **B** structures from the Protein Data Bank: 6b3r [156]. **C** and **D** traces adapted from [141].

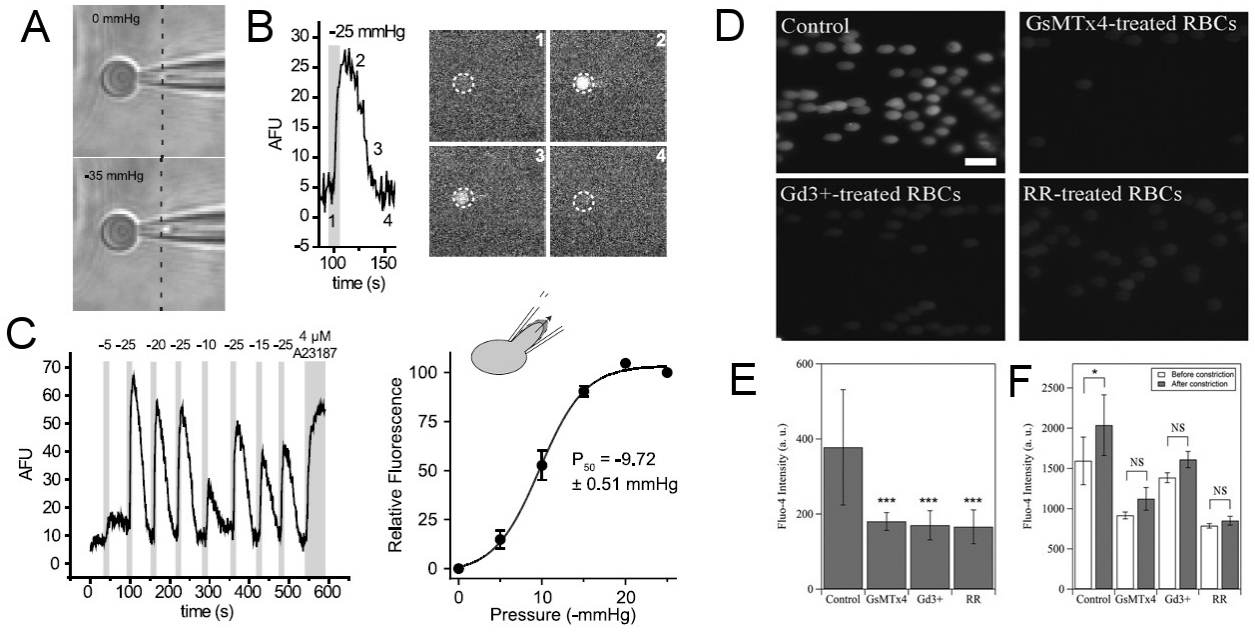

Figure 1.7: Piezo1-mediated calcium influx is pressure-dependent and occur during capillary passage.
(**A**) Brightfield images of an individual RBC before (top) and during (bottom) application of −35 mmHg. Dotted line indicates starting location of RBC membrane prior to stretching. (**B**) Left: representative plot of background subtracted Fluo-4 fluorescence of an individual RBC following application of −25 mmHg for the time indicated by the gray shaded area. Right: images of the RBC plotted on left at the times indicated. (**C**) Left: representative plot of background subtracted Fluo-4 fluorescence from an individual RBC when subjected to pressure pulses of different magnitudes. Pulse duration is as indicated by shaded areas on plot; magnitude of pressure in mmHg is indicated above lines. Right: pressure-response curve (mean ± SEM) generated from 8 RBCs subjected to varying pressures. Responses to each different pressure were normalized to the average of the flanking −25 mmHg pulses, and the order of each different pressure applied was randomized for each separate RBC. (**D**) Fluorescence images of Fluo-4-loaded control and Piezo1 inhibitor-treated RBCs stretched by shear in a microfluidic device. Calculated average shear stress is about 3.4 Pa. (Scale bar: 20 µm) (**E**) Average fluorescence intensity of control and Piezo1 inhibitor-treated single RBCs. The error bars are reported as the SDs of the mean (n = 3). ***P <0.001. (F) Average fluorescence intensity of control and Piezo1 inhibitor-treated RBCs (10% vol/vol) flowing before and after the constriction channel. The error bars are reported as the SDs of the mean (n = 8 and 3 for normal RBCs and treated RBCs, respectively). NS, not significant; RR, ruthenium red. *P <0.05. Figure adapted and merged from [166, 167].

activators that act on the upstream blade, in contrast to Yoda1, which acts on the downstream beam [164]. This study also demonstrated that Yoda1 potentiates poke-induced currents, unlike stretch-induced currents. Indeed, a blunt pipette is usually used to press into the membrane. There are other ways of probing mechanosensitivity. Suction, that is, negative pressure can elicit mechanosensitive currents. Shear stress, as experienced by cells in flow, stretches the membrane, as it is pulled in the direction of flow. Two Piezo structural domains are involved in mechanical and chemical transduction along the protein, called blade and beam. Production of Yoda1 analogs via chemical synthesis identified recently Dooku1 as a competitive inhibitor of Yoda1-evoked currents [165]. Nonetheless, it does not have any effect on mechanically-induced Piezo currents. Calcium can pass through Piezo1 during RBC stretching in small vessels as shown by experiments in microfluidic capillaries (**Fig. 1.7**). In addition, ATP release was observed in response to shear stress and dependent on critical extracellular calcium levels [166].

Non-Selective Voltage-Dependent Cation Channel

NSVDC is a Non-Selective Voltage-Dependent Cation Channel discovered by Halperin et al. [168]. Its molecular identity is unknown, but it has been thoroughly characterized during the last decades via several experimental approaches. It is active at positive membrane potentials. Given the strong chloride conductance setting the membrane potential at the equilibrium for chloride (Cl^-) NSVDC activation is typically achieved by diminishing the extracellular chloride concentration. Isotonic, Low Ionic Strength (LIS) extracellular solutions have been usually employed, such as sucrose solution, with the disadvantage of lowering the pH of unbuffered solutions. The so-called LIS effect was observed over a century ago when bovine RBCs were washed in sugar cane solutions and was shown in human RBCs with sucrose in 1939 [169, 170]. Enhanced conductances for Na^+ and K^+ observed in LIS conditions continued after the cells were resuspended in a solution of normal ionic strength. Importantly, this cation increase depended on Ca^{2+}. Addition of 1 mM Ca^{2+} to depolarized RBCs in a LIS solution lacking calcium caused a strong hyperpolarization, attributed to Gárdos as it could be inhibited by blockers such as carbocyanine. Ca^{2+} entered through the voltage-dependent pathway triggering Gárdos activation. NSVDC is opened at membrane potentials higher than 40 mV and is blocked by ruthenium red at low micromolar concentrations [168]. The first patch-clamp characterization using the inside-out configuration, showed complex gating and greater frequencies at high salt concentration. The channel is truly nonselective for Na^+, K^+ $NH4^+$ and Rb^+ and has a zero-current conductance of 35 pS. In addition, while it is firmly closed at membrane potentials between -20 and -30 mV, the open probability is 0.85 at 100 mV [130]. A striking realization was that the aforementioned first characterization in conditions nominally devoid of activators was likely made possible by the activating effects of nicotine on the channel brought about by contamination of utensils by smokers [171]. Subsequent experiments from non-smoking healthy donors established the channel as being of nicotinic subtype and capable of being activated by acetylcholine agonist carbachol, with desensitization at high concentration [171]. Nonetheless, NSVDC behavior differs much from cloned nicotinic acetylcholine receptors, in terms of selectivity and gating, therefore ruling out its belonging to this family [169]. It should be noted also that carbachol does not alter erythrocyte permeability in LIS solutions, suggesting the binding site could have been made accessible during the formation of inside-out patches [172]. The channel was found to display histeresis, that is, activity dependence on the previous history of the channel. If the channel was held at +100 mV and voltage reduced step-wise, the activity appeared greater than if the initial voltage was set at +20 mV and raised towards higher membrane potentials [172]. Another observation was the fact that the open probability is not close to 1 at high potentials for divalent cations as is the case with monovalent cations. Moreover, whereas inward currents of monovalent cations were only seen as tail-currents during deactivating voltage steps, rare gating events occurred for divalent cations at negative voltages [169, 172]. NSVDC is undoubtedly a major player in the cation permeability which develops when RBCs are placed in LIS solutions, despite ignoring so far its molecular nature.

There is some evidence for the presence of other cation channels in the erythrocyte plasma membrane. N-methyl-D-aspartate receptors, NDMAR, have been detected not only in erythroid progenitors, but also in mature RBCs. Copy numbers are reduced as maturation progresses, though NMDAR in mature RBCs were found to bind glycine and glutamate triggers Non Selective Cation Channel activity, with a measurable increase in calcium cytosolic levels [173]. This channel was found to be involved in SCD pathophysiology, with inhibition by memantine showing rehydration and partially preventing sickling [174]. Short Transient Receptor Potential Channel 6, TRPC6, is a Non Selective Cation Channel found at the mRNA and protein level in human

mature RBCs [133, 175].

Anion Channels

Erythrocytes count with anion channels in the plasma membrane whose primary function is to facilitate Band 3 operation. They balance chloride ions in and out of the cell so that Band 3 can move chloride depending only on P_{CO_2} and not on a chloride gradient. In this way, no energy needs to be spent in the process. Therefore, ultimately they indirectly favor gas transport and the correct operation of the Jacobs-Stewart cycle. Few anion channels have been identified at the molecular level. Cystic Fibrosis Transmembrane conductance Regulator, CFTR, was proven to be present at the plasma membrane of healthy RBCs, with a significant reduction seen in cystic fibrosis patients [176]. Although its particular function is unknown, ATP release by human RBCs was connected to their function as healthy, but not cystic fibrosis patient-derived RBCs were able to mediate ATP release [177]. Chloride channel protein 2, ClC-2, was found in mouse and human erythrocytes via immunoblots, but not in mouse knockouts [178]. Moreover, *Plasmodium* infected wild-type mice display increased whole-cell currents upon cell swelling contrary to mouse knockouts.

Anion channels revealed by malaria studies

Ion imbalance is present in a number of hematological disorders, including hereditary spherocytosis, hereditary stomatocytosis, sickle cell and infectious diseases such as malaria. Malaria infection causes an increase in membrane ion conductances, notably anionic conductances. The knowledge obtained regarding not only anion channels but Non Selective Cation channels through decades of study of *Plasmodium*-infected RBCs, and the development of the patch-clamp studies in this pathological model, notably by our laboratory, makes the topic of malaria relevant to the understanding of ion channels in both infected and uninfected RBCs.

Plasmodium spp. is the eukaryotic parasite causative of malaria. It arrives to the host via the bite of a female *Anopheles* mosquito. The propagative cycle is complex, and parasites have an initial replication cycle in the liver before they make their way into the bloodstream where they infect erythrocytes, normally one parasite per cell. Upon infection, *Plasmodium* is capable of producing the DNA, RNA and proteins necessary for 20-32 nascent parasites in only 48 hours. This remarkable metabolic rate is frenetic, up to 100 times greater than healthy RBCs [179]. Altering membrane permeability is essential to achieve it, both its own, plus the parasitophorous vacuole membrane (PVM) and the host membrane. Hence, the permeability of the plasma membrane is greatly enhanced and many varied solutes normally impermeant to the RBC membrane are, just 14 hours upon infection, able to cross. The increased permeability affects transport rates of peptides, amino acids, nucleosides, sugars, polyalcohols, small quaternary ammonium compounds, some monocarboxylates, monovalent inorganic anions and cations [180–184]. *Plasmodium* needs not only to provide for its extensive anabolic machinery but also assure fast and efficient export of hazardous metabolic end products. The acquired augmented permeability of parasitized RBCs was termed New Permeation Pathways (NPPs). NPPs display features of anion channels, although they are poorly selective and Na^+ and K^+ intracellular concentration reverse as infection progresses, thereby revealing an extensive leak or conductance for cations [184]. NPPs are inhibitable, which is strongly indicative of transporter or ion channel involvement rather than a direct modification of the lipid bilayer making it porous or leakier. Classical anion channel inhibitors NPPB (5-Nitro-2-(3-phenylpropylamino)benzoic acid), furosemide, niflumic acid glibenclamide and several quaternary ammonium compounds inhibit NPPs [181, 185–187]. First evidence of ion channels taking part in the permeability in-

crease postinfection came from patch-clamp studies. RBCs infected with *Plasmodium falciparum* trophozoites have a whole-cell anionic current 150 times greater than what is observed in uninfected RBCs. An inwardly rectifying anion channel of less than 10 pS of conductance was compatible with the observation assuming 1000 channels per cell. Moreover, the selectivity was shown to be shifted to anions, albeit cations can cross, and the channels were blockable by typical NPPs inhibitors such as NPPB, glibenclamide or furosemide. A search for putative membrane transporters on the *Plasmodium falciparum* annotated genome identified about one hundred such proteins based on hydropathy scores and thus the likeliness of having transmembrane domains and being exported to the membrane. However, only a few were thought to be putative channels and, critically, no homologs of known eukaryotic anion channels were found [188, 189]. In spite of this, CLAG3, a *Plasmodium* protein lacking several transmembrane domains (featured by almost all channels known), was found to form homoligomers enabling membrane integration and nutrient transport [190]. Whether CLAG3 forms alone the so-called Plasmodial Surface Anion Channel (PSAC) or complexes along with other proteins to form it is not yet clarified [191]. A poorly-selective anion channel observed in malaria-infected red cells is of host origin and up-regulated by the parasite, via phosphorylation or oxidation [192, 193].

VDAC Using the cell-attached configuration of patch-clamp, a maxi-anion channel was identified in RBCs. It is dormant in uninfected cells but opens upon exposure to serum. It shows multiple conductance levels, with very complex kinetics and gating properties. Several reports on small conductance anion channels match this channel's behavior under different conductance modes. It has been identified at the molecular level as the channel complex PBR/VDAC (Peripheral type Benzodiazepine Receptor/Voltage-Dependent Anion Channel). VDAC was originally discovered in mitochondria, but it is present in the plasma membrane alone or as member of the PBR complex. The PBR complex comprises at least three protein partners: Translocator Protein (TSPO), Adenosine Nucleotide Transporter (ANT) and VDAC. The complex is sensitive to benzodiazepine ligands Ro5-4864, PK11195 and diazepam with *Plasmodium* half growth inhibition being 1-10 times that of NPPB indicating a strong link between NPPs, parasite survival and PBR complex, which was validated by sorbitol lysis assessment [194]. An estimated number of 100-150 PBR complexes per red cell lends support to the hypothesis this pathway mediates the large anion conductance observed upon Gárdos activation, ultimately responsible for severe dehydration as it is within the same copy number range as Gárdos. Strictly speaking, VDAC is not an ion channel, but a member of the β-barrel pore family. Data gathered from studies on cancerization cellular processes in mitochondria suggests that the pore's closed state behaves like a cation channel [195]. This configuration, which depends on the oligomeric protein assembly, represents another putative route for cation leak at the RBC membrane and may reconcile the observation that the increase in anion, O^2 and cation permeabilities upon infection is susceptible to the same inhibitors than for uncharged solute permeabilities.

Cation imbalance

Erythrocytes must maintain a delicate ion balance lest their most important function, gas transport, be jeopardized. As previously mentioned the pump-leak equilibrium, that is, the coupling of cation leak with active pumping by ATPases ensures a stable volume and, thus, surface-volume ratio critical to RBC rheological properties. In addition, calcium inward leak must be especially kept in check as a failure to do so entails a severe loss of homeostasis through channels (such as Gárdos) and calcium-dependent processes which impact flexible cytoskeleton configuration leading to microvesiculation and loss of surface/volume ratio and the essential

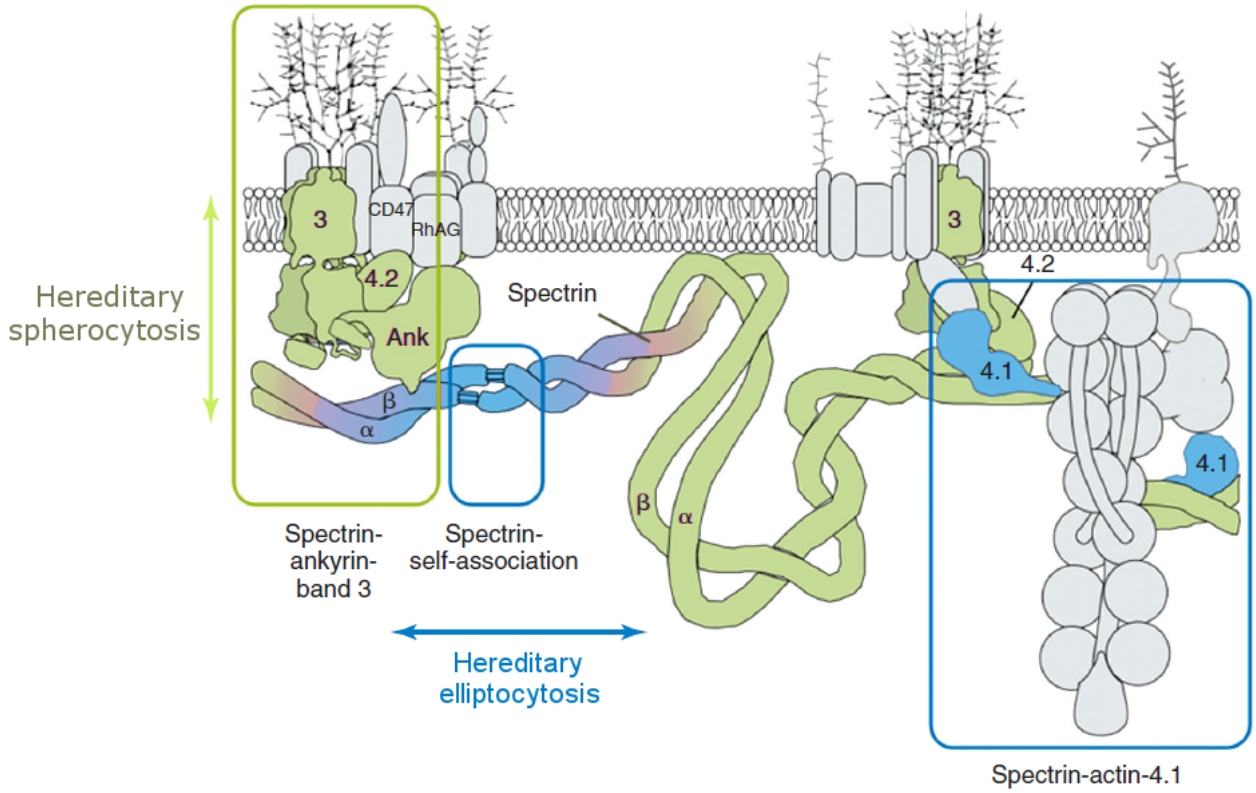

Figure 1.8: Structural proteins affected by mutations causing Hereditary Spherocytosis and Elliptocytosis.
Schematic showing membrane transporters and spectrin implicated in Hereditary Spherocytosis (so-called vertical interactions) and Hereditary Elliptocytosis (horizontal interactions).

discocytic morphology required to traverse through the microvasculature. Cation leak decreases as a function of temperature in healthy RBCs up to 8 °C, while fluxes increase if temperature is further reduced towards 0 °C. The leak was determined as $^{86}Rb^+$ influx in conditions where the Na^+/K^+ pump and NKCC were inhibited [196, 197]. Moreover, temperature dependence is different in several hematological disorders, not only in cryohydrocytosis where it is markedly altered at low temperature, but in all stomatocytoses with data fitting widely distinct functions [198]. Loss of the cationic steady-state has been reported since the earliest descriptions of anemia and since thought to contribute to the early demise of circulating mature RBCs. Many anemic disorders are hereditary in nature and mutations were found in proteins fundamental to the cellular physiology of RBCs. Well-known disorder classes where cation imbalance is found include hereditary spherocytosis (HS), hereditary elliptocytosis (HE) and hereditary stomatocytosis (HSt). Na^+ inward leak is mildly enhanced in HE RBCs, increasing ATP consumption by the pumps risking a catastrophic failure as erythrocytes age and Gárdos activates as consequence of unchallenged calcium influx into the cells [20, 199].

Hereditary stomatocytoses are disorders thus named due to stomatocytes tending to be the predominant abnormal morphology in RBC smears. Several membrane proteins are known to cause HSt if mutated. Mutations in Band 3 cause a wide range of different hematological disorders such as forms of HE and forms of HSt such as cryohydrocytosis (CHC). CHC has the particularity that affected erythrocytes display a huge leak at cold temperature. However basal leak is also enhanced at normal body temperature. These mutant Band 3 are unable to perform anion exchange. The hypothesis that mutated Band 3 mediates aberrant cation flux stems from the fact that CHC mutations fall in the transport domains of band 3 and experiments in transfected *Xenopus* oocytes recapitulate cation leak, which is sensitive to band 3 inhibitors [200]. Many other rare HSt variants have been

reported with disparate temperature dependencies and impact on anion exchange capabilities. Whereas Band 3-related HSt are relatively mild, overhydrated hereditary stomatocytosis (OHSt) increases the cation permeability of RBCs in affected patients up to 40 times greater than normal values and is linked to mutations in Rh-associated glycoprotein (RhAG). *In silico* predictions of the impact of the most common mutation, F65S, point to a widening of the transport channel, which normally carries ammonium or CO_2, so that it behaves as a non selective pore [89, 201]. Glycolysis rate is increased in OHSt individuals, presumably from high ATP demand by pumps, though an involvement of oxidation pathways has also been identified [202].

Southeast Asian Ovalocytosis (SAO) is also caused by Band 3 mutation, specifically a multi amino acid deletion which results in protein misfolding and loss of anion exchange function [203, 204]. Affected erythrocytes have been shown to display a cation leak at low temperature identical to that of CHC [205, 206]. However, at body temperature, aside from abnormal ovalocytic morphology, SAO RBCs are normal and patients have no anemia, with mild anemia seen in infants and rare cases [20]. Another mild, nearly asymptomatic condition is familial pseudohyperkalemia (FP) linked to ABCB6 and Piezo1 mutations [207, 208]. Cation leakage is only slightly above normal at 37 °C, but increases at cold temperature with leak rate and temperature threshold depending on specific FP-causing mutations.

Thalassemia patients show aberrant cation fluxes and akin sickle cell disease, mutations or deficiency in hemoglobin can dramatically alter membrane properties via complex pathophysiological mechanisms. Mutations in erythrocyte ion channels are causative of anemia. These disorders have been classified as HSt or Hereditary Xerocytosis (HX) with mutations in Gárdos and Piezo1 Detailed pathophysiology is discussed in Chapter 4 on page 95.

Sickle Cell Disease has a staggeringly complex pathophysiology and a cation permeability (called P_{sickle}) is increased through a pathway consistent with Non Selective Cation channel activity. Although the hemoglobin mutation affects this putative cation channel rather indirectly, its involvement in the positive-feedback loop leading to irreversibly sickle cells underscores how critical is for red cell to keep their cation balance and point to possible roles for NSCs in health. See page page 50 for an overview on P_{sickle}. Cation imbalance is not caused only by genetic disorders. Infectious diseases, such as malaria, display a loss of ion homeostasis. Though beneficial for the parasite, the alteration in membrane permeabilities spawned extensive research (importantly on ion channels through patch-clamp recordings), which has deepened our understanding not only of malaria pathophysiology but of endogenous RBCs ion channels.

RBCs nearing the end of their lifespan have altered cation composition due to enhanced leak fluxes. There is an ongoing imbalance in cation content that worsens throughout the life of RBCs, with progressive increase in cell density. Does the leak rate increase due to a mere metabolic failure in cells where proteins cannot be restored or is the enhanced *leak* an opening of a cation pathway with a physiological senescence function? Does it hasten removal of RBCs with subpar performance? Cation permeability is heavily altered in stored RBCs, such as those intended for transfusion. Storage conditions have been improved over the last decades allowing long-term storage of RBCs, yet the ion steady-state is soon lost and degrades during storage impacting efficiency and erythrocyte survivability. Senescence and the storage lesion is discussed in detail in page 51.

P_{sickle} — A NSC channel?

P_{sickle} is the term used for the increase in cation conductance observed in sickled RBCs. Tosteson and colleagues first described this phenomenon in 1952, reporting that erythrocytes from SCD patients gained Na^+ and lost K^+ upon deoxygenation [209]. Cation exchange could be reversed by reoxygenation and was prevented by carbon monoxide, which precludes sickling, even if oxygen was lacking.

KCC activity is low when the partial pressure of oxygen is also low, whereas sickle cells exhibit elevated activities for both KCC and P_{sickle} [68]. KCC is only active in very young cells in healthy individuals becoming dormant in fully matured RBCs [210, 211]. Both KCC and P_{sickle} are activated by oxidants. Sickle cells are on average younger than RBCs from healthy subjects, as their lifespan is severely reduced to about 20 days compared to 120 days of normal erythrocytes. Moreover, erythropoiesis, which becomes overactive in order to cope with the anemia, may produce RBCs with abnormal permeabilities in SCD [68, 212]. Sickle hemoglobin (HbS) polymerization activates P_{sickle} because sickling inhibitors abrogate P_{sickle} [213]. Well-known sickling inhibitors are a substituted benzaldehyde known as 12C79, which augments HbS oxygen affinity, and dimethyl adipimidate (DMA), which crosslinks hemoglobin lysines [214, 215]. Irreversibly sickle cells (ISC) are very dense, markedly dehydrated erythrocytes found in SCD patients, with severely impaired rheological properties. They began as sickle cell which underwent HbS polymerization due to oxygenation, activating P_{sickle}. Potassium efflux and sodium and calcium influx follows. Calcium activates, in turn, Gárdos, leading to marked K^+ exit and a change to negative membrane potentials, which favors concomitant Cl^- exit and, thus, water loss. Cytosolic pH becomes acidic due to outward flow of chloride, which disturbs the Jacobs-Steward cycle. Low pH stimulates KCC bringing about more KCl exit, dehydration and acidification in a positive feedback loop. Contrary to Psickle, KCC works in both oxygenated and deoxygenated conditions, with activation levels depending on KCC reticulocyte expression [216]. Irreversibly sickle cells can trigger a thrombotic event as they attempt to pass through a capillary. They were originally thought to correspond to the oldest fraction of the erythrocyte population in SCD patients, given that RBCs become naturally denser as they age. Despite this intuitive notion, reticulocytes were proven to turn into irreversibly sickled cells in as little as 4-7 days, being quickly removed from the bloodstream [216, 217]. Reticulocytes have higher transporter activity levels than RBCs.

Elevated intracellular calcium concentrations have been shown to lead to protein crosslinking, through the action of transglutaminase, contributing to irreversibly sickle cells' demise [218]. In addition, P_{sickle} is sensitive to DIDS and other stilbenes, which has prompted the association of P_{sickle} with a modified channel-like Band 3, although this hypothesis has not been validated [219, 220]. In contrast, patch-clamp recordings in whole-cell configuration have proven P_{sickle} to be inhibited partially by o-vanillin and GsMTx4 [221]. GsMTx4 is an inhibitor of MS NSC channels, including Piezo1, whereas the blocking effects of antisickling agent orthovanillin are expected given the requirement of sickling to trigger P_{sickle} opening. So either GsMTx4 is blocking P_{sickle} due to weakly specific inhibition of a related NSC channel or Piezo1 is P_{sickle} in those conditions. P_{sickle} shares with Piezo1, permeability to both monovalent (Na^+ and K^+) and divalent (Mg^{2+} and Ca^{2+}) cations, a feature of a Non Selective Cation channel. Gd^{3+} has been reported to inhibit P_{sickle} and even though it is a fairly unspecific NSC blocker, it had inhibitory effects at low concentrations ($IC_{50} = 2\mu M$) [222]. Yet another known P_{sickle} inhibitor is dipyridamole which is currently used in the clinic as adjuvant to prevent thrombosis [223]. It has anticoagulant and vasodilator properties. It has showed promise in clinical trials halving the number

of vaso-occlusive crisis in combination with acetylsalicylic acid [224]. It only blocks partially P_{sickle} but it displays additional inhibitory effects on the rate-limiting anion conductance responsible for marked dehydration upon Gárdos activation [223]. Despite studying P_{sickle} for decades the scientific community has not found the molecular nature of the cation pathway and even though a Non Selective Cation channel is the primary suspect, the puzzling pharmaca observed needs to be addressed.

Red blood cell aging and the storage lesion

Red blood cells have evolved an antioxidant system to hold off oxidation. The main system providing reducing power is the pentose phosphate pathway which yields NADPH keeping high concentrations of glutathione (GSH) in its reduced form. Should oxidized forms, such as glutathione-disulfide, become greater than glutathione levels, an ATP-fueled pathway takes it out of the cell. New GSH is produced to maintain a predominantly reducing redox ratio. Thus, GSH prevents the harmful effects of hydrogen peroxide and superoxide anions, which can oxidize cysteines in proteins producing aberrant conformations or crosslinking resulting in protein loss [225]. Even though protein oxidation plays a role in cell aging it cannot be its sole explanation as RBC removal is tightly regulated and nonrandom.

RBC lifespan Red cell lifespan has been studied since the early 20th century, with Ashby studies on differential agglutination and removal of transfused cells [226, 227]. First estimates covered a wide range, though in a couple of decades an improvement of the agglutination method led to an estimation of a mean 120 days for an erythrocyte's life in circulation [228]. Another technique yielding about 127 days red cell lifespan was labeling heme by providing nitrogen-15 glycine which is readily incorporated into heme after oral consumption and its disappearance can be followed, as heme is not reused but destroyed and made continuously [229]. A similar estimation is obtained by using carbon 14 [230, 231]. Radioisotopes have been extensively used too to determine red cell lifespan. Chromium was found to be present in both erythrocytes and plasma and radioactive chromium-51, especially in $^{51}CrC1_3$ form rather than in hexavalent form, binds to globins, including hemoglobin. Thus, a method was devised for lifespan determination in spite of the fact that chromium elutes from red cells, as this was thought to be able to be factored in [232, 233]. However, the elution rate is highly variable, so much (up to twofold range) as for the technique to be called "fundamentally flawed" [234]. Nevertheless, this technique was standardized in 1971 for survival studies and since widely performed in the clinical setting, i.e. measuring cell recovery after transfusion [235, 236].

Radioiron can be used as a tracer for red cell studies of iron metabolism and erythropoiesis as the radioactive decay can be follow as the isotope is taken for red blood cell production [237]. In as little as a day, intravenously injected radioiron is used for hemoglobin synthesis in the bone marrow [238]. Contrary to heme, iron itself is reused to meet the continuous requirement by erythropoiesis which would lead to the conclusion that radioiron is not suitable for red cell lifespan studies. However, by injecting very small doses of radioiron with high specific radioactivity in patients with increased iron excess or by stable iron injection in animals, the reuse rate can be minimized [238, 239]. Its use in human subjects is indeed highly questionable from an ethical point of view given the long half-life and long residence time of iron in the body. Another ingenious way of determining red blood cell survival is the measurement of endogenous carbon monoxide (CO) exhaled through the lungs. Endogenous CO production is intrinsically linked to red blood cell metabolism as it arises from the cleavage of α -methene bond of heme following red blood cell removal and breakdown. Thus, in healthy

individuals the rate of CO production matches that of erythrocyte destruction and is constant [240, 241]. Biotin is a widely used label that has the advantage of being nonradioactive and allows for enrichment of biotinylated cells therefore old cells may be sorted by this technique. A study with rabbits showed no difference in cell survival between carbon-14 and biotin labeling [242]. In humans a biotinylation method has been described that enables RBC survival studies with very small blood volumes and, owing to the use of multiple biotin densities, several measurements can be performed in the same individual. The original fractions are easily tracked by flow cytometry. These advantages are especially suitable in vulnerable subjects, such as children or pregnant women. In addition, reticulocyte counts are an indirect measure of erythropoietic activity and high proportions in blood indicate very low RBC survival [234].

Nonrandom removal of senescent erythrocytes Splenic red pulp macrophages participate in red cell clearance, though the fact that red cell lifespan is barely affected in splenectomized subjects indicates that the spleen is not necessary for RBC nonrandom removal [243]. It is indeed critical for removal of poorly deformable cells as thrombosis is a major complication of splenectomy. Since early experiments with iron-59 it was found that centrifuged erythrocytes separate in a gradient according to age, as younger erythrocyte were found in the top fraction and old erythrocytes in the bottom fraction [244]. This indicates that density increases with age. Dehydration due to ion efflux (mainly K^+ and Cl^-) must be the main mechanism behind this observation [225, 245]. Although the hemoglobin concentration was thought to stay constant throughout the life of the cell [245], hemoglobin-containing vesicles have been detected, with a preponderance in old cell fraction [246]. Traversal of the splenic slits may be responsible for the enhanced vesiculation observed because the decrease in Hb is not seen in splenectomized subjects [246]. Hemoglobin-spectrin crosslinking, lipid peroxidation, methemoglobin, hemichromes and elevated GSSH levels were detected in old RBCs and are characteristic of oxidative damage, validating the intuitive notion that oxidative stress is a major driver of RBC aging. All these changes decrease erythrocyte deformability which would at least increase spleen passage time as an increase in internal viscosity by itself is expected to increase the probability of contact with macrophages [247]. Even though there is a strong correlation of density and red cell age, an old cell subpopulation was found that had elevated Na^+ levels and was, thus, rehydrated and less dense [248]. Care should be taken in considering the densest cells as the oldest, because the possibility remains that very old cells prior to removal may rehydrate due to reversal of Na^+/K^+ gradients [249]. An increase in Na^+ permeability was linked to Ca^{2+} and shrinkage [250]. Ca^{2+} pump activity decreases with age so that intracellular calcium levels rise and Gárdos activates, however Na^+ influx exceeds K^+ in the oldest RBCs. This emerging Na^+ permeability with cell age was termed P_{cat} and its properties are compatible with a Non Selective Cation channel [251]. Its activity would be predominant in the final stages of cell senescence prior to removal.

Many markers and correlations have been described for RBC aging: density, PMCA activity loss, protein 4.1b/a ratio or hemoglobin glycation [244, 251, 252] . Yet, what are the mechanisms promoting destruction of red cells by macrophages? Enhanced phagocytosis was found to occur when RBCs were incubated with autologous immunoglobulins, specifically IgG. If cells were fractioned by density, phagocytosis occurred preferentially with minimal phagocytosis of young cells. This proved the role of autoantibodies on aged red cell removal. Early experiments showed that exposed glycoproteins in which sialic acid has been lost could be a target of autoantibodies [253–255]. Most plasma glycoproteins disappear from the circulation if sialic acid is

removed [256]. The work of Kay brought the identification of two small regions of Band3 as the senescent antigens that could be recognized by autologous IgG, thus linking senescence and Band3 autoantibodies [257]. Peptides targeting these regions abolish IgG binding to RBCs dose-dependently [258].

A proposed model for erythrocyte removal has been proposed [259] by which the antigenic region 812-830 of Band 3 can flip from the intracellular to the extracellular side of the membrane by a rare conformational event. This would induce anti-Band 3 antibody binding. These bivalent IgGs would promote clustering of Band 3. Oxidation would increase the levels of hemichromes, which bind to Band 3 and induce its clustering. These bound complexes are inactive, thereby reducing both oxygen-carrying capacity and anion exchange. Combined hemichrome- and IgG-induced clusters would expose large targets for macrophage recognition along with complement (C3d) opsonization [260]. The fact that hemoglobin can more easily bind to the membrane as its iron's oxidation state increases [261] shows that oxidative stress is likely essential in the clustering process of Band 3. Loss of sialic acid may enhance opsonization by complement and antibodies and together with shrinkage towards the end of the lifespan would ensure contact and recognition by macrophages.

Finally, it was reported that phosphatidylserine (PS) is increased on the outer leaflet of old cell membranes, a common marker for cell removal, and which would increase during aging to promote senescent RBC removal from the circulation [262]. Despite many reports on this subject for the last 15 years its importance on RBC physiology is still under debate. A report found no such increase in PS despite a reduction in aminophospholipid translocase activity in aged cells although the authors found a loss of membrane phospholipid asymmetry [263]. Moreover, homozygous thalassemia and sickle cell disease patients are afflicted with chronic severe thromboembolism as a consequence of extensive phosphatidylserine exposure by their RBCs. Therefore, how could have senescent RBC phagocytosis been evolved to rely on such a potent thrombogenic stimulus [264]?

The storage lesion and its parallelisms with RBC aging It has long been known that a proportion of transfused RBCs disappear from the circulation within one day of injection [226], owing to aforementioned methods for measuring RBC survival: radioiron, biotinylation and mainly, radiochromium, have been used for post-transfusion determination. In fact, FDA regulations require that no less than 75% of transfused cells remain after the intervention. This was revised in 2004 to allow 3 in 24 or 2 in 20 healthy subjects to have recoveries below 75% to account for natural variation [265]. European regulations likewise require that storage duration should ensure 75% recovery 24 hours post-transfusion, although only hemolysis is systematically controlled [266]. It shall not exceed 0.8% of red cell mass in 90% of units tested. This finding highlights the underlying storage lesions which render RBCs more fragile. A depletion in glucose and adenine during storage leads to failure to sustain glycolysis and provide ATP for other processes, such as NADPH production and antioxidant enzymes. In an oxygenated environment such a PVC bag, oxidation entails of both proteins and lipids. Lack of surrounding plasma proteins, including notably albumin, promotes microvesiculation, leading to a loss of surface-ratio and discocyte morphology. Cation cytosolic levels are altered and if stored for more than three weeks, erythrocytes dehydrate. An unexpected ally in RBC preservation is diethylhexyl phthalate (DEHP). It was observed that polyvinyl chloride (PVC) bags, commonly used to store RBCs since mid-20th century due to mechanical and manufacturing advantages, were leaching DEHP, the plasticizer used to polymerize PVC. Interestingly, rather than having a toxic effect on cells, DEHP was shown to stabilize RBCs membranes and lengthen the storage time of RBCs [267, 268]. Several RBCs parameters improve in the presence of DEHP such as osmotic fragility, hemolysis, vesiculation and morphology [267, 269] ATP and 2,3-DPG concentration stay

unaltered. These finding have turned PVC bags into a virtual requirement for long term storage of erythrocytes.

Senescent cells present several characteristics: i) K^+ and water efflux, ii) oxidation of proteins and lipids, iii) autoantibodies against aggregated Band3, iv) opsonization of old RBCs by complement and, in common with accelerated aging in transfusion bags: v) decline in enzymatic activity, vi) loss of surface area by microvesiculation and vii) reversal of the Na^+/K^+ ratio. These alterations are very similar to the storage lesion and it has sometimes thought of as an accelerated *in vitro* aging. However, in senescence the immune system is involved, as there is loss of *self*, accounting for nonrandom removal. The process is not fully elucidated. In transfusion practice, immune cells are obviously avoided to prevent serious adverse reactions. Leukoreduction, i.e. filtering blood to remove leukocytes, is routinely performed in developed countries to ensure depletion of granulocytes and lymphocytes. If there is leukoreduction, leukocytes cannot exceed five million per unit [266]. For Buffy-Coat-Removed Red cell Units no more than 1.2×10^9 leukocytes must remain.

Therefore senescence and storage injures feature metabolic failure, cellular oxidation and cation imbalance.

Thesis objectives

In spite of extensive research carried out for decades on RBCs transport pathways the nature and origin of leak pathways has not been elucidated. Most passive transporters and ion channel are silent in resting conditions raising the question of what role they play in erythrocyte physiology. Ion channel activity was considered negligible owing to low whole-cell currents displayed by RBCs, smaller than 50 pA in resting conditions. However, ion channels dramatically alter cellular dynamics in both genetic and infectious diseases and evidence points to their involvement in senescence. RBCs possess a high anion conductance orders of magnitude above the cation conductance. Nonetheless, increases in cation permeability affects cell volume, cell energy consumption and cytoskeletal organization, among other cellular processes. Untimely or abnormally frequent ion channel openings can lead to hemolysis or impaired cellular functions and removal by macrophages. Knowledge of cation channel activity, especially by Non-Selective Cation Channels, is lacking despite their prominent role in pathophysiology. Furthermore, cation imbalance is known to occur in cell senescence and red cell concentrate storage, but whether it is a consequence of ion channel activity has not been yet clarified. Consequently, I set the following objectives:

First Determine a pharmacological approach facilitating the study of Non-Selective Cation channel activity via its impact on the membrane potential.

The study of cation channels in RBCs is hindered by the massive chloride conductance which renders invisible the effect of ion channel activity on the membrane potential, except for the powerful Gárdos channel. A typical approach to circumvent this problem is by using chloride conductance inhibitors. Many exist, such as DIDS, NPPB or NS1652. NS3623 is the most efficient inhibitor known to date and hence it was thoroughly studied. In addition, cation conductances other than Gárdos have only been observed via membrane potential estimation RBCs are depolarized, that is, their membrane potential is positive. I devised a experimental strategy to study cationic conductances and notably, Non Selective Cation channels, in hyperpolarizing conditions.

Second Develop procedures enabling the functional study of ion channel activity in RBCs derived from patients with mutations in Gárdos and Piezo1.

Most hereditary anemias affect RBCs structural proteins with tens of Band 3 and spectrin mutations described to date. They were classically diagnosed via morphological inspection of abnormal RBCs in blood smears, complemented with hematological parameters such as hemoglobin blood values. Although red cell cation imbalance is present in some of these disorders, the advent of inexpensive next-generation sequencing shifted the scientific community's attention to genetics. Finding the exact Single Nucleotide Polymorphism (SNP) within a gene is unequivocal for diagnosis, especially with morphological and hematological data. Thus, knowledge on ion channels involvement in hereditary anemias is scant. Shortly after the discovery of Piezo1, mutations were uncovered affecting the erythroid lineage, including matured RBCs and cause disease. Examination of Gárdos gene, *KCNN4*, brought also to light missense mutations causing hemolytic anemia. These patients were previously diagnosed with rare anemia of unknown origin. Excessive activity of these ion channels leads to hemolysis. Even though studies have been carried out via patch-clamp, most address mutant channel activity heterologously expressed in

cell line, so that insight is lacking on the actual behavior of RBCs with the mutant channels at their membranes, that is, on patients cells. I aimed to study ion channel activity from RBCs derived from patients samples sent by collaborating laboratories, devising the required protocols suitable for each mutation and allowing discrimination of healthy and pathological RBCs.

Third Assess ion channel activity throughout 42-day storage of Red Blood Cell Concentrates intended for transfusion.

Ion channel activity is unknown in the context of the storage lesion, the set of cellular alterations known to develop when RBCs destined for transfusion are placed in CPD-SAGM and stored for a maximum of 42 days at 4 °C. These storage conditions are the only authorized in most of the European Union for Red Blood Cell Concentrate (RBCC). Six weeks was chosen as a limit upon the knowledge that RBCs increasingly deteriorate at the metabolic and morphological level over the storage duration. Among storage solutions developed over the years, CPD-SAGM was mainly adopted due to being inexpensive and because it prevents substantial hemolysis from taking place in the bag, with a maximum of 0.8% being authorized. Ion channel activity directly affects ion distribution, including notably calcium, which in turn affects cell volume and, thus, morphology. Hence, information is needed to account for the impact of ion channel activity in the storage lesion for an eventual development of improved storage procedures allowing longer storage periods and improved cell survivability and function, which may reduce the frequency of transfusion in patients requiring chronic transfusions.

Recording membrane potential changes

Chapter 2

Preliminary notes: Recording membrane potential changes

In science men have discovered an activity of the very highest value in which they are no longer, as in art, dependent for progress upon the appearance of continually greater genius, for in science the successors stand upon the shoulders of the predecessors; where one man of supreme genius has invented a method, a thousand lesser men can apply it.

Bertrand Russell

Monitoring the membrane potential of human RBCs in real time

Membrane potential estimation is central to this thesis, ergo a detailed explanation of the technique and the electrophysiological rationale behind it is warranted. Materials and methods are found within each chapter.

Ion channel are electrogenic so that their opening entails a dynamic change of the membrane potential (V_M) until their closure. The membrane potential is the separation of charges, ions, across an insulator, the lipid bilayer and refers to the voltage between the extracellular medium and the cytosol. Voltages, by convention, refer to the inside with respect to the outside. Hence the potential or voltage can be described by the Ohm law:

$$I = \frac{V}{R} \qquad G = \frac{1}{R} \qquad I = GV \tag{Eq. 2.1}$$

An ion is considered at equilibrium regardless its relative concentrations at either side of the membrane if the free energy variation (ΔG) is zero.

$$\Delta G = RT \ln \frac{[ion]_i}{[ion]_o} + zF(E_i - E_0) \tag{Eq. 2.2}$$

Thus, the potential at which an ion is at equilibrium, $E_i - E_0$ is defined at:

$$(E_i - E_0) = E_{ion} = -\frac{RT}{zF} \ln \frac{[ion]_i}{[ion]_o} \tag{Eq. 2.3}$$

The potential of ions asymmetrically distributed across a membrane depends on their concentrations and is termed equilibrium or Nernst potential (E_{ion}).

$$E_{ion} = -\frac{RT}{zF} \ln \frac{[ion]_i}{[ion]_o} \tag{Eq. 2.4}$$

Symbols: R is the ideal gas constant, T the absolute temperature, z the ion charge, F the Faraday constant, G_{ion} the respective ion conductance, [ion], the ion concentration, with *i* being inside or *o* being outside the cell and ΔG is the free energy.

$$I_{ion} = G_{ion}(V_M - E_{ion}) \tag{Eq. 2.5}$$

Where V_M is the membrane potential difference called henceforth, for simplicity, membrane potential. Hence the electrical current of moving ions depends on their concentrations across the membrane. If the membrane potential matches the ion equilibrium potential, there is no net ion movement and current is zero.

As a result, the membrane potential is a contribution of the equilibrium potentials, which depend on electrochemical gradients, and the conductance for every ion, given by leak permeability and/or ion channels. It is given by Goldman-Hodgkin-Katz equation:

$$V_M = -\frac{RT}{zF}\ln\frac{G_{K^+}[K^+]_o + G_{Na^+}[Na^+]_o + G_{Cl^-}[Cl^-]_i + G_{Ca^{2+}}[Ca^2+]_o + G_{Mg^{2+}}[Mg^2+]_o}{G_{K^+}[K^+]_i + G_{Na^+}[Na^+]_i + G_{Cl^-}[Cl^-]_o + G_{Ca^{2+}}[Ca^2+]_i + G_{Mg^{2+}}[Mg^2+]_i} \quad \text{(Eq. 2.6)}$$

At the resting state in RBCs:

$$G_{Cl^-} \gg G_{K^+} = G_{Na^+} \gg G_{Ca^{2+}} \gg G_{Mg^{2+}} \text{ then:}$$

$$V_M = -\frac{RT}{zF}\ln\frac{G_{Cl^-}[Cl^-]_i}{G_{Cl^-}[Cl^-]_o} \quad \text{(Eq. 2.7)}$$

G_{Cl^-} is constant. The excess of negative charges inside cells (proteins are overall negatively charged) pushes chloride ions out of the cell until they reach an equilibrium dictated by the membrane potential. Contrary to most other cell types, however, erythrocytes have an anion exchanger, Band 3, at the erythrocyte membrane, so chloride is exchanged by bicarbonate electroneutrally, thus raising intracellular chloride levels compared to cell types with very negative membrane potentials. Anion channels ensure chloride equilibrium so that Band 3 can operate without energy expenditure. As a result and given that cationic conductances are negligible in the resting state, the membrane potential is – 10 mV in RBCs.

$$V_{M^{rest}} \simeq E_{Cl^-} = -10mV$$

If a potassium channel opens, for instance, such as Gárdos:

$$G_{K^+} > G_{Cl^-} \gg G_{Na^+} \gg G_{Ca^{2+}} \gg G_{Mg^{2+}} \text{ then:}$$

$$V_M = \frac{RT}{F}\ln\frac{G_{K^+}[K^+]_o + G_{Cl^-}[Cl^-]_i}{G_{K^+}[K^+]_i + G_{Cl^-}[Cl^-]_o} \quad \text{(Eq. 2.8)}$$

V_M will change over time towards E_{K^+} until the dissipation of the driving force.

There are four approaches for membrane potential determination.

i Microelectrode cell impalement.

ii Fluorescent dyes sensitive to the membrane potential.

iii Patch-clamp in current clamp mode.

iv CCCP method.

Intracellular measurements via an electrode have been widely performed in *Amphiuma spp.* RBCs owing to their large size, but the technique is not amenable to human RBCs small dimensions.

Fluorescent dyes such as 3,3'-dihexyl-2,2'-oxacarbocyanine allow the determination of human RBCs as the fluorescence intensity varies according to the membrane potential [102]. However it has serious shortcomings:

it increases inward leaks for Na^+ and K^+ and it is toxic to RBCs which leads to lysis at longer exposures. Classically, membrane potentials could be estimated from Cl^- distribution, but it is only valid when RBCs are at the resting state and this approach could not be used when the K^+ permeability, for instance, was increased.

Patch-clamp can be used not only to record ion channel or cell current upon a fixed voltage, but by the reverse, setting a fixed current in order to record the membrane potential, what is called current clamp. Membrane potential measurements recorded in this way are however limited by the access resistance as whole-cell configuration must be reached for these recordings.

Macey, Adorante, and Orme [270] described in 1978 a simple technique where membrane potentials are determined according to the distribution of protons, which are also at equilibrium. The method is based on the unique features of red blood cells that contain very high amounts of hemoglobin, which happens to be an excellent buffer. Thereby, if the extracellular solution is left unbuffered, a RBC suspension will buffer pH to about 7.2 in a matter of seconds! As there is an inward driving force for H^+, which are positively charged, their equilibration reflects the membrane potential. If H^+ equilibration and, thus, H^+ conductance is raised, the technique allows for the determination of fast changes in membrane potential, such as those entailed by a channel opening. This is achieved by the use of small concentrations of H^+ ionophores, such as CCCP, which increase the permeability to H^+ by orders of magnitude. Therefore, by following extracellular changes in pH of unbuffered medium the membrane potential of a RBC population can be determined (**Fig. 2.1**).

$$V_M = \frac{RT}{F} \ln \frac{[H^+]_o}{[H^+]_i} = 2.303 \frac{RT}{F} (pH_i - pH_o) \qquad \text{(Eq. 2.9)}$$

As the cytoplasm is buffered, pH_i can be assumed to be constant. Lysing a red cell suspension at the end of an experiment with a detergent removes all plasma membranes hence $V_M = 0mV$, and $pH_i = pH_o$ so pH_i when $V_M = 0mV$ can be obtained from this final measurement of the lysed RBC suspension. This calibration, $pH_i = pH_{lysate} = pH_{V_M=0}$, is then used to determine V_M for the duration of the experiment (**Fig. 2.2**) [124].
Calculating the constants, at 37 °C, the membrane potential is obtained by the simple equation:

$$V_M = -61.51(pH_o - pH_{V_M=0}) \qquad \text{(Eq. 2.10)}$$

The CCCP method is possible on red blood cells due to the H^+ distribution being at equilibrium and the lack of organelles, especially mitochondria, which often maintain considerable H^+ gradients. In addition, the cytoplasm is filled with hemoglobin, with a huge buffering capacity. If the medium was heavily buffered, then the intracellular pH would change rather than the extracellular pH. The latter is far easier to measure and requires only fast, responsive electrodes. Moreover, the relationship between the membrane potential and pH_o is kept accurate to very low hematocrits, as low as 3%.

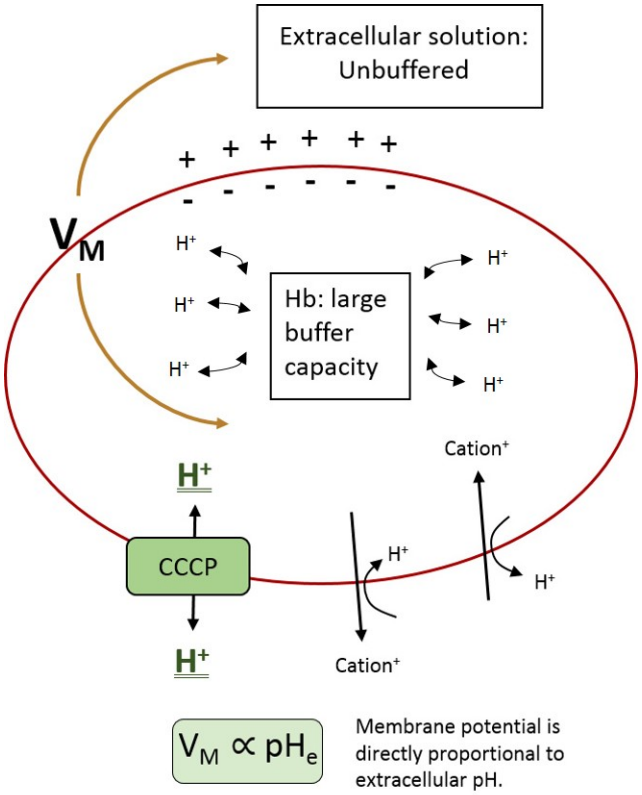

Figure 2.1: Drawing showing the principle of membrane potential determination via use of protonophore CCCP. Schematic showing H^+ movements being linked to cation movements due to the effect on the membrane potential. Cations leaving an erythrocyte leads to a more negative membrane potential, favoring H^+ uptake to balance the charge. Almost instantaneous equilibration of H^+ is achieved with proton ionophore CCCP. As the extracellular solution is left unbuffered, the membrane potential is directly proportional to the extracellular pH and can be measured with a pH meter.

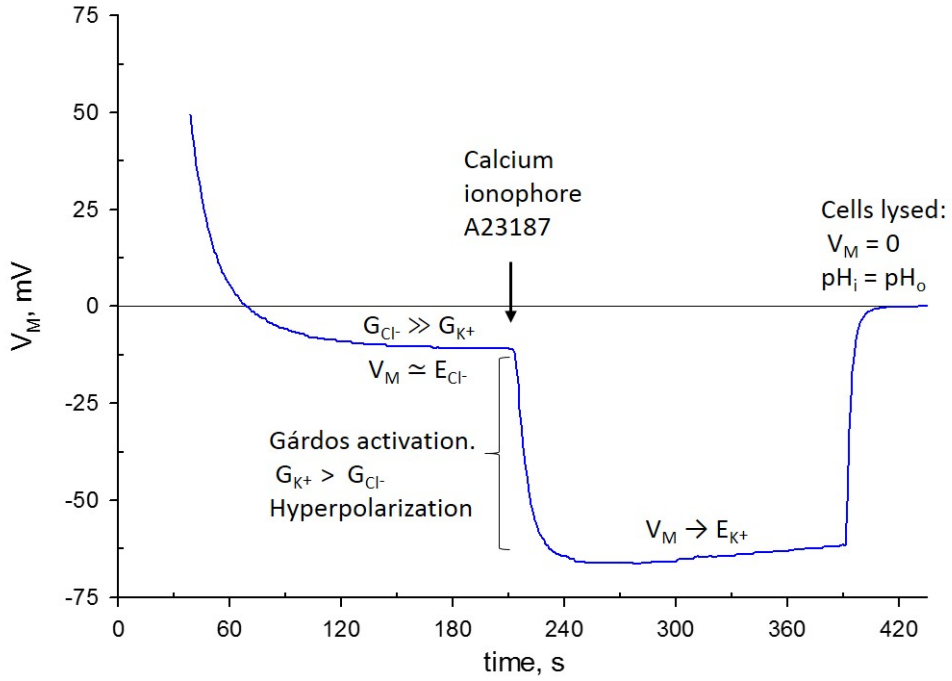

Figure 2.2: Typical recording of membrane potential changes and steps of an experiment.
Schematic showing a typical membrane potential plot. CCCP is added to an unbuffered saline solution and pH_o recording is started. Cells are injected into the solution. They quickly buffer it and the resting state, which matches the equilibrium for chloride, is reached. A calcium ionophore, A23187, is added leading to a sudden increase in calcium permeability. Gárdos opens when intracellular calcium levels are raised and a hyperpolarization (meaning that the membrane potential becomes more negative than at the resting state) develops. The membrane potential then tends to the equilibrium of potassium and other ions. At the end of the experiment detergent is added to the RBC suspension to lyse the cells and determine the intracellular pH at 0 mV. As the cells have been lysed intracellular pH is equal to the pH of the lysate. The trace is calculated with this calibration point as a reference.

Experimental approaches

Membrane potential estimation in real time of a RBC population gives insight on ion channel activity as it is proportional to the contribution of every ion conductance. As a channel can increase the conductance for an ion by several orders of magnitude, the extent of channel activation can be inferred. Using different pharmacological approaches and conditions we can influence ion channel activity and reveal deviations from typical RBC populations compared to senescent or pathological populations.

Pharmacological approach

G_{Cl^-} inhibition Blocking the chloride conductance, which is dominant in RBCs and responsible for the membrane potential being -10 mV (E_{Cl^-}), is often essential to discern the small cationic currents that would have otherwise little effect on the membrane potential. Even channels carrying large currents such as Gárdos can have a small impact on the membrane potential due to the compensating effects of chloride leaving the cell at the same time. Compounds I have used to this end include: NS3623 (low concentration; 10 μM) and NPPB.

Gárdos activation A Ca^{2+}-dependent K^+ channel, Gárdos has a strong effect on the membrane potential, especially when G_{Cl^-} is inhibited and maximally activated. Its activation entails cellular dehydration and hyperpolarization, that is, the membrane potential becomes more negative than at the resting state. It can be activated by use of: calcium ionophore A23187 which greatly increases calcium permeability leading to instantaneous maximal activation. NS309 lowers the intracellular calcium concentration threshold needed for Gárdos activation, hence Gárdos can be activated in this manner without artificially raising the intracellular calcium levels. In addition, extracellular calcium levels can be nominally zero, to study submaximal activation states or in the millimolar range to study physiological activations.

In order to study Non Selective Cation channels the equilibrium characteristic of the resting state must be perturbed so that driving force is present and channel activity can be measured.

Gárdos inhibition A way to verify the contribution of Gárdos to a delta in membrane potential is to use its selective blocker Tram34.

Piezo1 activation Piezo1 is a mechanosensitive Non Selective Cation channel which can be activated by agonist Yoda1. However, because Piezo1 is permeable to calcium, use of Yoda1 also entails Gárdos activation and the impact on the membrane potential come primarily from Gárdos activity.

Piezo1 inhibition GsMTx4 is a toxin which blocks mechanosensitive channels. It can be use to probe whether Piezo1 is involved in observed NSC activity.

Enhancement of NSC activity At large concentrations, in addition to inhibiting the chloride conductance, NS3623 enhances NSC activity in hyperpolarizing conditions which favor Na^+ entry. See chapter 3 on page 69 for an article providing evidence that NS3623 enhances NSC activity.

Alternative strategies

Substitution of a permeant cation by an impermeant one An approach to ascertain whether sodium is involved in a process (such as movement through a cationic pathway) is the removal of the ion from solution. To keep osmolarity constant an impermeant cation must be replaced in its stead. Choline cannot cross conductive pathways therefore fulfilling that role in most conditions.

Use of Low Ionic Strength Solutions Replacement of sodium by sucrose leads to an instantaneous depolarization to very positive membrane potentials, a condition where a Non Selective Cation channel is known to operate. In these conditions addition of calcium to the medium gives rise to Gárdos opening and hyperpolarization. Moreover, the aforementioned agonists and antagonists can be employed to study several ion channel at once, such as the interplay between Piezo1 and/or NSC and Gárdos.

A thorough characterization of ion channel activity is obtained by combining different approaches and is applicable to the study of senescent populations, the storage lesion (how its effect on ion channel activity impacts erythrocytes) and in anemic disorders.

Nomenclature used in membrane potential recordings (CCCP method)

The membrane potential V_M is the separation of charges across the insulating lipid bilayer. By convention, the voltage on the external side of the insulator, that is, of the membrane is considered zero: $V^{out} = 0$. The resting membrane potential, V_M^{rest}, is equal to -10 mV in human erythrocytes. Ion channel openings alter the membrane potential as charges, i.e. ions, can move in or out the cell through the ion channel pore which crosses the lipid bilayer. Living cells have a V_M different from zero. Generally $V_M^{rest} < 0$ for all cells, including RBCs, although they do have a V_M much less negative than most cell types. As ion gradients are an absolute requirement for homeostasis (including for cells devoid of organelles such as RBCs) for ATP generation and cell signaling, a stable $V_M = 0$ means generally cell death. Breakdown of the plasma membrane is synonym with cell lysis and indeed $V_M = 0$ in such instance. For membrane potential determination via CCCP method, erythrocytes are routinely lysed at the end of experiments in order to determine a baseline upon which all other V_M can be calculated (this is indicated by a horizontal line at $V_M = 0$ in plots). Terms related to membrane potential change refer to deviations from V_M^{rest}:

- Hyperpolarization conveys a change towards very negative membrane potential values, smaller than the resting membrane potential. If $V_M < -10mV$, there is a hyperpolarization, V_M^{hyp}. A maximum hyperpolarization, V_M^{maxhyp}, is the smallest V_M value recorded for a cell population. If an equilibrium is reached, cells may stay at such small V_M for long time period, i.e., they may stay hyperpolarized.

- Depolarization denotes a change towards positive membrane potential values, that is, greater than the resting membrane potential. If $V_M > -10mV$, there is a depolarization, V_M^{dep}.

- Repolarization expresses a change towards the resting membrane potential either from a previous state of hyperpolarization or depolarization. It refers to a transient state after a hyperpolarization or depolarization has taken place where V_M is returning to -10 mV.

In addition, the membrane potential change rate, v, can be calculated over a period of time, as V_M can change suddenly very strongly, or drift slowly over a long period. All v are calculated using time intervals corresponding to the linear part of slopes, and hence they are termed initial rates v_0. Units are millivolts per second, mV/s. According to the process these can be:

- Hyperpolarization rate, v_0^{hyp}, conveys the change in V_M to values smaller than -10 mV over a period of time v_0^{hyp}. In the results herein presented hyperpolarizations typically take place after Gárdos activation, thus, the rate is calculated immediately after Gárdos agonist addition.

- Depolarization rate, v_0^{dep}, denotes the the change in V_M to values greater than -10 mV over a period of time. In the results herein presented depolarizations only occur in Low Ionic Strength conditions.

- Repolarization rate, $v_0^{rep} = v_0^{posthyp} = v_0^{postdep}$, expresses the change in V_M towards -10 mV, V_M^{rest}, over a period of time. Consequently, it may refer to either a change in V_M after a hyperpolarization, $v_0^{posthyp}$ or a depolarization, $v_0^{postdep}$. In the results herein presented repolarizations occur immediately after a maximum hyperpolarization has been reached or immediately after RBCs are placed in Low Ionic Strength solutions, as they depolarize instantaneously and V_M changes towards V_M^{rest}.

Enhancement of NSC channels in hyperpolarizing conditions

The chloride conductance inhibitor NS3623 enhances the activity of a non selective cation channel in hyperpolarizing conditions

Monedero Alonso David[1,2], Pérès Laurent[1,2], Bouyer Guillaume[1,2], Egée Stéphane[1,2*]

[1] Sorbonne Université, CNRS, UMR 8227 LBI2M, Station Biologique de Roscoff SBR, 29680 Roscoff, France

[2]Laboratory of Excellence GR-Ex, Paris, France.

*** Correspondence:**
Corresponding Author
egee@sb-roscoff.fr

Keywords: Non selective cation channel, erythrocyte, membrane potential, chloride channel inhibitor, CCCP method, red blood cell

Abstract

It is stated in handbooks of physiology that the strategy adopted by RBCs for keeping constant the cell volume is to maintain a very low membrane permeability for cations. However, enhanced cation permeability can be measured and observed in specific physiological and pathophysiological situations such as senescence, sickle cell anaemia and many other genetic defects. Among cation permeabilities, cation channels are able to dissipate rapidly the gradients that are built and maintained by the sodium and calcium pumps. These situations have been very well documented but a mechanistic understanding of complex electrophysiological events underlying ion transports is still lacking. In addition, non-selective cation channels present in the red blood cell membrane have proven difficult to molecular identification and functional characterization. For instance, NSC channel activity can be elicited by Low Ionic Strength conditions (LIS): the associated change in membrane potential triggers its opening in a voltage dependent manner. But, whereas depolarizing media produce a spectacular activation of NSC channel, Gárdos channel-evoked hyperpolarizations have been shown to induce sodium entry through a pathway thought to be conductive and termed P_{cat}. Using the CCCP method, we show here i/ that hyperpolarization elicited by Gárdos channel activation triggers sodium entry through a conductive pathway, ii/ that chloride conductance inhibition unveils such conductive cationic conductance, iii/ that the use of the specific chloride conductance inhibitor NS3623 (a member of the NS1652 family), at concentrations above what is needed for full anion channel block, potentiates the trans-membrane non-selective cation conductance.

These results indicate that a non-selective cation channel is likely activated by the changes in the driving force for cations rather than a voltage dependence mechanism *per se*.

1 Introduction

The most prominent feature of erythrocyte ionic permeability is the selectivity for anions. Hydrophilic anions such as Cl^- and HCO_3^- cross the membrane about one million times faster than hydrophilic cations of similar size such as Na^+ or K^+. Thus, human erythrocytes display a relatively high chloride conductance (G_{Cl-}) of about 25 $\mu S.cm^{-2}$ (Bennekou, 1999). The dominance of G_{Cl-} over the other conductances clamps the membrane potential of red blood cells (RBCs) close to the Nernst equilibrium for Cl^- (−12 mV), facilitating by such CO_2 transport within the blood thanks to fast hydration within RBCs by the carbonic anhydrase coupled to the fast exchange of produced bicarbonate through the chloride/bicarbonate exchanger AE1 or Band 3, the so-called “chloride shift” (Hoffman and Geibel, 2005). Cation movements, on the contrary, have to stay low in order to maintain homeostasis and rheological properties constant in the steady state. Small leaks are swiftly corrected for by the action of powerful pumps such as the $3Na^+/2K^+$ pump and the Plasma Membrane Ca^{2+} ATPase (PMCA) (Tosteson and Hoffman, 1960). However, the human red cell membrane is endowed with numerous cationic permeabilities, notably ionic channels, that may represent a threat if their activity and generated fluxes are above pump capacity (Thomas et al., 2011). Among the cationic channels, the human red blood cell membrane contains 150 to 200 copies of a K^+ channel activated by Ca^{2+} ions (IK1, KCa3.1, KCNN4). The so-called Gárdos channel is the most well-described in the literature (Hamill, 1983; Maher and Kuchel, 2003; Lew and Tiffert, 2017). At intracellular physiological Ca^{2+} concentrations (30 to 60 nM) (Tiffert and Lew, 1997), the Gárdos channel is inactive. The activation threshold is reached at 150 nM and the maximum activity at around 2 µM (Dunn, 1998); the transmembrane K^+ flux is then multiplied by a thousand: the massive output of K^+ ions hyperpolarizes the membrane, whose potential then shifts toward the equilibrium potential for K^+ ions (E_K) and creates a favorable electrochemical gradient for anion release, usually leading to massive dehydration.

On the contrary, the picture for Non Selective Cation channels (NSC) also present in the red cell membrane is rather more complex and their molecular identity remains elusive. Indeed, NSC channels carry Na^+, K^+ and Ca^{2+} down their respective electrochemical gradients and may, once active, dissipate the gradient maintained by the pumps. Numerous reports describe these conductances functionally but it is still unknown whether different types of channels with specific roles exist or, rather, a single NSC can operate under different modes of action. Nevertheless, there is evidence for several channel proteins that may account for the cation exchange observed in physiological or pathophysiological conditions (Bennekou, 1999). Piezo1, a mechanosensitive pore-forming NSC channel has been shown to be critical for RBC ion homeostasis as its impairment impacts cell hydration (Cahalan et al., 2015) and was reported as the primary link to Hereditary Xerocytosis (HX, MIM #194380) when mutated (Zarychanski et al., 2012; Bae et al., 2013;

Andolfo et al., 2018). Moreover, it has been hypothesized to play a role in capillary passage in association with the Gárdos channel (Dyrda et al., 2010; Faucherre et al., 2014; Danielczok et al., 2017b). The Transient Receptor Potential Channel 6 (TRPC6), a NSC channel member of the TRP superfamily, was detected at the RNA level in erythroid progenitors and at the protein level in mature RBCs in humans and mice (Foller et al., 2008; Danielczok et al., 2017a). N-methyl-D-aspartate Receptors (NMDAR) are ligand-gated NSC channels ten times more permeant to Ca^{2+} than monovalent cations. Glycine, glutamate and homocysteine are able to activate the channels (Makhro et al., 2013). They have been found in greater numbers in Sickle Cell Disease (SCD) erythrocytes compared to controls, especially after hemolytic crisis which addresses why sickled cells display abnormal Ca^{2+} level (Hänggi et al., 2014). Memantine, used currently for Alzheimer's disease, is being explored as a treatment for SCD as it is an antagonist of NMDARs.

In addition, many situations have been demonstrated to involve cation leak through NSC channels. The non-selective cation conductance observed in sickle cells, termed P_{sickle} (Lew and Bookchin, 2005), is triggered by deoxygenation and is sensitive to pH changes (Ma et al., 2012; Cytlak et al., 2013). SCD dehydration is thought to arise from calcium influx mediated by P_{sickle} followed by Gárdos channel activation, which entails massive K^+ efflux. The increased cation permeability of terminal senescent RBCs has been referred to as P_{cat} and leads to cation gradient reversal, that is, with Na^+ influx exceeding K^+ influx (Lew et al., 2007; Cueff et al., 2010). The Non-Selective Voltage Dependent Cation channel (NSVDC) has been extensively characterized at the functional level and is largely responsible for the repolarization of RBCs observed when erythrocyte membrane potential is changed to positive values, as it happens when they are immersed in Low Ionic Strength solutions (Bennekou et al., 2004; Moersdorf et al., 2013).

However, in any case, study of the cationic conductances of RBCs is hindered by the strong anionic conductance (G_{Cl}−), so that in order to study cation movements chloride inhibitors are routinely employed. Chloride pathway inhibitors include DIDS (4,4'-Diisothiocyano-2,2'-stilbenedisulfonic acid), shown to bind covalently Band 3 and know to inhibit G_{Cl}− (Cabantchik and Greger, 1992), NPPB (5-nitro-2-(3-phenylpropylamino)benzoic acid) (Cabantchik and Greger, 1992) and Neurosearch-developed NS1652 (2-(N8-trifluoromethylphenyl)ureido)-benzoic acid) (Bennekou et al., 2000) and NS3623 (N-(4-bromo-2-(1H-tetrazol-5-yl)phenyl)-N'-(3-trifluoromethyl-phenyl)urea) compounds (Bennekou et al., 2001). The latter was proven, in a seminal work on SCD, to be the most effective chloride inhibitor to date, even more so than NS1652, with an IC_{50} of 210 nM versus 620 nM for NS1652 (Bennekou et al., 2001).

Measuring membrane potential changes via the CCCP (carbonylcyanide-m-chloro-phenyl-hydrazone) method has proven to be a valuable tool in the study of NSC activity (Macey et al.,

1978). For instance, inhibition of G_{Cl}− in Low Ionic Strength conditions (LIS) revealed NSC channel activity (Bennekou et al., 2003) which are the correlate of NSVDC channels previously described by patch-clamp at the single level (Christophersen and Bennekou, 1991; Kaestner et al., 1999; Kaestner et al., 2000).

Thus, inhibiting G_{Cl}− allows the magnification of the NSC contribution to any changes in membrane potential. Herein we present data showing that NS3623, the most efficient chloride channel inhibitor, acts as an enhancer of the cation conductance at concentrations above 10 µM. Interestingly, this activity occurs after Gárdos channel-induced hyperpolarization, in conditions where the driving force favors Na^+ entry at a membrane potential for which NSCs were thought to be in the closed state.

2 Materials and Methods

Reagents

All salts were acquired from Sigma and of analytical grade or better. Nominal calcium-free solutions amount to 4 µM Ca^{2+} due to typical salt contamination.

Solutions

Normal Ringer: 154 mM NaCl, 2 mM KCl. Calcium Ringer: 154 mM NaCl, 2 mM KCl, 1 mM $CaCl_2$. Choline-substituted Ringers: **0%**: 154 mM NaCl, 2 mM KCl**. 25%:** 115.5 mM NaCl, 38.5 mM Choline Chloride, 2 mM KCl **50%**: 77 mM NaCl, 77 mM Choline Chloride. 2 mM KCl **100%** 154 mM Choline Chloride, 2 mM KCl.

Red Blood Cells

Blood from healthy human donors was drawn into heparinized vacuum tubes, washed thrice with unbuffered saline by centrifugation for 5 min at 5000 rpm, the buffy coat and plasma removed then with a final step of 1 minute at 12 000 rpm, and the packed cells stored at 4 ºC until use.

Ethical Statement

Blood from healthy volunteers was withdrawn upon written informed consent (EFS, Etablissement Français du Sang), in accordance with the recommendations of institutional (CNRS) Health, Safety and Ethical committee in accordance with the guidelines of the Helsinki Declaration of 1975, as revised in 2008.

Drugs

A23187 (calcymicin; 5-(methylamino)-2-[[(2S,3R,5R,6S,8R,9R) -3,5,9-trimethyl-2-[(2S)-1 -oxo-1-(1H-pyrrol-2-yl)propan-2-yl] -1,7-dioxaspiro[5.5]undecan-8-yl]methyl] -1,3-benzoxazole-4-carboxylic acid); Valinomycin (Cyclo(L-Val-D-HyIva-D-Val-L-Lac-)3: HyIva = -Hydroxyisovaleric acid, Lac = Lactic acid); CCCP (carbonyl cyanide 3-chlorophenylhydrazone), DIDS (4,4'-Diisothiocyano-2,2'-stilbenedisulfonic acid) were purchased from Sigma-Aldrich (Saint Quentin Fallavier, France); NPPB (5-nitro-2-(3-phenylpropylamino)benzoic acid); NS3623 (N-(4-bromo-2-(1H-tetrazol-5-yl)phenyl)-N'-(3-trifluoromethyl-phenyl)urea) and NS309 (6,7-Dichloro-1*H*-indole-2,3-dione 3-oxime) were purchased from Tocris (France).

Membrane potential estimation

The CCCP method was used for the monitoring of membrane potential evolution (Macey et al., 1978; Bennekou and Christophersen, 1986). When erythrocytes are suspended in nominally buffer-free solution in the presence of the protonophore CCCP, changes in extracellular pH reflect membrane potential changes, since protons are kept at equilibrium across the membrane. The membrane potential can thus be estimated from:

$$V_M = 61.51\,mV \cdot (pH_i - pH_o)$$

Due to the high red cell buffer capacity, the intracellular pH remains constant (at about 7.2) throughout an experiment and can be estimated as the pH of the solution after lysis with Triton-X-100 at the end of the experiment.

Relative chloride conductance units

The chloride conductance was calculated based on maximum hyperpolarizations reached after valinomycin treatment (not shown). This allows to examine the efficacy of NS3623. Valinomycin is a K^+ ionophore, hence, the K^+ conductance increase is constant for a given concentration of valinomycin and since the Cl^- ground leak is also constant, the membrane potential reached reflects the activity of both conductive pathways. Accordingly, the anion conductance change can be calculated with known Nernst potentials for K^+ ($E_K = -110mV$) and Cl^- ($E_{Cl} = -12mV$) and the membrane potential (V_M) measured in the presence of valinomycin.

$$G_K^{val} = G_{Cl^0} \frac{E_{Cl} - V_M}{V_M - E_K}$$

$$G_{Cl^-} = G_K^{val} \frac{V_M - E_K}{E_{Cl} - V_M}$$

Cell water, Na^+ and K^+ content determination

0.5 ml aliquots of the cell suspension, with drugs (if any) added at indicated times, were distributed in polyethylene micro test tubes and centrifuged at 20 000×g for 10 min at 4°C. After centrifugation the packed cell mass was separated from the supernatant by slicing the tube with a razor blade below the top of the red cell column.

Water content:

After weighting, the packed cells were dried to constant weight for at least 24 h at 90°C and re-weighted. RBC volume depends on the intracellular water content, which is estimated to be about 90 fl for a healthy discocyte. Shape change can be misleading in the estimation of the cell's water content due to the great plasticity of the red cell membrane. These measurements are independent of cell shape.

Na^+ and K^+ content:

The packed cells within the sliced tube were lysed in 1 ml MilliQ water. Proteins were denatured to ease separation by addition of 231.9 µM of perchloric acid. The tubes were spun at 16 900 g for 7.5 min at 4°C and the supernatant passed onto sample tubes and diluted 10 times. The ionic content was measured using a flame photometer (PFP7, Jenway). The amounts of Na^+ or K^+ measured are reported as µmol/g dry cell solid.

3 Results

NS3623 was previously reported as a chloride conductance inhibitor with a higher affinity than that of the hitherto most effective blocker NS1652 (Bennekou et al., 2001). We set to incorporate this novel compound in our research, as it is the best-known blocker of the human erythrocyte chloride conductance. A range of NS3623 concentrations was tested and the corresponding G_{Cl^-} values were log-transformed, plotted and fitted to a sigmoid equation in a dose-dependent manner (Fig. 1A). As reported, the compound is an excellent inhibitor with 99% block of G_{Cl^-} at a concentration of 10 µM. However, this inhibition is lost at concentrations above 10 µM. Such deviation suits two different scenarios: either NS3623 loses its affinity for G_{Cl^-} targets at concentrations greater than 10 µM or the reduced maximal hyperpolarization is caused by the activation of a cationic conductive pathway that lets Na^+ into the cells due to the huge electrochemical gradient brought about by the hyperpolarization. Given the unlikely prospect that a compound with such high affinity would fail to do so at high concentrations that are still within the micromolar range, we set to investigate whether this compound directly enhances the cation conductance.

Another way to hyperpolarize quickly RBCs is by increasing drastically the Ca^{2+} permeability. This is achieved by employing A23187, a potent calcium ionophore, which will immediately activate the Gárdos channel. Considering that G_{Cl^-} and Gárdos channel (if active) are the strongest conductances of RBCs, the greater the G_{Cl^-} inhibition, the more the cell will hyperpolarize as Gárdos channel activity will bring the membrane potential to very negative membrane potential values.

Pretreating cells with 0, 10 or 100 µM NS3623 does not change the resting membrane potential, then once cells are exposed to A23187 a hyperpolarization follows which is dependent on the concentration of NS3623 (Fig.1B). Whereas without inhibitor the potential reaches −59.9 ± 7.6 mV (n=22), the use of 10 µM NS3623 brings the membrane potential to −85.3 ± 2.8 mV (n=12). But again, surprisingly, at 100 µM the hyperpolarization attains only −60.6 ± 2.9 mV (n=4), considerably reduced compared to 10 µM. Strikingly, a delayed onset of the hyperpolarization occurs after A23187 treatment. The latter observation strengthens the hypothesis of Na^+ entry being caused by NS3623, considering that valinomycin and A23187 hyperpolarize the cell by two independent mechanisms and that an inhibitor actually increasing the Cl^- conductance is not plausible.

In order to test the hypothesis that Na^+ enters via a cationic pathway, erythrocytes were resuspended in solutions with reduced concentrations of Na^+, keeping the osmolarity constant by using choline chloride. Choline is a cation unable to cross the plasma membrane through ion channels. Cells were

treated with 0, 10 or 100 µM NS3623 followed by A23187. RBCs hyperpolarize to the same extent: −81.7 ± 3.3 mV – regardless of the degree of Na^+ available when the chloride conductance is inhibited by 10 µM NS3623 (Fig.2A). At this concentration, no significant difference was found in terms of maximum hyperpolarization between choline-free and choline-containing solutions (p=0.084). However, when RBCs are subjected to 100 µM NS3623, the subsequent hyperpolarizations are dependent on Na^+ concentration, in an inversely proportional manner: the less Na^+ present the more the cells hyperpolarize, with the strongest hyperpolarization happening in solutions containing only choline and no Na^+ (Fig. 2B). Those in 0% choline chloride reach (mean ± SD) −60.8 ± 6.9 mV (n=3) compared to those in Na^+-free solutions hyperpolarizing to −86.1 ± 1.3 mV (n=3) ($p < 0.001$). In addition, the repolarization observed when Na^+ is available, is completely absent in solutions devoid of Na^+ (Fig.2B). Therefore, Na^+ is involved in the differential effect observed between 10 and 100 µM NS3623. The latter is thought to induce Na^+ influx via a NSC. To directly confirm this influx, RBCs were treated with 0, 10 or 100 µM NS3623 followed by A23187 and sampled at 5 and 30 minutes for subsequent analysis of intracellular water, K^+ and Na^+ content.

Cells begin to dehydrate immediately after A23187 addition, however the inhibition of the chloride conductance by NS3623 hinders the exit of water as Cl^- movement is blocked and there is less osmotically obliged water following KCl exit. After 5 minutes, uninhibited cells have lost 14.5 % ± 4.4 % (n=5) of their internal water compared to 2.2 % ± 4.1 % (n=5) of 100 µM NS3623 pre-treated cells (p=0.008). Cells untreated with NS3623 dehydrate fast so by 30 minutes the dehydration due to Gárdos channel activity is severe, a 41.1 % ± 3.6 % reduction in water content (Fig. 2C) whereas 10 and 100 µM NS3623 pre-treated cells have only lost 22.7 % ± 5.8 % and 20.8 % ± 4.6 % respectively ($p<0.001$).

Dehydration is accounted for by intracellular K^+ measurements showing a decrease from (mean ± SEM) 240.8 ± 8.5 to 80.4 ± 5.3 µmol/g dry cell mass by 30 min (n=5, Fig. 2D). Both 10 and 100 µM NS3623-treated cells displayed decreased dehydration and K^+ loss owing to the blocked chloride conductance, as chloride is rate-limiting. This indicates, importantly, that the chloride conductance is indeed inhibited at 100 µM NS3623 as otherwise a greater loss of water and K^+ would be expected. Na^+ measurements show that erythrocytes treated with 100 µM NS3623 take in Na^+ over time after Gárdos channel activation is triggered by A23187 exposure. This Na^+ influx is increased as early as 5 minutes for 100 µM NS3623 pre-treated cells. 30 minutes after A23187 treatment, intracellular Na^+ significantly increased to 60.6 ± 5.2 µmol/g dry cell solid in 100 µM NS3623 pre-treated erythrocytes, whereas 0 and 10 µM NS3623 pretreated cells contained 42.2 ± 3.4 µmol/g dry cell and 44.6 ± 3.4 µmol/g dry cell solid, respectively (p=0.016 and p=0.031)

(Fig. 2E). Notably, NS3623 by itself, either at 10 or 100 µM, does not alter water, K^+ nor Na^+ content as late as 40 minutes after addition, underscoring that hyperpolarizing conditions are a requirement for its enhancing effect on the cation conductance.

NS309 is a compound that lowers Gárdos channel sensitivity to calcium so that a smaller intracellular calcium concentration is enough to open the channel. In this manner, NS309 does not increase the intracellular calcium concentration contrary to A23187, allowing for the study of Gárdos channel-induced hyperpolarizations in stable calcium levels. To ascertain whether the phenomenon set off by NS3623 is independent on $[Ca^{2+}]_i$ variation we subjected RBCs to NS309 at two different extracellular $[Ca^{2+}]_o$: first in conditions meeting those of previous experiments, i.e. 4 µM Ca^{2+} and then in a more physiological condition with 1 mM Ca^{2+}. Our hypothesis postulates that a NSC is activated after treatment with 100 µM NS3623, which entails a Na^+ increase, as has been shown, and a calcium influx. As expected, hyperpolarizations are much greater when the chloride conductance has been blocked than when it is not: −68.7 ± 5.2 mV (n=3) compared to −26.5 ± 10.9 mV (n=3) (p=0.002). The initial rate of hyperpolarization (v_0^{hyp}) is also larger: −0.79 ± 0.07 mV/s (n=3) for 10 µM NS3623 pre-treated cells in contrast to −0.21 ± 0.21 mV/s (n=3) of untreated cells (p=0.003). However, when 100 µM NS3623 is used, the hyperpolarization achieved is closer to that of uninhibited cells: −31.5 ± 8.8 mV (n=3) reached by inhibited cells compared to −26.5 ± 10.9 mV (n=3). This is 37.2 mV lower than values reached by 10 µM NS3623-treated cells (p=0.003). 100 µM NS3623 also delays the onset of hyperpolarization with v_0^{hyp} −0.09 ± 0.05 mV/s (n=3) in contrast to −0.79 ± 0.07 mV/s (n=3) of RBCs treated with 10 µM NS3623 (p <0.001, Fig. 3A).

If these experiments are performed with solutions containing millimolar concentrations of calcium the picture changes. First, Gárdos channel-induced hyperpolarization becomes maximal, attaining −44.1 ± 2.5 mV (n=3) for 0 µM NS3623-treated cells and −87.3 ± 2.4 for 10 µM treated cells (p<0.001). Even though 100 µM treated cells hyperpolarize to greater extents, −81.2 ± 2.0 mV, getting close to 10 µM NS3623 levels though distinctly different (p=0.028), they do so at a slower pace than 10 µM treated cells: v_0^{hyp} is −0.35 ± 0.08 mV/s (n=3) for 100 µM pretreated RBCs whereas it is −1.29 ± 0.16 mV/s (n=3) for 10 µM pretreated cells (p <0.001) (Fig. 3B). This may be explained by an influx of calcium through the NSC (see discussion).

We quantified intracellular water, Na^+ and K^+ after Gárdos channel activation in stable intracellular Ca^{2+} conditions by employing NS309 in low and high extracellular calcium solutions. Contrary to what is observed with A23187, NS3623 has no clear effect on cell volume upon NS309-induced

hyperpolarization. Indeed, the dehydration and K^+ loss are reduced due to Gárdos channel partial activation given the low intracellular concentration dictated by the nominal extracellular calcium concentration (4 µM) and the pumping activity of the PMCA. Cells with G_{Cl^-} uninhibited lost 25.7 % ± 4.9 % (n=5) intracellular water by 30 minutes whereas 100 µM NS3623 pretreated RBCs lost 19.6 % ± 4.9 % (n=5, p=0.069, Fig.3C). The K^+ loss at 30 min, as anticipated, was greatest for uninhibited cells with a final content of 128 ± 7.6 µmol/g dry cell mass (n=5) whereas for 100 µM NS3623 pretreated cells it was 154.5 ± 4.6 µmol/g dry cell mass (p=0.019, n=5, Fig.3E). A small increase in Na^+, 43.3 ± 6.9 µmol/g dry cell mass is observed once the cells are subjected to 100 µM NS3623, compared to 36.7 ± 2.17 µmol/g dry cell mass for those not treated with NS3623, although it is not significant (p=0.056, Mann-Whitney, Fig. 3E, n=5).

Experiments carried out with 1 mM Ca^{2+} Ringers show the high impact of calcium availability on water and cation content when Gárdos channel is opened. As early as 5 minutes there is a 14.1 % ± 3.0 % (n=3) decrease in water content whereas 10 and 100 µM NS3623 pre-treated cells have only lost 4.82% ± 2.76 % and 0.80 % ± 1.49 % respectively (p=0.008 and p=0.003, Fig. 3D). This dehydration progresses to extreme levels surpassing those of A23187 by 30 minutes for untreated cells. As K^+ efflux is behind the dehydration, the reduction in K^+ is equivalent to that of water, with G_{Cl^-} moderating K^+ efflux. By 30 minutes, intracellular K^+ was 75.8 ± 12.3 µmol/g dry cell mass (n=3) for untreated cells in contrast to 132.3 ± 12.0 µmol/g dry cell mass (n=3) in 100 µM NS3623 pretreated cells (p=0.03, Fig.3F). In these conditions there is a significant Na^+ increase as soon as 5 minutes: cells treated with 10 µM NS3623 have 35.1 ± 0.9 µmol/g dry cell mass (n=3) whereas those treated with 100 µM NS3623 have 39.0 ± 0.3 µmol/g dry cell mass (p=0.013) (n=3). After 30 minutes, cells reach 35.3 ± 1.4 µmol/g dry cell mass (n=3) and 40.8 ± 1.4 µmol/g dry cell mass (n=3) for 10 and 100 µM NS3623 treatments, respectively (p=0.012, Fig. 3F).

Considering the high accuracy of the measurements, the wide variability observed in experiments conducted with 4 µM Ca^{2+} and the fact that it decreases considerably with 1 mM Ca^{2+} leads us to the tempting conclusion that Ca^{2+} may also influence the NSC *per se*. This assertion is strengthened by the hyperpolarization rate under NS309 and 100 µM NS3623 (see discussion).

Nevertheless, when this is performed with 1 mM extracellular Ca^{2+}, the dehydration is fast and extreme (within 30 minutes a full dehydration occurs), about 70% of the intracellular K^+ is lost via Gárdos channel in NS3623-untreated cells whereas only about 40% for NS3623-treated cells. Na^+ intake increases over time only in 100 µM NS3623-treated cells in a significant manner as early as 5 minutes.

4 Discussion

Using 100 µM NS3623 prior to hyperpolarization with either valinomycin or A23187 prevents cells from reaching a maximum hyperpolarization, staying at values similar to those untreated with the compound, contrary to the fast hyperpolarization development occurring after 10 µM NS3623 pretreatment. However, experiments with choline chloride dispelled the possibility that chloride conductance was not inhibited at high concentrations. The Na^+-dependence points clearly to the emergence of a cation conductance: cells treated with 100 µM NS3623 and 10 µM A23187 in solutions lacking Na^+ hyperpolarized to similar values as cells treated with 10 µM NS3623 and 10 µM A23187 regardless of the proportions of Na^+ and choline chloride present.

Moreover, measurements of changes in intracellular water, K^+ and Na^+ provide strong evidence on the activation of a non-selective cation conductance by NS3623 at a concentration above 10 µM. It is a matter of fact that a significant Na^+ influx was reported as measurable after three hours when they have been loaded with Ca^{2+} by employing A23187, to activate Gárdos channel and then placed in an ionophore-free solution triggering PMCA-mediated Ca^{2+} extrusion (Lew et al., 2007; Lew and Tiffert, 2017). The pathway responsible for such Na^+ movement, concomitant to cell shrinkage and cell hyperpolarization, was named P_{cat} (Lew et al., 2007; Cueff et al., 2010). Interestingly, the reported Na^+ intake was partially dependent on fast anion exchange possible due to SCN^- use whereas we observed very fast Na^+ intake, in 5 minutes, compared to a 3-hour timespan under the influence of a $G_{Cl}-$ inhibitor. In addition, a decrease in Na^+ uptake is observed upon use of EGTA, hinting at Ca^{2+} involvement in the P_{cat} response, even though it was still active in its absence (Tiffert et al., 2007). Considering that under physiological conditions the normal human red cell has a high conductance for chloride, about 25 µS/cm² (Bennekou, 1984; Egee et al., 2002), shrinkage after Gárdos channel activation will be rate-limiting by the availability of chloride to accompany the efflux of K^+. Thus, if the chloride conductance is inhibited, less K^+ leaves the cell through the Gárdos channel as there is no chloride for electrical compensation and consequently much less water leaves the cell. The fact that 100 µM NS3623-treated cells lose as much water and K^+ as 10 µM NS3623-treated cells after Gárdos channel activation strengthens the assumption that $G_{Cl}-$ is inhibited at both concentrations. These experiments also showed an increase in intracellular Na^+ over time only for 100 µM NS3623-treated cells. The only known conductive pathway able to carry large amounts of Na^+ in such short timespans (as early as 5 minutes) in RBCs are Non Selective Cation Channels (Christophersen and Bennekou, 1991; Kaestner et al., 2000; Duranton et al., 2002).

Importantly, it is worth noting that NS3623 (even at 100 µM) itself does not alter neither membrane potential nor Na^+ and K^+ content of RBC at resting membrane potential. NS3623 is still able to inhibit the chloride conductance and to trigger, at high concentrations, NSC activity even if Gárdos

channel-elicited hyperpolarization is already fully developed (Fig. S1). This undoubtedly indicates that NS3623 action relies on the driving force and not on Gárdos channel activation *per se*.

Such behavior indicates either that the effect of the compound is voltage dependent or that the channel itself is voltage dependent *per se*. Such an observation suggests that the pathway activated could be the previously described NSVDC (Bennekou et al., 2004). The voltage dependence hypothesis is seemingly ruled out since experiments performed with reduced driving force for K^+ efflux via Gárdos channel do not alter the repolarization rate when Na^+ is present (Fig. S3). This phenomenon remains concentration-dependent at this reduced K^+ driving force, displaying the same Na^+ dependence (compare Fig. S3B with Fig. S2B).

However, A23187 raises the intracellular Ca^{2+} concentration permanently. In order to decipher whether Ca^{2+} or the driving force triggers NSC activity, NS309 was used. This compound increases the sensitivity of Gárdos channel to calcium so that nominal intracellular calcium is sufficient to evoke channel openings (Strobaek et al., 2004) and, more importantly, it keeps the intracellular calcium levels stable and thus maintains the Plasma Membrane Calcium ATPase (PMCA) at resting activity (Baunbaek and Bennekou, 2008). It should be noted that even though the PMCA will keep intracellular calcium levels below the Gárdos channel threshold of activation in physiological conditions, $[Ca^{2+}]_i$ will indeed be higher than RBCs resuspended in nominal Ca^{2+}-free solutions as the PMCA extrusion capacity is greater the more calcium there is, until ATP exhaustion. Thus, NS309 induced-hyperpolarizations are a function of the extracellular calcium concentration (Strobaek et al., 2004; Baunbaek and Bennekou, 2008).

Using NS309 in nominally calcium-free solutions with 0, 10 or 100 µM NS3623 pretreatment displays smaller overall hyperpolarizations, as the Gárdos channel is not maximally activated, with 0 and 100 µM NS3623-pretreated cells attaining similar membrane potential values albeit at a slightly faster rate for 100 µM NS3623-pretreated cells. Nevertheless, performing these experiments with physiological (1 mM) calcium content shows that, amid the greater hyperpolarizations in the context of greater Gárdos channel activation, 100 µM NS3623-pretreated cells reach values close to those of 10 µM NS3623 cells by five minutes with the hyperpolarization rate increasing over time. A possible explanation may reside in the fact that the Gárdos channel is not fully activated even with an extracellular calcium concentration of 1 mM and the chloride conductance blocked so when 100 µM NS3623 enhances the activity of the NSC, there is calcium intake, as there is a huge driving force towards the cytoplasm, and Gárdos channel activity increases slightly over time towards the maximum, only in 100 µM NS3623-pretreated cells. The maximum hyperpolarization difference between low or high calcium solutions was 17.60 ± 6.79 mV (n=3) and 18.65 ± 4.38 mV (n=3) for 0 or 10 µM NS3623-pretreated cells, whereas the difference for

100 µM NS3623-pretreated cells reached 49.67 ± 7.30 mV (n=3), highlighting the strong synergistic effect of calcium and NS3623 (100 µM). Such an interplay between Ca^{2+}, Gárdos channel and NSVDC was already reported in depolarizing conditions (LIS conditions) (Bennekou et al., 2003).

When calcium is scarce, Gárdos channel activity is limited and water and K^+ loss is contained. Even though Na^+ flows in over time in 100 µM NS3623-pretreated cells, the increase is minimal. However, interestingly, in high calcium solutions the loss of water and K^+ after NS309 treatment is even more pronounced than for A23187-treated cells and Na^+ is significantly increased as early as 5 minutes only in 100 µM NS3623 pretreated cells, even though the maximum amounts reached are smaller than those of A23187-treated cells. The amount of intracellular Na^+ increases after 100 µM NS3623 addition, significantly when cells are resuspended in solutions containing millimolar concentrations of calcium. Thus, there is a NSC-mediated Na^+ current upon 100 µM NS3623 treatment which electrically counteracts the hyperpolarizing K^+ loss. Positive charges are leaving (K^+) and entering (Na^+) the cell, bringing some electroneutrality even though the Gárdos channel is more powerful which may explain the more pronounced slope as there is a long-term tendency towards E_{K+}. This prevents 100 µM pretreated cells to attain such negative membrane potentials as those of 10 µM NS3623 pretreated-cells. In nominal Ca^{2+} free conditions, the extracellular calcium is so low that its entry through 100 µM NS3623-enhanced NSC is not enough to boost Gárdos channel activity.

This emphasizes the importance of calcium in red cell physiology as it reliably acts as a pervasive secondary messenger throughout the population, composed of billions of cells, quickly coordinating the overall response. Lack of calcium compromises this and the response will depend more on the individual status of the cells such as ATP availability, protein oxidation, cell age (Baunbaek and Bennekou, 2008; Seear and Lew, 2011)… etc. *In vivo,* it may mean enabling an ultra-fast shrinking response for capillary passage together with Piezo1 mechanosensitive activity, as has been proposed (Dyrda et al., 2010; Danielczok et al., 2017b). Although calcium does not activate the cation conductance pathways it may directly either modulate it by affecting channel gating or open probability or, at the very least, favor a subsequent Na^+ pathway opening. More interestingly, it may represent a fast feedback loop for transient hyperpolarization due to Gárdos channel activation in the narrowest of the capillaries. Indeed, it was shown that mechanical force causes calcium influx into RBCs that is dependent on Piezo1 expression (Cahalan et al., 2015). Such activation causes Ca^{2+} influx and eventually Gárdos channel-dependent RBC dehydration, with certainty the scenario leading to hereditary xerocytosis with the majority of Piezo1 mutated channels described so far (Zarychanski et al., 2012; Cahalan et al., 2015; Andolfo et al., 2018). But for healthy RBCs, such

transient activation (a few ms), will offer i) a simple opportunity to adjust the cell volume without altering shape or deformability of the erythrocyte in capillaries below their own volume, ii) back to the normal bloodstream, activation of a NSC will tend to let Na^+ entering the cell, allowing nearly the restoration of cell volume, iii) which eventually should give enough time for the Na^+/K^+ pump (considering the rate of exchange) to finely tune the intracellular Na^+/K^+ ratio to maintain homeostasis.

In conclusion, NSC activity can take place in hyperpolarizing conditions via a pharmacological approach with a hitherto reported efficient chloride conductance inhibitor NS3623 and with calcium as a positive modulator. Except for Piezo1 agonist Yoda1 and Jedi-related compounds (Syeda et al., 2015; Syeda et al., 2016), no activator of NSCs has been described. We argue that concomitant NSC enhancement and chloride inhibition is a key advantage, as it will allow studies of the cationic conductances of the RBC with a single supplementary drug.

5 Conflict of Interest

The authors declare that the research was conducted in the absence of any commercial or financial relationships that could be construed as a potential conflict of interest.

6 Author Contributions

SE, DMA, LP and GB defined the study, performed the experiments, interpreted the data, and drafted the manuscript. All authors listed have made a substantial, direct and intellectual contribution to the work, and approved it for publication.

7 Funding

This study was supported by the European Framework “Horizon 2020” under grant agreement number 675115 (RELEVANCE, DMA and SE), and the Laboratory of Excellence GR-Ex, reference ANR-11-LABX-0051; GR-Ex is funded by the program “Investissements d’avenir” of the French National Research Agency, reference ANR-11-IDEX-0005-02.(SE, GB, LP)

8 Acknowledgments

We thank Poul Bennekou for his inspiring work, including on this chloride conductance inhibitor.

9 References

Andolfo, I., Russo, R., Gambale, A., and Iolascon, A. (2018). Hereditary stomatocytosis: An underdiagnosed condition. *Am J Hematol* 93(1)**,** 107-121. doi: 10.1002/ajh.24929.

Bae, C., Gnanasambandam, R., Nicolai, C., Sachs, F., and Gottlieb, P.A. (2013). Xerocytosis is caused by mutations that alter the kinetics of the mechanosensitive channel PIEZO1. *Proc Natl Acad Sci U S A* 110(12)**,** E1162-1168. doi: 10.1073/pnas.1219777110.

Baunbaek, M., and Bennekou, P. (2008). Evidence for a random entry of Ca2+ into human red cells. *Bioelectrochemistry* 73(2)**,** 145-150.

Bennekou, P. (1984). K+-valinomycin and chloride conductance of the human red cell membrane. Influence of the membrane protonophore carbonylcyanide m-chlorophenylhydrazone. *Biochim Biophys Acta* 776(1)**,** 1-9.

Bennekou, P. (1999). The feasibility of pharmacological volume control of sickle cells is dependent on the quantization of the transport pathways. A model study. *J Theor Biol* 196(1)**,** 129-137.

Bennekou, P., Barksmann, T.L., Kristensen, B.I., Jensen, L.R., and Christophersen, P. (2004). Pharmacology of the human red cell voltage-dependent cation channel. Part II: inactivation and blocking. *Blood Cells Mol Dis* 33(3)**,** 356-361.

Bennekou, P., and Christophersen, P. (1986). Flux ratio of valinomycin-mediated K+ fluxes across the human red cell membrane in the presence of the protonophore CCCP. *J Membr Biol* 93(3)**,** 221-227.

Bennekou, P., de Franceschi, L., Pedersen, O., Lian, L., Asakura, T., Evans, G., et al. (2001). Treatment with NS3623, a novel Cl-conductance blocker, ameliorates erythrocyte dehydration in transgenic SAD mice: a possible new therapeutic approach for sickle cell disease. *Blood* 97(5)**,** 1451-1457.

Bennekou, P., Kristensen, B.I., and Christophersen, P. (2003). The human red cell voltage-regulated cation channel. The interplay with the chloride conductance, the Ca(2+)-activated K(+) channel and the Ca(2+) pump. *J Membr Biol* 195(1)**,** 1-8.

Bennekou, P., Pedersen, O., Moller, A., and Christophersen, P. (2000). Volume control in sickle cells is facilitated by the novel anion conductance inhibitor NS1652. *Blood* 95(5)**,** 1842-1848.

Cabantchik, Z.I., and Greger, R. (1992). Chemical probes for anion transporters of mammalian cell membranes. *Am J Physiol* 262(4 Pt 1)**,** C803-827.

Cahalan, S.M., Lukacs, V., Ranade, S.S., Chien, S., Bandell, M., and Patapoutian, A. (2015). Piezo1 links mechanical forces to red blood cell volume. *eLife* 4. doi: 10.7554/eLife.07370.

Christophersen, P., and Bennekou, P. (1991). Evidence for a voltage-gated, non-selective cation channel in the human red cell membrane. *Biochim Biophys Acta* 1065(1)**,** 103-106.

Cueff, A., Seear, R., Dyrda, A., Bouyer, G., Egee, S., Esposito, A., et al. (2010). Effects of elevated intracellular calcium on the osmotic fragility of human red blood cells. *Cell Calcium* 47(1)**,** 29-36. doi: S0143-4160(09)00175-4 [pii] 10.1016/j.ceca.2009.11.002.

Cytlak, U.M., Hannemann, A., Rees, D.C., and Gibson, J.S. (2013). Identification of the Ca2+ entry pathway involved in deoxygenation-induced phosphatidylserine exposure in red blood cells from patients with sickle cell disease. *Pflügers Archiv - European Journal of Physiology* 465(11)**,** 1651-1660. doi: 10.1007/s00424-013-1308-y.

Danielczok, J., Hertz, L., Ruppenthal, S., Kaiser, E., Petkova-Kirova, P., Bogdanova, A., et al. (2017a). Does Erythropoietin Regulate TRPC Channels in Red Blood Cells? *Cellular Physiology and Biochemistry* 41(3)**,** 1219-1228.

Danielczok, J.G., Terriac, E., Hertz, L., Petkova-Kirova, P., Lautenschläger, F., Laschke, M.W., et al. (2017b). Red Blood Cell Passage of Small Capillaries Is Associated with Transient Ca2+-mediated Adaptations. *Frontiers in Physiology* 8(979). doi: 10.3389/fphys.2017.00979.

Dunn, P.M. (1998). The action of blocking agents applied to the inner face of Ca(2+)- activated K+ channels from human erythrocytes. *J Membr Biol* 165(2)**,** 133-143.

Duranton, C., Huber, S.M., and Lang, F. (2002). Oxidation induces a Cl(-)-dependent cation conductance in human red blood cells. *J Physiol* 539(Pt 3)**,** 847-855.

Dyrda, A., Cytlak, U., Ciuraszkiewicz, A., Lipinska, A., Cueff, A., Bouyer, G., et al. (2010). Local membrane deformations activate Ca2+-dependent K+ and anionic currents in intact human red blood cells. *PLoS One* 5(2)**,** e9447. doi: 10.1371/journal.pone.0009447.

Egee, S., Lapaix, F., Decherf, G., Staines, H.M., Ellory, J.C., Doerig, C., et al. (2002). A stretch-activated anion channel is up-regulated by the malaria parasite Plasmodium falciparum. *J Physiol* 542(Pt 3)**,** 795-801.

Faucherre, A., Kissa, K., Nargeot, J., Mangoni, M.E., and Jopling, C. (2014). Piezo1 plays a role in erythrocyte volume homeostasis. *Haematologica* 99(1)**,** 70-75. doi: 10.3324/haematol.2013.086090.

Foller, M., Kasinathan, R.S., Koka, S., Lang, C., Shumilina, E., Birnbaumer, L., et al. (2008). TRPC6 contributes to the Ca(2+) leak of human erythrocytes. *Cell Physiol Biochem* 21(1-3)**,** 183-192.

Hamill, O.P. (1983). "potassium and chloride channels in red blood cells," in *Single channels recording.*, eds. E. Neher & sackmann. (New-York: Plenum), 451-477.

Hänggi, P., Makhro, A., Gassmann, M., Schmugge, M., Goede, J.S., Speer, O., et al. (2014). Red blood cells of sickle cell disease patients exhibit abnormally high abundance of N-methyl D-aspartate receptors mediating excessive calcium uptake. *British Journal of Haematology* 167(2)**,** 252-264. doi: doi:10.1111/bjh.13028.

Hoffman, J.F., and Geibel, J.P. (2005). Fluorescent imaging of Cl- in Amphiuma red blood cells: how the nuclear exclusion of Cl- affects the plasma membrane potential. *Proc Natl Acad Sci U S A* 102(3)**,** 921-926.

Kaestner, L., Bollensdorff, C., and Bernhardt, I. (1999). Non-selective voltage-activated cation channel in the human red blood cell membrane. *Biochim Biophys Acta* 1417(1)**,** 9-15.

Kaestner, L., Christophersen, P., Bernhardt, I., and Bennekou, P. (2000). The non-selective voltage-activated cation channel in the human red blood cell membrane: reconciliation between two conflicting reports and further characterisation. *Bioelectrochemistry* 52(2)**,** 117-125.

Lew, V.L., and Bookchin, R.M. (2005). Ion transport pathology in the mechanism of sickle cell dehydration. *Physiol Rev* 85(1)**,** 179-200.

Lew, V.L., Daw, N., Etzion, Z., Tiffert, T., Muoma, A., Vanagas, L., et al. (2007). Effects of age-dependent membrane transport changes on the homeostasis of senescent human red blood cells. *Blood* 110(4)**,** 1334-1342.

Lew, V.L., and Tiffert, T. (2017). On the Mechanism of Human Red Blood Cell Longevity: Roles of Calcium, the Sodium Pump, PIEZO1, and Gardos Channels. *Frontiers in Physiology* 8(977). doi: 10.3389/fphys.2017.00977.

Ma, Y.L., Rees, D.C., Gibson, J.S., and Ellory, J.C. (2012). The conductance of red blood cells from sickle cell patients: ion selectivity and inhibitors. *J Physiol* 590(9)**,** 2095-2105. doi: 10.1113/jphysiol.2012.229609.

Macey, R.I., Adorante, J.S., and Orme, F.W. (1978). Erythrocyte membrane potentials determined by hydrogen ion distribution. *Biochim Biophys Acta* 512(2)**,** 284-295.

Maher, A.D., and Kuchel, P.W. (2003). The Gárdos channel: a review of the Ca2+-activated K+ channel in human erythrocytes. *The International Journal of Biochemistry & Cell Biology* 35(8)**,** 1182-1197. doi: https://doi.org/10.1016/S1357-2725(02)00310-2.

Makhro, A., Hanggi, P., Goede, J.S., Wang, J., Bruggemann, A., Gassmann, M., et al. (2013). N-methyl-D-aspartate receptors in human erythroid precursor cells and in circulating red blood cells contribute to the intracellular calcium regulation. *American journal of physiology. Cell physiology* 305(11)**,** C1123-1138. doi: 10.1152/ajpcell.00031.2013.

Moersdorf, D., Egee, S., Hahn, C., Hanf, B., Ellory, C., Thomas, S., et al. (2013). Transmembrane potential of red blood cells under low ionic strength conditions. *Cellular physiology and biochemistry* 31(6)**,** 875-882. doi: 10.1159/000350105.

Seear, R.V., and Lew, V.L. (2011). IKCa agonist (NS309)-elicited all-or-none dehydration response of human red blood cells is cell-age dependent. *Cell Calcium* 50(5)**,** 444-448. doi: http://dx.doi.org/10.1016/j.ceca.2011.07.005.

Strobaek, D., Teuber, L., Jorgensen, T.D., Ahring, P.K., Kjaer, K., Hansen, R.S., et al. (2004). Activation of human IK and SK Ca2+ -activated K+ channels by NS309 (6,7-dichloro-1H-indole-2,3-dione 3-oxime). *Biochim Biophys Acta* 1665(1-2)**,** 1-5.

Syeda, R., Florendo, Maria N., Cox, Charles D., Kefauver, J.M., Santos, Jose S., Martinac, B., et al. (2016). Piezo1 Channels Are Inherently Mechanosensitive. *Cell Reports* 17(7)**,** 1739-1746. doi: http://doi.org/10.1016/j.celrep.2016.10.033.

Syeda, R., Xu, J., Dubin, A.E., Coste, B., Mathur, J., Huynh, T., et al. (2015). Chemical activation of the mechanotransduction channel Piezo1. *Elife* 4. doi: 10.7554/eLife.07369.

Thomas, S.L., Bouyer, G., Cueff, A., Egee, S., Glogowska, E., and Ollivaux, C. (2011). Ion channels in human red blood cell membrane: actors or relics? *Blood Cells Mol Dis* 46(4)**,** 261-265. doi: S1079-9796(11)00058-1 [pii] 10.1016/j.bcmd.2011.02.007.

Tiffert, T., Daw, N., Etzion, Z., Bookchin, R.M., and Lew, V.L. (2007). Age decline in the activity of the Ca2+-sensitive K+ channel of human red blood cells. *J Gen Physiol* 129(5)**,** 429-436.

Tiffert, T., and Lew, V.L. (1997). Apparent Ca2+ dissociation constant of Ca2+ chelators incorporated non-disruptively into intact human red cells. *J Physiol* 505 (Pt 2)**,** 403-410. doi: 10.1111/j.1469-7793.1997.403bb.x.

Tosteson, D.C., and Hoffman, J.F. (1960). Regulation of cell volume by active cation transport in high and low potassium sheep red cells. *J Gen Physiol* 44**,** 169-194. doi: 10.1085/jgp.44.1.169.

Zarychanski, R., Schulz, V.P., Houston, B.L., Maksimova, Y., Houston, D.S., Smith, B., et al. (2012). Mutations in the mechanotransduction protein PIEZO1 are associated with hereditary xerocytosis. *Blood* 120(9)**,** 1908-1915. doi: 10.1182/blood-2012-04-422253.

Figure Legends

Figure 1

NS3623 inhibits chloride conductance up to 10 µM, another effect is unveiled at higher concentrations.

(**A**) Dose-response curve of NS3623 effect on G_{Cl-}, measured via valinomycin treatment. In blue, the experimental data can be fitted to a sigmoid curve up to 10 µM. In red, at higher concentrations the points deviate from this curve. (**B**) Evolution of membrane potential from cells injected into normal Ringer solution at t=30 s with exposure to 0 µM (green, mid trace, n=22), 10 µM (cyan, bottom trace, n=12) or 100 µM (red, top trace, n=4) of NS3623 before hyperpolarization was triggered by 10 µM A23187 addition. Dashed lines indicate ± SD.

Figure 2

NS3623 becomes a potential NSC activator at high concentrations.

(**A**, **B**) Evolution of membrane potential from cells injected into respective choline chloride-substituted Ringers (0 to 100% choline), treated with 10 µM (**A**) (n=3) or 100 µM (**B**) (n=3) of NS3623 and hyperpolarized with A23187 (10 µM). Average of n=5 experiments (**C**, **D** and **E**) Intracellular water content (wet weight/dry weight) (**C**) and quantity of K^+ (**D**) and Na^+ (**E**) in packed RBCs washed with normal Ringer buffered with HEPES (pH=7.4) and treated with 0 (green), 10 (cyan) or 100 µM (red) of NS3623 and with (closed symbols, black lines) or without (open symbols, gray lines) 10 µM A23187 over time. Bars denote SEM. Average of five independent experiments.

Figure 3

NSC activity enhanced by high concentrations of NS3623 in hyperpolarizing conditions is driving force dependent.

(**A**, **B**) Evolution of membrane potential from cells injected into normal Ringer solutions containing 4 µM (**A**) or 1 mM (**B**) extracellular $CaCl_2$, treated with 0 µM (green), 10 µM (cyan) or 100 µM (red) of NS3623 and hyperpolarized with NS309 (100 µM). Average of n=3 experiments, dashed lines indicate ± SD.

(**C**-**F**) Intracellular water content (wet weight/dry weight) (**C, D**) and quantity of Na^+ (bottom traces) and K^+ (top traces) (**E, F**) of red cells treated with 0 (green), 10 (cyan) or 100 µM (red) of NS3623 and with (closed symbols, colored lines) or without (open symbols, gray lines) 100 µM NS309, in the presence of 4 µM (**C, E**) or 1 mM (**D, F**) of extracellular $CaCl_2$. Bars denote SEM, average of five (**C**,**E**) or three (**D,F**) independent experiments.

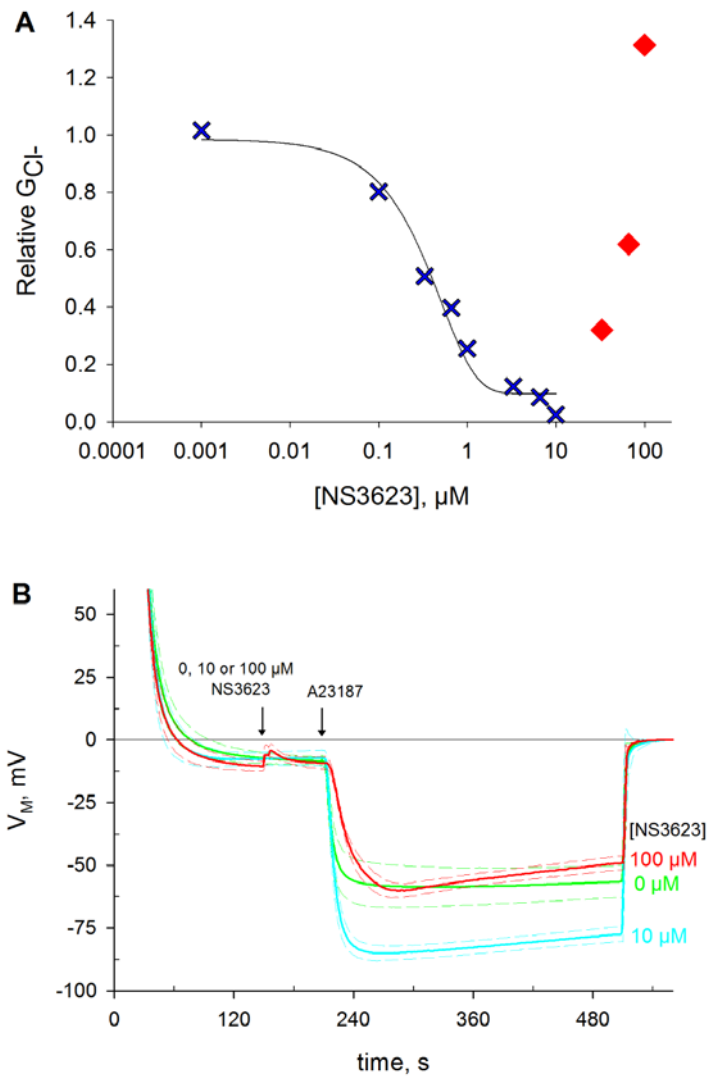
A
Relative GCl-
1.4
1.2
1.0
0.8
0.6
0.4
0.2
0.0
0.0001
0.001
0.01
0.1
1
10
100
[NS3623], µM
B
VM, mV
50
25
0
-25
-50
-75
-100
0, 10 or 100 µM
NS3623
A23187
[NS3623]
100 µM
0 µM
10 µM
0
120
240
360
480
time, s

Figure 1

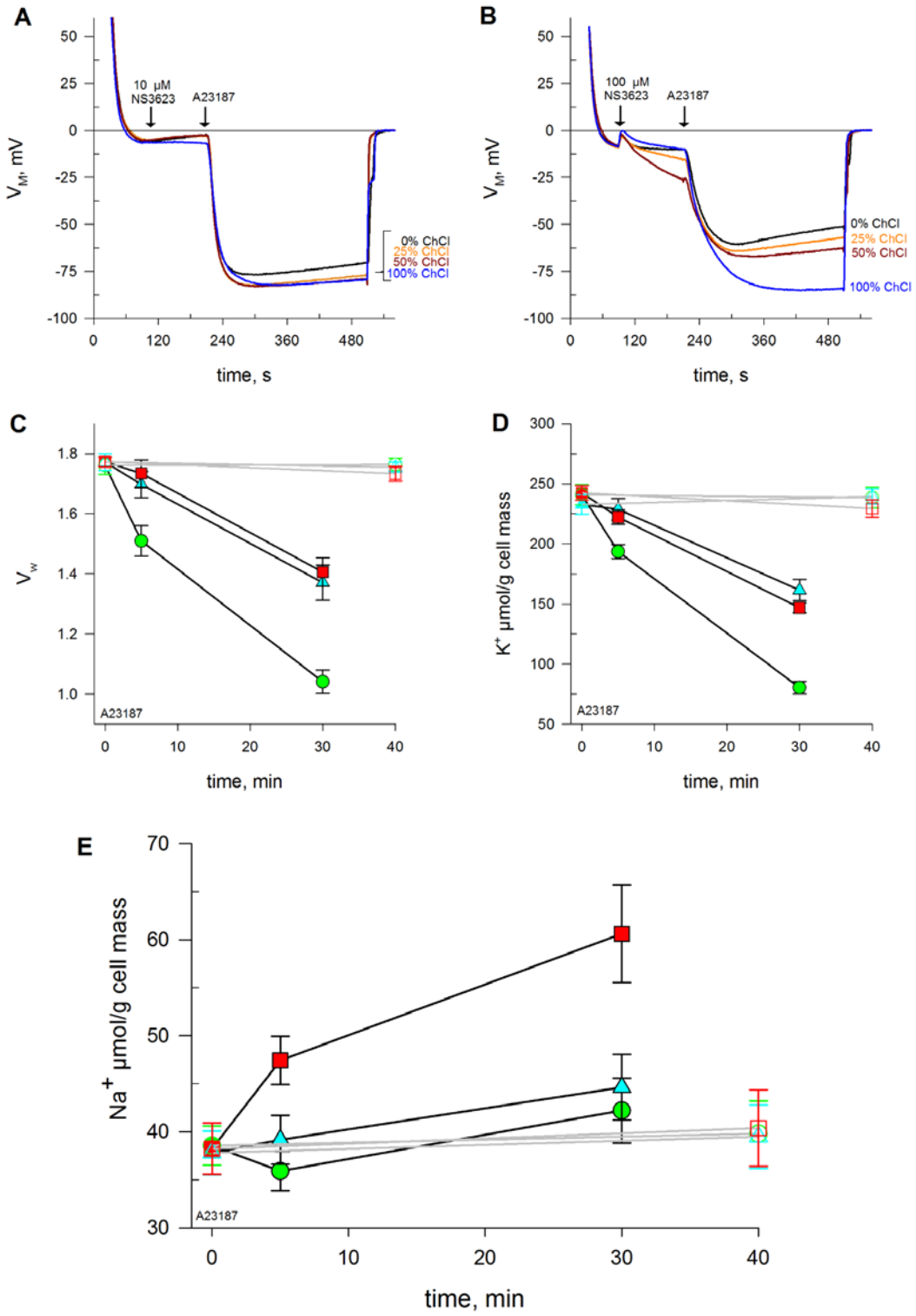
A
B
C
D
E
10 µM
NS3623
A23187
100 µM
NS3623
A23187
0% ChCl
25% ChCl
50% ChCl
100% ChCl
V_M, mV
time, s
V_w
K+ µmol/g cell mass
Na+ µmol/g cell mass
time, min

Figure 2

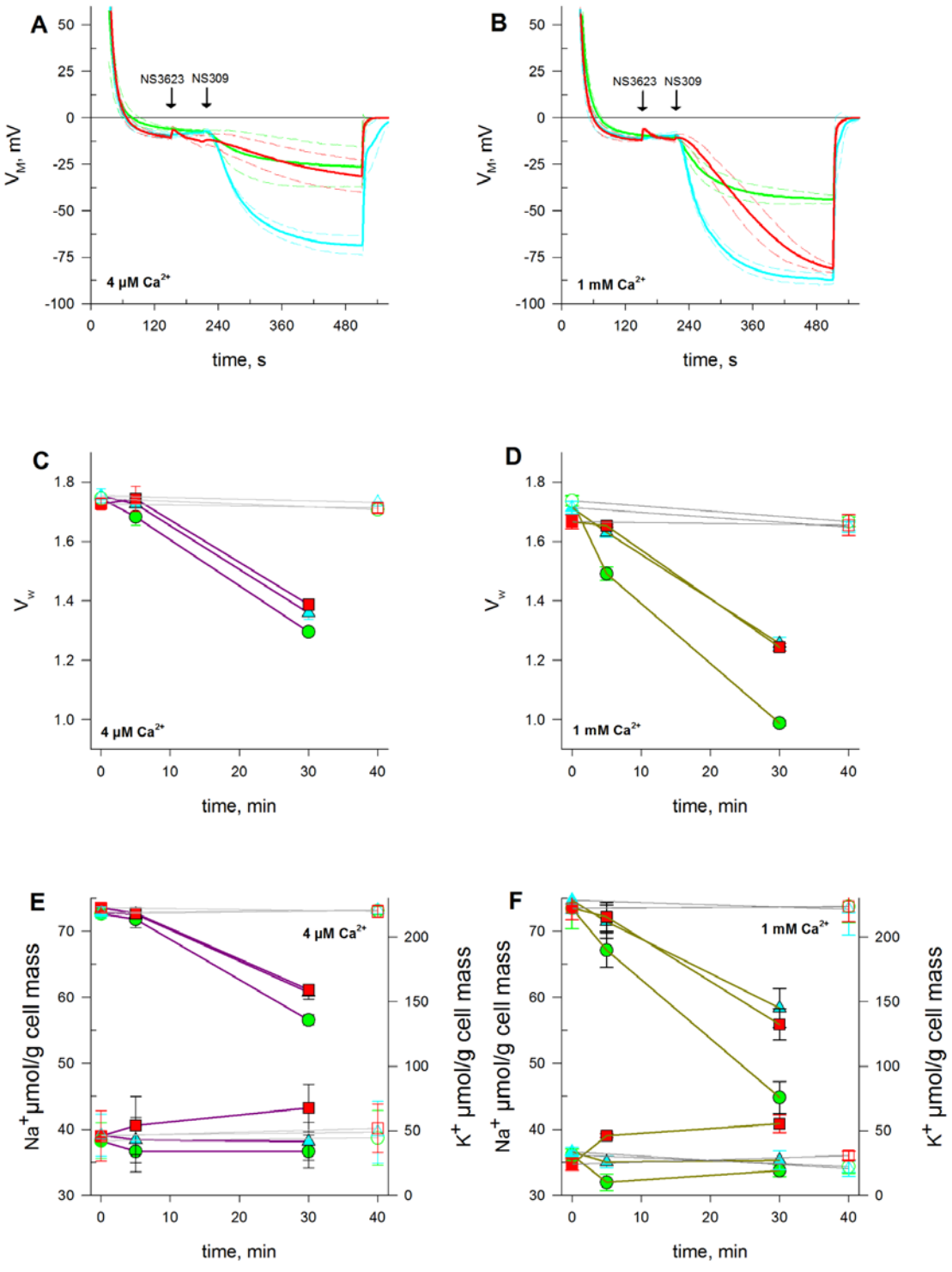
A
B
C
D
E
F
NS3623 NS309
4 µM Ca2+
1 mM Ca2+
VM, mV
time, s
Vw
time, min
Na+µmol/g cell mass
K+ µmol/g cell mass
K+ µmol/g cell mass

Figure 3

Supplementary Figure S1

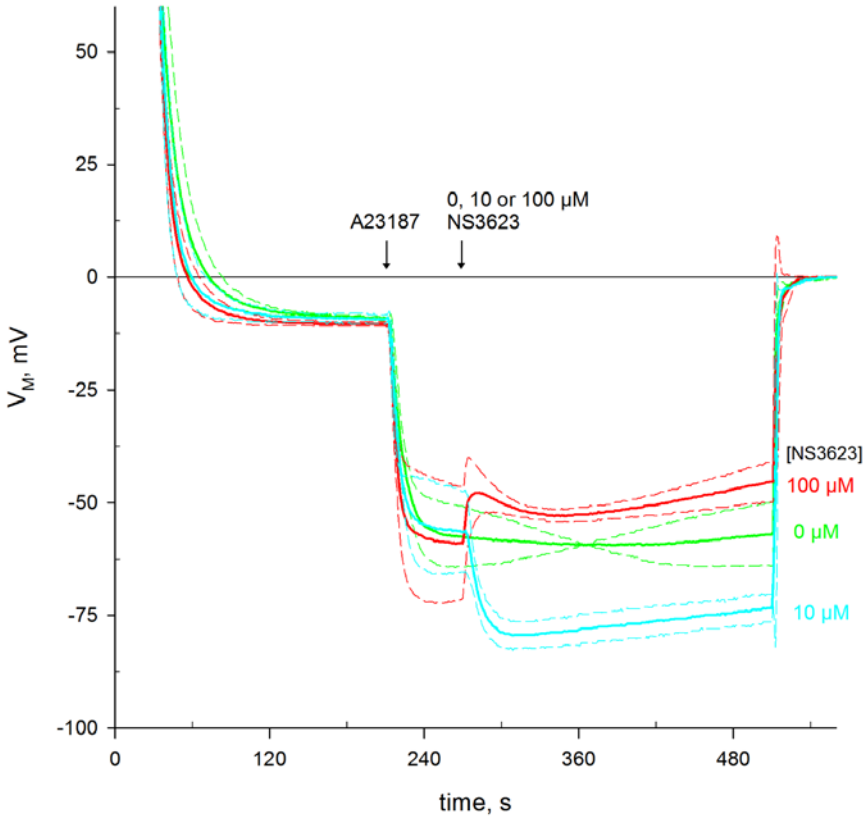

Figure S1

NS3623 inhibits the chloride conductance at 10 µM and becomes a potential NSC activator at 100 µM even when the hyperpolarization has already maximally developed.

Evolution of membrane potential from cells injected into normal Ringer solution at t=30 s with 0 µM (green, mid trace), 10 µM (cyan, bottom trace) or 100 µM (red, top trace) of chloride conductance inhibitor NS3623 provided after hyperpolarization was triggered by 10 µM A23187. Average of n=3 experiments, dashed lines indicate ± SD.

Supplementary Figure S2

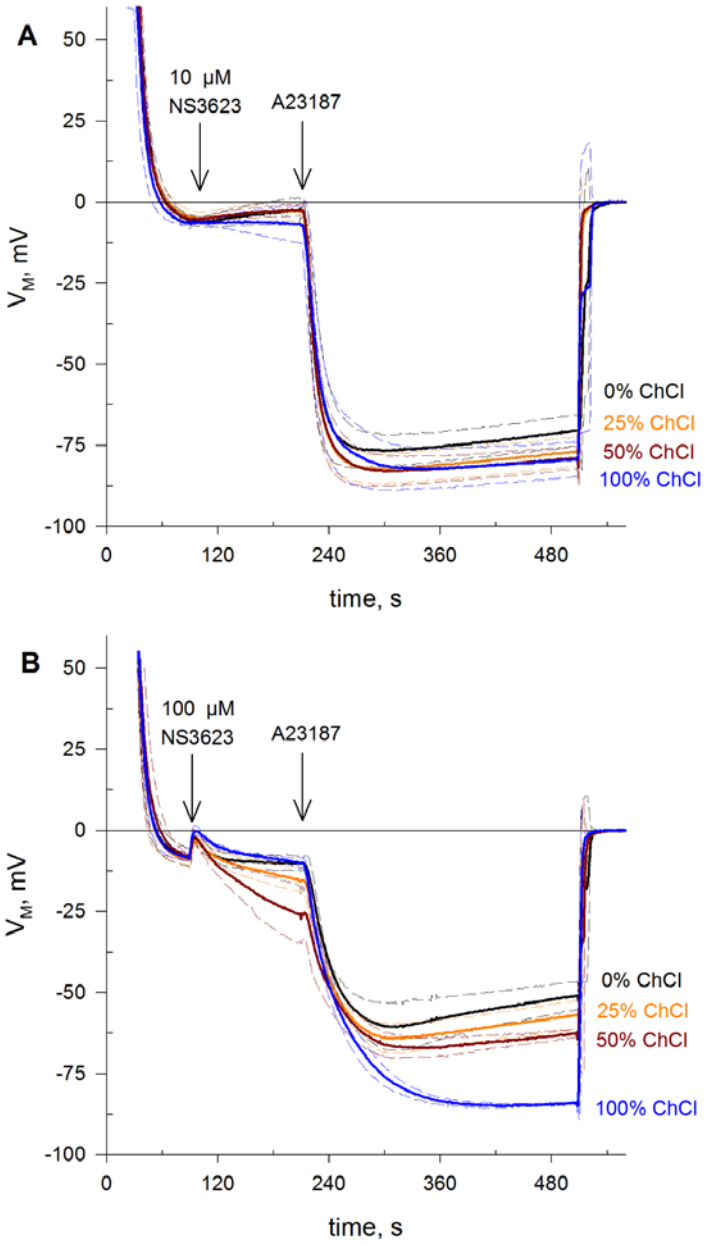

Figure S2

Removing Na^+ from the extracellular solution has barely no impact on Gárdos hyperpolarization after inhibiting the chloride conductance with 10 µM NS3623, whereas the use of 100 µM NS3623 clearly reveals a sodium dependency in the extent of hyperpolarization. This is further confirmed by the abolition of the repolarization occurring after A23187-induced hyperpolarization. It strongly suggests that 100 µM NS3623 enhances a NSC mediating Na^+ influx.

Evolution of membrane potential from cells injected into respective choline chloride-substituted Ringers, treated with 10 µM (**A**) or 100 µM NS3623 (**B**) and hyperpolarized with A23187 (10 µM). Average of n=3 experiments, dashed lines indicate ± SD.

Supplementary Figure S3

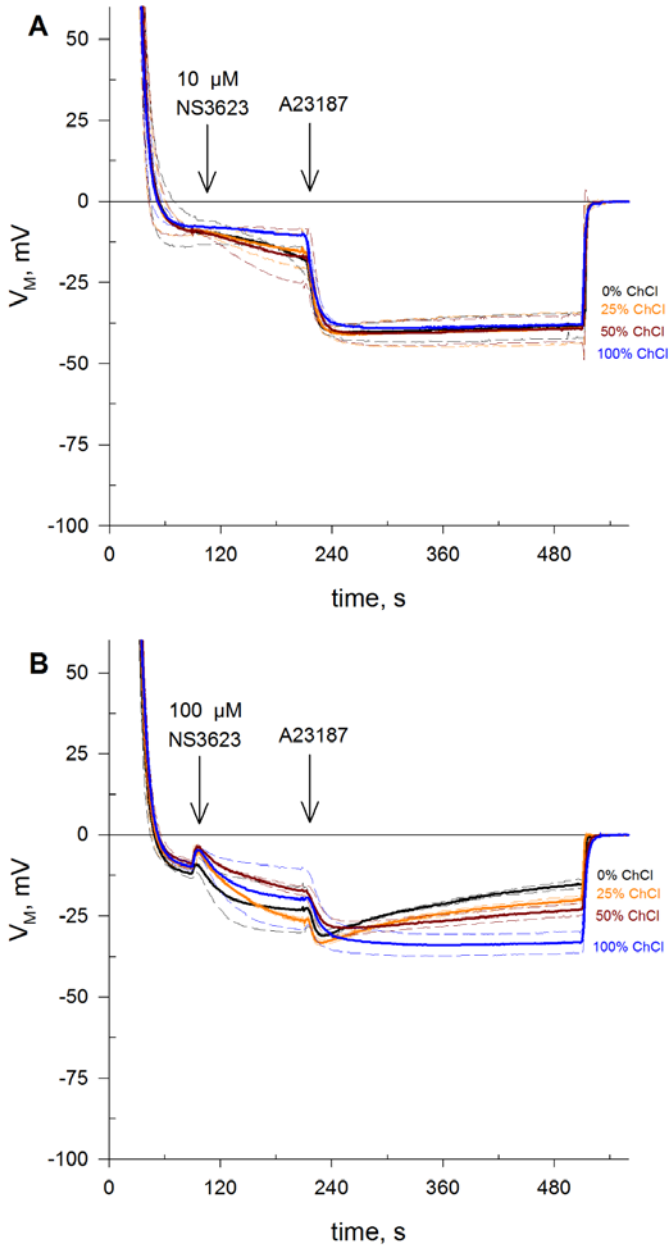

Figure S3

A smaller driving force for potassium via the use of a higher concentration (25 mM) in the extracellular solution does not preclude a differential hyperpolarization according to Na^+ available after use of 100 µM NS3623, pointing to enhanced NSC activity. NSC activity is absent or minimal at 10 µM NS3623.

Evolution of membrane potential from cells injected into respective choline chloride-substituted Ringers, treated with 10 µM (**A**) or 100 µM NS3623 (**B**) and hyperpolarized with A23187 (10 µM). Average of n=3 experiments, dashed lines indicate ± SD. Traces/solutions, top to bottom: 0, 25, 50 and 100 % Choline Chloride (ChCl) degree of substitution, with 0% = 131 mM NaCl; 25 mM KCl and 100% 131 mM ChCl; 25 mM KCl.

Functional study of RBCs from patients with mutations in Gárdos and Piezo1 channels

Chapter 4

Functional study of RBCs from patients with mutations in Gárdos and Piezo1 channels

Classical hereditary anemias, such as Hereditary Spherocytosis (HS) and Hereditary Elliptocytosis (HE), described more than a century ago, have generally been classified according to cell morphology. Hence anemias causing abnormally predominant spherocytic or elliptocytic RBC shapes, HS and HE respectively, are the most studied disorders. These diseases are caused by mutations in structural proteins or the cytoskeleton. Spectrin, ankyrin, protein 4.2 or band 3 are affected in HS, disrupting the interaction anchoring the cytoskeleton to the lipid bilayer, the so-called *vertical* interactions. HE patients display mutations in proteins tying the cytoskeleton together such as in spectrin self-association sites or protein 4.1-spectrin binding sites, termed *horizontal* interactions. However, hematological disorders involving ion channels have only recently been described thanks to facilitating sequencing methods being now available. These anemias were also named according to morphology, yet RBCs shape can be highly variable between patients leading sometimes to misdiagnosis if exome sequencing is not performed. (Dehydrated) Hereditary Stomatocytosis or Hereditary Xerocytosis have been reported in patients with mutations in Gárdos and Piezo1, with dehydration and stomatocytes being found in some, but not all cases [207, 271–275]. To avoid any ambiguity these hereditary anemias are henceforth called in this thesis Gárdos-HSt for the hematological disorder presenting mutations in Gárdos channel and Piezo1-HX for the anemia caused by mutations in Piezo1. These hematological disorders are characterized by wide heterogeneity in morphology and severity which has prevented the identification of Gárdos-HSt and Piezo1-HX as distinct anemias until very recently [276, 277]. Currently, either genetic panels (also called targeted-Next-Generation-Sequencing, t-NGS) are performed for diagnosis, as single-gene analysis was proven insufficient to establish causality of many hereditary anemias [278]. Even so, tNGS approaches have false-negative diagnosis rates of about 20%, requiring in those cases whole exome sequencing for unequivocal diagnosis. Common symptoms comprise muscle weakness, chronic fatigue and abdominal pain due to splenic enlargement [276]. Even though splenectomy has often been performed on Gárdos-HSt and Piezo1-HX patients, it is contraindicated in current clinical practice. Establishing the causative mutation of hereditary anemias is fundamental for clinicians as complications vary between Gárdos-HSt and Piezo1-HX. Prevalence is thought to be about one in 50 000 births [276], although genetic-based diagnoses only started to be carried out in the last decade, so more time will be necessary for detailed epidemiology studies. A recent epidemiological study focusing on phenotipic markers of HX has provided a prevalence estimate using a large US database on hematological parameters giving a tentative HX prevalence of 1 in 8 000 [279]. However, the study focuses only into dehydration markers, excluding some forms of Hereditary Stomatocytosis where dehydration is not present, some involving Gárdos mutations. Subsequent screenings based on this data will help to clarify the frequency of these anemias, at least in the US population.

In the present study, we monitor membrane potentials via CCCP method and use patch-clamp to characterize ion channel activity in patients having point mutations either in Gárdos or Piezo1 channels. The main objective of this transversal study was double:

1. Support diagnosis and link tNGS and exome sequencing results to functional activity of ion channels.

2. Develop a simple targeted method for diagnosis and disorder severity purposes through membrane po-

tential determination (CCCP method).

This chapter is divided in two parts. The first one contains results obtained from RBCs coming from patients affected with a mutation in gene KCNN4, the Gárdos channel. The second part deals with a series of mutations from patients afflicted with Piezo1-HX.

Materials and Methods

Reagents All salts were acquired from Sigma and of analytical grade or better. Nominal calcium-free solutions amount to 4 μM Ca^{2+} due to typical salt contamination [124].

Solutions normal Ringer: 154 mM NaCl, 2 mM KCl. Calcium Ringer: 154 mM NaCl, 2 mM KCl, 1 mM $CaCl_2$. Low Ionic Strength solution: 264 mM Sucrose, 2 mM KCl.

Drugs

CCCP (Sigma): (carbonyl cyanide 3-chlorophenylhydrazone)

A23187 (Sigma): (calcymicin; 5-(methylamino)-2-[[(2S,3R,5R,6S,8R,9R)-3,5,9-trimethyl-2-[(2S)-1-oxo-1-(1H-pyrrol-2-yl)propan-2-yl] -1,7-dioxaspiro[5.5]undecan-8-yl]methyl]-1,3-benzoxazole-4-carboxylic acid)

NS309 (Alomone): 6,7-Dichloro-1H-indole-2,3-dione 3-oxime

Yoda1 (Tocris): 2-[5-[[(2,6-Dichlorophenyl)methyl]thio]-1,3,4-thiadiazol-2-yl]pyrazine

Tram34 (Tocris): 1-[(2-Chlorophenyl)diphenylmethyl]-1H-pyrazole

Chloride inhibitors:

NPPB (Tocris): (5-nitro-2-(3-phenylpropylamino)benzoic acid)

NS3623 (Alomone) (N-(4-bromo-2-(1H-tetrazol-5-yl)phenyl)-N'-(3-trifluoromethyl-phenyl)urea)

GsMTx4 (Alomone): Peptide with sequence GCLEFWWKCNPNDDKCCRPKLKCSKLFKLCNFSF.

All were prepared as stock solutions in DMSO except for GsMTx4, which was dissolved in ultrapure water. DMSO concentrations did not exceed 0.3%, which is known not to cause any effect in fluxes nor membrane potentials [124].

Red blood cells Blood from either healthy human donors or patients with a mutation in Gárdos (gene KCNN4) or Piezo1 (gene Piezo1) channels was drawn into vacuum tubes and shipped from collaborating laboratories at 12-15 °C. Upon arrival blood was split according to experiments, with water, sodium and potassium content determination and smear imaging done with whole blood, whereas blood intended for membrane potential determination experiments was washed thrice with unbuffered saline by centrifugation for 5 min at 3 000 *g*, the buffy coat and plasma removed, with a final step of 1 minute at 15 294 *g*, and packed cells stored at 4 ° C until use.

Membrane potential determination The CCCP method was used for membrane potential determination [270]. See Chapter 2 on page 59 for a detailed explanation of the technique.

Cell water, Na^+ and K^+ content determination 0.5 ml aliquots of whole blood from either wild-type, Gárdos-HSt or Piezo1-HX as appropriate, were distributed in polyethylene micro test tubes and centrifuged at 20 000×*g* for 10 min at 4 °C. After centrifugation the packed cell mass was separated from the supernatant by slicing the tube with a razor blade below the top of the red cell column [280]. After weighing, the packed cells were dried to constant weight for at least 24 h at 90 °C and re-weighed.

RBC volume depends on the intracellular water content which is estimated to be about 90 fl for a healthy discocyte. Shape change can be misleading in the estimation of the cell's water content due to the great plasticity of the red cell membrane. These measurements are independent of cell shape.

The packed cells within the sliced tube were lysed in 1 ml MilliQ water. Proteins were denatured to ease separation by addition of 231.9 µM of perchloric acid. The tubes were spun at 16 900 g for 7.5 min at 4 °C and the supernatant passed onto samples tubes and diluted 10 times. The ionic content was measured using a flame photometer (PFP7, Jenway). Na^+ or K^+ measured are reported as concentration in mmol/cell water or as amount in µmol/g dry cell solid.

Patch-clamp

The patch-clamp technique was invented in 1976 by Neher and Sakmann [90] and developed in following years [91–93]. Their work earned them the Nobel Prize in 1991. The method enables the recording of membrane current or potentials using a single pipette containing an electrode. Hamill [94] made the first patch-clamp report in RBCs, hitherto considered unpatchable due to their small size. The electrode is made of Ag/AgCl with another reference electrode in the bath so that voltage can be zeroed.

In short, the experimenter approaches a solution-containing pipette with a blunt, cone-shaped end (with a diameter of about 1 µm and a pipette resistance of 10-15 MΩ) to a cell and briefly applies suction (about 4 kPa) allowing the formation of a very tight seal, which much be of a resistance higher than 1 GΩ. Gigaohm sealing is required for red cell patching in order to avoid leakage between the pipette and the membrane as the resulting noise would preclude any recording of actual cellular electrical events. Single channel currents can be measured in this way, what is termed cell-attached mode. If suction and a brief pulse of around one volt are applied at once on the membrane, it will rupture around the tip of the pipette, thus gaining access to the cytoplasm and allowing the recording of the every electrogenic source in the cell. This recording configuration is called whole-cell. Currents are typically measured by *clamping* the voltage (voltage-clamp, the reverse current-clamp enables measurements of voltages), that is, fixing it to a set value and recording the current change. Sequences of voltage changes in a step-wise manner for a range of milliseconds can be applied so that currents may be known for all physiological potentials.

Pipettes were pulled and heat polished from borosilicate glass capillaries (GC 150F Clark Electromedical) using an universal pipette-puller (DMZ, Zeitz Instruments).

The following solutions, providing notably calcium and potassium gradient, were employed:

Pipette solution (in mM): 145 KCl, 1.22 $MgCl_2$, 10 Hepes, 1.29 $CaCl_2$, 5 EGTA. Bath solution (in mM): 145 NaCl, 5 KCl, 1 $MgCl_2$, 10 Glucose, 10 Hepes.

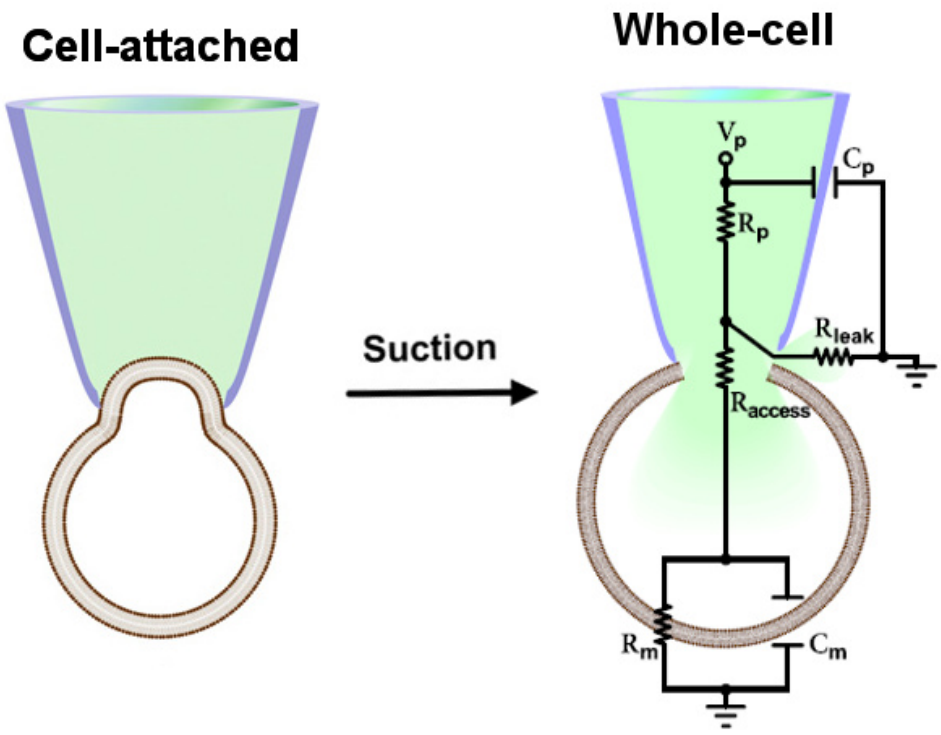

Figure 4.1: Overview of whole-cell configuration of patch-clamp.
Schematic showing the switch to whole-cell mode and its recording configuration equivalent circuit. V_p, R_p and C_p denote the voltage, axial resistance and capacitance of the pipette. V_m, R_m and C_m stand for the voltage, resistance and capacitance of the membrane. R_{access} is the resistance of the membrane hole created upon switch to whole-cell via the application of negative pressure. R_{leak} denotes the leak resistance which depends on the tightness of the seal between the glass of the pipette and the membrane. Only recordings where seals are greater than 1 GΩ are considered, precisely to minimize leak through the gap, which is key for human RBC patch-clamping given their small size. Adapted from [281].

Morphology

Erythrocyte morphology was assessed via smears on slides fixed with methanol and stained 10 min with 5% Giemsa (Sigma-Aldrich). Images were acquired and shape descriptors, such as projected area, were obtained with software ImageJ.

Roundness was obtained with ImageJ according to the formula:

$$Roundness = 4 \times \frac{[Area]}{\pi \times [MajorAxis]^2}$$

Circularity was obtained with ImageJ according to the formula:

$$Circularity = 4\pi \frac{[Area]}{[Perimeter]^2}$$

Gárdos channelopathy

A mutation-causing disease on the Gárdos channel was first described in 2015 and classified as a variant of hereditary xerocytosis [271–273]. Elliptocytes, acanthocytes, dacryocytes and schistocytes were found in patients' blood, but stomatocytes were very rare, which is why the disease is sometimes termed xerocytosis instead of dehydrated hereditary stomatocytosis (dHSt). Gárdos-HSt has been described in several families and linked to point mutations in gene KCNN4, which encodes the Gárdos channel, such as R352H or V282M/E mutations,

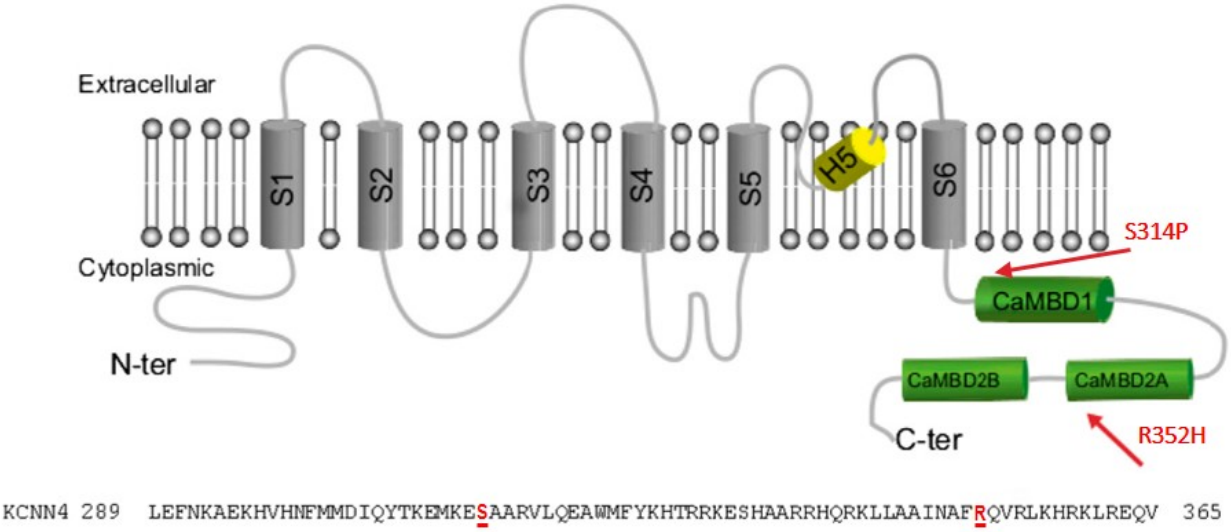

Figure 4.2: Gárdos protein domains.
Scheme showing the general structure of a Gárdos channel monomer with the Calmodulin Binding Domains in green and the mutations studied marked with an arrow. The functional channel arranges itself as a homotetramer, with each subunit binding to one calmodulin. Adapted from [271]

.

among others [271, 272, 282]. The main clinical consequence of the disease is said to be red cell dehydration which leads to hemolysis, hence the term 'xerocytosis'. The dehydration would be explained by the fact that a small calcium influx, such as one triggered by Piezo1 activation during capillary passage stretching, entails a strong and more sustained activation of Gárdos in affected RBCs rather than the brief opening of a healthy erythrocyte. Nevertheless, lack of dehydration has been observed in patients with mutation R352H, differentiating the disorder with hereditary xerocytosis [282].

In the present study, in the frame of a collaboration with Paola Bianchi's group (Milan, Italy), I studied erythrocytes from patients affected by two mutations: i) the already described R352H and ii) the nondescribed S314P. Both mutations are located near or within Calmodulin Binding Domains (CBD) 1 and 2 of the Gárdos channel (**Fig. 4.2**). It has been hypothesized that such a mutation, at least for R352H, makes the channel more sensitive to calcium, thus leading to an abnormal, increased open probability [271, 282]. Calmodulin binds tightly to CaMDB1 via its C-lobe, whereas the N-terminal binds CaMDB2 in a Ca^{2+}-dependent manner, acting on the S4-S5 linker which changes conformation and opens the pore [139]. One calmodulin associates for each Gárdos monomer for a total four calmodulins in the assembled tetramer. S314P mutation falls within CaMDB1 while R352H mutations occurs at CaMDB2.

R352H Gárdos RBCs

We present data from 5 different patient samples, summarized in **Table 4.1** with relevant hematological parameters. However, due to low blood volumes precluding some experiments or their replication while encountering technical problems, not all samples (n=5) are featured in every figure. Experiments are consistent with literature findings.

R352H Gárdos Patients	P1	P2	P3	P4	P5
Date	June 2017	September 2017	April 2018	June 2019	June 2019
Hematocrit (%)	30.2	32	29.9	—	—
MCV (fl)	82.5	104.9	87.7	—	—
Reticulocytes (%)	7.8	11.1	—	—	—

Table 4.1: R352H Gárdos-HSt patient blood samples
Gárdos-HSt patients with mutation R352H who have participated in this study and selected hematological parameters, when available. Note that they do not appear in every figure due low blood volumes precluding some experiments or their replication while encountering technical problems. Pooled data is consistent with clinical reports.

Intracellular water, cation content and morphology of R352H Gárdos RBCs

Upon arrival, measurements of intracellular water, Na^+ and K^+ were performed on control and patient erythrocytes. Control blood from a healthy donor was always included in the shipment to account for transportation alterations, as it is known blood transport affects cells [283, 284]. Hence, the behavior of donor cells, either from healthy volunteers or patients, differs not only according to typical interpersonal variability but also due to the effect of transporting conditions on cells.

R352H Gárdos RBCs appear larger and a number of aberrant shapes are found such as schistocytes, acanthocytes and swollen nondiscoid red cells (**Fig. 4.3B**). R352H Gárdos RBCs are also less round, more elliptical as confirmed not only visually but by calculation of the roundness ratio ($p<0.001$, Mann-Whitney) (**Fig. 4.3C**). In addition, their circularity is reduced compared to wild-type RBCs, as cells present spurs in their surface, and acanthocytes are indeed found ($p<0.001$, Mann-Whitney)(**Fig. 4.3D**). Whereas discocytes from a control donor had an area of 39.1 ± 0.1 μm^2 (mean ± SEM, n=2226), R352H Gárdos displayed a significantly larger area: 46.2 ± 0.2 μm^2 (mean ± SEM, n=1911) ($p<0.001$, Mann-Whitney)(**Fig. 4.3E**). Therefore, erythrocytes in R352H Gárdos patients' blood are in general more elliptical, spurred and have an increased surface area.

Gárdos activation leads to exit of K^+ and osmotically obliged water, causing cell shrinkage. Albeit, R352H Gárdos RBCs were found to be overhydrated, contrary to the expectation that increased sensitivity of the mutated channel to calcium should entail frequent channel openings and thus potassium, and water, efflux. RBCs from Patient 1, Patient 2 and Patient 4 have 7.1% (**Fig 4.4A**), 8.9% and 5.1% (**Fig. 4.4C**), respectively, more intracellular water than control cells. Excluding Patient 3 as an outlier this increase is significant ($p=0.049$, n=3), otherwise it is not ($p=0.572$, n=4). Severe hemolysis and erythrocyte fragility on sample arrival precluded accurate measurements for Patients 3 and 4, and may account for the discrepancy. Hence, cation amounts are shown in order to elucidate whether cation movements actually occur. Intracellular sodium amount is increased by 43.91 % ± 26.09 % (n=4) in contrast to control RBCs. In terms of concentration, there is also a mean increase of 7.4 ± 4.9 µmol/l cell water ($p=0.076$). Both sodium concentrations and amounts are elevated in Patients 2, 4 and 5 explaining overhydration via sodium influx (**Fig. 4.4C-F**). Thereby, overhydration is not masking cation movements, but revealing them. Intracellular potassium levels of R352H RBCs display a modest decrease of -9.21 % ± 4.36 % ($p=0.107$, n=4) compared to control (**Fig. 4.4A, C and E**). Potassium amounts are similar to control, so potassium efflux due to Gárdos activation is restrained by another mechanism.

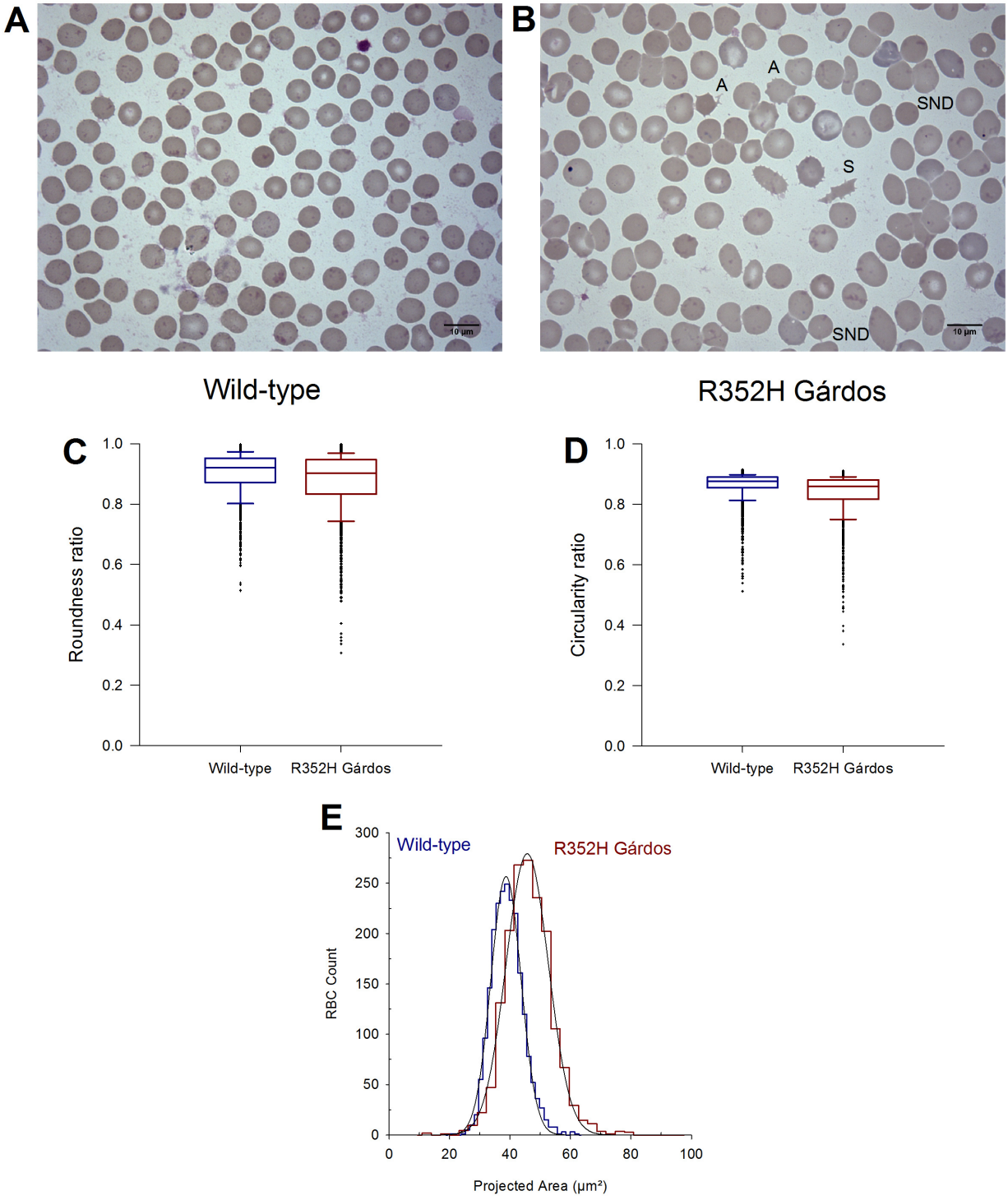

Figure 4.3: Morphology of R352H Gárdos RBCs.

Erythrocyte photographs from a wild-type donor (**A**) and R352H Gárdos patient 2 (**B**). It is representative of all R352H Gárdos RBCs analyzed, save for cellular area being lower than control in Patient 3. Arrows point to abnormal shapes. Roundness (**C**), circularity (**D**) and projected cell area (E) of wild-type and R352H Gárdos RBCs. Roundness and circularity are ratios and hence dimensionless. They are calculated according to: $Roundness = 4 \times \frac{[Area]}{\pi \times [MajorAxis]^2}$ and $Circularity = 4\pi \frac{[Area]}{[Perimeter]^2}$ Roundness, circularity and projected cell area are significantly different between wild-type and R352H Gárdos RBCs ($p<0.001$, Mann-Whitney). Aberrant RBCs in Panel B: A denotes acanthocyte; S, schistocyte; SND, Swollen NonDiscoid cell.

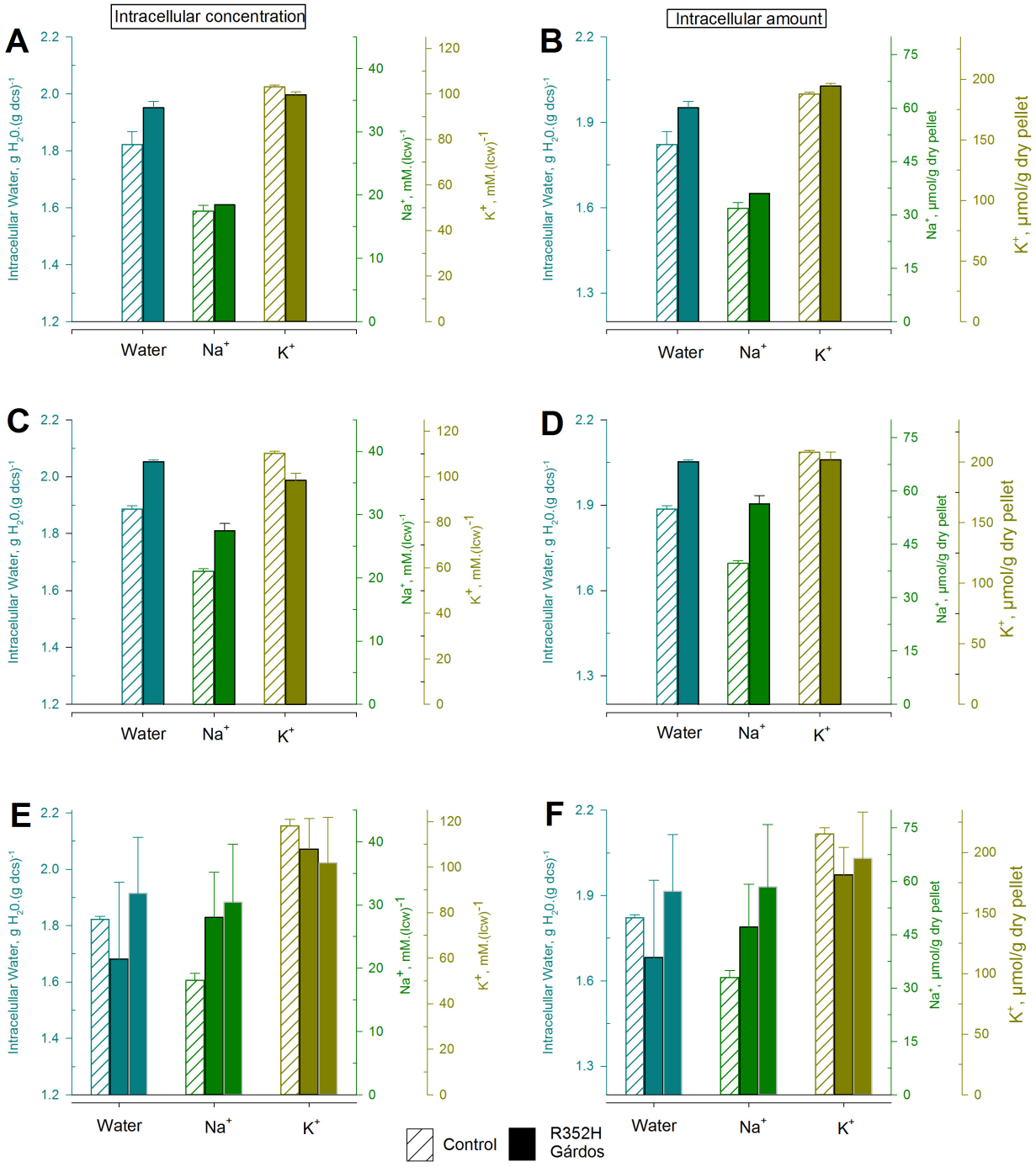

Figure 4.4: Cell water, sodium and potassium content of R352H Gárdos erythrocytes.
Intracellular concentrations (**A**, **C** and **D**) and amounts (**B**, **D** and **F**) of water, Na^+ and K^+ of RBCs from patients with R352H Gárdos mutation. Patient 1 (**A** and **B**), Patient 2 (**C** and **D**) and Patients 4 and 5 (**E** and **F**) are shown. Shipped controls are striped bars whereas Gárdos mutants are solid bars.

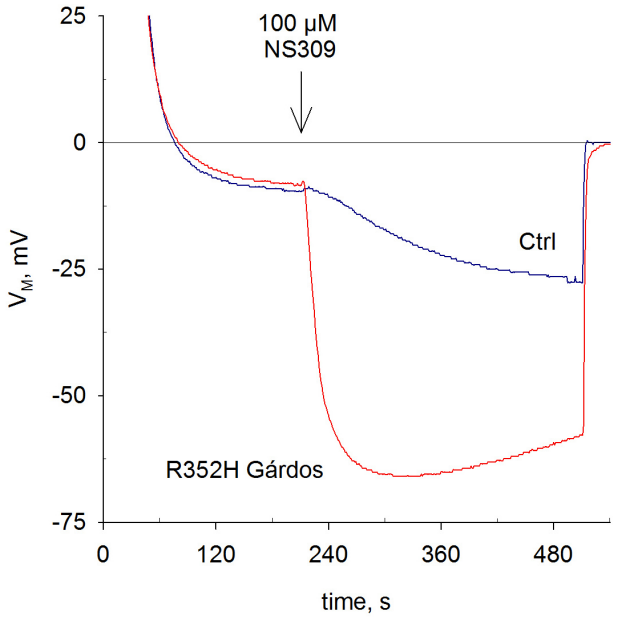

Figure 4.5: R352H Gárdos RBCs display enhanced calcium sensitivity.
Membrane potential traces from control and R352H Gárdos cells injected into normal Ringer and treated with Gárdos activator NS309 (100 µM). Patient 1 is shown.

Determination of calcium sensitivity of R352H Gárdos

As previously mentioned, R352H mutation impacts CaMDB2 (**Fig. 4.2**). Certainly such a mutation affects Gárdos Ca^{2+} sensitivity, as previously claimed [285], enhancing the open probability of the channel. Previous experiments have proven the value of NS309 as a potent Gárdos activator that does not induce Ca^{2+} entry (Chapter 3 on page 69) [286]. Indeed NS309 lowers the calcium concentration threshold needed for channel activation. Treating RBCs with NS309 immediately reveals the increased sensitivity to calcium of R352H Gárdos erythrocytes compared to control (**Fig. 4.5**). The maximum hyperpolarization reached is 38.2 mV greater for R352H Gárdos RBCs than wild-type cells.

In order to determine the extent of the increase in calcium sensitivity, control and R352H patient cells were subjected to 10, 50 and 100 µM NS309 in nominally calcium-free solution (**Fig. 4.6**). In both patient and control RBCs, the increase in maximum hyperpolarization is dose-dependent. The higher the concentration, the larger the hyperpolarization reached. However, whatever the concentration employed, hyperpolarization of R352H Gárdos RBCs is always much more pronounced compared to control erythrocytes ($p \leq 0.008$). Even more importantly, the lowest concentration of NS309 (10 µM) triggers a stronger hyperpolarization than those recorded in control RBCs at the highest concentration (100 µM) ($p=0.060$). 10, 50 or 100 µM NS309 addition leads R352H Gárdos cells reach hyperpolarizations 4.7 ± 0.8 (n=4), 3.4 ± 1.0 (n=4) or 2.2 ± 0.7 (n=4) times larger than wild-type erythrocytes, respectively. A ten-fold lower concentration of NS309 elicits a stronger channel response in R352H Gárdos cells than wild-type erythrocytes. Concomitantly, a measurable slight repolarization immediately follows Gárdos-induced hyperpolarization indicating that either an anionic or cationic pathway is then active. Hence, R352H RBCs display a calcium sensitivity several times higher than wild-type calcium thresholds for Gárdos activation.

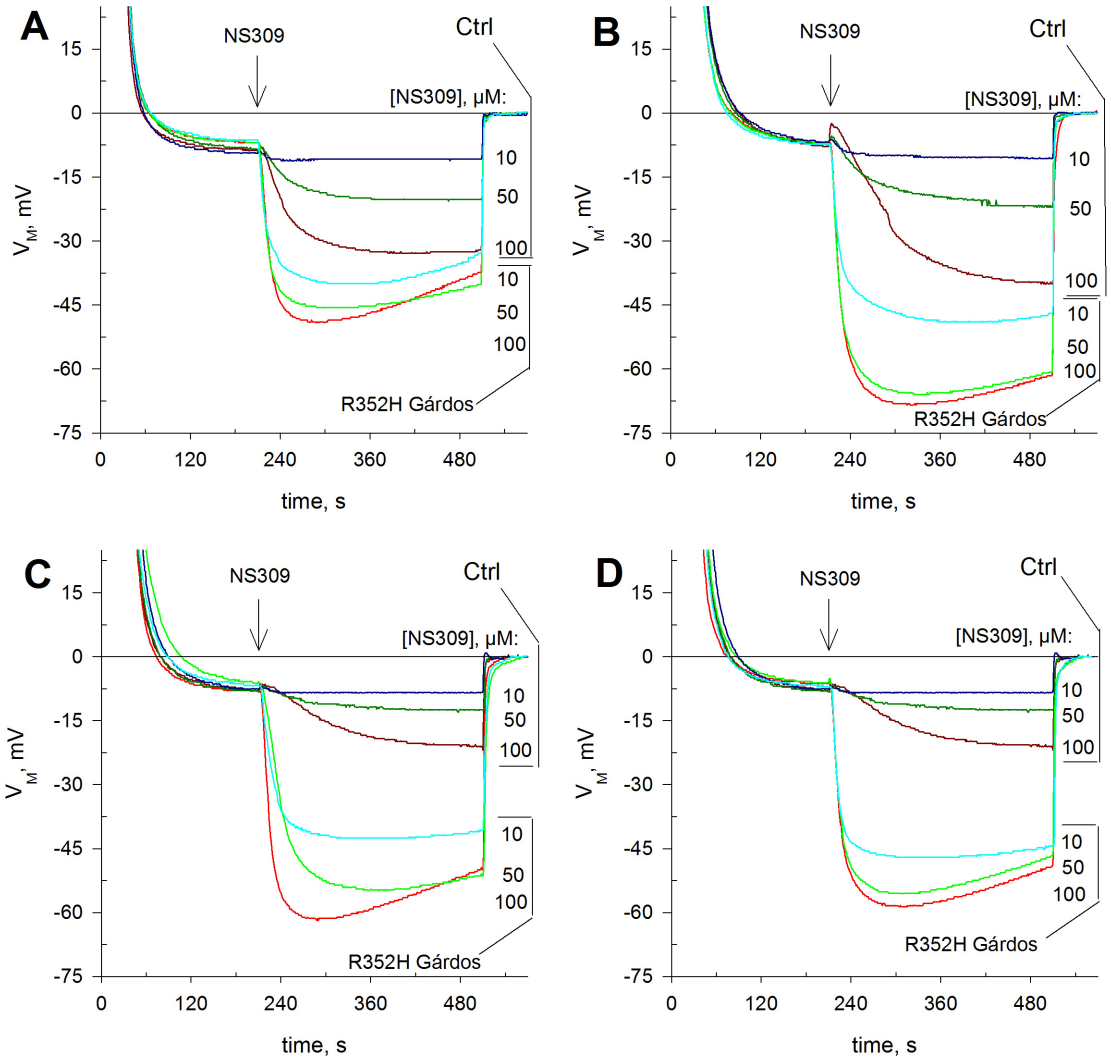

Figure 4.6: Enhanced calcium sensitivity of R352H Gárdos RBCs is one order of magnitude above wild-type. (**A-B**) Membrane potential traces from control and patients' erythrocytes with R352H Gárdos mutation injected into normal Ringer solutions and treated with 10, 50 or 100 µM of Gárdos activator NS309. On the right, order of NS309 concentration of each trace, top to bottom: 10, 50 and 100 µM NS309. R352H Gárdos traces are in bright colors with concentrations underlined. Patient 2 (**A**), 3 (**B**), 4 (**C**) and 5 (**D**) are shown. Each panel is an independent measurement from different donors, except in panels C and D where controls are the same, as there was a common shipped control for two patient samples.

Chloride conductance inhibition to reveal full channel activity

The chloride conductance is predominant in human RBCs. When a cationic conductive pathway, such as Gárdos, is opened in addition to the cation efflux an anionic efflux will follow due to the favorable driving force. In this manner, the extent of the activation and its impact on V_M is partially masked by a current of opposite sign. Hence, inhibition of the chloride conductance allows to study the full extent of Gárdos activity and the increased activity conferred by the mutation. In the presence of 10 µM NS3623, R352H Gárdos cells reach a mean maximum hyperpolarization of -89.2 ± 3.5 mV (n=5) whereas controls cells attain -60.6 ± 10.5 mV (n=5) ($p \leq 0.001$)(**Fig. 4.7**). A key finding is the instantaneous hyperpolarization that ensues only in R352H cells after NS309 treatment. This response closely resembles a typical A23187-induced hyperpolarization of wild-type cells, due to huge calcium influx. The initial rate of hyperpolarization (v_0^{hyp}) was -0.42 ± 0.15 mV/s

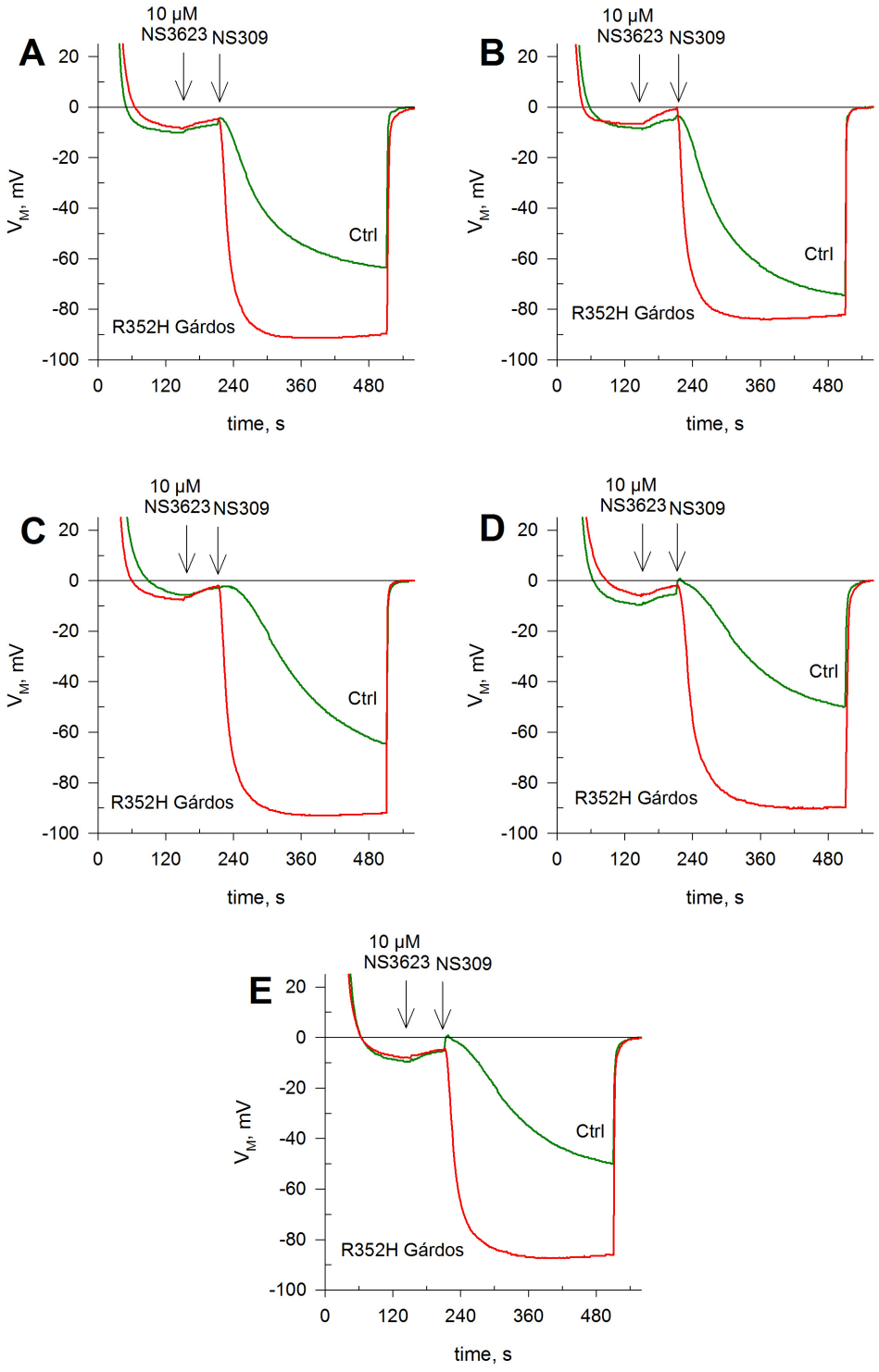

Figure 4.7: R352H Gárdos RBCs reach the Nernst equilibrium for potassium upon channel activation when G_{Cl^-} is blocked.

Membrane potential traces from control and patients' erythrocytes with R352H Gárdos mutation injected into normal Ringer solutions and treated with chloride conductance inhibitor NS3623 (10 µM) followed by Gárdos activator NS309 (100 µM). Patient 1 (**A**), 2 (**B**), 3 (**C**), 4 (**D**) and 5 (**E**) are shown. Each panel is an independent measurement from different donors, except in panels D and E where the same nonshipped control is shown, as the common shipped control volume was insufficient to carry out the experiment, therefore requiring the use of nonshipped wild-type RBCs.

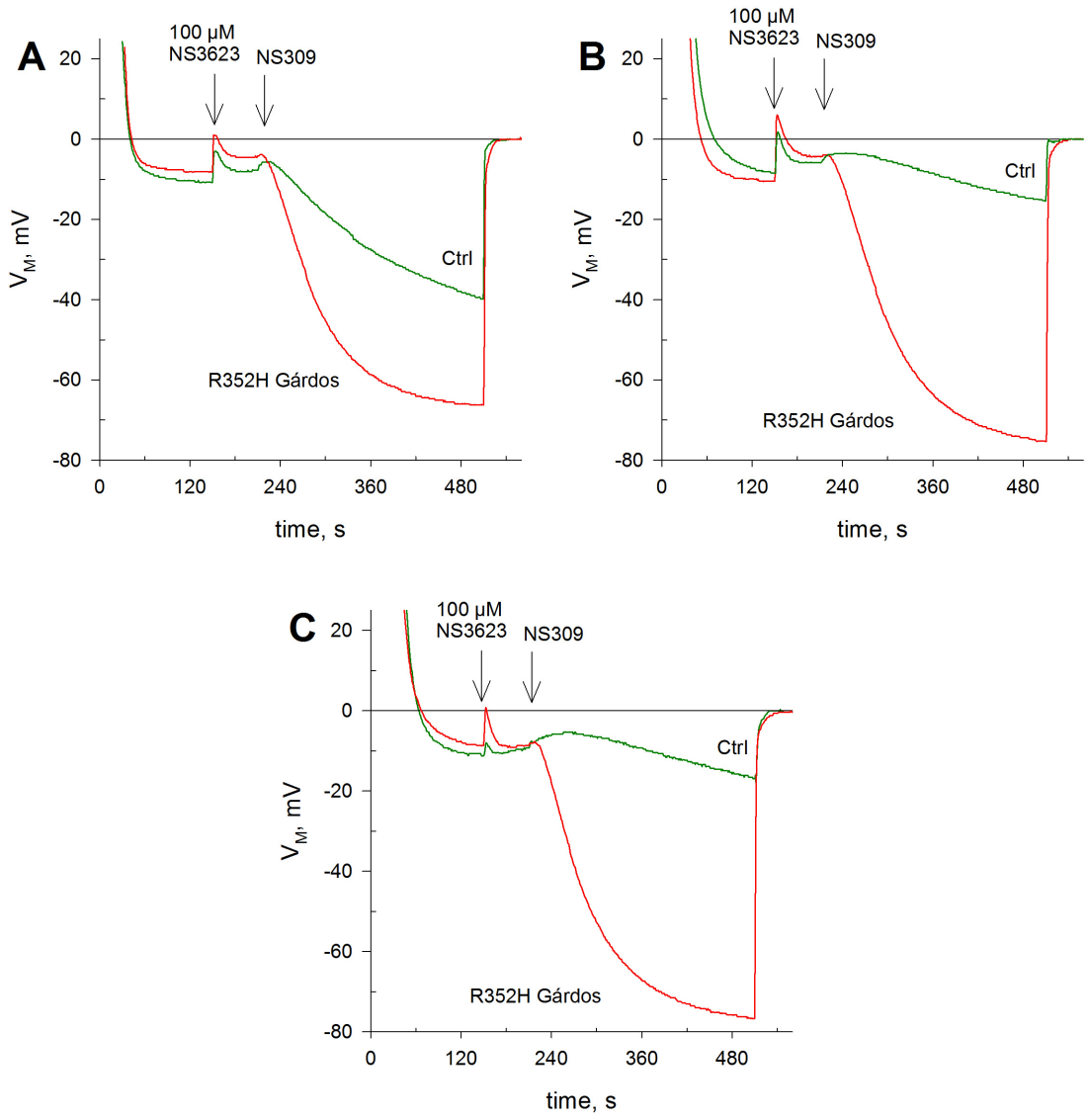

Figure 4.8: Strong Gárdos activation of R352H Gárdos RBCs despite the enhancement of NSC activity. Membrane potential traces from control and patients' erythrocytes with R352H Gárdos mutation injected into normal Ringer solutions and treated with chloride conductance inhibitor and NSC enhancer NS3623 (100 µM) followed by Gárdos activator NS309 (100 µM). Patient 2 (**A**), 3 (**B**) and 4 (**C**) are shown. Each panel is an independent measurement from different donors. Due to low blood volume availability, Panel C displays a response from nonshipped wild-type RBCs.

(n=5) for control RBCs compared to -3.19 ± 0.49 mV/s (n=5) of R352H Gárdos erythrocytes ($p<0.001$). A finding consistent with the reported augmented sensitivity to calcium as well as with experiments shown before (**Fig. 4.6**). Calcium levels stay at the nanomolar range in wild-type cells at rest and, therefore, below the threshold for Gárdos activation. R352H Gárdos RBCs, in contrast, have a lower threshold of activation, so that the same small calcium influx activates the Gárdos channel.

Enhancement of NSC in R352H Gárdos RBCs

Treating R352H Gárdos cells with 100 µM NS3623, as well as inhibiting the chloride conductance, enables the opening of a Non Selective Cation Channel (NSC) in hyperpolarizing conditions (Chapter 3 on page 69) [286]. Thus, it allows us to ascertain what impact the NSC has in the strong maximal Gárdos current seen in R352H Gárdos cells as it is a gateway for Ca^{2+}. Treatment with 100 µM NS3623 plus NS309 (100 µM) caused a marked

hyperpolarization in Gárdos R352H RBCs compared to control red cells. Mean maximum hyperpolarizations were -24.6 ± 13.3 mV (n=3) for control RBCs compared to -72.7 ± 5.7 mV (n=3) of R352H Gárdos erythrocytes (p=0.005). Variation among controls and patients is widespread and highlights the interest of this technique as it allows to measure the actual channel activity that may vary between subjects with the same mutation. Hence, whereas **Figure 4.8A** shows a difference of 26.36 mV between wild-type and R352H Gárdos RBCs, **Figure 4.8B** displays a difference of 59.89 mV. The initial rate of hyperpolarization, v_0^{hyp}, was -0.09 ± 0.07 mV/s (n=3) for controls, whereas it was -0.61 ± 0.05 mV/s (n=3) for R352H RBCs, though control RBCs on **Figure 4.8A** deviate from the others (p=0.1, Mann-Whitney). Calcium variability in shipped controls is a finding reported in a study identifying calcium as a marker of anemia [283]. Following treatment of R352H Gárdos erythrocytes with 100 μM NS3623 plus NS309 (100 μM), maximum hyperpolarizations were not altered or only slightly compared to 10 μM NS3623, but rather the rate of hyperpolarization was, so it is evident that NSC channel activity is masking the hyperpolarization. These experiments allowed to test whether an increase in intracellular calcium levels, without calcium addition to the medium but via stimulation of a calcium conductive pathway such as the NSC, would lead to a greater Gárdos activation compared to 10 μM NS3623 pretreated red cells. Indeed, the fact that V_M^{maxhyp} is greater in 10 μM NS3623 pretreated R352H Gárdos RBCs and that an equilibrium is reached by the end of the experiment strongly suggest R352H Gárdos erythrocytes undergo maximal Gárdos activation under NS309 stimulation.

Gárdos activation via calcium ionophore

A calcium ionophore, A23187, was employed to make a comparative analysis between control and R352H Gárdos erythrocytes where Gárdos is maximally activated. Upon A23187, RBCs quickly load up with calcium triggering a Gárdos opening and an instantaneous hyperpolarization. A23187 treatment of R352H cells induces a slightly reduced hyperpolarization compared to control cells. R352H Gárdos RBCs hyperpolarize to -58.8 ± 12.3 mV (n=5) compared to -65.20 ± 9.35 mV (n=5) of wild-type erythrocytes (p=0.421)(**Fig. 4.9**). Even though there is variation in the extent of hyperpolarization, the repolarization observed after reaching the new equilibrium is significantly faster in R352H Gárdos erythrocytes overall than control cells. Hence, R352H RBCs repolarize at a rate of 0.050 ± 0.014 mV/s (n=5) compared to 0.026 ± 0.016 mV/s (n=4) of wild-type cells (p=0.048). As both wild-type and R352H Gárdos channels must be maximally activated under the effect of A23187, which equilibrates extra- and intracellular calcium concentrations, R352H Gárdos RBCs' reduced hyperpolarization is explained by either reduced intracellular potassium levels or increased NSC activity, which reduces the driving force. Potassium levels are similar between wild-type and R352H Gárdos red cells (**Fig. 4.4**). Once a maximum hyperpolarization has been reached, a Na^+ influx is apparent as confirmed by the heightened repolarization rates observed.

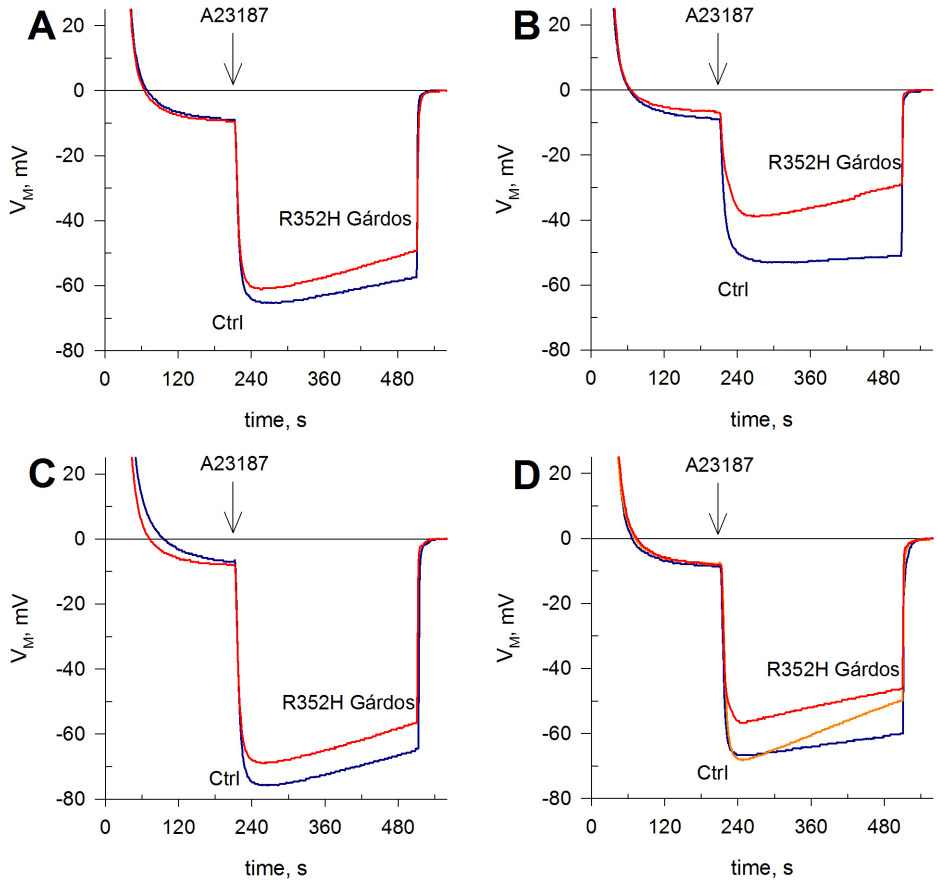

Figure 4.9: Reduced hyperpolarizations of R352H Gárdos RBCs when cytosolic calcium levels are at saturation.

(**A-E**) Membrane potential traces from control (blue trace) and patients' erythrocytes with R352H Gárdos mutation (red or orange traces) injected into normal Ringer solutions and treated with 10 µM NS3623 followed by calcium ionophore A23187 (10 µM). Patient 1 (**A**), 2 (**B**), 3 (**C**), 4 (**D**, red trace) and 5 (**D**, orange trace) are shown. Each panel is an independent measurement from different donors.

Patch-clamp protocol for Gárdos activation

Even though membrane potential estimation is a powerful method to investigate ion channel activity alterations upon mutations, it only gives a populational picture while the specific behavior at the cell level may be concealed when looking at the whole population. As mentioned before, although laborious, patch-clamp allows such an investigation. Performing both techniques enables us to gather information at both cell and population level, shedding light on the pathophysiology of the mutation. Considering that according to the literature, Gárdos is activated by Ca^{2+} entry through Piezo1 channel openings, I developed a specific protocol amenable to trigger Gárdos currents via pharmacological activation of Piezo1. Such protocol in whole-cell configuration requires triggering Piezo1 activity by use of Yoda1 (5 µM). For the sake of simplicity, in order to preserve seal resistance by limiting the number of perfusion procedures, as well as to avoid any prior mechanical Ca^{2+} entry upon seal formation [140], sealing is performed in calcium-free medium. Yoda1 is subsequently added in to a solution containing 1 mM Ca^{2+} (final concentration) and thus current changes are followed by successive stimulation sweeps of different voltages. The origin of membrane currents thus elicited are assessed by pharmacological approaches: i) by using the specific Gárdos channel inhibitor Tram34, ii) Gd^{3+}+ as an inhibitor of mechanosensitive channels and iv) if the seal remains stable, by washing the bathing solution out, restoring a

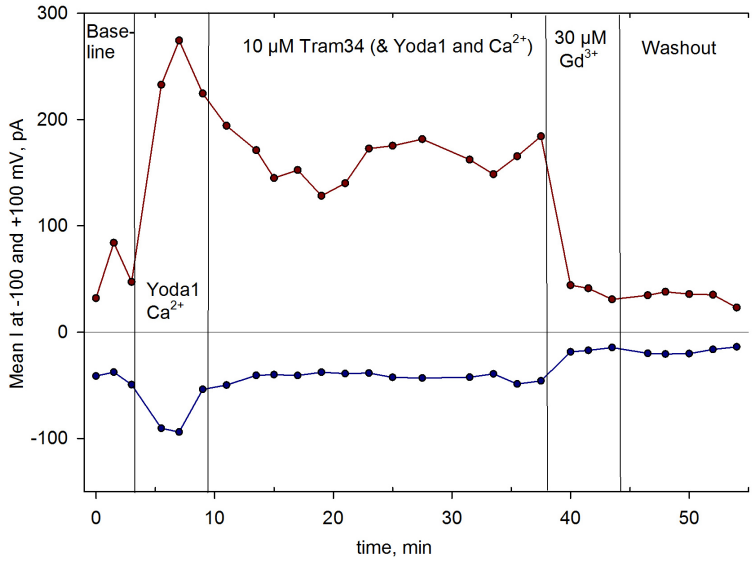

Figure 4.10: Typical patch-clamp current evolution when performing a protocol developed to observe Gárdos activity.

Representative experiment (from **Fig. 4.11** data) of Gárdos activation protocol via Piezo1 pharmacological stimulation. Mean whole-cell currents (pA) at +100 mV or -100 mV evolution over time upon addition of agonist- or inhibitor-containing solutions. Washout indicates baseline solution without any compound nor calcium. See materials and methods for details.

calcium-free solution at the end of experiment (**Fig. 4.10**).

At baseline, the solution surrounding the RBC lacks calcium, whereas there are minute amounts in the pipette. Yoda1 (5 µM) stimulation along with $CaCl_2$ elicits, in a subset of RBCs patched, a sudden current increase within 200-300 pA as early as 90 seconds after application, though wide variability is observed between cells. Yoda1-evoked currents may spontaneously decrease over time, pointing to channel closure. Tram34 inhibits most of the current if subsequently applied, revealing Gárdos contribution to the overall current. Moreover, unspecific Non Selective Cation channel inhibitor Gd^{3+} blocks nearly any residual current. A final washout, with bathing solution devoid of calcium, restores the cell medium to the original calcium-free solution, bringing whole-cell currents to baseline levels and underscoring the need of calcium for channel openings. Seals that are stable over 30 minutes are rare, thereby precluding the use of some inhibitors in some cells. It is considered more desirable to allow more time to record the response to Yoda1 and to allow for Tram34 inhibition, which has been observed to take long in contrast with Gd^{3+} which is nearly instantaneous. The fact that the conductance is outwardly rectified is in agreement with K^+ efflux via Gárdos. Thus, larger currents are observed at positive voltage than at equal voltages of opposite sign. Only cells with a seal above 1 GΩ after whole-cell access and 5 minute stability of such resistance were considered. Furthermore, only a fraction of cells were found to respond to Yoda1 stimulation (not shown), about 20%, by account of current increase. It is unknown why Piezo1 fails to open in those cases, but three interrelated possibilities may be considered: i) patching RBCs up to gigaohm resistance requires suction (negative pressure) so that Piezo1 may be refractory to pharmacological due to the sustained mechanical stimulation and closes quickly after patching, before recording begins. ii) patching imposes a spherical shape on RBCs, potentially disrupting the lipid bilayer curvature required for activation either by mechanical stimulation or due to loss of access to Yoda1-binding amino acids. iii) switching to whole-cell mode implies access to the cytoplasm by rupturing the membrane bleb the pipette is on, therefore Piezo1 may be removed in this manner, given there are few channels and they may be clustered.

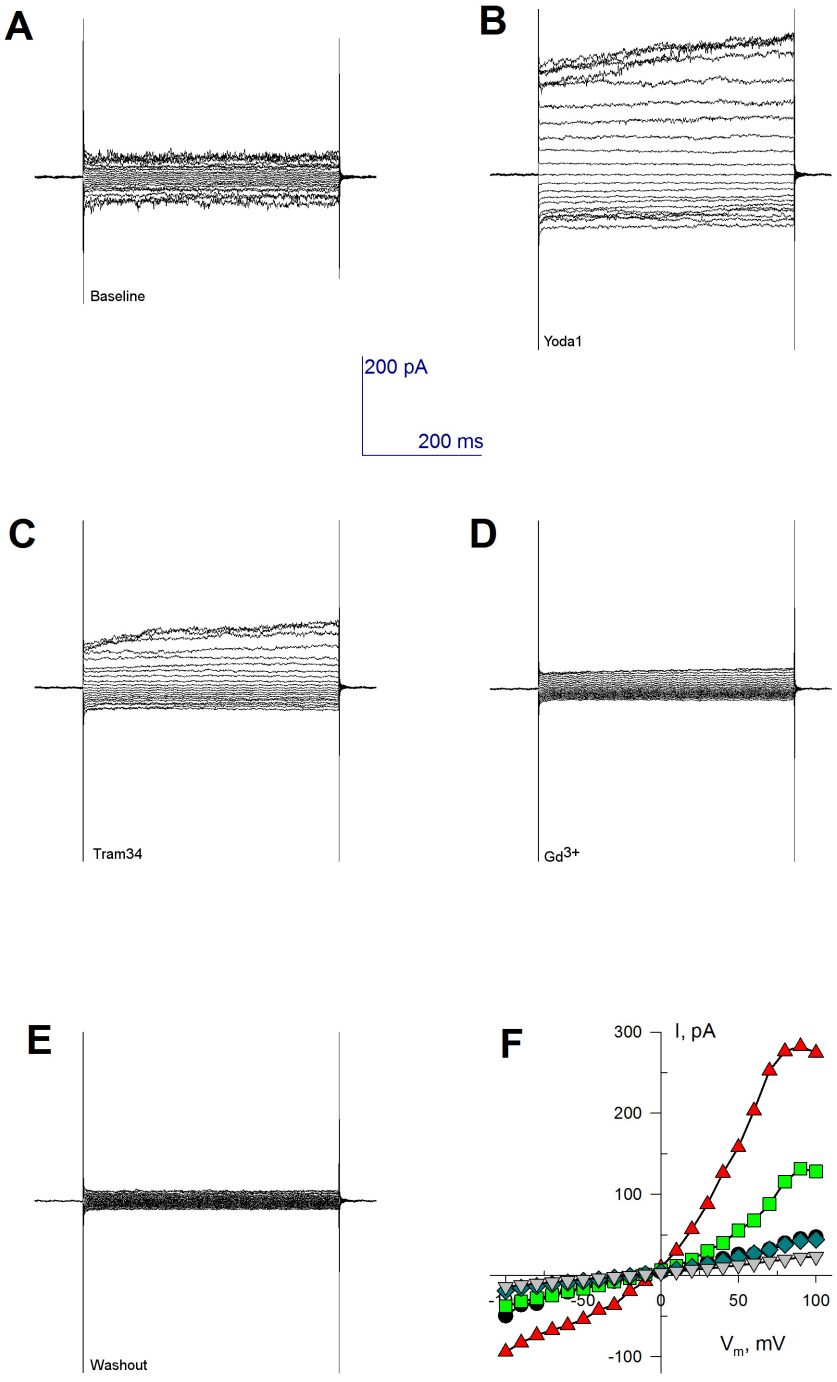

Figure 4.11: Piezo1-mediated Gárdos activity of a wild-type cell in whole cell mode configuration of patch-clamp.

Whole-cell currents (pA) over time (ms) during a voltage ramp from -100 mV to 100 mV in the span of 300 ms. **A**. Baseline current. **B**. 3 min after addition of Yoda1 (5 µM). **C**. 5 min after addition of Tram34 (10 µM). **D**. 1.5 min after addition of Gd^{3+} (30 µM). **E**. 9 min after washout (baseline solution). **F**. I/V curve of A-E. Black circles: baseline. Red triangles: Yoda1. Green squares: Tram34. Teal diamonds: Gd^{3+}. Gray triangles: washout.

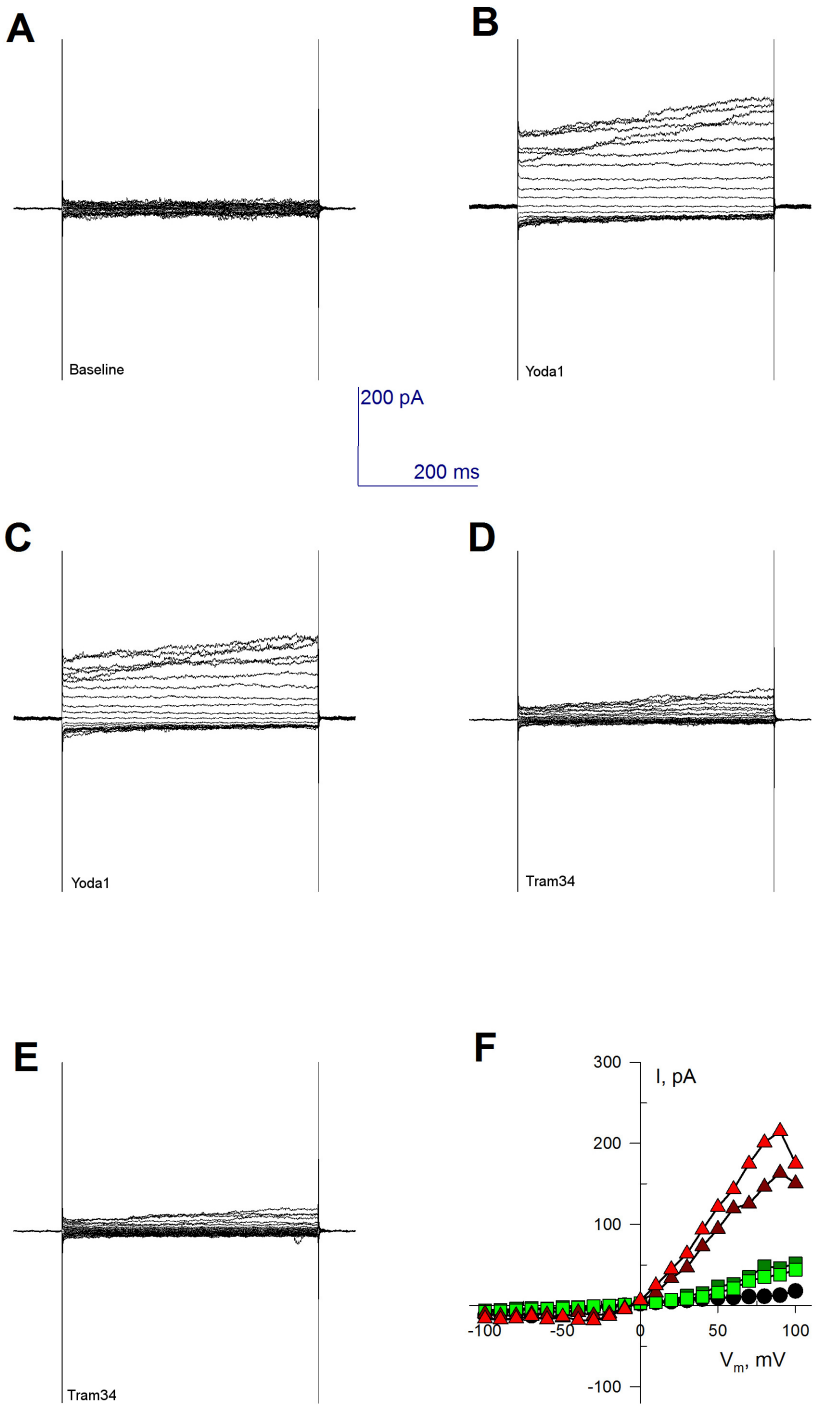

Figure 4.12: Piezo1-mediated Gárdos activity of a wild-type cell in whole cell mode configuration of patch-clamp.

Whole-cell currents (pA) over time (ms) during a voltage ramp from -100 mV to 100 mV in the span of 300 ms. **A**. Baseline current. **B**. 1.5 min after addition of Yoda1 (5 µM). **C**. 5 min after addition of Yoda (5 µM). **D**. 1.5 min after addition of Tram34 (10 µM). **E**. 3.5 min after addition of Tram34 (10 µM). **F**. I/V curve of A-E. Black circles: baseline. Red (bright: 1.5 min; dark: 5 min) triangles: Yoda1. Green (bright: 3.5 min; dark: 1.5 min) squares: Tram34.

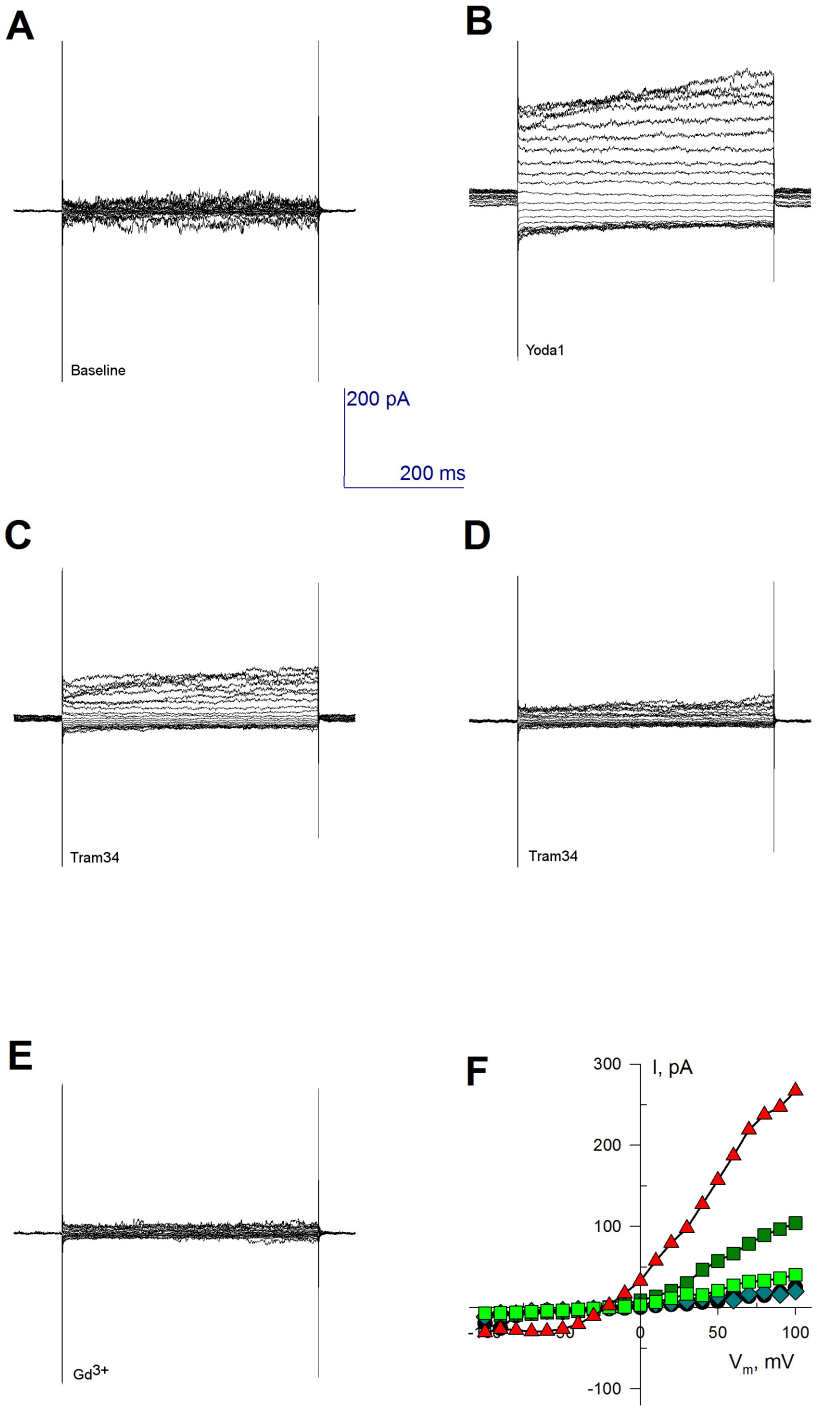

Figure 4.13: Piezo1-mediated Gárdos activity of a wild-type cell in whole cell mode configuration of patch-clamp.

Whole-cell currents (pA) over time (ms) during a voltage ramp from -100 mV to 100 mV in the span of 300 ms. **A**. Baseline current. **B**. 1.5 min after addition of Yoda1 (5 µM). **C**. 1.5 min after addition of Tram34 (10 µM). **D**. 4 min after addition of Tram34 (10 µM). **E**. 1.5 min after addition of Gd^{3+} (30 µM). **F**. I/V curve of A-E. Black circles: baseline. Red triangles: Yoda1. Green (bright: 4 min; dark: 1.5 min) squares: Tram34. Teal diamonds: Gd^{3+}.

Three representative wild-type recordings are shown, with variable timing being due to seal stability and to ascertain the maximum extent of activation or inhibition, which varies from one cell to another. **Figure 4.11** shows an erythrocyte with an overall current of around 50 pA at +100 mV at rest (**Fig. 4.11A**). Yoda1 stimulation brings the current almost to 300 pA at +100 mV (**Fig. 4.11**B, F). Yoda1 also allows the development of inward currents, which are increased up to -100 pA, suggesting that part of this current can be accounted for by Na^+ entry through Piezo1. This assumption is supported by the failure of Tram34 to fully inhibit this current, even at a concentration above reported IC_{99} [117]. In addition, it is important to note that Tram34 inhibitions kinetics may not be immediate as shown in **Figure 4.12**. Nonetheless, addition of the unspecific inhibitor Gd^{3+}+ abolishes the remaining current almost completely, supporting this notion. Finally, a washout procedure confirmed calcium dependence of Yoda1-evoked currents. Minimal whole-cell current is observed 9 minutes after washout of calcium- and compound-containing medium (**Fig. 4.11E**). Albeit with changes in overall amplitude, **figure 4.12** and **figure 4.13** present similar results with two other wild-type RBCs.

This protocol was proven successful with healthy, wild type cells. Its use on erythrocytes from a patient with mutations in Gárdos should provide with better characterization of Gárdos channel activity within a single cell, thus allowing to know the extent of the augmented abnormal current. It is noteworthy that all mutants described so far are heterozygotes, meaning that they carry both wild-type and malfunctioning channels. Most channelopathies have proven that point mutations can alter different ion channel properties such as ligand affinity, open probability, desensitization and gating properties.

Figure 4.14 shows whole-cell currents from a R352H Gárdos-HSt erythrocyte increasing dramatically to about 200 pA 90 seconds after Yoda1 stimulation, and beyond, up to 500 pA at 100 mV 5 min after Piezo1 agonist addition (**Fig. 4.14B, C, F**). Significant inhibition of outward current is observed as early as 90 s after Tram34 exposure, with a near-baseline block by 3 minutes indicating that Gárdos is the main contributor to the current recorded (**Fig. 4.14D, E**). The current increase is about 10 times that observed on stimulated shipped control RBCs (not shown). It is in agreement with one-order-of-magnitude increase in calcium sensitivity seen in membrane potential determination experiments with NS309 where Gárdos activation induced by 10 µM NS309 is more pronounced in R352H Gárdos RBCs than that induced by 100 µM NS309 in wild-type erythrocytes (**Fig. 4.6**).

S314P Gárdos RBCs

Intracellular water, cation content and morphology of S314P Gárdos RBCs

As part of this study on Gárdos-HSt RBCs, within the frame of the collaboration with Paola Bianchi's laboratory, we had the opportunity to test the hypothesis that calcium sensitivity is deregulated in novel Gárdos mutants. A new variant was identified with a mutation located within Calmodulin Binding Domain 1 (CaMDB1), in position 314 of Gárdos polypeptide chain (S314P). Samples provided came from two patients, who were kin: a father and his son, who inherited the mutation.

S314P Gárdos RBCs appear to be slightly dehydrated (**Fig. 4.16**). However, a shipped control sample was not provided along with the patient sample, therefore a mean shipped control average from previous measurements is plotted. Moreover, there was little blood available, hence only a single measurement was performed (n=1). More S314P Gárdos samples will be required to draw a conclusion on the impact of this mutation on hydration and cation content. Nevertheless, morphological data support dehydration of S314P RBCs. Elliptocytes

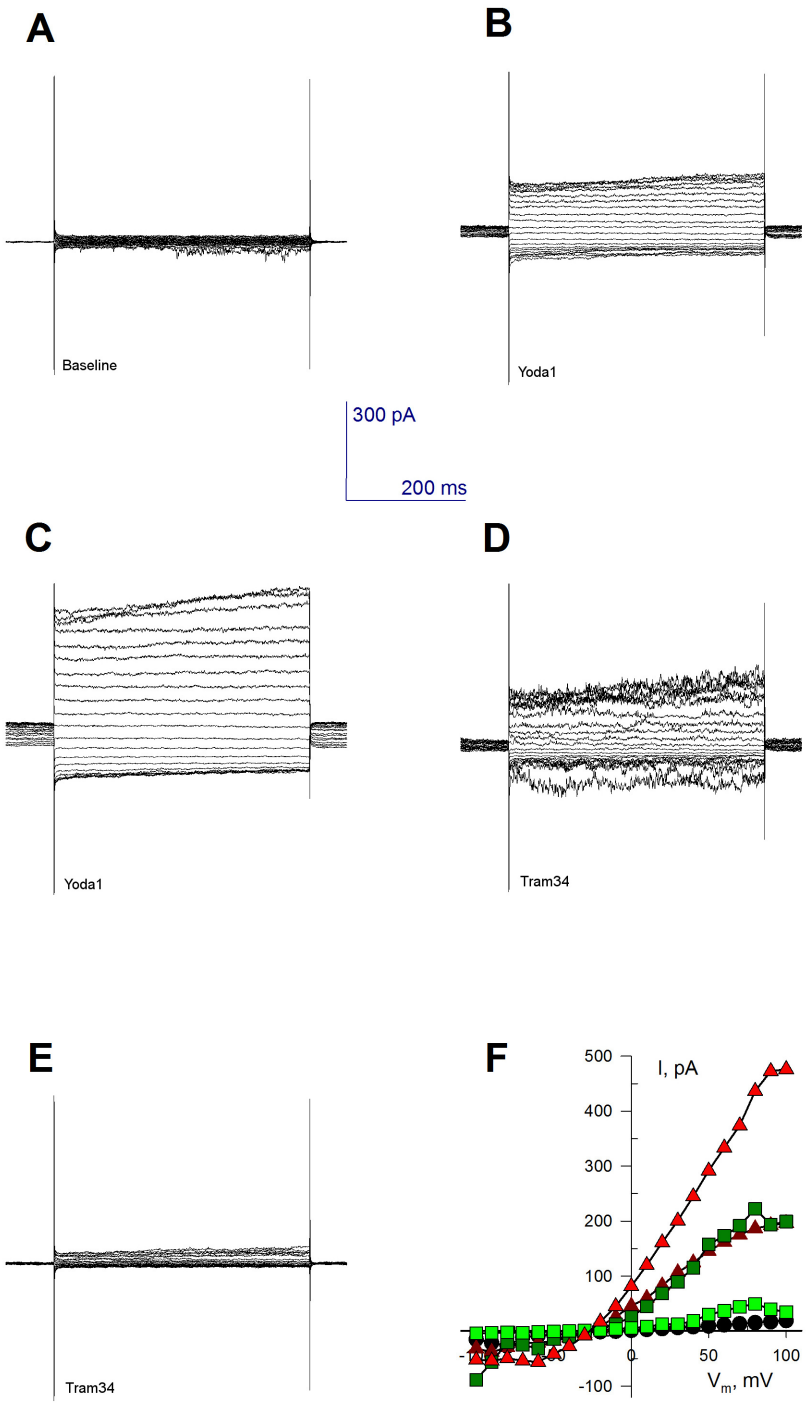

Figure 4.14: Piezo1-mediated Gárdos activity of a R352H Gárdos RBC in whole cell mode configuration of patch-clamp.

Whole-cell currents (pA) over time (ms) during a voltage ramp from -100 mV to 100 mV in the span of 300 ms. A. Baseline current. B. 1.5 min after addition of Yoda1 (5 µM). C. 5 min after addition of Yoda1 (5 µM). D. 1.5 min after addition of Tram34 (10 µM). E. 3 min after addition of Tram34 (10 µM). F. I/V curve of A-E. Black circles: baseline. Red (bright: 5 min; dark: 1.5 min) triangles: Yoda1. Green (bright: 3 min; dark: 1.5 min) squares: Tram34.

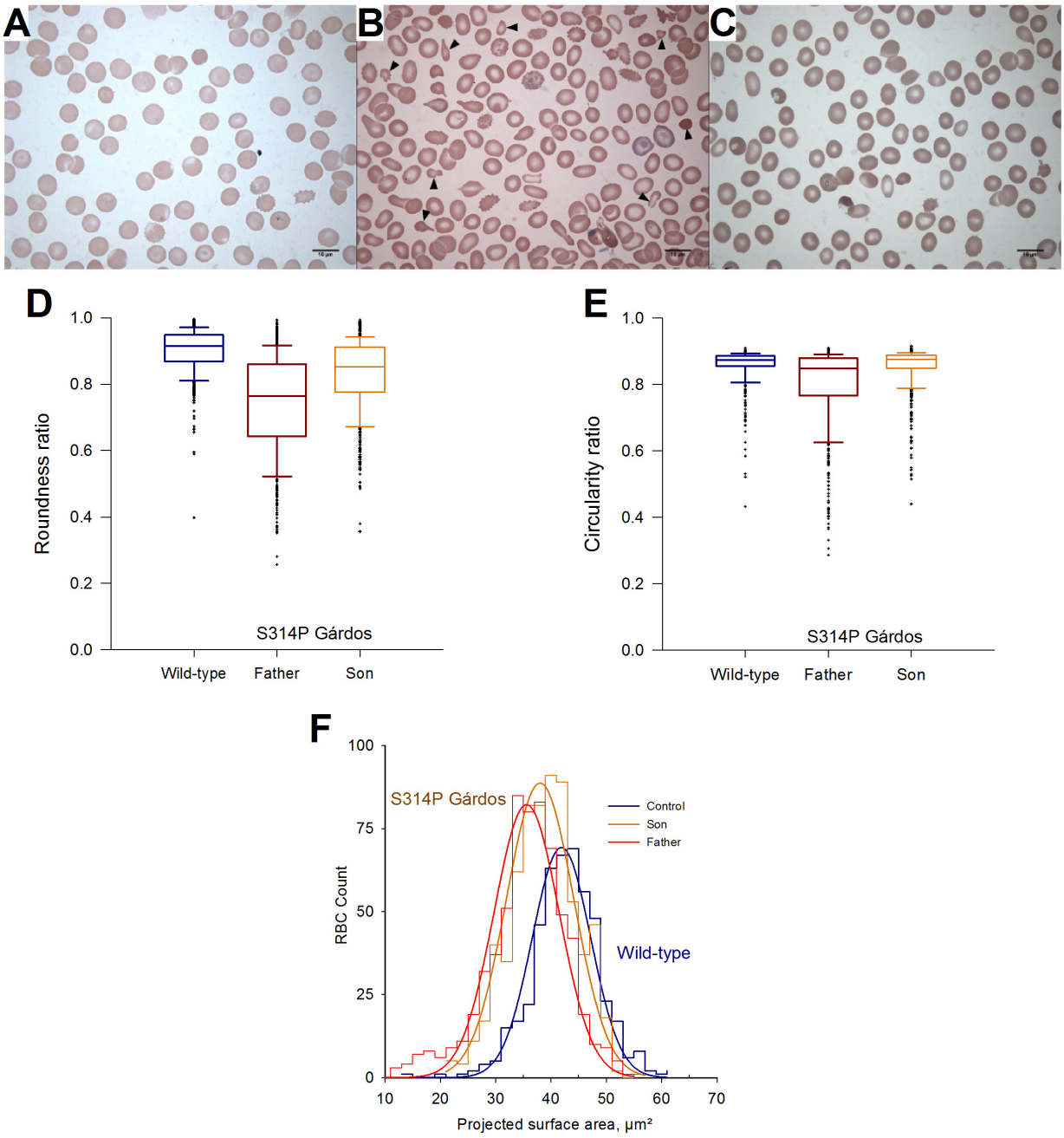

Figure 4.15: Morphology of S314P Gárdos RBCs.

Erythrocyte photographs from a wild-type donor (**A**) and S314P Gárdos patients: father (**B**) and son (**C**). Arrows point to abnormal shapes. Roundness (**D**), circularity (**E**) and projected cell area (**F**) of wild-type and S314P Gárdos RBCs. Roundness and circularity are ratios and hence dimensionless. They are calculated according to: $Roundness = 4 \times \frac{[Area]}{\pi \times [MajorAxis]^2}$ and $Circularity = 4\pi \frac{[Area]}{[Perimeter]^2}$ Roundness, circularity and projected cell area are significantly different between wild-type and S314P Gárdos RBCs ($p<0.001$, Kruskal-Wallis), except for the son's erythrocyte circularity ratio ($p=0.301$, Kruskal-Wallis)

and microcytes are present in patient's blood smears (**Fig. 4.15A-C**). RBCs from the father show numerous dacryocytes, perhaps in relation to his splenectomy (**Fig. 4.15B**). Roundness and circularity differ significantly between wild-type and patient RBCs ($p < 0.001$, Kruskal-Wallis), except for the son's erythrocyte circularity ratio which is similar to that of wild-type cells ($p = 0.301$)(**Fig. 4.15D, E**). Both patients display RBCs with significantly smaller projected surface area ($p < 0.001$, Kruskal-Wallis), as gauged visually by microcytosis (**Fig. 4.15F**).

Gárdos activity of S314P RBCs

The protocol used to study R352H Gárdos mutants was also carried out on S314P Gárdos erythrocytes to test the hypothesis whether Gárdos defect comes from altered calcium sensitivity.

Contrary to R352H Gárdos mutants, S314P RBCs reach similar hyperpolarizations as control RBCs when subjected to A23187 (10 µM) (**Fig. 4.17B**). This may be explained by the fact that A23187 forces maximal Gárdos openings. Since cell volume and intracellular potassium levels seem not to be altered in patient RBCs, maximum hyperpolarization therefore depends only on electrochemical gradients for K^+. On the other hand, when S314P erythrocytes are subjected to NS309 stimulation, a much more pronounced hyperpolarization develops compared to wild-type red cells. As a result, S314P Gárdos RBCs either contain more cytosolic calcium or its mutant Gárdos is more sensitive to Ca^{2+}.

Interestingly, the son's erythrocytes reach more negative maximum hyperpolarization values, which may be related to the fact that the father was splenectomized with RBCs presenting many aberrant cell shapes compared to his son (**Fig. 4.15B, C**). The son's disorder severity is rather clear in **Figure 4.17B** which indicates either increased sensitivity or intracellular calcium levels in son's RBCs compared to the father's with a maximum hyperpolarization difference of -31.9 mV and -19.5 mV, respectively, against control. Although, further analysis is required to draw conclusions on this mutation, these measurements highlight the variability in channel responses between patients, even with the same mutation and common genetic background.

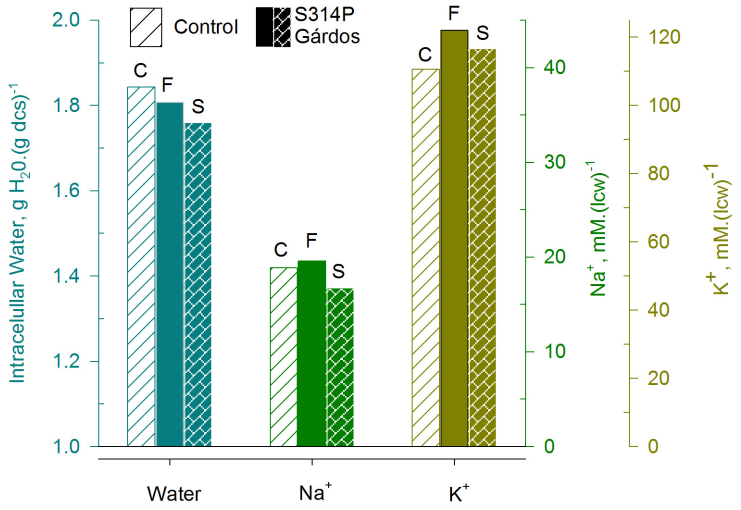

Figure 4.16: Cell water, sodium and potassium content of S314P Gárdos erythrocytes.
Intracellular amounts of water, Na^+ and K^+ of RBCs from two patients with S314P Gárdos mutation. Control was averaged from controls from **Fig. 4.4**. Wild-type is noted by striped bars whereas S314P Gárdos-HSt are indicated by solid bars. A single measurement (n=1) is shown.C, F and S denote Control, Father and Son, respectively.

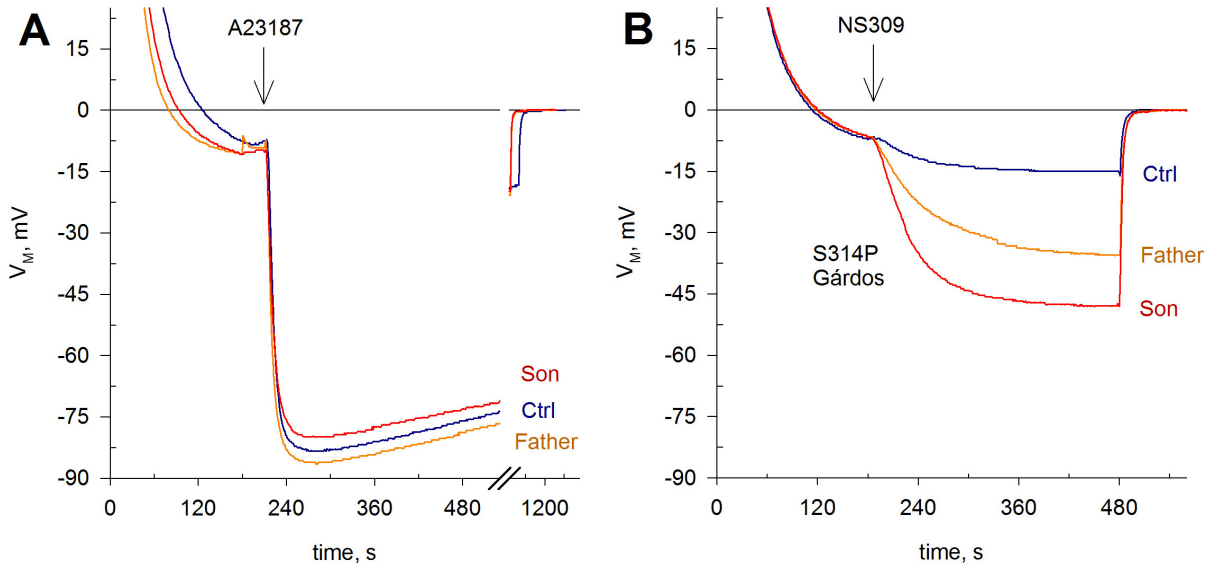

Figure 4.17: S314P Gárdos RBCs display enhanced calcium sensitivity.
Membrane potential traces from control (blue trace) and patients' erythrocytes with S314P Gárdos mutation (Father, orange trace and son, red trace) injected into normal Ringer solutions and treated with calcium ionophore A23187 (10 µM) (**A**) or Gárdos activator NS309 (100 µM) (**B**). Each trace is an independent measurement from a different donor.

Discussion

The Gárdos channel is a homotetrameric calcium-dependent K^+ channel [139]. Recent studies in wild-type erythrocytes proved that mechanical stimulation in a range compatible with shear stress that RBCs encounter within the bloodstream, triggers transient increases in intracellular calcium levels which may activate, in turn, Gárdos [140]. The main hypothesis for Gárdos-HSt would be enhanced Gárdos activity leading to marked K^+ efflux and the disorder is sometimes classified as Hereditary Xerocytosis. However, for the already described R352H mutation as well as the new mutation S314P, no reduction in volume, as measured by water content, nor in intracellular potassium were found. Despite, shape analysis of both mutations indicates a strong alteration of the discocytic shape, worsened in the splenectomized patient, the father (**Fig. 4.15B**). Moreover, morphological descriptors such as cell area and cell roundness show a significant deviation from normal values. See **Table 4.2** on page 141 for an overview.

More importantly, all patients, with R352H or S314P mutation, display altered Gárdos Ca^{2+} sensitivity, as confirmed by increased hyperpolarizations when R352H or S314P Gárdos cells are exposed to NS309 and by increased whole-cell currents inhibitable by Gárdos blocker Tram34. Hence, calcium sensitivity is at least one order of magnitude greater in R352H erythrocytes compared to the standard sensitivity of wild-type Gárdos. NS309 increases the calcium sensitivity of wild-type Gárdos nearly as much as the R352H mutation does. As a result, use of NS309 on R352H RBCs will left-shift the calcium sensitivity curve and half-maximal Gárdos activations can occur with as little as 1000-fold less calcium than with wild-type channels (**Fig. 4.18**).

However our data shows RBC overhydration due to sodium influx. Such an observation has already been reported for R352H mutant [271, 282]. Moreover, dehydration is faster after Ca^{2+} pump block by vanadate, in R352H Gárdos RBCs than wild-type [271]. Contrary to what is expected from erythrocytes with enhanced K^+ efflux, the sole explanation, which is confirmed by Na^+ measurements, is that Na^+ takes place via compensating mechanisms. MCV values in the first study on affected individuals were in the normal range, with one individual being above the normal range. Another report found a high MCV value in an individual from

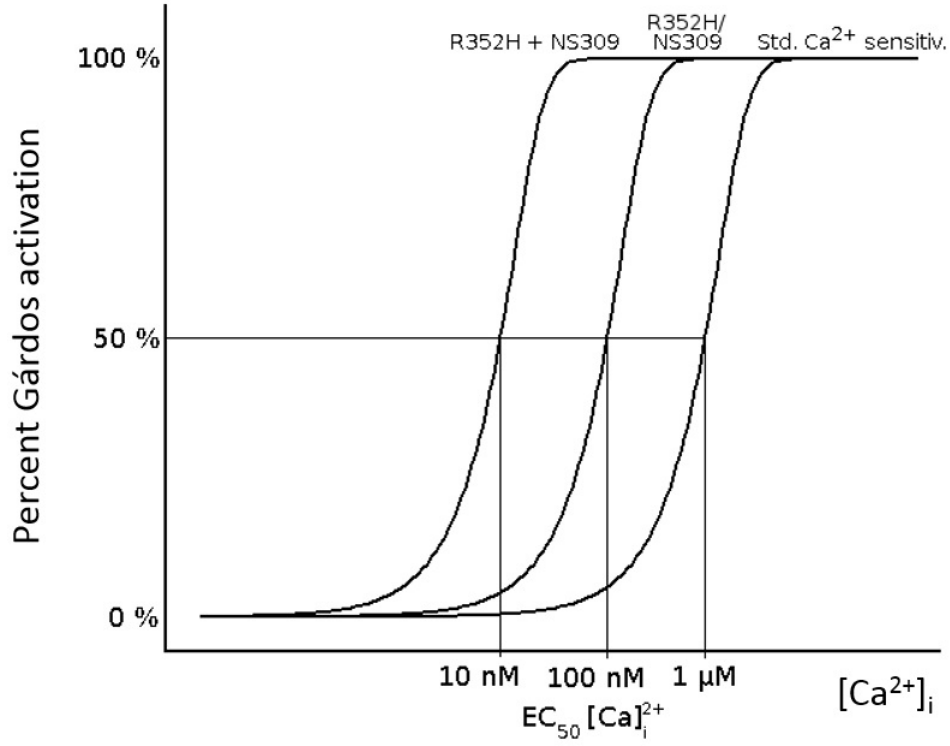

Figure 4.18: Schematic of calcium sensitization of Gárdos by mutations or activator NS309.
Schematic showing intracellular calcium concentration plotted against the extent of Gárdos activation. Half-maximal effective calcium concentration (EC_{50} $[Ca]^2+_i$) is indicated and its left-shift according to the effects of Gárdos agonist NS309 and/or the gain-of-function mutation R352H.

an independent family and his child had a MCV within the normal range [282]. MCV is highly influenced by storage conditions [287]. Nevertheless, they all presented with low hemoglobin concentration and, importantly, very high reticulocyte counts which are indicative of an overall young population due to reduced RBC lifespan. A fragile subpopulation may lyse early as soon as RBCs are *ex vivo*. Transportation can alter cation levels. Blood is shipped at 10-15 ° C, and the temperature is bound to change during transport depending on ambient temperature. The Na^+/K^+ pump is inhibited by low temperature leading to cation imbalance. Afterwards, handling may cause lysis of the most fragile red cell fraction during centrifugations and washing steps.

In vivo, constant work overload of Na^+/K^+ and Ca^{2+} ATPases places a huge strain on ATP pools and glycolysis. ATP will be less available for other processes including, importantly, antioxidant defense which may lead to increased oxidation of cellular proteins and early cell death. Splenectomy has an overall positive outcome in R352H Gárdos patients as transfusions after hemolytic crises are normally no longer necessary and, other forms of HSt notwithstanding, no thrombosis was reported after the intervention [282]. If the most fragile fraction of the RBC population is partially lost before measuring, then the pathophysiology is more complex than envisaged. Nonetheless, assuming that what we observe is representative of the whole population, a hypothesis arises regarding the pathophysiology. A NSC channel is *a priori* the only pathway for significant sodium uptake, as channels can carry a significant ion capacity. However, enhanced NSC activity leads also to Ca^{2+} uptake which would entail a permanent activation of R352H Gárdos and dehydration, which would be incompatible with our findings. Therefore, a normally silent transporter must be considered as being responsible of sodium influx. Symporter NKCC (Na^+, K^+, 2 Cl^- cotransporter) is able to bring sodium into the cell in response to cation imbalance. It is regulated by phosphorylation and activates upon water and chloride loss. Chloride

leaves the cell along with potassium during Gárdos opening, therefore there is also a chloride imbalance which strongly favors NKCC activation. NKCC action might restore K^+ and Cl^- levels, but raising at the same time Na^+ levels, in agreement with our observations and with the notion of an overactive Na^+/K^+ pump. As mentioned, heavy ATP consumption by the ATPases may lead to reduced energy for antioxidant defense and oxidative stress leading to premature hemolysis or removal from the circulation. Reduced pathological RBC lifespans require hematopoietic compensation in the form of increased cell production. Reticulocytes thus produced are known to have higher passive transporter activities which may abnormally continue in mature RBCs due to osmotic stress and chloride deficiency. NKCC has already been proposed, among several other transporters which are inactive in healthy RBCs, as responsible for Na^+ and K^+ uptake leading to overhydration [282].

The current approach, via membrane potential estimation, is not amenable to probe electroneutral transporters, which do not alter the membrane potential as they are not electrogenic. Ion movement through passive transporter is rate-limited by protein conformational changes, with ion binding before translocation takes place. In addition, passive transporters do not employ ATP and therefore ion movement can only occur down the electrochemical gradient. NKCC activity can be studied via inhibition of the Na^+/K^+ pump with ouabain and the symporter itself with bumetanide. Then, precise measurements of ion change both intra- and extracellularly should shed light on NKCC involvement. As the Na^+/K^+ pump is inhibited by cold during transport, a shipped control will be especially required for comparison unless measurements can be performed at the place of blood withdrawal.

A potential treatment may be derived by using Gárdos inhibitors. The most studied compound so far in the clinic is senicapoc. Senicapoc (also known as ICA-17043) was discovered in 2003 and is a small aromatic molecule with powerful Gárdos inhibitory properties. Its use on the SAD mouse model of Sickle Cell Disease showed amelioration of hematological parameters [288]. The drug has also been tested on human subjects in a phase 2 trial with positive outcomes including higher hemoglobin levels than placebo, decreased reticulocytosis and good tolerance [289]. A good record on human subjects and given the molecular target for the SCD treatment is also Gárdos may speed clinical trials. Preliminary tests with senicapoc show that it is also effective against the mutated channel and ameliorates dehydration-related alterations *in vitro* [290]. Therefore, a therapeutic strategy for overhydrated Gárdos-HSt remains to be devised. The pathophysiology needs to be clarified including whether there is an involvement of NKCC.

Piezo1 Hereditary Xerocytosis

If Gárdos is a well-described ion channel in RBCs, another more recently discovered, Piezo1, crystallizes interest in hematology nowadays. Indeed, since the first report in 2010 that linked the protein to the mechanosensitive channel we have been chasing for more than 20 years [141], channel mutations were associated to Hereditary Xerocytosis in 2012 [207, 274, 275]. Since then, numerous mutations have been described with the most recent publication on the subject listing more than 40 mutations [291], with another 40 mutations in various meta-analysis for which the pathological incidence is not always clear [292, 293].

Most mutations described happen to be relatively close to the C-terminal end, which has been shown to include the pore region. Thus, these mutations were interpreted as a partial “gain-of-function”, since experiments have demonstrated a slower inactivation of the channel leading to a longer opening time that may eventually

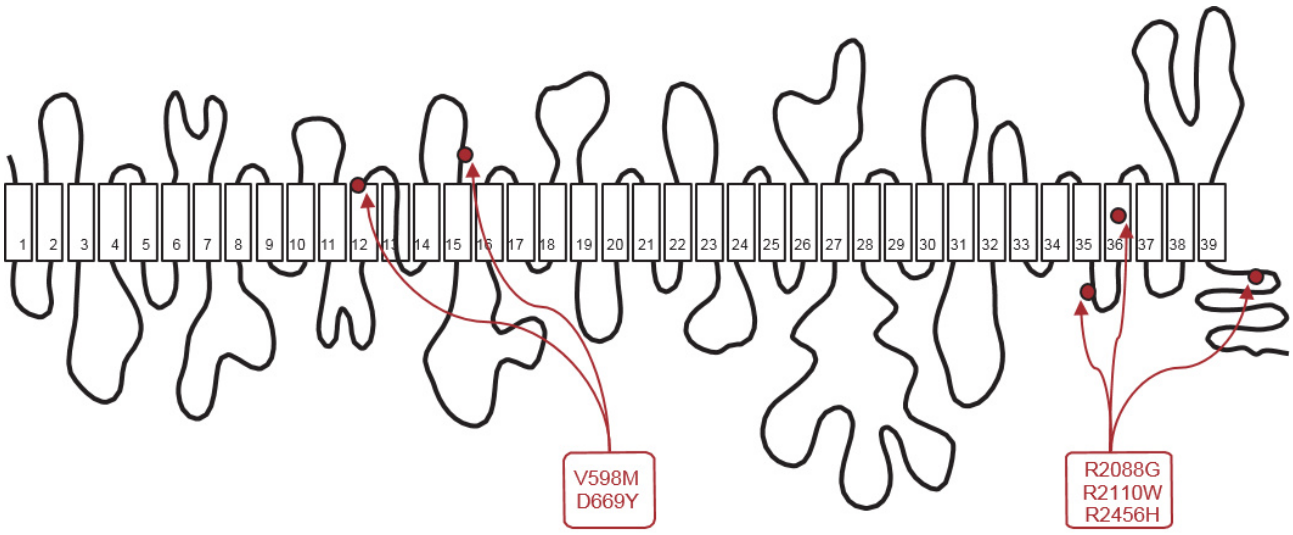

Figure 4.19: Location of Piezo1 mutations studied in a Piezo1 2D representation.
2D schematic of Piezo1 showing its transmembrane domains and the localization of the mutations studied.

enhance Ca^{2+} influx, which will in turn promote substantial activation of Gárdos followed by loss of osmotically obliged water and, in consequence, dehydration. Nevertheless, keeping in mind that Piezo1 is a Non Selective Cation channel, an exchange 1:1 Na^+:K^+ also occurs, although in hyperpolarizing conditions, i.e. after Gárdos activation, it is mainly a pathway for Na^+ and Ca^{2+} due to the favorable driving force. Today pharmacological tools are available to study functional effects of mutation on Piezo1 activity. For instance, treating wild-type red cells with Piezo1 activator Yoda1 leads to calcium entry, mimicking how with most mutations small mechanical stimuli entail sustained activation.

In the present study, within the frame of a collaboration with the groups of Paola Bianchi (Milan, Italy), Richard van Wijk (Utrecht, The Netherlands) and Lamisse Mansour-Hemdili (Paris, France), I was able to analyze a range of Piezo1 mutations (2088G, R2110W, R2456H, V598M and one unknown mutant). Furthermore, a dedicated case study of mutation D669Y, which affects the mechanosensing blade domain, is presented at the end of the chapter as a draft manuscript for publication. In the same way that Gárdos mutants have been studied, a series of experiments have been conducted for each Piezo1 mutant including an analysis of cell volume, cation content, morphology and a set of experiments carried out using CCCP method for membrane potential estimation in order to challenge Non Selection Cation channel activity hence determining whether cation balance has been impaired and, if so, to what extent it has.

Study of a Gárdos mutation close to the Calmodulin Binding Domain allows to easily test the susceptibility of the Gárdos channel to calcium by using NS309. Although Yoda1 may be used for a direct approach, the complexity seen in the pathophysiology of Piezo1-HX patients and their channel behavior requires a range of strategies in order to pinpoint channel activity alterations which vary not only among mutations but also display idiopathic variation.

Different strategies enable us to measure NSC activity whatever the protein responsible for these cation movements, via membrane potential determination, namely:

- Low Ionic Strength Condition, i.e. sucrose solutions. Using or not chloride conductance blockers (NS3623 or NPPB), allowing to directly measure the strength of NSC channel activity.
- GsMTx4, an inhibitor of mechanosensitive channels which will highlight the underlying basal Piezo1

activity in a given experimental condition (i.e. LIS) when there is no direct activation via mechanical or pharmacological stimuli.

- Yoda1, which enables transient channel activations at low concentrations.
- A23187, which facilitates the assessment of the maximal Gárdos activity and, moreover, by measuring repolarization the strength of NSC channels in hyperpolarizing conditions.

Every condition present some advantage and provide us with a way to probe specific hypotheses that I will explain when necessary. Some of them directly or indirectly act on Piezo1, whereas others act on Gárdos, since there is significant interplay between them.

Even if all conditions have been tested systematically on every patient, to the limit of blood volume available, only significant results relevant for discussion will be shown herein. Pooled mean values from different mutants are also offered in order to show the suitability of the protocol to study Piezo1-HX caused by different mutations.

Morphology of Piezo1-HX RBCs

Smears from Piezo1-HX R2088G patient blood samples show numerous stomatocytes, much more predominant than in R2110W patient blood, as well as acanthocytes (**Fig. 4.20B**). Despite being stomatocytic, these RBCs are actually less round than control cells ($p<0.001$, Mann-Whitney) (**Fig. 4.20C**). Acanthocytes likely contribute to the overall reduced circularity which is also reduced ($p<0.001$, Mann-Whitney)(**Fig. 4.20C**). Cell projected area is 28.0 % ± 0.7 % (mean ± SEM, n=1504) higher in R2088G Piezo1-HX cells than in wild-type ($p<0.001$, Mann-Whitney) (**Fig. 4.20E**). Even though it may seem counterintuitive, given that R2456H Piezo1 red cells are dehydrated, cell surface is measured as the projected area of a 3D object, therefore if a RBC shrinks it may extend on the support when it sediments, appearing to be larger. Moreover, shrinkage may also alter shape *per se*, for instance by flattening red cells, thus they appear larger when the projected surface is measured. Hence, dehydration is compatible with a higher projected cell area. Other factors might play a role, such as the fact that reticulocytes levels are elevated. Certainly, reticulocytes are barely recognizable by Giemsa staining, however, the reticulocyte proportion does not exceed 10%, therefore it cannot skew the data.

RBCs from a Piezo1-HX patient with a mutation at R2110W were found to be stomatocytic and smaller. Acanthocytes were also present (**Fig. 4.21B**). Despite finding some rod-shaped, elliptical cells, there was no difference in either roundness nor circularity ratio (p=0.903 and p=0.181, respectively. Mann Whitney) (**Fig. 4.21C-D**). Even though there is spread in R2110W RBC size, they have overall significantly smaller surface area than control cells, 37.6 ± 0.2 μm^2 (mean ± SEM, n=1160) and 43.2 ± 0.2 μm^2 (mean ± SEM, n=827) respectively ($p<0.001$, Mann-Whitney) (**Fig. 4.21E**).

R2456H Piezo1 erythrocytes are stomatocytic with numerous codocytes and spurred cells (**Fig. 4.22B**). Shapes are highly irregular and as a result roundness and circularity is markedly decreased in R2456H Piezo1 RBCs compared to control ($p<0.001$, Mann-Whitney) (Fig. 4.22C-D). Surface area is increased by 22.2 % ± 0.6 % (mean ± SEM, n=1225) in R2456H compared to wild-type cells (**Fig. 4.22E**).

V598M Piezo1 blood samples feature schistocytes, acanthocytes and occasional stomatocytes (**Fig. 4.23B**). Many angular cells are observed, resulting in roundness and circularity ratios smaller than wild-type (**Fig. 4.23C, D**) ($p<0.001$, Mann-Whitney). V598M erythrocytes have a projected surface area 15.2% ± 0.6% (mean

± SEM, n=1572) greater than wild-type cells ($p<0.001$, Mann-Whitney).

To conclude, cell shape analysis indicates Piezo1-HX erythrocytes are heavily altered. Importantly, all mutations cause an increased projected area compared to wild-type, with the exception of mutation R2110W. These results show how misleading Piezo1-HX is when doing a visual inspection of blood smears, with wide variability in morphology confirming the difficulty to classify the pathology.

Intracellular water and cation content of Piezo1-HX RBCs

In order to correlate shape analysis to the actual cell hydration state, all patient samples and respective shipped controls were subjected, upon arrival, to measurements of intracellular water, sodium and potassium. All patients' RBCs studied displayed cell dehydration, the main clinical feature of hereditary xerocytosis (**Fig. 4.24**). Whereas wild-type cells had mean water levels of 1.83 ± 0.09 (n=6) g cellular wet mass/g cellular dry mass, all Piezo1 mutants studied had a mean intracellular water content of 1.63 ± 0.06 (n=7) g cellular wet mass/g cellular dry mass, a significant reduction ($p<0.001$). Thus, these Piezo1-mutants had 11.01 % ± 5.5 % (n=7) less intracellular water than control RBCs. This water loss is due to a K^+ loss, though the extent of this loss varies among Piezo1 mutants. Shipped controls display variability in intracellular K^+ levels which may stem from transportation conditions. Piezo1-mutants studied had, on average, 87.3 ± 17.9 µmol/l cell water (n=7) compared to 107.0 ± 22.0 µmol/l cell water (n=7) in control (p=0.122). In addition, a significant Na^+ influx was observed for all Piezo1 mutants studied, with an average intracellular concentration of 37.4 ± 9.3 µmol/l cell water (n=7) compared to 26.30 ± 8.40 µmol/l cell water (n=6) of wild-type erythrocytes (p=0.048) (**Fig. 4.24**).

In conclusion, analyses of the the actual hydration state and cation homeostasis clearly indicate that Piezo1 mutants tend to dehydrate. More importantly, the cation balance (Na^+, K^+ and Ca^{2+}) is disrupted [283] pointing to the nature of Piezo1 as a Non Selective Cation channel.

Gárdos activation via calcium ionophore

Considering the previous finding, the next step is to elucidate up to what extent Non Selective Cation channel activity is enhanced in these Piezo1 mutants. In order to achieve this, I carried out membrane potential measurements via CCCP method. Although the study of NSC channel activity is challenging in these conditions, several strategies were developed.

Use of A23187 allows for the study of NSC activity indirectly. As a Gárdos activation brings the membrane potential to very negative values it sets a favorable driving force for sodium, then if a NSC is overactive compared to control a faster repolarization will be observed. Piezo1 mutants studied hyperpolarize upon A23187 treatment to similar extents as control red cells (**Fig. 4.25**). Mean maximum hyperpolarizations were -75.6 ± 7.6 mV (n=6) and -78.1 ± 5.1 mV (n=7) for controls and Piezo1 mutants, respectively. Even though intracellular sodium levels are raised, potassium levels are reduced, thus balancing the internal total cation amount. Strong repolarizations are observed after hyperpolarization for every Piezo1 mutant studied, with a rate of 0.085 ± 0.018 mV/s (n=7) in contrast to 0.036 ± 0.010 mV/s (n=6) in control red cells (p=0.001, Mann-Whitney test). Repolarizations develop as Na^+ enters through the NSC to counterbalance the loss of cation, K^+, by Gárdos. The repolarization rate is 1.25-fold higher than what is observed after A23187 treatment of R352H Gárdos

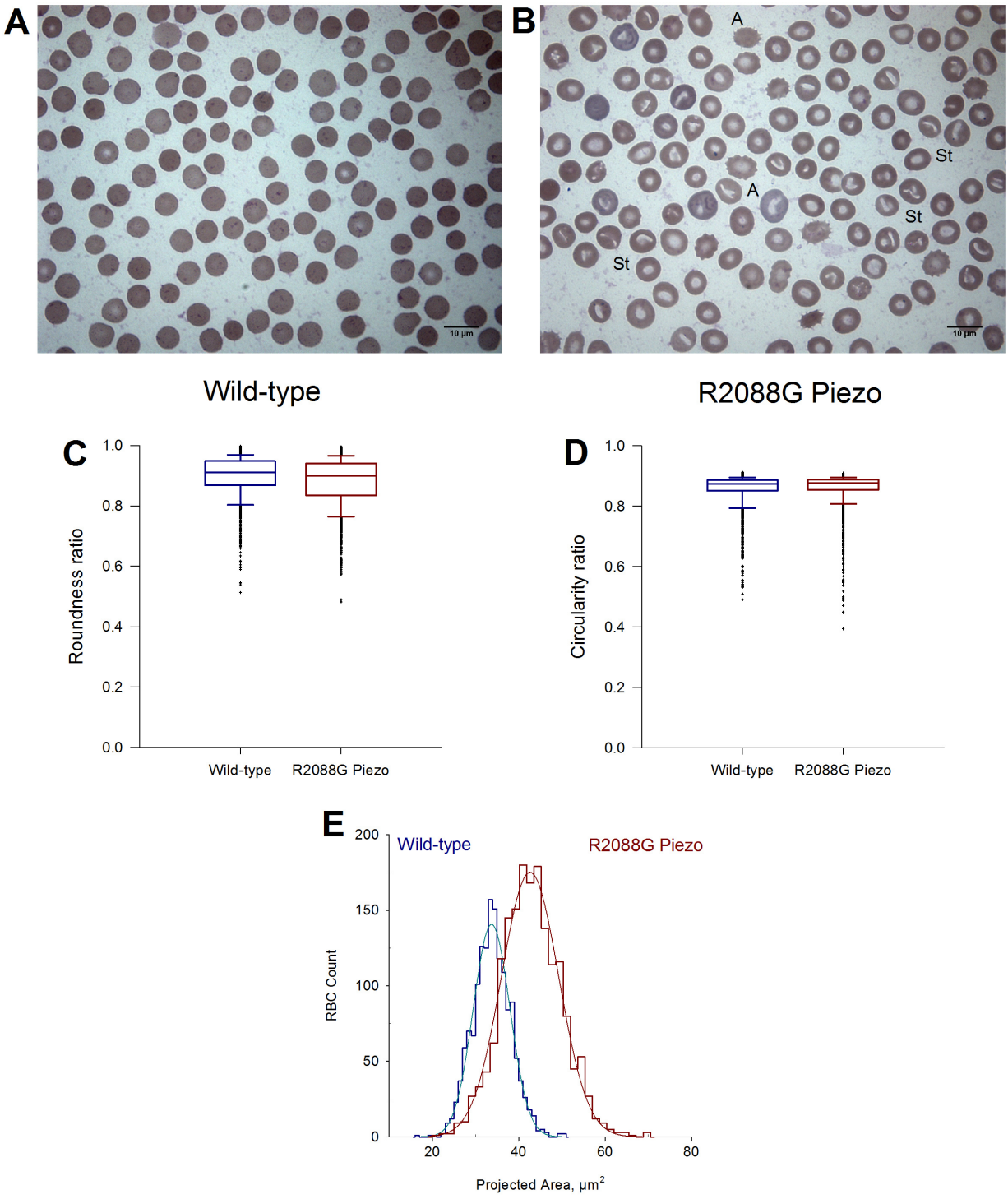

Figure 4.20: Morphology of R2088G Piezo1 RBCs.

Erythrocyte photographs from a wild-type donor (**A**) and R2088G Piezo1 patient (**B**). Arrows point to abnormal shapes. Roundness (**C**), circularity (**D**) and projected cell area (E) of wild-type and R2088G Piezo1 RBCs. Roundness and circularity are ratios and hence dimensionless. They are calculated according to: $Roundness = 4 \times \frac{[Area]}{\pi \times [MajorAxis]^2}$ and $Circularity = 4\pi \frac{[Area]}{[Perimeter]^2}$ Roundness, circularity and projected cell area are significantly different between wild-type and R2088G Piezo1 RBCs ($p<0.001$, Mann-Whitney). Aberrant RBCs in Panel B: A denotes acanthocyte and St, stomatocyte.

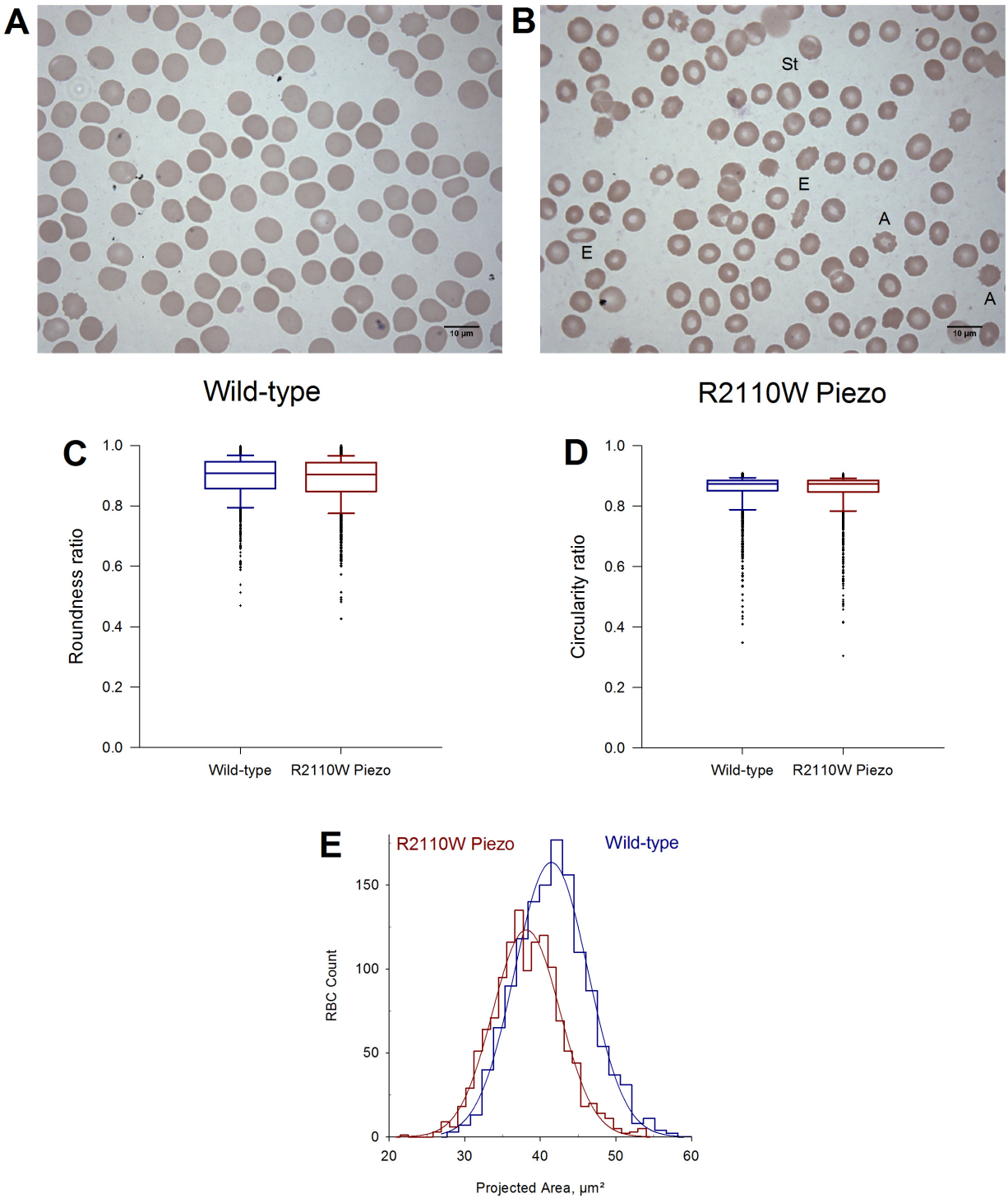

Figure 4.21: Morphology of R2110W Piezo1 RBCs.

Erythrocyte photographs from a wild-type donor (**A**) and R2110W Piezo1 patient (**B**). Arrows point to abnormal shapes. Roundness (**C**), circularity (**D**) and projected cell area (E) of wild-type and R2110W Piezo1 RBCs. Roundness and circularity are ratios and hence dimensionless. They are calculated according to: $Roundness = 4 \times \frac{[Area]}{\pi \times [MajorAxis]^2}$ and $Circularity = 4\pi \frac{[Area]}{[Perimeter]^2}$ Roundness and circularity ratios are not significant (p=0.903 and p=0.181 Mann-Whitney, respectively) while projected cell area is significantly different between wild-type and R2110W Piezo1 RBCs ($p<0.001$, Mann-Whitney). Aberrant RBCs in Panel B: A denotes acanthocyte; E, elliptocyte and St, stomatocyte.

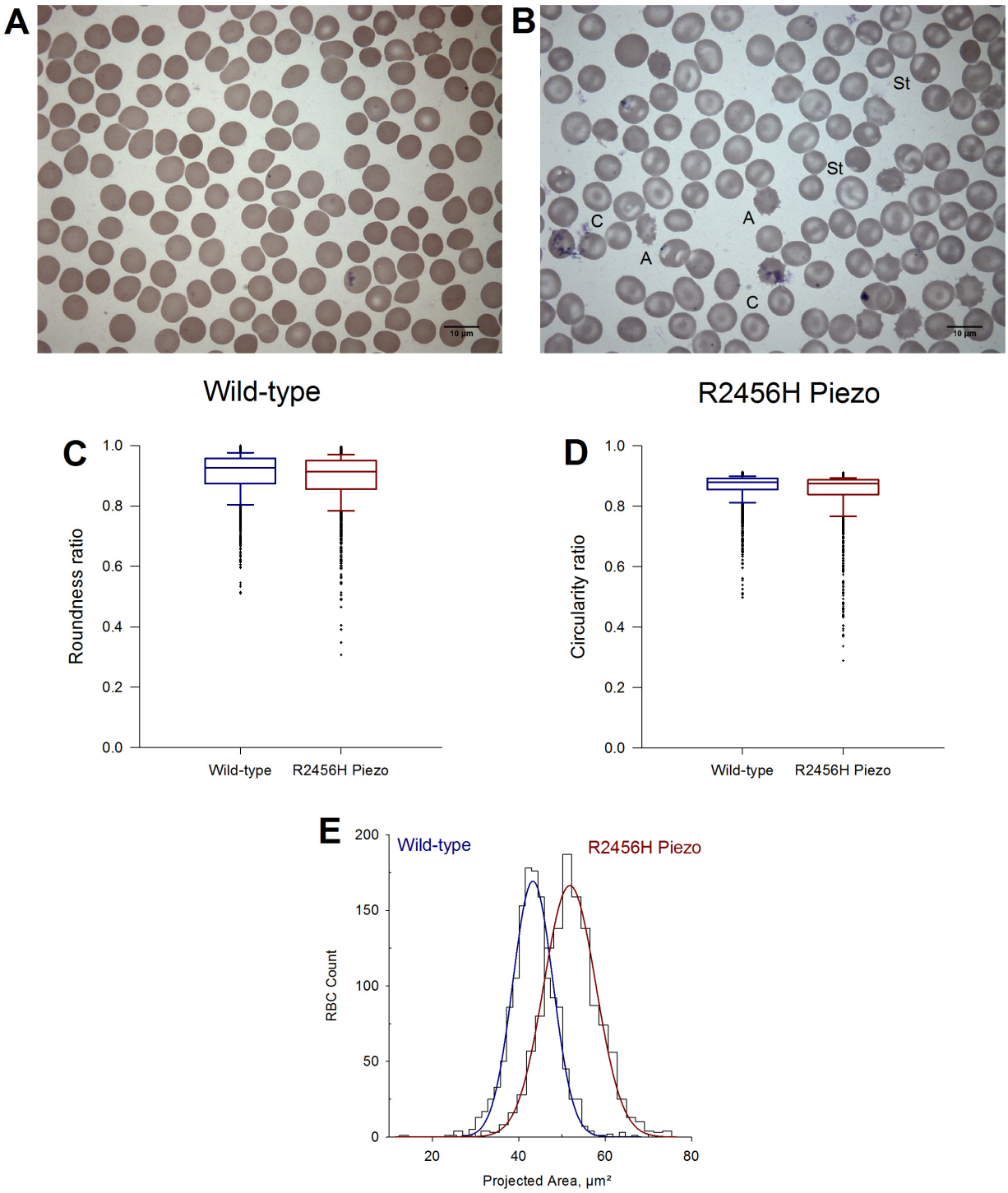

Figure 4.22: Morphology of R2456H Piezo1 RBCs.

Erythrocyte photographs from a wild-type donor (**A**) and R2456H Piezo1 patient (**B**). Arrows point to abnormal shapes. Roundness (**C**), circularity (**D**) and projected cell area (E) of wild-type and R2456H Piezo1 RBCs. Roundness and circularity are ratios and hence dimensionless. They are calculated according to: $Roundness = 4 \times \frac{[Area]}{\pi \times [MajorAxis]^2}$ and $Circularity = 4\pi \frac{[Area]}{[Perimeter]^2}$ Roundness, circularity and projected cell area are significantly different between wild-type and R2456H Piezo1 RBCs ($p<0.001$, Mann-Whitney). Aberrant RBCs in Panel B: A denotes acanthocyte; St, stomatocyte and C, codocyte.

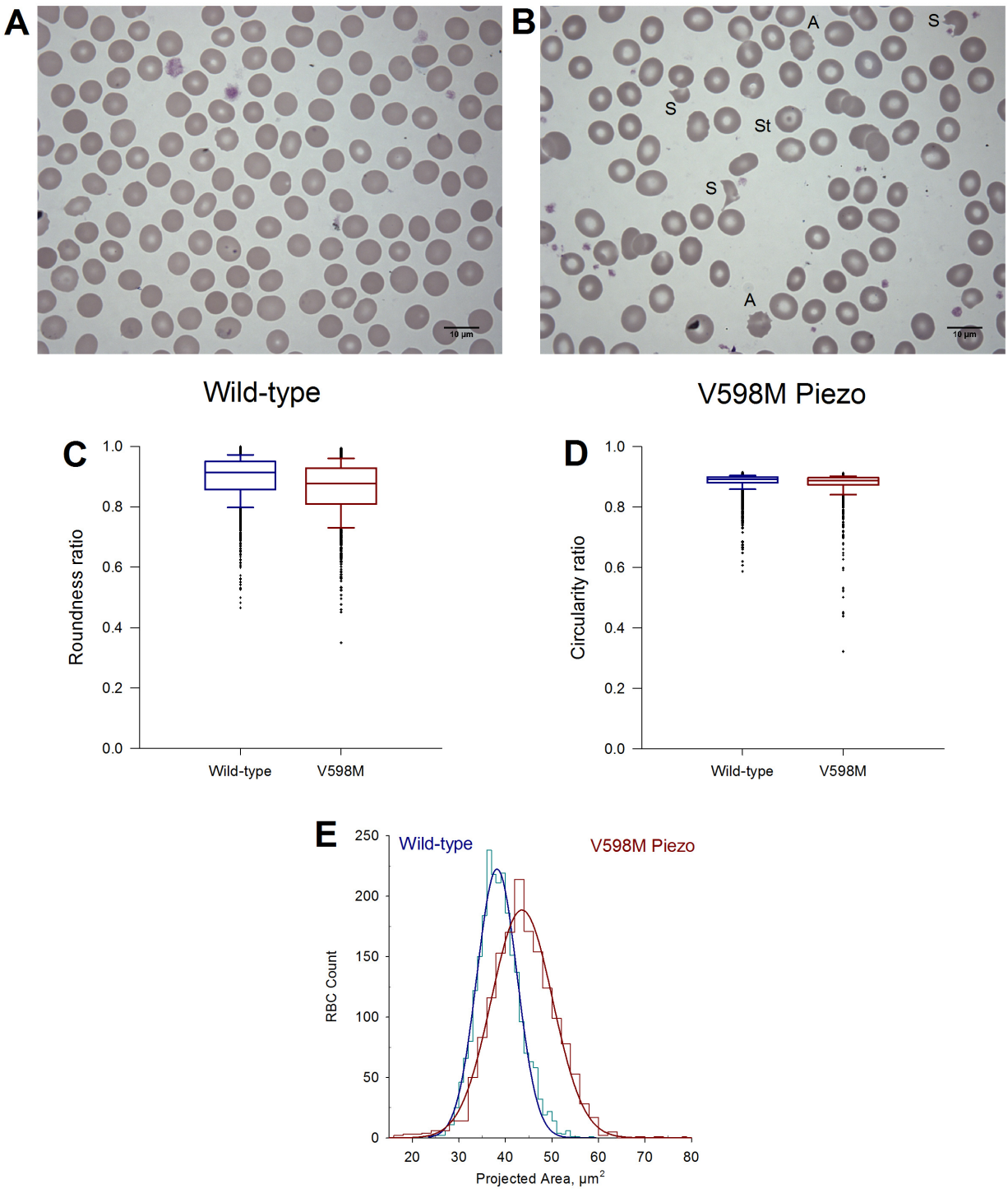

Figure 4.23: Morphology of V598M Piezo1 RBCs.

Erythrocyte photographs from a wild-type donor (**A**) and V598M Piezo1 patient (**B**). Arrows point to abnormal shapes. Roundness (**C**), circularity (**D**) and projected cell area (E) of wild-type and V598M Piezo1 RBCs. Roundness and circularity are ratios and hence dimensionless. They are calculated according to: $Roundness = 4 \times \frac{[Area]}{\pi \times [MajorAxis]^2}$ and $Circularity = 4\pi \frac{[Area]}{[Perimeter]^2}$ Roundness, circularity and projected cell area are significantly different between wild-type and V598M Piezo1 RBCs ($p<0.001$, Mann-Whitney). Aberrant RBCs in Panel B: A denotes acanthocyte; S, schistocyte and St, stomatocyte.

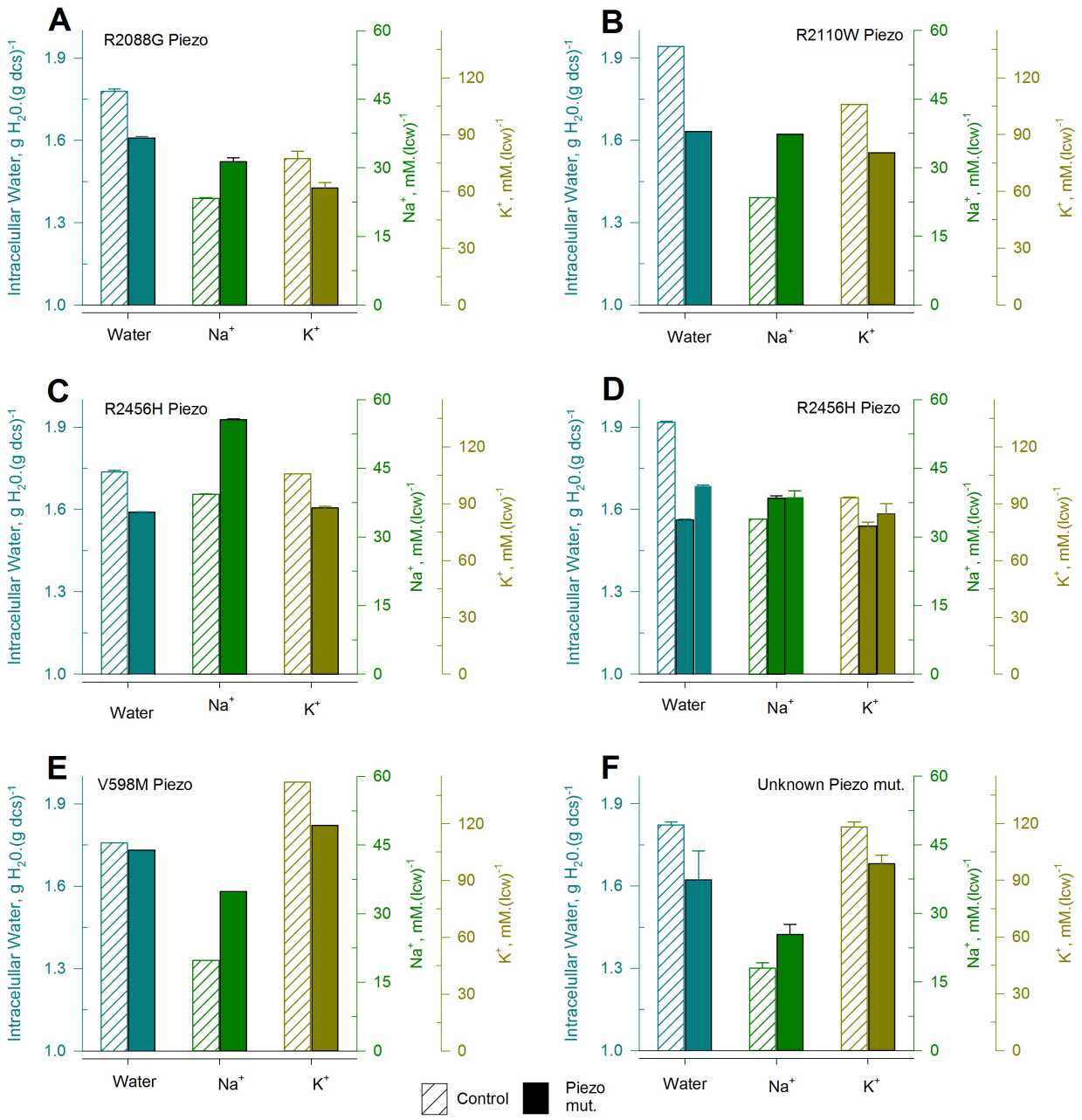

Figure 4.24: Cell water, sodium and potassium content of Piezo1-HX erythrocytes.
Intracellular amounts of water, Na^+ and K^+ of RBCs from patients with R2088G (**A**), R2110W (**B**), R2456H (**C** and **D**), V598M (**E**) and an unknown Piezo1 mutation (**F**). Controls are striped bars whereas Piezo1 mutants are solid bars.

RBCs, indicating that NSC channel conductance is with certainty constitutively more active, at rest, in Piezo1 patients.

Direct pharmacological activation of Piezo1 via Yoda

Yoda1, a Piezo1 agonist, is a straightforward approach to look at Piezo1 activity by activating the channel pharmacologically. A thorough analysis of Yoda1 dose-responses identified 625 nM as the best concentration to study NSC channel activity via its effect on the membrane potential (not shown). The choice of such a low concentration of Yoda1 aims to prevent a flood of calcium into the cytoplasm, keeping the activation as physiologically close as possible. Yoda1 (625 nM) elicits a transient hyperpolarization in control cells,

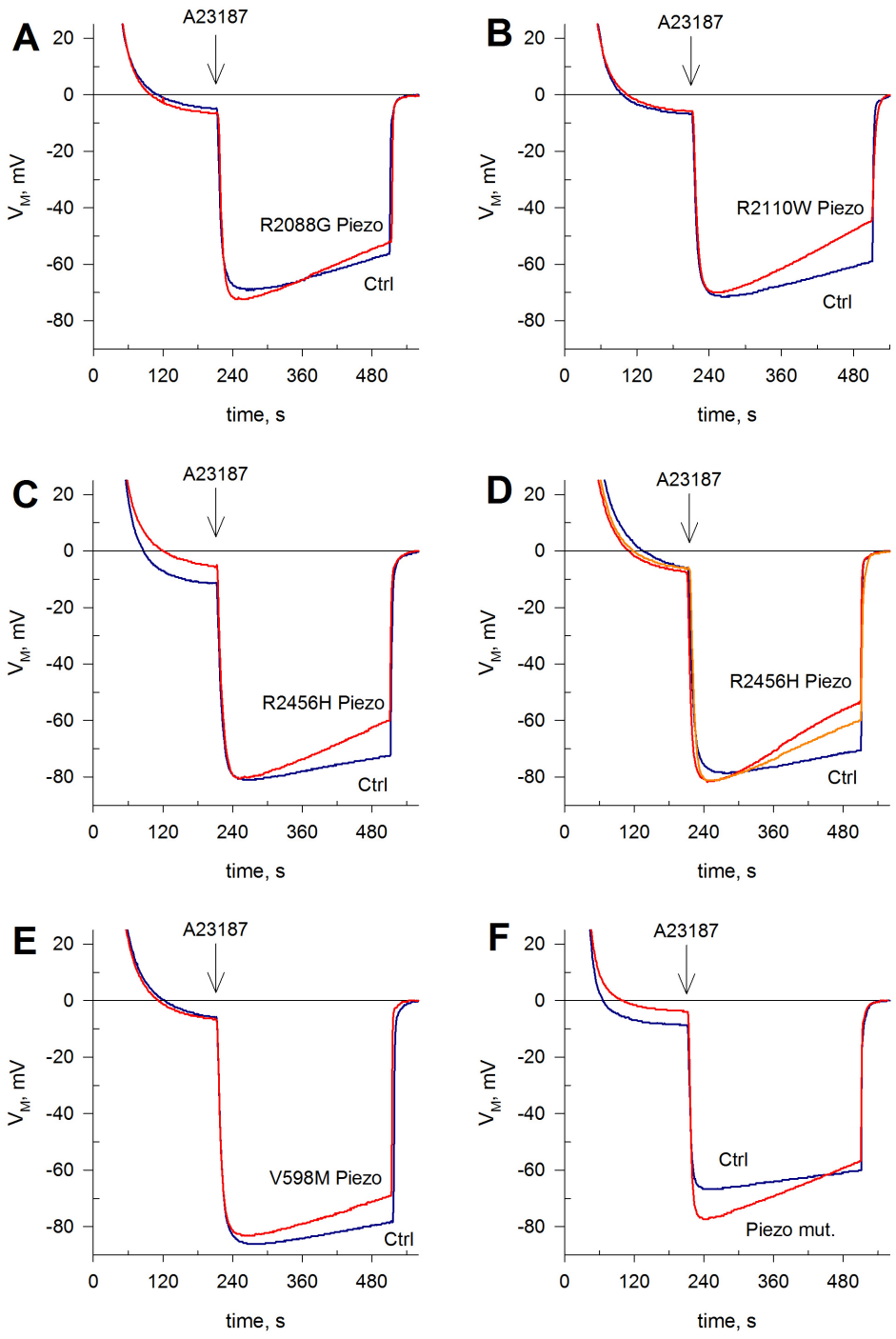

Figure 4.25: Piezo1-HX RBCs repolarize following strong A23187-induced Gárdos activation.
Membrane potential traces from control (blue trace) and patients' erythrocytes (red trace) with R2088G (**A**), R2110W (**B**), R2456H (**C** and **D**), V598M (**E**) and unknown (**F**) Piezo1 mutation injected into normal Ringer solutions and treated with calcium ionophore A23187 (10 µM). Each trace is an independent measurement from a different donor.

whereas Piezo1 patients studied displayed a sustained hyperpolarization reflecting the longer inactivation time of mutant Piezo1 channels. RBCs from patients with R2456H (three different patients), an unknown variant and V598M Piezo1 patient were subjected to 625 nM Yoda1. Nonetheless, **figure 4.26D** shows both control and V598M Piezo1 mutant patient being divergent from the other Piezo1 patients studied. Given it could only be measured once, it was considered as an outlier and excluded from overall analysis. There is a significant difference between control and patient RBCs in maximum hyperpolarizations reached, with -56.1 ± 2.2 mV

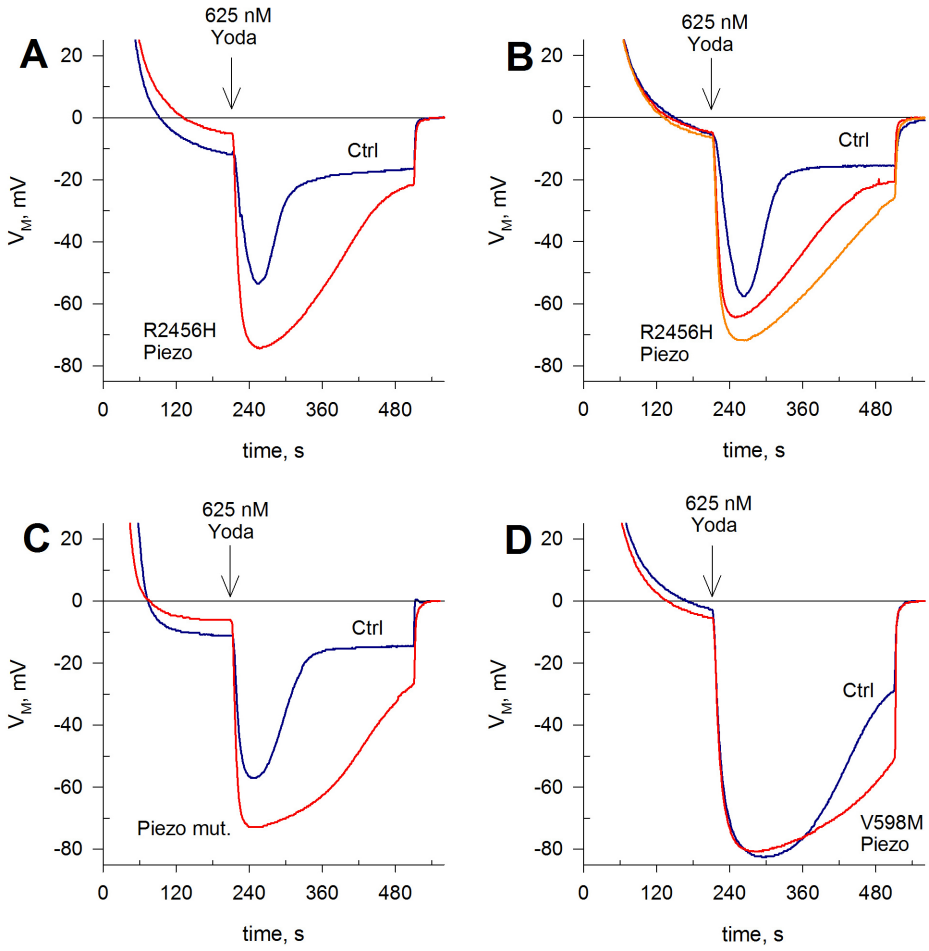

Figure 4.26: Piezo1-HX RBCs display strong Yoda-induced openings with delayed inactivation.
Membrane potential traces from control (blue trace) and patients' erythrocytes (red trace) with R2456H (**A** and **B**), unknown (**C**) and V598M (**D**) Piezo1 mutation injected into calcium Ringer solutions and treated with Piezo1 activator Yoda1 (625 nM). Each trace is an independent measurement from a different donor.

(n=3) attained by control cells and -70.9 ± 4.4 mV (n=4) by patients erythrocytes (p=0.003) (**Fig. 4.26A-C**). Following hyperpolarization due to Gárdos opening caused by calcium entry through Yoda-activated Piezo1, erythrocytes repolarize. Control cells repolarize fast owing to a transient Gárdos activation, with a $v_0^{posthyp}$ of 0.62 ± 0.064 mV/s (n=3). Piezo1 mutants analyzed repolarize at a significantly reduced rate: 0.12 ± 0.040 mV/s (n=4) (p <0.001) (**Fig. 4.26A-C**). This points to a prolonged Gárdos activity due to additional calcium entry through mutant Piezo1, which remains open longer. Sodium entry may also contribute to the repolarization kinetics observed.

Low Ionic Strength-induced NSC activity

Subjecting RBCs to Low Ionic Strength Solution (LIS) is known to elicit an instantaneous depolarization, attaining very positive membrane potential values, due to the lack of ions in the extracellular solution. In these conditions, a Non Selective Cation channel as well as chloride channel opens to allow potassium and chloride out of erythrocytes in an attempt to bring the membrane potential to physiological values (-10 mV). Hence, it can be observed whether Piezo1 mutations have an impact in NSC activity. In addition, as this solution is nominally calcium-free, supplementation with 1 mM $CaCl_2$ during repolarization immediately activates Gárdos,

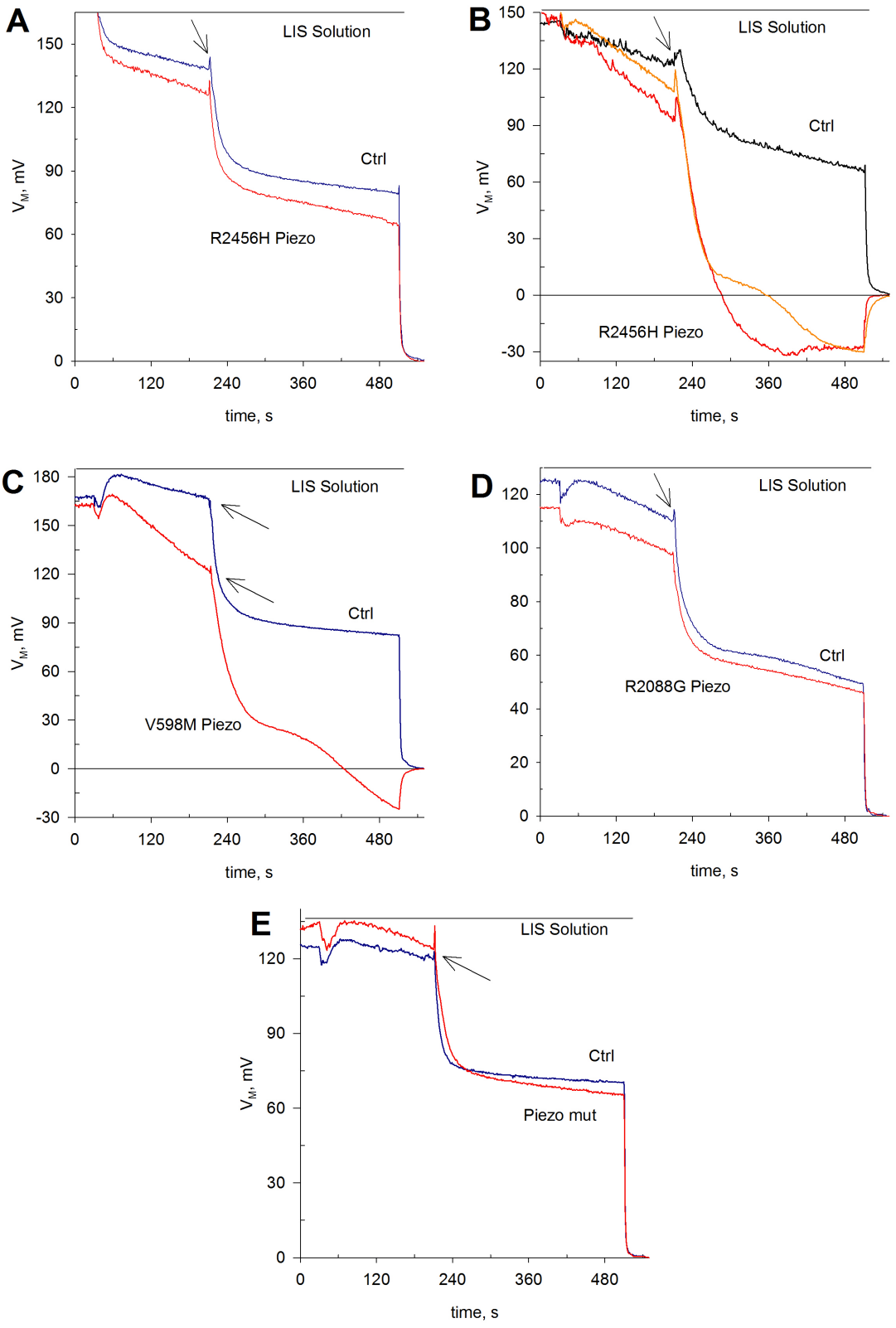

Figure 4.27: NSC channel activity is often increased in Piezo1-HX RBCs resuspended in LIS solutions. Membrane potential traces from control (blue trace) and patients' erythrocytes (red trace) with R2456H (**A** and **B**), V598M (**C**), R2088G (**D**) or unknown (**E**) Piezo1 mutation injected into Low Ionic Strength Ringer. Arrows indicate calcium addition (1 mM). Each trace is an independent measurement from a different donor. R2456H patients: Patient 1 in panel A, Patient 2 in Panel B red trace and Patient 3 in panel B orange trace. Axes were set for the best fit that shows better the initial slopes.

as there is an opened pathway for Ca^{2+} [172, 294]. This approach allows for the study of NSC and Gárdos simultaneous activities without the use of agonists. As the unknown Piezo1 mutant deviates from all other mutants analyzed in these conditions, it was considered as an outlier and excluded from overall analysis. Axes were chosen to fit the plots in order to allow better comparison of trace slopes. Upon cell resuspension in LIS solution, erythrocytes repolarize towards less positive membrane potentials. The rate at which cells repolarize depends on the chloride conductance and the activity of NSCs, hence on chloride and potassium efflux. For the membrane potential to decrease over time the efflux of potassium must be greater to the exit of chloride, thus reflecting the extent of NSC activity. The average initial post-depolarization rate ($v_0^{postdep}$) of wild-type red cells is -0.089 ± 0.024 mV/s (n=5), slower than Piezo1 mutants studied at a rate of 0.188 ± 0.104 mV/s (n=6) (p=0.247, Mann-Whitney) (**Fig. 4.27A-E**). There is wide variability with only two patient's RBC showing a significant difference in $v_0^{postdep}$. R2456H and V598M Piezo1 RBCs display an enhanced NSC activity in LIS conditions. They repolarize at a rate of -0.280 ± 0.039 mV/s (n=3) in contrast to control erythrocytes that do at a rate of -0.089 ± 0.024 mV/s (n=5) ($p<0.001$, Mann-Whitney). RBCs from a R2456H and R2088G Piezo1-HX patient as well as a patient with an unknown Piezo1 mutation repolarize no faster than control RBCs.

To test whether Ca^{2+} through Piezo1 or another NSC channel is enhanced in patient cells during repolarization, 1 mM Ca^{2+} is injected in order to elicit a Gárdos channel opening [295]. The mean delta in membrane potential between calcium addition and maximum hyperpolarization was 97.0 ± 44.2 mV for all Piezo1-HX RBCs samples studied compared to 62.5 ± 12.7 mV for controls (p=0.247, Mann-Whitney)(**Fig. 4.27**). Nonetheless, it is evident that there are two subgroups of Piezo1-HX patients, with pronounced Gárdos activation after calcium addition to the medium in two out of three R2456H mutants and V598M mutant (**Fig. 4.27B-C**), whereas the other mutants display no stronger Gárdos-mediated response to calcium than wild-type (**Fig. 4.27A, D, E**). This large difference observed between R2456H and V598M mutants (**Fig. 4.27B-C**) and wild-type indicates that the cation conductance is increased in these Piezo1 mutants in LIS conditions as more calcium is able to pass through a cationic conductive pathway heightening intracellular calcium levels and assuming the chloride conductance is constant. LIS approach revealed the tremendous difference in NSC channel activities between patients with the same mutation (**Fig. 4.27A-B**).

It is worth noting that the greater the V_M at which cells initially depolarize and the faster cells repolarize after the initial depolarization, the more pronounced is the hyperpolarization. Because if NSCs are more active in LIS conditions, then more calcium can traverse the channel(s) and activate, in turn, Gárdos triggering a hyperpolarization. Hence, the slow pace at which R2456H, R2088G and unknown mutants ((**Fig. 4.27A, D and E**) repolarize is indicative of reduced NSC activity in these conditions compared to other mutants. The variability likely stems from the fact that NSC channels, NSVDC and Piezo1, are in very low copy numbers and both may vary according to genetic background and protein partition and degradation, though we do record the average response of the cell population.

Interestingly, in **Figure 4.27B-C**, erythrocytes from R2456H and V598M Piezo1 patients display delayed kinetics before attaining a maximum hyperpolarization after Gárdos opening. Only two phenomena are possible, either the chloride conductance is briefly altered due to the sudden decrease in membrane potential and the opening of another, stronger potassium pathway or the direction of potassium flow through the NSC is momentarily reversed as the efflux through Gárdos is much stronger. An equilibrium is eventually reached, according to the potassium driving force. An entry of sodium is impossible in these conditions as it is lacking in the extracellular solution. It is unknown why this phenomenon was not observed for Patient 3 (**Fig. 4.27B**, red

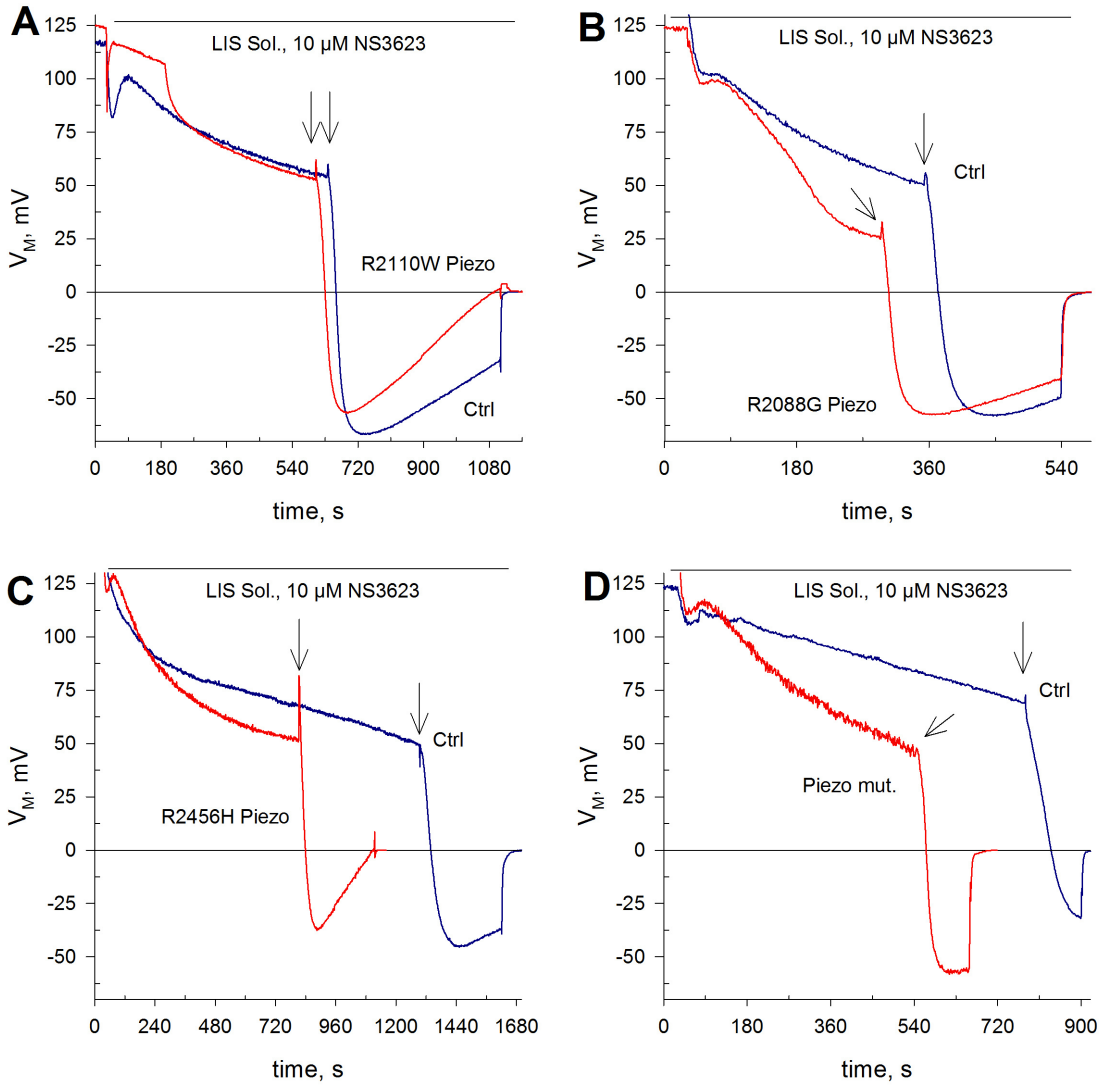

Figure 4.28: NSC channel activity of Piezo1-HX RBCs is further accelerated in LIS conditions when G_{Cl^-} is inhibited.

Membrane potential traces from control (blue trace) and patients' erythrocytes (red trace) with R2110W (**A**), R2088G (**B**) and R2456H (**C**) and unknown (**D**) Piezo1 mutation injected into Low Ionic Strength Ringer in the presence of chloride conductance inhibitor NS3623 (10 µM). Arrows indicate calcium addition (1 mM). Each trace is an independent measurement from a different donor. Axes were set for the best fit that shows better the initial slopes.

trace) as the $v_0^{postdep}$ and V_M^{maxhyp} are largely identical.

In LIS conditions there are only two predominant ionic pathways: i) the chloride conductance, ii) NSC due to the strong depolarization and, if calcium is added to the medium, a third one, Gárdos, with a higher potassium conductance than NSCs, i.e. capable of carrying more K^+ through. Hence, use of a chloride conductance blocker such as NS3623 (10 µM) allows to look directly at NSC activity from the start and subsequently, Gárdos upon calcium stimulation, since they are the only predominant pathways in these conditions. Axes were chosen to fit the plots in order to allow better comparison of trace slopes. There is a difference of 0.088 mV/s (n=4) in the mean repolarization rates at the onset of RBCs exposure to both 10 µM NS3623 and a LIS medium between wild-type and Piezo1 mutant erythrocytes, though it is not statistically significant (p=0.339) (**Fig. 4.28**). However, it is obvious that for R2008G, R2456H and unknown Piezo1 mutants, the repolarization

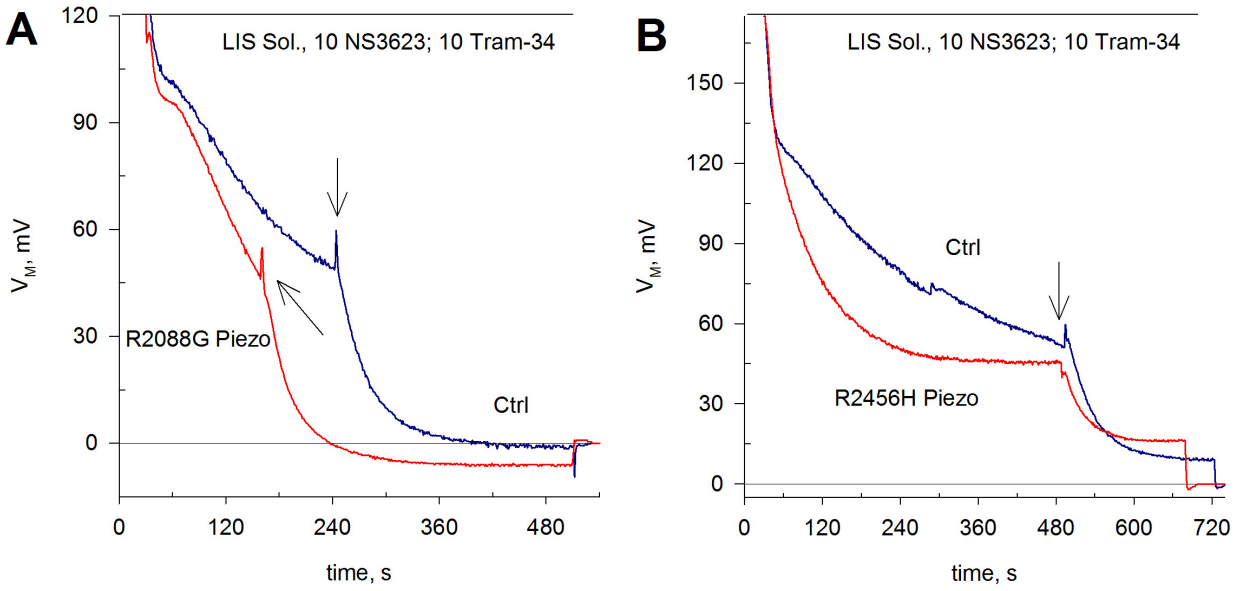

Figure 4.29: NSC channel activity of Piezo1-HX RBCs is further accelerated in LIS conditions when G_{Cl^-} is inhibited by NS3623 and Gárdos by Tram34.

Membrane potential traces from control (blue trace) and patients' erythrocytes (red trace) with R2088G (**A**) or R2456H (**B**) Piezo1 mutation injected into Low Ionic Strength Ringer in the presence of chloride conductance inhibitor NS3623 (10 µM) and Gárdos inhibitor Tram34 (10 µM). Arrows indicate calcium addition (1 mM). Each trace is an independent measurement from a different donor. Axes were set for the best fit that shows better the initial slopes.

rate is faster compared to their respective controls. R2110W mutant, on the contrary, seems similar to control. Unfortunately, the experiment without NS3623 was artifactual and thus no conclusion could be drawn for this particular mutant (R2110W). The maximum hyperpolarization after Ca^{2+} addition does not differ between mutants and controls (-50.6 ± 15.2 mV and -52.4 ± 9.9 mV, respectively)(**Fig. 4.28**). On the other hand, the repolarization towards zero membrane potential observed immediately after attaining the new equilibrium following Gárdos activation is faster in the Piezo1 mutants studied compared to control RBCs. The unknown Piezo1 variant was excluded from this analysis as there is insufficient information for rate calculation (**Fig. 4.28D**). Hence, whereas control cells repolarize at a rate of 0.074 ± 0.018 mV/s (n=3), Piezo1 mutants display a significantly different repolarization rate of 0.145 ± 0.036 mV/s (n=3), a significant difference (p=0.036)(**Fig. 4.28A-C**).

Employing two inhibitors: Tram34 (10 µM) targeting Gárdos and NS3623 (10 µM) targeting the chloride conductance removes the only two conductances possible in LIS conditions out of the equation leaving NSC as the sole and predominant one. However, despite high reported affinity of Tram34, some Gárdos activity or calcium-induced hyperpolarization is observed after calcium addition, though considerably reduced compared to Tram34-free experiments. The NSC is more active in R2088G and R2456H Piezo1 erythrocytes in these conditions, confirming initial observations made with NS3623 (10 µM) alone. Initial repolarization rates, $v_0^{postdep}$, were -0.275 mV/s for wild-type erythrocytes compared to -0.532 mV/s of R2088G Piezo1 RBCs (**Fig. 4.29A**). $v_0^{postdep}$ was even more pronounced in R2456H Piezo1 red cells at -0.914 mV/s, for -0.372 mV/s of control RBCs. Furthermore, whereas wild-type erythrocytes reach a maximum hyperpolarization of -1.6 mV or 8.6 mV, R2088G and R2456H Piezo1 RBCs attain -6.4 mV and 15.7 mV, respectively. A new equilibrium is quickly reached after hyperpolarization. Importantly, it is worth noting that Ca^{2+} still induces hyperpolariza-

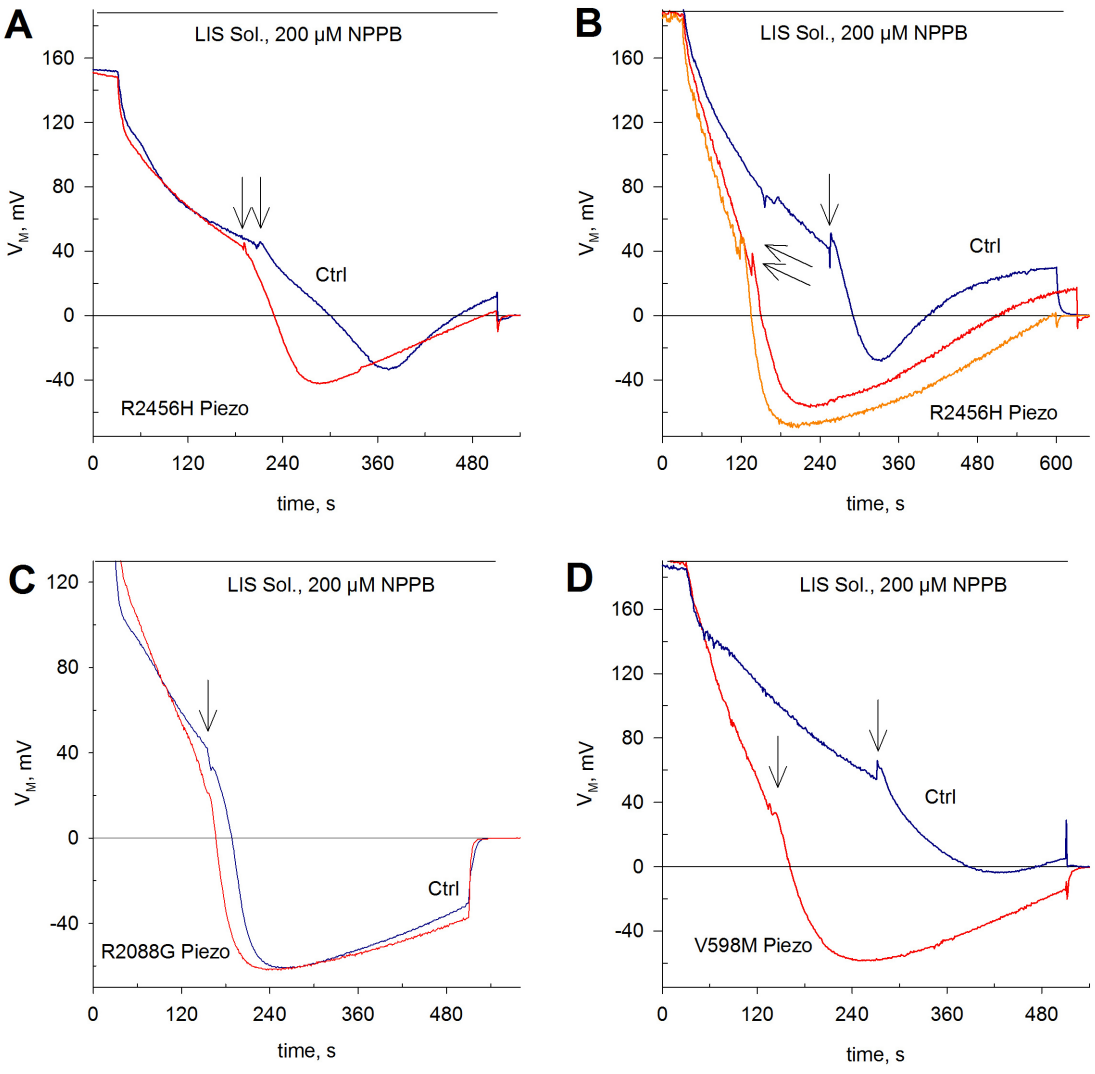

Figure 4.30: NSC channel activity of R2456H RBCs is further accelerated in LIS conditions when G_{Cl^-} is inhibited by NPPB.

Membrane potential traces from control (blue trace) and patients' erythrocytes (red trace) with R2456H (**A** and **B**), R2088G (**C**) or V598M (**D**) Piezo1 mutation injected into Low Ionic Strength Ringer in the presence of chloride conductance inhibitor NPPB (200 µM). Arrows indicate calcium addition (1 mM). Each trace is an independent measurement from a different donor. Axes were set for the best fit that shows better the initial slopes.

tion when Gárdos is inhibited raising the question whether Tram34 is fully inhibiting the channel as it would be expected for such a high concentration or more presumably the repolarization originates from two distinct NSC channels for which at least one is Ca^{2+} dependent.

As there is wide interpersonal variability among channel activities of both healthy and anemic donors' RBCs and knowing that different chloride inhibitors give rise to different initial repolarization profiles, another such blocker was employed to supplement data obtained with 10 µM NS3623 treatment. Chloride inhibitor NPPB was employed, as it displays high efficacy in Low Ionic Strength conditions. Thus, as with NS3623 (10 µM), NSC activity can be recorded without chloride conductance compensation. NSC-mediated initial repolarization, v_0^{rep}, is greatly accelerated as no anions leave the cell along with potassium (**Fig. 4.30**). Axes were chosen to fit the plots in order to allow better comparison of trace slopes.

No statistically significant difference in $v_0^{postdep}$ between Piezo1 mutants (-1.018 ± 0.389 mV/s (n=5)) and

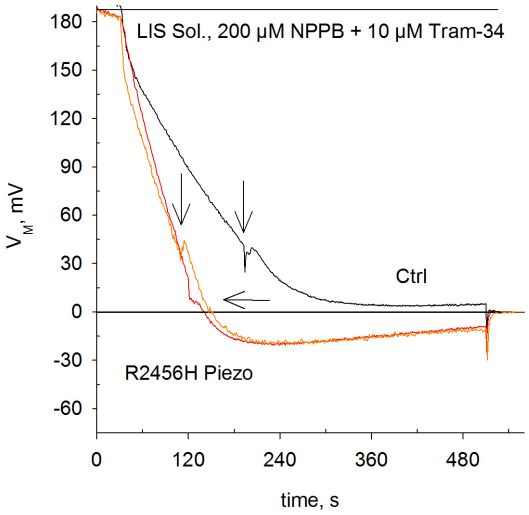

Figure 4.31: NSC channel activity of Piezo1-HX RBCs is further accelerated in LIS conditions when G_{Cl^-} is inhibited by NPPB and Gárdos by Tram34.

Membrane potential traces from control (blue trace) and patients' erythrocytes (red and orange traces) with R2456H Piezo1 mutation injected into Low Ionic Strength Ringer in the presence of chloride inhibitor NPPB (200 µM) and Gárdos inhibitor Tram34 (10 µM). Arrows indicate calcium addition (1 mM). Each trace is an independent measurement from a different donor. Axes were set for the best fit that shows better the initial slopes.

wild-type (-0.579 ± 0.198 mV/s (n=4)) RBCs was found (0.081) (**Fig. 4.30**). However if a R2456H mutant (**Fig. 4.30A**) is excluded, as it is clear the initial slope is identical to that of control, a difference of -0.589 mV/s (n=4) is found between groups (p=0.008).

Right after calcium addition, the hyperpolarization rate, v_0^{hyp}, was -1.262 ± 0.663 mV/s (n=4) for control RBCs compared to -2.011 ± 0.622 mV/s (n=5) of Piezo1 mutants analyzed (p=0.125). Piezo1 mutants studied hyperpolarize to further extents than wild-type RBCs: -57.8 ± 10.0 mV (n=5) for -31.6 ± 23.4 mV (n=4), respectively (p=0.056). R2456H and V598M Piezo1 RBCs, which show the strongest hyperpolarizations among mutants studied, reach a mean maximum hyperpolarization significantly larger than wild-type cells: -56.83 ± 11.20 mV (n=4) compared to -21.91 ± 15.95 mV (n=3), respectively (p=0.019). The subsequent repolarization rate, $v_0^{posthyp}$, however, was not different between groups.

In these conditions, if erythrocytes are pretreated with Tram34 (10 µM) as well as NPPB in LIS medium, the Gárdos channel is mostly inhibited and as a result the NCS becomes the predominant conductance in these conditions (**Fig. 4.31**). Axes were chosen to fit the plots in order to allow better comparison of trace slopes. R2456H Piezo1 RBCs repolarized faster at the onset with rates of -1.72 and -1.53 mV/s (n=1) compared to -0.83 mV/s (n=1) of control red cells. Maximum hyperpolarizations following calcium addition were much reduced by Tram34-mediated Gárdos inhibition. Whereas wild-type erythrocytes reached only 3.6 mV, a value matching the resting membrane potential in typical solutions, R2456H Piezo1 RBCs further hyperpolarized to -24.97 and -29.73 mV (n=1). The subsequent repolarization frequently observed after Gárdos stimulation was minimal. Control red cells displayed a rate of -0.01 mV/s (n=1) in contrast to 0.05 and 0.03 mV/s (n=1).

Piezo1 inhibition via toxin GsMTx4

GsMTx4 has been reported as a potent inhibitor of mechanosensitive channels, including Piezo1. Use of this blocker in LIS conditions, where there is continuous NSC activity slows down considerably $v_0^{postdep}$ in

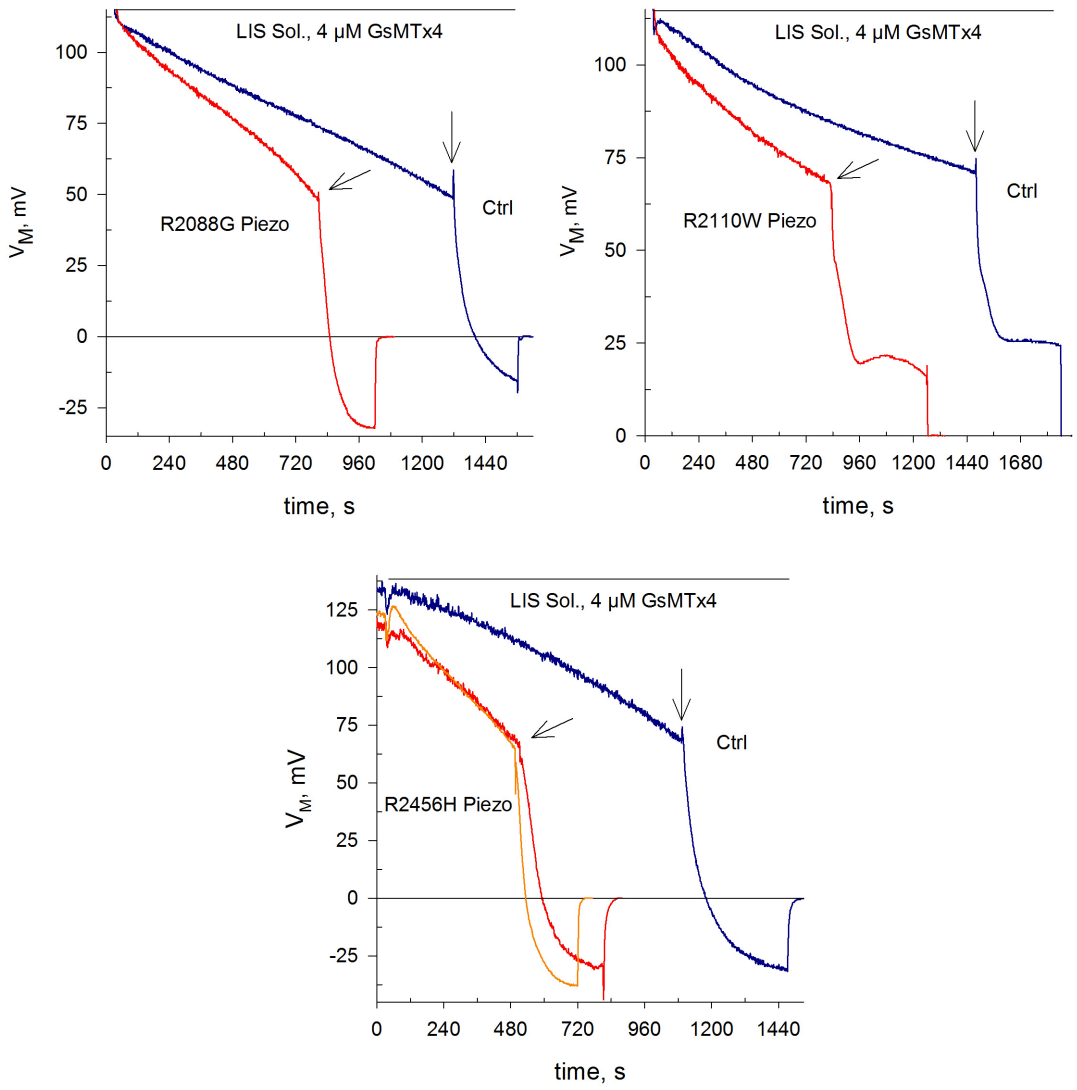

Figure 4.32: Piezo1-HX RBCs display strong NSC channel activity in LIS conditions despite GsMTx4 inhibition.

Membrane potential traces from control (blue trace) and patients' erythrocytes (red trace) with R2088G (**A**), R2110W (**B**) and R2456H (**C**) Piezo1 mutation injected into Low Ionic Strength Ringer in the presence of mechanosensitive channel inhibitor GsMTx4 (4 µM). Arrows indicate calcium addition (1 mM). Each trace is an independent measurement from a different donor. Axes were set for the best fit that shows better the initial slopes.

wild-type cells, indicating by such that Piezo1 is involved as a NSC in the LIS effect. Note the time axis. Nevertheless, the fact that the membrane potential does change in the presence of GsMTx4 shows that there is another NSC, distinct from Piezo1, involved in the LIS NSC activity. Hence, at least two Non-Selective cation Channels ought to be involved to account for the cation movements observed in LIS conditions. Axes were chosen to fit the plots in order to allow better comparison of trace slopes. The initial repolarization rate, v_0^{rep}, was -0.047 ± 0.008 mV/s (n=3) for control RBCs and -0.097 ± 0.034 mV/s (n=4) for the Piezo1 mutants studied (**Fig. 4.32A-C**). The difference falls short of statistical significance (p=0.062). However, R2008G and R2456H Piezo1 mutants repolarize significantly faster than wild-type erythrocytes in these conditions. v_0^{rep} were -0.047 ± 0.008 mV/s (n=3) and -0.109 ± 0.0282 mV/s (n=3) for R2008G and R2456H Piezo1 and wild-type RBCs, respectively (p=0.021) (**Fig. 4.32A, D**). R2110W RBCs take nonetheless 12 min less than wild-type cells to reach 70 mV (**Fig. 4.32B**). R2008G attain a membrane potential of 50 mV within 13 min, compared to 24.58

min of control RBCs. R2456H Piezo1 RBCs are about 10 min faster than wild-type erythrocytes at the onset to reach 70 mV. Upon calcium addition to the medium, Gárdos opens as calcium is able to enter the cell via a NSC in spite of Piezo1 inhibition, considering the finding that NSC activation in LIS conditions gives rise to two distinct NSC activities. Control erythrocytes attained a maximum hyperpolarization of -9.03 ± 29.53 mV (n=3) in contrast to -21.20 ± 25.28 mV (n=4) of the Piezo1 mutants studied (p=0.4, Mann-Whitney). An increased channel activity at the baseline may explain these findings, as GsMTx4 is know to act via direct action on the lipid membrane rather than the channel itself, although the effect of a conformational change, including at the quaternary level, in the local shape of the plasma membrane and hence on the binding affinity of GsMTx4 on the lipid bilayer surrounding the channel cannot be ruled out [161].

Discussion

Even though stomatocytes are found in patient blood samples, they are rare (except for R2088G Piezo1 RBCs), and the overall morphology is largely unremarkable which together with clinical parameters overlapping other disorders have made difficult the diagnosis of this disorder. Erythrocytes affected with mutations in Piezo1 typically display an increase in Na^+, due to the opening of Piezo1 itself, and a decrease in K^+, which causes cell dehydration and which is a consequence of Gárdos activation due to calcium influx through Piezo1. See **Table 4.2** on page 141 for a summary of findings. Due to severe life-threatening thrombotic complications found in hereditary xerocytosis splenectomized patients, splenectomy is nowadays contraindicated [296, 297]. Transfusion-independent iron overload is featured in many Piezo1-HX patients and they often develop secondary hemosiderosis requiring chelation. How the mutation may impair iron metabolism is unknown, perhaps via hepcidin dysregulation [278]. Most mutations described occur in near the C-terminal domain, close to the pore assembly region, which indicates that a mutation in this region is likely to be deleterious, especially changes in charged residues which directly affect channel properties [207, 298]. Na^+ and K^+ intracellular amounts were also reported to increase and decrease, respectively, after overnight transport. Na^+ influx is favored by Gárdos activation, as the driving force shifts due to K^+ exit and the membrane potential becomes more negative, as observed in the repolarizations occurring after Gárdos activation which are generally faster the larger the previous hyperpolarization was (**Fig. 4.25**). Cell-attached patch-clamp experiments show spontaneous currents on RBCs from an anemic individual affected by R2456H mutation in response to pressure and applied voltage, not seen in wild-type erythrocytes, with full inhibition when GsMTx4 was present in the pipette [207]. The mutated channel displays an increased open probability and slow inactivation kinetics in response to mechanical stimuli [207, 298, 299].

These findings are in agreement with ours as we have found cation reversal in the cell population and Yoda1 experiments (**Fig. 4.26**) reveal a significant delay in the repolarization which occurs after Gárdos-induced hyperpolarization due to calcium entry. Membrane potential change occurs in much longer timespans than current activity and although low concentrations of agonist were employed, Piezo1 activity is sustained when using Yoda1, contrary to mechanical stimulation. Hence, as the mutated channel shows prolonged activation upon cell stretching, the mutation is considered gain-of-function [291]. All disease-causing mutations in erythrocytes reported so far have been gain-of-function, suggesting that mutations reducing channel activity are less deleterious, at least in RBCs. Concerning V598M mutation, a patch-clamp study found higher currents after extinction of a large initial conductance in wild type erythrocytes exposed to Yoda1 than in V598M RBCs in the absence of stimulation [300]. Although, the combination of the gain-of-function mutation plus Yoda1

activation is expected to result in greater whole-cell currents than wild-type it may partially account for our puzzling observation where the initial hyperpolarization of wild-type RBCs matches that of V598M erythrocytes. Treating V598M Piezo1 erythrocytes with Gárdos inhibitor senicapoc was shown to reduce spontaneous currents whole-cell demonstrating Gárdos is involved via Ca^{2+} influx through Piezo1 [300].

Piezo1 is more abundant in erythroid progenitors than in mature RBCs so it is thought to play a role in erythropoiesis [301]. The kinetics alterations of mutated Piezo1 point to either a destabilization of the inactivated state or a stabilization of the open state [298]. Considering Piezo1 opens very briefly (in the order of 100 ms) in response to mechanical stimulus as shown via patch-clamp, an increase in the basal channel activity in the absence of mechanical stimuli must be considered [207, 275, 299]). Contribution in this manner to the basal Ca^{2+} leak of RBCs would explain better the more severe phenotypes encountered. A sustained entry of Ca^{2+} (and Na^+) puts a heavy strain on Na^+/K^+ and calcium pumps, depleting the cells of ATP especially as cells get older in the circulation. Such a process may entail early erythrocyte death and explain thrombotic complications as Ca^{2+} is important in cytoskeleton function, with an excess potentially destabilizing it and impairing deformability within the microvasculature. Compatible evidence with this hypothesis has been shown [302]. Importantly, a very recent publication addresses the question of post-translational regulation of Piezo1 by phosphorylation upon mechanical stimulus [303]. Indeed, the ability to perform phosphorylation depends directly on ATP availability. Attention to this issue is lacking and further experiments will be required for clarification.

Piezo1 can be active in wild-type red cells independently of mechanical stimulus, as seen in Low Ionic Strength Conditions (**Fig. 4.28** and **4.32**), with membrane potential change being delayed by GsMTx4 in both wild-type and Piezo1-HX cells, but considerably more so in wild-type cells. Considering the mode of action of GsMTx4 [161], such an observation would demonstrate that changes in the behavior of mutant Piezo1 channels are variable. Indeed, mutations may affect the open probability as well as the inactivation time of the channel [275, 298, 299]. But we may also consider that the surrounding environment is particularly important for a mechanosensitive channel. Thus the lipid composition of patients' erythrocytes should also be studied since such alterations may contribute to the symptomatic variability observed. An initial study seems to support this notion [304]. Among ion pathways, only Piezo1, Gárdos and plasma membrane ATPases (by failing to counter the cation imbalance) are involved in Piezo1-HX pathophysiology. Cotransporters, including NKCC, were found not to be overactive in Piezo1-HX patients [207]. RBCs from hematopoietic-specific mouse knockout were found to be overhydrated and thus swollen, were more easily trapped in the spleen and were more osmotically fragile [305].

Dehydration observed is caused by frequent Gárdos activations due to abnormally high calcium levels. NS3623 does not inhibit Gárdos, but by blocking the chloride conductance it can significantly decrease Gárdos-caused dehydration as the loss of potassium is rate-limited by that of chloride and water loss is the result of salt loss and osmotic movement. This strategy was proven successful in SAD mice improving sickle cell disease symptoms such as hematocrit and a reduced irreversibly sickled cell fraction [306].

Piezo1 is not only permeable to divalent cations but to monovalent cations as well. Hence, at resting membrane potentials its activation ought to cause an exchange 1:1 of Na^+ and K^+ as they move down their gradient for the time of channel opening. Experiments in RBC suspensions treated with Yoda1 demonstrate cation reversal in a few minutes. Potassium efflux surpasses sodium influx due to the calcium influx activating Gárdos, which is selective for potassium and highly dissipative (**Fig. 4.33**). Hence, there is net cation efflux and

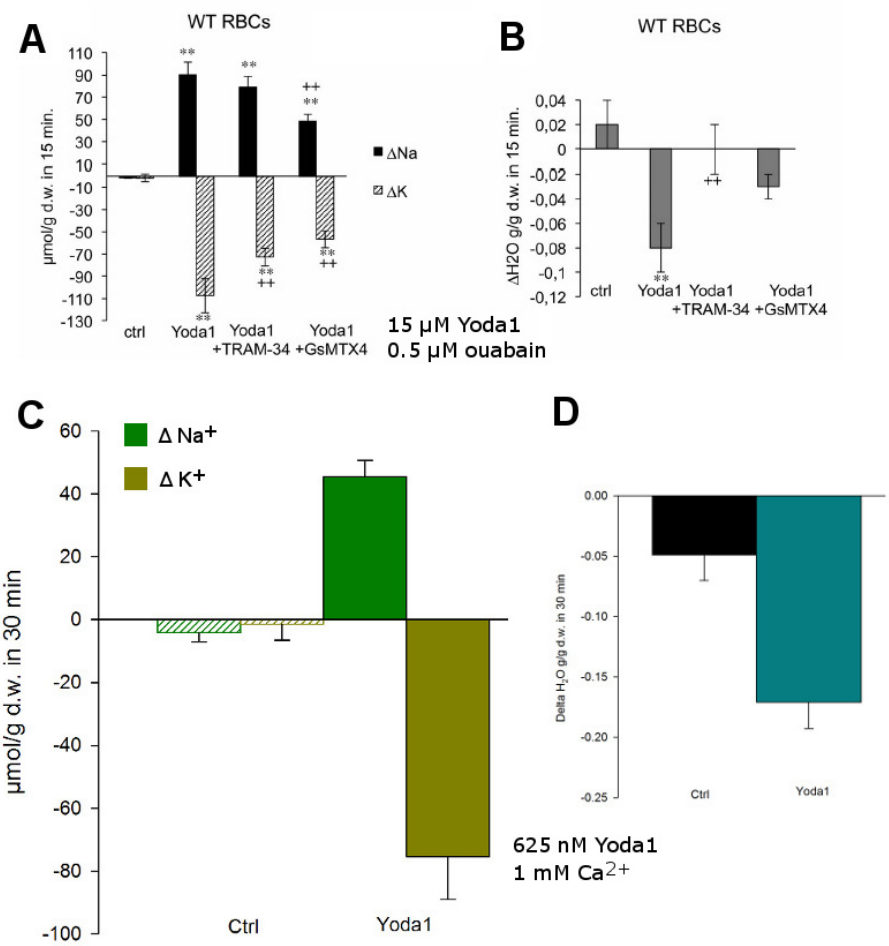

Figure 4.33: Cell water, sodium and cation content of wild-type RBCs following treatment of Piezo1 agonist Yoda1.

Cation (**A**) and water (**B**) movements in control RBCs stimulated by Yoda1. Washed RBC suspension was set to 30% hematocrit and 0.5 µM ouabain was added. At time zero, 15 µM of Yoda1 was added to cell suspension either containing 10 µM TRAM-34, 10 µM GsMTx4 or DMSO. Samples were collected 15, 30 and 60 minutes after Yoda1 addition and cell water, Na^+ and K^+ contents were measured. Data shows the variation in 15 minutes, means ± SEM of 4 experiments. **P<0.001 comparison of control condition with the 3 conditions with Yoda1. ++P<0.001 comparison between Yoda1 and Yoda1 + inhibitors. Mann-Whitney test. Cation (**C**) and water (**D**) movements in control RBCs stimulated by Yoda1. Washed RBC suspension was set to 15% hematocrit in the presence of 1 mM Ca^{2+} and 625 nM of Yoda1 was added to cell suspension. Samples were collected 30 minutes after Yoda1 addition and cell water, Na^+ and K^+ contents were measured. Data shows the variation at 30 minutes, means ± SEM of 3 experiments. Panels A and B are adapted from [300]. Panels C and D are own data.

water follows by osmosis causing cell dehydration. Figure 4.33A-B shows Piezo1 activation by use of high concentrations (15 µM) of Yoda1 in the presence of Na^+/K^+ pump inhibitor ouabain. Gárdos contribution to K^+ efflux is seen after Tram34 inhibition and importantly it abrogates cell water loss. GsMTx4 blocks only partially Na^+ and K^+ movements through Piezo1, suggesting lower specificity for Piezo1 than is currently expected. Cation distribution reversal via Piezo1 opening can also be observed if small concentrations of Yoda1 are used, provided there are millimolar levels of calcium in the medium as erythrocytes find in plasma (**Fig. 4.33C**). This approach intends to resemble a sustained mechanical activation, considering high concentrations of Yoda1 are highly deleterious to RBCs due to the massive calcium entry, with echinocytes and even spheroechinocytes forming in a few seconds, as we observed under the microscope (not shown). Marked dehydration is also

observed in this setting as K^+ exit is greater than Na^+ entry, further confirmation that Piezo1 openings can lead to strong Gárdos activation. Ouabain was not employed as ion movements through the Na^+/K^+ pump are negligible compared to those carried by an ion channel in the timespan of the experiment. Piezo1 activation *in vivo* likely consist in brief openings lasting milliseconds, with Gárdos activity being thus limited in scope, far from an activation lasting minutes. However, it proves Piezo1 malfunction has severe consequences for cation content and, hence, cell hydration.

Disorder	Mutation	Ion channel activity	Cell water	$[K^+]_i$	$[Na^+]_i$	Cell shape	Cell roundness	Cell circularity	Cell surface area
Gárdos-HSt	R352H	Calcium sensitivity is augmented	Increased	Slightly decreased	Increase	Acanthocytes, schistocytes	Decreased	Decreased	Increased
Gárdos-HSt	S314P	Calcium sensitivity is augmented	Slightly decreased	Increased	As wild-type	Elliptocytes, microcytes	Decreased	Decreased or as wild-type	Decreased
Piezo1-HX	R2110W	NSC activity is increased in hyperpolarizing conditions. Strong NSC activity despite GsMTx4 inhibition	Marked decrease	Decrease	Markedly increased	Stomatocytes, acanthocytes	As wild-type	As wild-type	Decreased
Piezo1-HX	R2088G	Strong NSC activity upon G_{Cl^-} inhibition. Strong NSC activity despite GsMTx4 inhibition	Decreased	Decreased	Increased	Stomatocytes, acanthocytes	Decreased	Decreased	Increased
Piezo1-HX	R2456H	Strong Yoda-induced opening with delayed inactivation. Strong NSC activity in LIS conditions, also in the presence of inhibitor GsMTx4.	Decreased	Decreased	Increased	Stomatocytes, acanthocytes, codocytes	Decreased	Decreased	Increased
Piezo1-HX	V598M	Delayed inactivation upon Yoda-induced opening. Strong NSC activity in LIS conditions.	Slightly decreased	Decreased	Markedly increased	Stomatocytes, schistocytes	Decreased	Decreased	Increased
Piezo1-HX	Unknown	Strong Yoda-induced opening with delayed inactivation. Strong NSC activity upon G_{Cl^-} inhibition.	Decreased	Decreased	Increased	—	—	—	—

Table 4.2: Summary of results of Gárdos-HSt and Piezo1-HX studied.

Table summarizing findings of intracellular, water, sodium, potassium, morphology and ion channel activity of RBCs from Gárdos-HSt and Piezo1-HX patients studied as compared to wild-type. Cell shape refers to abnormal cell shape found in blood smears.

Conclusion: Diagnostic potential

Genetic hematological disorders have been described affecting Gárdos and Piezo1 with Single Nucleotide Polymorphisms (SNPs) and resulting missense amino acid change causing increased channel activity leading to hemolysis. Use of the aforementioned approaches allow us to gauge the extent of cationic conductive activity in real time and it is thus a valuable complementary tool for diagnosis of these channelopathies. Membrane potential estimation gives functional information of channel activity which is lacking in clinical practice as diagnosis is based on morphology (often insufficient for differential diagnosis as is highly variable in channelopathy patients) and/or on exome sequencing. Although patch-clamp is the gold standard in regard to functional characterization of conductive pathways it deals with single cells and experiments are often done with heterologously expressed mutants in cell lines, which may not yield the full picture as interacting partners present or absent in RBCs can influence their activity. Experiments on human RBCs have been performed but owing to cell fragility compounded by cell transport their scope is limited (see data on Gárdos channelopathy cells on 113). Automatic patch-clamp is a technique which provides the robustness and accuracy of patch-clamp with high-throughput and great amounts of data can be thus obtained. However high-throughput automated patch-clamp devices are expensive and impose harsh conditions on RBCs (akin to manual patch-clamp) such as shear stress, which is a concern in the study of Piezo1 activity and its downstream effects.

Membrane potential estimation is inexpensive as it only requires a pHmeter and appropriate drugs. Moreover, low blood volumes are enough to perform experiments and it could be set up with ease in a hospital laboratory. Hence in case where morphology is puzzling and information is scant to make a diagnosis, functional ion channel activity information can be useful prior or in addition exome sequencing as fast and accurate result can be delivered quickly provided a healthy control is analyzed under the same conditions. The technique gives information on severity and screenings on the proband's family can be performed with just a few milliliter of blood and a response within a day. Limitations include the fact that measurements are carried out on large cell populations, so the enhanced ion channel activity of the cells more prone to lysis is averaged with those with little channel activation, potentially underestimating the impact extent. It requires fresh blood, given that channel activity changes with cell age and, especially, transportation has a deleterious effect, so it must be as fast as possible. A wild-type control must be included in any shipment to account for these transportation effects. The main shortcoming is the high variability observed between individuals including wild-type controls, which may have especially high ion channel activity or undiagnosed conditions of their own leading to misinterpretation.

New Piezo1 variant D669Y

New Piezo1 variant with enhanced cation permeability: an unexpected phenotype

Laurent Pérès[1*], David Monedero Alonso[1*], Morgane Nudel [2], Martin Figeac[3,4], Judith Bruge[2], Shéhérazade Sebda[3], Véronique Picard[5], Wassim El Nemer[6], Claude Preudhomme [3], Stéphane Egée[1#], Guillaume Bouyer[1#]

[1] CNRS UMR8227, Station Biologique de Roscoff, Sorbonne Université, Labex GR-Ex, France

[2] Hôpital Saint Vincent de Paul, Université Catholique, Lille

[3] Univ-Lille, Plate-forme de Génomique Fonctionnelle et Structurale, F-59000 Lille, France

[4] CHU Lille, cellule bioinformatique, plateau commun de séquençage, F-59000 Lille, France

[5] Hématologie biologique, CHU Bicêtre, Le Kremlin Bicêtre

[6] Inserm, UMR_S 1134, Institut National de la Transfusion Sanguine INTS, Paris

*contributed equally to this work

#contributed equally to this work

Human erythrocytes need to tightly control their membrane permeability to preserve their volume and deformability properties within the circulation. Most notably, defects in proper maintenance of cation permeability and cell content are implicated in several diseases (1). Dehydrated Hereditary Stomatocytosis (DHS), also termed Hereditary Xerocytosis (HX) (OMIM 194380), is a rare autosomal dominant congenital haemolytic anaemia, characterized by decreased intracellular K^+ concentration, not compensated by an increase in Na^+ content. This leads to erythrocyte dehydration with resulting increased Mean Corpuscular Haemoglobin Corpuscular Concentration (MCHC), and decreased osmotic fragility (1). Patient Red Blood Cells (RBCs) properties can be characterized by ektacytometry, where they display a maximal Elongation Index (EI_{max}) within normal range, while O_{min} and O_{hyper} are largely decreased (2, 3). Mutations affecting two cation channels have been linked to the disease: Piezo1, a mechanosensitive non-selective cation channel (4) and Gárdos channel, a K^+ selective channel activated by intracellular Ca^{2+} (5, 6). Regarding Piezo1, several mutations have been described leading to HX in the recent years (7, 8), nevertheless functional characterization of mutant ion channel properties remained mostly restricted to studies using heterologous expression. Here we use complementary techniques to describe cation channel activity within RBCs from a patient having a mutation in Piezo1 channel (D669Y) previously linked to HX but never functionally characterised.

The patient has been suffering from episodic haemolytic anaemia since he was 5 years old. Biological parameters measured so far indicate a Hb concentration of 11.4 g/dl, an MCV (Mean Corpuscular Volume) of 101 fl, an MCHC of 35g/dl, with no obvious drastic morphological changes of erythrocytes on smears at first observation. Circulating reticulocytes level was 177G/L (5.6%). Furthermore, this patient had a bilirubinemia of 20 mg/l of which 17mg/l unbound. Etiological investigations conducted since early childhood has not provided

any diagnosis, although an enhanced osmotic resistance associated and an increase of foetal haemoglobin up to 2.1 % was observed.

The *de-novo* comparative study, by whole exome sequencing, of the two parents and of the *propositus*, revealed one *in-silico* predicted deleterious single anomaly: a heterozygous variation of *PIEZO1* gene present in exon 16 (NM_001142864.2:c.2005 G>T), leading to the mutation D669Y in the *propositus*. This site is rather distal compared to the previous descriptions of the different mutations (fig. 1A, and 3D structure in supplementary fig. 1). Notably, the mutated residue lies within one of the two putative extracellular domains responsible for the mechanotransduction properties described for mPiezo1 homologous channel (9) located in the peripheral blade-like structure. This mutation has been reported in two unrelated recent reports compiling data on large sets of HX patients (7, 8), that lacked functional characterisation. Further smears analysis for control and patient RBCs revealed the presence of aberrant shapes (fig. 1B), such as dacryocytes (tear-drop cells), achantocytes and target cells. Piezo1 D669Y RBCs also displayed an enlarged projected area (fig. 1C), consistent with an increased deformability, and are slightly elliptocytic as confirmed by the decreased cell roundness calculated from smear analysis (fig. 1D).

Ektacytometry revealed a mild DHS type profile for D669Y Piezo1 RBCs (fig. 2A): O_{min} is reduced, revealing as expected an increased osmotic resistance, EI_{max} is increased which shows an increased deformability and O_{hyper} is only slightly reduced, reflecting a mild dehydration. This was confirmed by osmotic fragility curves (fig. 2B), and by measuring hydration and cation concentration status of RBCs. As expected, intracellular K^+ was significantly decreased, but surprisingly intracellular Na^+ is increased (although not significantly) and cell water content is preserved (fig. 2C). When checking total intracellular cation content, we observed that K^+ decreased content was nearly compensated by increased Na^+: 139.4 vs 128.5 mmol/lcw for control and patient respectively (fig. 2D), an unusual feature for DHS. This raised two questions about the pathway(s) involved in Na^+ entry: (i) is it Piezo1 channel itself or another cation transporter regulated downstream? (ii) Is this linked to constant Na^+ small leakage into the cell, or to bursts of activity that Na^+/K^+ pump is unable to cope with?

To study the activity of cation channels within patient RBCs, we monitored the evolution of membrane potential in response to various stimulation, using the CCCP method (10). First, in a Normal Ringer solution, we injected control or D669Y Piezo1 RBCs. Rapidly for both cell types, the membrane potential stabilized to a value close to the theoretical membrane potential for RBCs (–12mV), indicating that this mutation does not alter chloride conductance or Band3 efficiency. We then challenged the membrane potential by addition of A23187, a Ca^{2+} ionophore that leads to a fast and maximal activation of the Gárdos channel (fig. 3A). Hyperpolarization peak reached the same amplitude both cell types, leading to the conclusion that Gárdos channel activity is not affected by the mutation. The repolarization occurring after maximal hyperpolarization corresponds to a cation influx (Na^+, the only permeant cation in the extracellular medium) through another conductive pathway. This repolarisation is accelerated in D669Y Piezo1 RBCs (fig. 3A), unveiling an increase in the activity of a cation channel, most likely Piezo1. In another series of experiments, cells were placed in a Low Ionic Strength (LIS) media that is known to activate Non Selective Cation Channel (NSC) activity in human RBCs (11). In D669Y Piezo1 RBCs, this NSC channel activity was faster than in control RBCs (fig. 3B). Injection of Ca^{2+} with subsequent activation of Gárdos channel confirmed our previous observations. The same experiment in LIS media

was repeated with the addition of 100µM NPPB to inhibit chloride conductance, revealing a much faster NSC channel activity in D669Y Piezo1 RBCs (fig 3C). Whether this activity can be attributed directly to the mutant Piezo1 channel or to a secondary mechanism remains to be determined. We then monitored Ca^{2+} content and uptake by using Fluo-4 loaded cells and Yoda1 activation of Piezo1 channels (fig. 3D). We observed that (i) basal Ca^{2+} content was significantly higher and (ii) Ca^{2+} uptake via Yoda1 activation was magnified in *propositus* RBCs compared with control RBCs, suggesting either an enhanced susceptibility of Piezo1 channel to the activator, or an increased maximal activity of the channel. Altogether, these results show that NSC activity is enhanced in patient RBCs and can provide a route for Na^+ and Ca^{2+} entry, likely via a direct increase of Piezo1 channel activity.

Finally, we used the patch clamp technique to monitor direct cation channel activity in RBCs membrane. The whole cell conductance of D669Y Piezo1 RBCs revealed an enhanced cation channel activity, whereas in control cells spontaneous cation current always remained minimal (fig. 3E). In patient cells, membrane currents are globally increased but when looking in details, only 4/7 cells displayed increased cation current (fig. 3F). This suggest that only in some D669Y Piezo1 RBCs, a spontaneous cation channel activity is increased. Two hypothesis can be proposed: this increase could be linked (i) to cell aging, a phenomenon that seems accelerated in patient RBCs; or (ii) to differential expression of the mutant channel in progenitor cells, since the proband is heterozygous for Piezo1 channel. For cells that displayed channel activity, membrane current was inwardly rectified, suggesting a more important activity for cations entering the cell at highly negative membrane potentials. This phenotype is rather different than other electrophysiological reports on Piezo1 mutant RBCs associated with HX where R2456H or R2088G Piezo1 RBCs displayed no difference from control, whereas C426R Piezo1 RBCs showed higher outward current and E2496ELE Piezo1 RBCs had a decreased current (12). A study using high throughput automated patch clamp on R2110W Piezo1 RBCs also showed increased current with an enhanced response to Yoda1 (13).

Altogether, we used different complementary approaches to investigate the effects of a Piezo1 mutation that has been linked to HX but not functionally investigated. Our characterization of cation channel activity using patient RBCs revealed a gain-of-function mutation for Piezo1 channel. This is almost always the case for HX, whereas loss-of-function mutations tend to have milder impact on RBCs, but have multiple consequences on other cell lineages, causing notably Generalised Lymphatic Dysplasia (OMIM 616843) (14, 15).

D669Y Piezo1 RBCs displayed as usual increased osmotic resistance and deformability but surprisingly no significant or very little cell dehydration. CCCP method proves that Gárdos channel susceptibility to Ca^{2+} and maximal activity are preserved, but Non Selective Cation Channel activity is enhanced, providing a route for Na^+ and Ca^{2+} to enter RBCs, and can compensate K^+ loss and restore membrane resting potential. In suspension, basal Ca^{2+} is not able to activate Gárdos channel. However Ca^{2+} relative measurements using Fluo-4 revealed a higher permeability to Ca^{2+} for patient cells when stimulated with Piezo1 activator Yoda1.

Consequently, we can speculate that the decreased lifespan of D669Y Piezo1 RBCs within the circulation proceeds via an accelerated aging of RBCs, which can be magnified by sudden and more frequent activation of the Gárdos channel when the threshold for its activation is exceeded. Finally, patch-clamp single cell study revealed the heterogeneity of cation channel activity in D669Y Piezo1 RBCs, illustrating the complexity of the consequences of the mutation

that likely depend on cell age. This also reflects the diversity of cell shapes observed in smear analysis.

Acknowledgement

We thank the patient and his family who gave informed written consent and generously provided blood samples for this study. This work is dedicated to the memory of Pr. Christian Rose, who followed the patient and initiated the collaboration between all groups.

Disclosures

The authors declare no relevant conflicts of interest. LP, DMA, WEN, GB and SE are supported by the Laboratory of Excellence Labex GR-Ex, reference ANR-11-LABX-0051; GR-Ex is funded by the program “Investissements d’avenir” of the French National Research Agency, reference ANR-11-IDEX-0005-02.

Author contributions

GB and SE designed the study and supervised the study. All authors performed research and data analysis. GB, VP and SE wrote the manuscript and designed the figures. All authors revised the manuscript.

References

1. Glogowska E, Gallagher PG. Disorders of erythrocyte volume homeostasis. Int J Lab Hematol. 2015;37:85-91. doi:10.1111/ijlh.12357.

2. Delaunay J. The molecular basis of hereditary red cell membrane disorders. Blood Reviews. 2007;21(1):1-20. doi:http://dx.doi.org/10.1016/j.blre.2006.03.005.

3. Andolfo I, Russo R, Gambale A, Iolascon A. New insights on hereditary erythrocyte membrane defects. Haematologica. 2016;101(11):1284-1294. doi:10.3324/haematol.2016.142463.

4. Zarychanski R, Schulz VP, Houston BL, Maksimova Y, Houston DS, Smith B, Rinehart J, Gallagher PG. Mutations in the mechanotransduction protein PIEZO1 are associated with hereditary xerocytosis. Blood. 2012;120(9):1908-1915. doi:10.1182/blood-2012-04-422253.

5. Glogowska E, Lezon-Geyda K, Maksimova Y, Schulz VP, Gallagher PG. Mutations in the Gardos channel (*KCNN4*) are associated with hereditary xerocytosis. Blood. 2015;126(11):1281-1284. doi:10.1182/blood-2015-07-657957.

6. Rapetti-Mauss R, Lacoste C, Picard V, Guitton C, Lombard E, Loosveld M, Nivaggioni V, Dasilva N, Salgado D, Desvignes J-P, Béroud C, Viout P, Bernard M, Soriani O, Vinti H, Lacroze V, Feneant-

Thibault M, Thuret I, Guizouarn H, Badens C. A mutation in the Gardos channel is associated with hereditary xerocytosis. Blood. 2015 2015-09-10 00:00:00;126(11):1273-1280. doi:10.1182/blood-2015-04-642496.

7. Picard V, Guitton C, Thuret I, Rose C, Bendelac L, Ghazal K, Aguilar-Martinez P, Badens C, Barro C, Bénéteau C, Berger C, Cathébras P, Deconinck E, Delaunay J, Durand J-M, Firah N, Galactéros F, Godeau B, Jaïs X, de Jaureguiberry J-P, Le Stradic C, Lifermann F, Maffre R, Morin G, Perrin J, Proulle V, Ruivard M, Toutain F, Lahary A, Garçon L. Clinical and biological features in PIEZO1-hereditary xerocytosis and Gardos-channelopathy: A retrospective series of 126 patients. Haematologica. 2019:haematol.2018.205328. doi:10.3324/haematol.2018.205328.

8. Andolfo I, Russo R, Rosato BE, Manna F, Gambale A, Brugnara C, Iolascon A. Genotype-phenotype correlation and risk stratification in a cohort of 123 hereditary stomatocytosis patients. American Journal of Hematology. 2018;93(12):1509-1517. doi:10.1002/ajh.25276.

9. Zhao Q, Zhou H, Li X, Xiao B. The mechanosensitive Piezo1 channel: a three-bladed propeller-like structure and a lever-like mechanogating mechanism. The FEBS Journal. 2019;286(13):2461-2470. doi:10.1111/febs.14711.

10. Macey RI, Adorante JS, Orme FW. Erythrocyte membrane potentials determined by hydrogen ion distribution. Biochim Biophys Acta 1978 1978/09/22/;512(2):284-295. doi:https://doi.org/10.1016/0005-2736(78)90253-5.

11. Bennekou P, Kristensen BI, Christophersen P. The Human Red Cell Voltage-regulated Cation Channel. The Interplay with the Chloride Conductance, the Ca2+-activated K+ Channel and the Ca2+ Pump [journal article]. The Journal of Membrane Biology. 2003 July 01;195(1):1-8. doi:10.1007/s00232-003-2036-6.

12. Petkova-Kirova P, Hertz L, Danielczok J, Huisjes R, Makhro A, Bogdanova A, Mañú-Pereira MdM, Vives Corrons J-L, van Wijk R, Kaestner L. Red Blood Cell Membrane Conductance in Hereditary Haemolytic Anaemias [Original Research]. Frontiers in Physiology. 2019 2019-April-16;10(386). English. doi:10.3389/fphys.2019.00386.

13. Rotordam MG, Fermo E, Becker N, Barcellini W, Brüggemann A, Fertig N, Egée S, Rapedius M, Bianchi P, Kaestner L. A novel gain-of-function mutation of Piezo1 is functionally affirmed in red blood cells by high-throughput patch clamp. Haematologica. 2019;104(5):e179-e183. doi:10.3324/haematol.2018.201160.

14. Martin-Almedina S, Mansour S, Ostergaard P. Human phenotypes caused by PIEZO1 mutations; one gene, two overlapping phenotypes? The Journal of Physiology. 2018;596(6):985-992. doi:10.1113/jp275718.

15. Murthy SE, Dubin AE, Patapoutian A. Piezos thrive under pressure: mechanically activated ion channels in health and disease [Review Article]. Nature Reviews Molecular Cell Biology. 2017;18:771. doi:10.1038/nrm.2017.92.

Figure legend

Figure 1. Morphological description of D669Y Piezo1 RBCs.

(A) Topology model for mPiezo1, modified from (9). D669Y mutation is indicated, as well as 36 other mutation sites (green dots) linked to HX families reported in (7). (B) Control (left) and patient (right) RBCs peripheral blood smears (100x objective), arrows indicate several aberrant shapes. Scale bar 10 µm. (C-D) Distribution of cell projected area (C) and cell roundness (D) from control (blue) and patient (red) RBCs, measured from peripheral blood smears and quantified using imageJ. n>1000 cells for both cell types. Cell roundness is defined as $4\times[Area]/\pi\times[Major\ axis]^2$

Figure 2. Mechanical properties of D669Y Piezo1 RBCs.

(A) Ektacytometry profile of patient (red) and control (blue) RBCs. Dots indicate O_{min}, EI_{max} and O_{hyper}. (B) Osmotic fragility curves for patient (red) and control (blue) RBCs. (C) content in water (left), Na^+ (middle) and K^+ (right) of control (blue) and patient (red) RBCs. (D) Total cation content of RBCs from control (blue) and patient (red) with addition of Na^+ and K^+ intracellular concentrations. (C-D) Averages +/ – SEM from n=3 independent experiments.

Figure 3. Functional characterization of cation channel activity in D669Y Piezo1 RBCs.

(A-C) Monitoring of membrane potential using CCCP technique. (A) Control (blue) and patient (red) RBCs in a normal Ringer solution, followed by addition of A23187 (10µM). (B) Control (blue) and patient (red) RBCs in a LIS solution, followed by addition of Ca^{2+} (1mM). (C) Control (blue) and patient (red) RBCs in a LIS solution with 100µM NPPB all the time, followed by addition of Ca^{2+} (1mM). (D) Fluorescence of Control (blue) and Patient (red) RBCs loaded with Fluo-4, before and 3min after addition of Yoda1 (10µM). Insert shows together initial Ca^{2+} fluorescence at a smaller scale. (E) Patch clamp whole cell recording from control (blue) and patient (red) RBCs, stimulated from V_m= +100 mV to V_m= –100 mV by ramps of 500 ms (black). (F) Patch clamp whole-cell corresponding I/V curves from Control (blue circles, n=6) and Patient (red circles, n=7) RBCs. Patient RBCs show heterogeneous profile, with no cation current (pattern A, red triangles up, n=3) or spontaneous cation channel activity (pattern B, red squares, n=4).

Figure 1

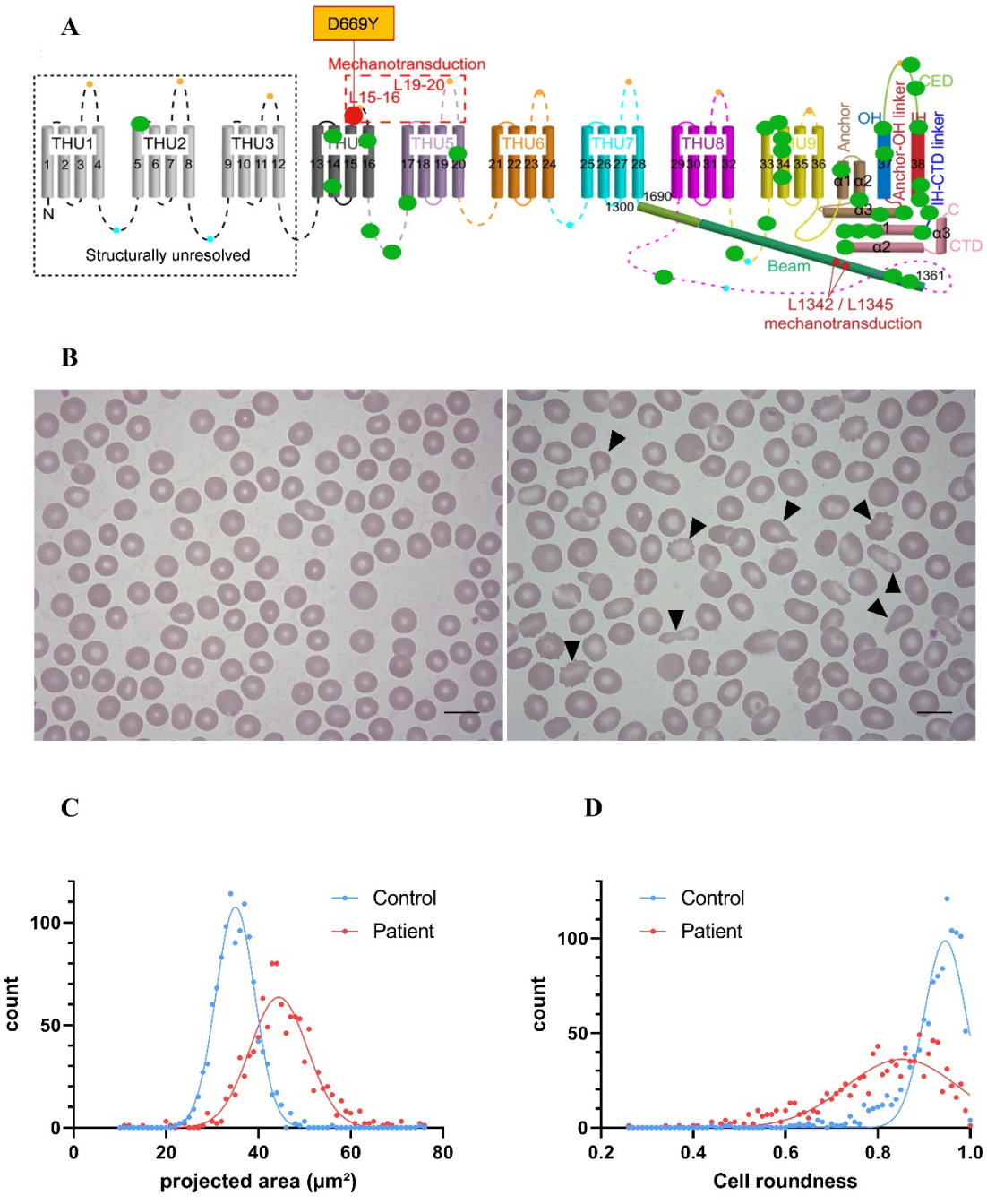
A
D669Y
Mechanotransduction
L15-16
L19-20
THU1
THU2
THU3
THU4
THU5
THU6
THU7
THU8
THU9
N
Structurally unresolved
Anchor
OH
CED
Anchor-OH linker
IH
IH-CTD linker
C
CTD
α1
α2
α3
α1
α2
α3
1690
1300
Beam
1361
L1342 / L1345
mechanotransduction
B
C
Control
Patient
count
projected area (μm²)
D
Control
Patient
count
Cell roundness

Figure 2

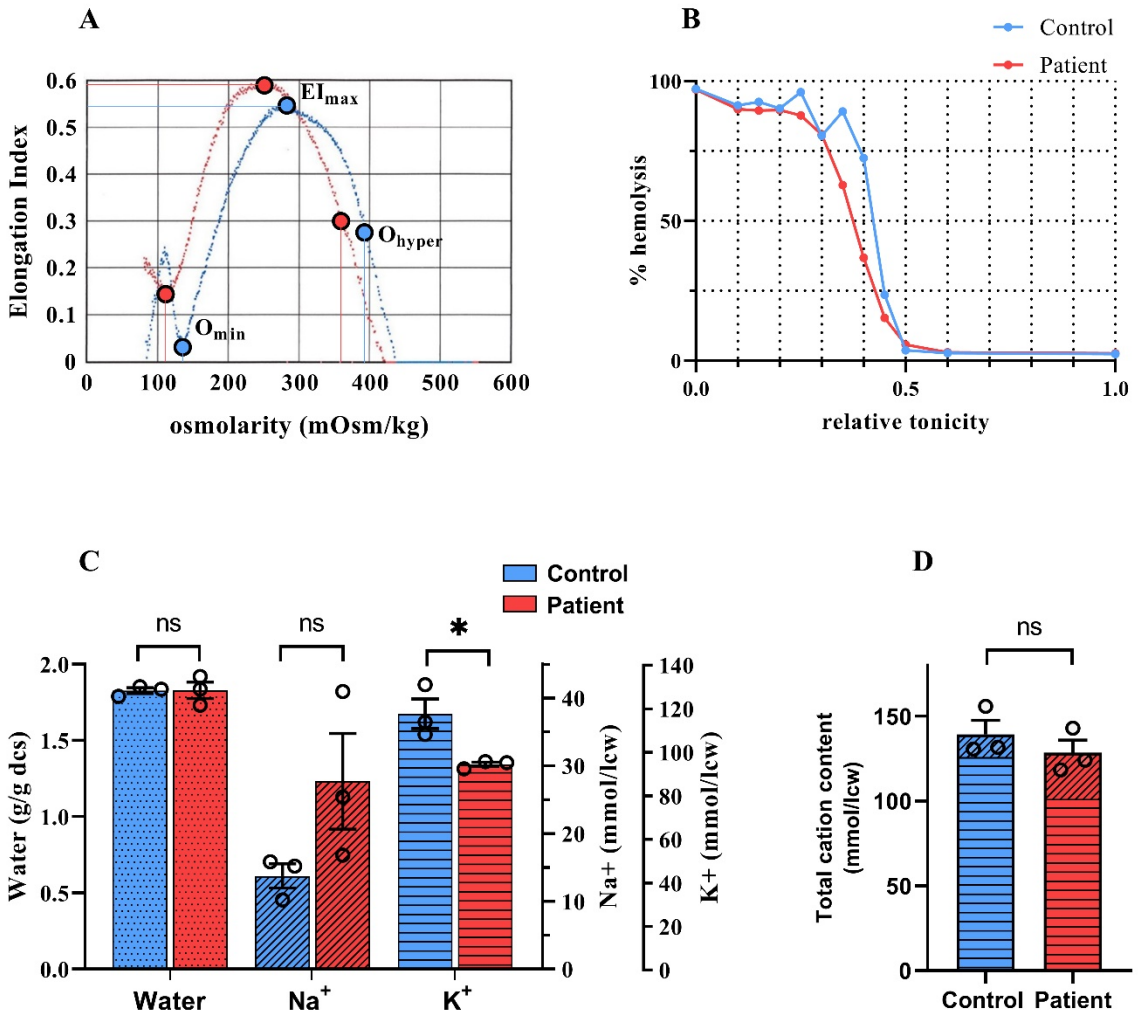
A
Elongation Index
0.6
0.5
0.4
0.3
0.2
0.1
0
EImax
Ohyper
Omin
0
100
200
300
400
500
600
osmolarity (mOsm/kg)
B
Control
Patient
% hemolysis
100
50
0
0.0
0.5
1.0
relative tonicity
C
Control
Patient
ns
ns
*
Water (g/g dcs)
2.0
1.5
1.0
0.5
0.0
Na+ (mmol/lcw)
40
30
20
10
0
K+ (mmol/lcw)
140
120
100
80
60
40
20
0
Water
Na+
K+
D
ns
Total cation content (mmol/lcw)
150
100
50
0
Control
Patient

Figure 3

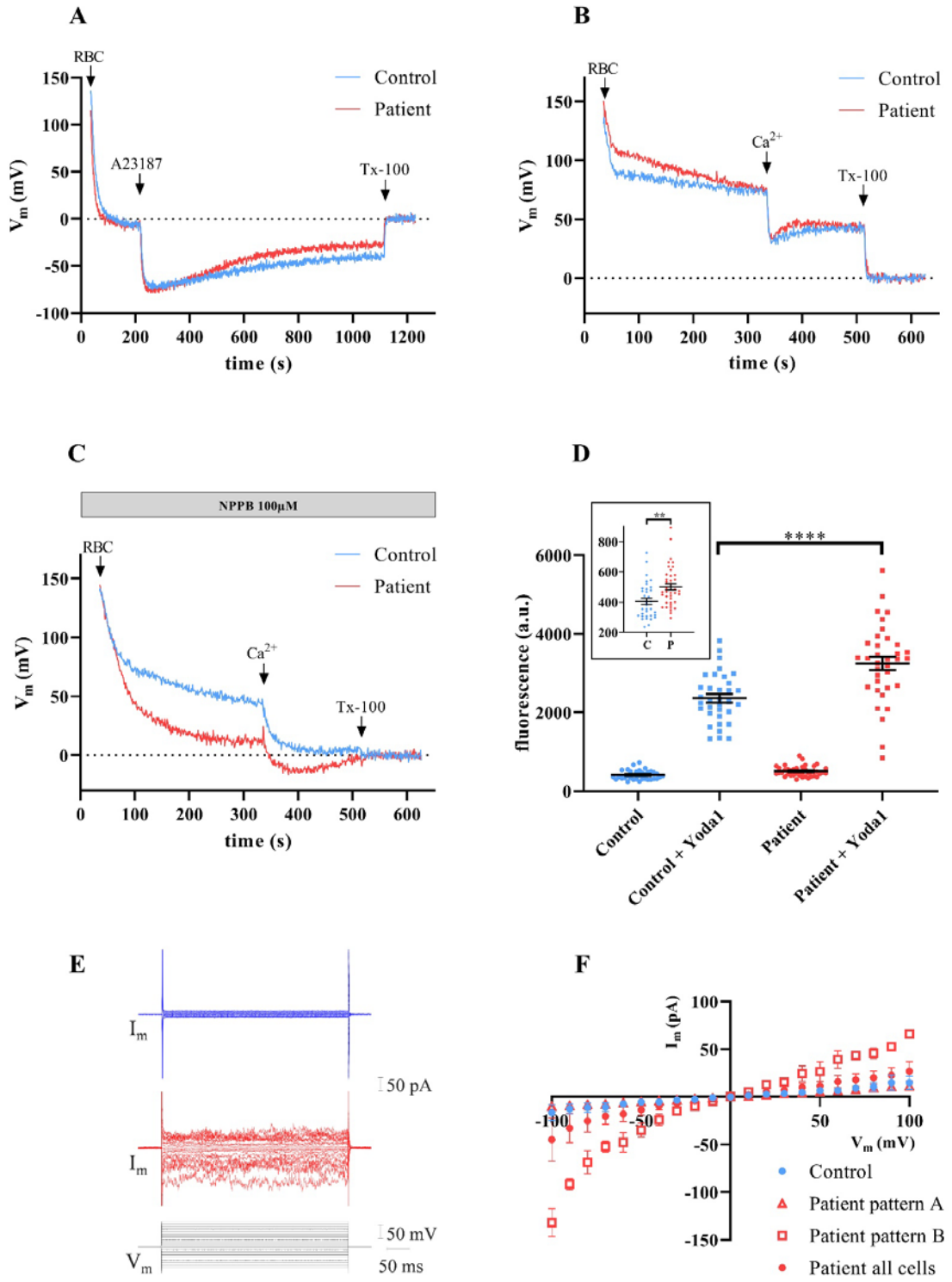
A
RBC
Control
Patient
A23187
Tx-100
V_m (mV)
time (s)
B
RBC
Control
Patient
Ca^{2+}
Tx-100
V_m (mV)
time (s)
C
NPPB 100µM
RBC
Control
Patient
Ca^{2+}
Tx-100
V_m (mV)
time (s)
D
fluorescence (a.u.)
**
****
C
P
Control
Control + Yoda1
Patient
Patient + Yoda1
E
I_m
50 pA
I_m
50 mV
V_m
50 ms
F
I_m (pA)
V_m (mV)
Control
Patient pattern A
Patient pattern B
Patient all cells

Influence of the storage lesion on cation channel activity

Chapter 5

Non Selective Cation Channel activity increases during storage of human red blood cells

Introduction

Transfusions are an essential, life-saving procedure in modern medicine. Meeting the demand of blood products is only possible thanks to long-term storage of blood components, especially RBCs. RBCC state-of-the-art storage is for a maximum of six weeks with no more than 0.8% hemolysis in the bag and 25% cell loss *in vivo*. Even though RBC storage has been possible since the early 20th century, owing to the discovery of anticoagulant solutions [307], many improvements were required until blood or RBCCs reached these storage standards currently enforced in most of the world.

These improvements include plastic bags and preservative solutions. Plastic bags were a critical innovation as they vastly improved logistics with lightness and flexibility. In addition, erythrocytes deteriorated quickly due to the well-known glass effect. A wide array of plastics were initially tested with hemorepellence and resistance to sterilization as the most important factor [308]. Polyvinyl chloride softened with di-2-ethylhexyl-phthalate (DEHP) was proven to be best for erythrocyte storage, to the point where DEHP was found to act as preservative as it leaked out of the plastic during storage. DEHP was found to reduce osmotic fragility, hemolysis, microvesicle release and improve morphology over several weeks of refrigerated storage [267, 269]. Nevertheless, hepatic toxicity was detected in rats and monkeys after numerous transfusions, though this would affect only patients with chronic diseases receiving twenty transfusions or more per year [308]. Alternative plasticizers have been tested in order to circumvent use of bioaccumulating DEHP. PVC plasticized with butyryl-n-trihexyl-citrate was found to allow RBC storage for 42 days in SAGM (Saline-Adenine-Glucose-Mannitol) with similar quality control parameters as PVC-DEHP [309].

Long-termed storage of RBCs requires additive solutions. The lengthy process that led to the advent of current solutions began with the use of citrate, which prevents coagulation by chelating calcium. Glucose was quickly incorporated into these solutions to enable cell energy production during storage. Phosphate was a component to be introduced in the 1950s as it was shown it leaks from stored erythrocytes. It also supports ATP pathways without compromising diphosphoglycerate levels [268, 310]. Acidified citrate-glucose (ACD) solutions were developed mainly to counter the caramelization problems appearing when autoclaving alkaline glucose solutions [311] but it CPD (Citrate-Phosphate-Dextrose) saw more use. Adenine was incorporated into CPD as a way to further support ATP metabolic pathways and was first proposed in 1962 [310, 312]. Thus, CDPA (Citrate-Phosphate-Dextrose-Adenine) become the gold standard of whole blood preservation. However, instead of storing whole blood, red cells can be centrifuged and stored as Red Blood Cell concentrates (RBCC) with a simple solution, the first of which was SAG (Saline-Adenine-Glucose). Whereas potassium loss and microaggregate content was reduced compared to whole blood, hemolysis increased slightly [313]. Addition of mannitol, an impermeant small sugar alcohol, acts as an osmoprotector as well as helping to decrease hemolysis, allowing rates under 1% for blood stored 49 days [314, 315]. Its addition into SAG gave rise to SAGM, which is widely used worldwide to this day. Buffy coat removal and, more recently, leukoreduction greatly reduce hemolysis, by eliminating granulocytes responsible of protease release *in vitro*. In spite of all of these

advances allowing to keep red cells *ex vivo* for six weeks, cellular damages occur, since substrates diminish while products build up causing toxic effects. This is put to test during storage and failure of these metabolic and enzymatic pathways entails irreversible oxidation of proteins.

The set of injures and alterations RBCs develop during storage are termed the storage lesion. These comprise metabolic, protein and morphological changes that impair RBC function. As cells are kept refrigerated their metabolism is reduced 40-fold [315]. While it helps slow down the aging, it has a negative impact in active processes like ion pumping or enzymatic reactions. A loss of critical metabolites, such as 2,3-DPG (2,3-diphosphoglycerate), urate and critically ATP, inhibiting many ATP-fueled processes, including the Na^+/K^+ ATPase, which is also inactivated by cold. Loss of 2,3-DPG happens early during storage, by the second week its levels become abnormally low. The hemoglobin oxygen affinity increases as a consequence. If pH turns too acid a phosphatase further reduces 2,3-DPG concentration, which happens as lactic acid forms via glycolysis [315]. Erythrocytes have an efficient antioxidant machinery to cope with the permanent threat of protein oxidation. Metabolic deregulation and loss of NADP replenishment results in the inability to prevent protein and lipid oxidation. Furthermore, membrane is lost through microvesiculation and red cells tend to spherocytic shapes reducing deformability. Microvesicles have been linked to thrombotic events and they are more abundant in stored blood from female or older donors [316, 317].

Great efforts in storage lesion research have gone into elucidating whether 'fresh' rather than 'old' stored blood has a clinical impact on transfused patients. Many storage alterations affect cellular functions and six-week old RBCs are especially abnormal with over 50% presenting aberrant morphologies [267]. Several observational studies established a link between RBC units which had been stored longer and clinical complications, however many studies are contradictory and subsequent meta-analyses reached no conclusions [318, 319] or a lack of link between 'old' transfusion units and mortality or worse clinical outcomes [320, 321]. Albeit, a meta-study also found a correlations between 'fresher' transfusions and higher rates of adverse reactions including infections despite absence of increased mortality [322]. Therefore, research bridging the storage lesion and clinical performance with biomarkers is still ongoing.

Although numerous reports exist on biochemical aspects of the storage lesion, insight on the mechanisms involving potassium loss and sodium intake and their potential relation with ion channels is lacking. The Gárdos channel is a powerful Ca^{2+}-activated K^+-selective channel capable of fast cell dehydration, although CPD-SAGM lacks any calcium and potassium rendering the channel fully inhibited in the absence of hemolysis. Non Selective Cation channels, e.g. Piezo1, are dissipative conductive pathways that may, once activated, interfere with cation homeostasis. Their activity, which allow cation movements down their gradients, may explain Na^+ intake and K^+ efflux, considerably boosting cation leaks revealed by inhibition of the Na^+/K^+ pump at 4 °C. Therefore, we aimed to study ion channel activity throughout a 42-day period of red cell concentrate in CPD-SAGM provided according to clinical regulations. Herein we challenge the cell with experimental protocols which may simulate physiological conditions that RBCs encounter when they are reinfused into the circulation.

Materials and Methods

Reagents All salts were acquired from Sigma and of analytical grade or better. Nominal calcium-free solutions amount to 4 µM Ca^{2+} due to typical salt contamination [124].

Solutions normal Ringer: 154 mM NaCl, 2 mM KCl. Calcium Ringer: 154 mM NaCl, 2 mM KCl, 1 mM $CaCl_2$. Choline-substituted Ringers: 0% 154 mM NaCl, 2 mM KCl. 25%: 115.5 mM NaCl, 38.5 mM Choline Chloride. 50%: 77 mM NaCl, 77 mM Choline Chloride. 100% 154 mM Choline Chloride, 2 mM KCl. RPMI medium was provided by Fisher and supplemented with 10% human serum AB was acquired from the French Blood Establishment (EFS).

Drugs

CCCP (Sigma): (carbonyl cyanide 3-chlorophenylhydrazone)

A23187 (Sigma): (calcymicin; 5-(methylamino)-2-[[(2S,3R,5R,6S,8R,9R)-3,5,9-trimethyl-2-[(2S)-1-oxo-1-(1H-pyrrol-2-yl)propan-2-yl] -1,7-dioxaspiro[5.5]undecan-8-yl]methyl]-1,3-benzoxazole-4-carboxylic acid)

NS309 (Alomone): 6,7-Dichloro-1H-indole-2,3-dione 3-oxime

Yoda1 (Tocris): 2-[5-[[(2,6-Dichlorophenyl)methyl]thio]-1,3,4-thiadiazol-2-yl]pyrazine

Tram34 (Tocris): 1-[(2-Chlorophenyl)diphenylmethyl]-1H-pyrazole

Chloride inhibitors:

NPPB (Tocris): (5-nitro-2-(3-phenylpropylamino)benzoic acid)

NS3623 (Alomone) (N-(4-bromo-2-(1H-tetrazol-5-yl)phenyl)-N'-(3-trifluoromethyl-phenyl)urea)

All were prepared as stock solutions in DMSO. DMSO concentrations did not exceed 0.3%, which is known not to cause any effect in fluxes nor membrane potentials [124].

Red blood cells Two PVC bags of red cell concentrate (O negative blood group, male and female, processed according to French and European transfusion regulations, leukoreduced, mixed with anticoagulant CPD (Citrate, Phosphate, Dextrose) and resuspended in SAGM (Saline, Adenine, Glucose, Mannitol) solution at hematocrit of approximately 80 % were provided by the French Blood Establishment (Établissement Français du Sang, EFS) two days after blood withdrawal, according to French and European regulations [266, 323]. The bags were kept in blood bank conditions at 4 °C. RBCs were aseptically collected from the bag every 3 or 4 days for measurements. RBCs were compacted with a centrifugation for 1 minute at 15 294 *g* and the packed cells stored at 4 °C until use.

Membrane potential determination The CCCP method was used for membrane potential determination [270]. See Chapter 2 on page 59 for a detailed explanation of the technique.

Erythrocytes were kept unwashed as packed cells, in ice until use, then at the start of every experiment they were directly resuspended in an unbuffered solution according to the experiment performed.

Cell water, Na^+ and K^+ content determination 0.5 ml aliquots of the unwashed cell suspension (hematocrit being about 80%, containing SAGM), with drugs (if any) added at indicated times, were distributed in polyethylene micro test tubes and centrifuged at 20 000×g for 10 min at 4 °C. After centrifugation the packed cell mass was separated from the supernatant by slicing the tube with a razor blade below the top of the red cell column [280]. After weighing, the packed cells were dried to constant weight for at least 24 h at 90 °C

and re-weighed. RBC volume depends on the intracellular water content which is estimated to be about 90 fl for a healthy discocyte. Shape change can be misleading in the estimation of the cell's water content due to the great plasticity of the red cell membrane. These measurements are independent of cell shape. The packed cells within the sliced tube were lysed in 1 ml MilliQ water. Proteins were denatured to ease separation by addition of 231.9 µM of perchloric acid. The tubes were spun at 16 900×g for 7.5 min at 4 °C and the supernatant passed onto samples tubes and diluted 10 times. The ionic content was measured using a flame photometer (PFP7, Jenway). The amounts Na^+ or K^+ measured are reported as µmol/g dry cell solid.

Results

Hydration state and cation content of stored erythrocytes

Extracellular sodium and potassium values of blood or red cell concentrate units are regularly reported in the literature, as automated devices are available at hospitals allowing the measurement of several biochemical parameters including lactate, glucose or iron, among others. However, intracellular measurements are lacking as they require a more laborious approach. Cellular water is commonly reported as the Mean Corpuscular Volume (MCV) which is calculated from flow cytometer cell counts. Herein are shown the evolution of intracellular water, sodium and potassium throughout the storage duration of two red cell concentrate bags used as transfusion units. These measurements generally show a decrease in K^+ and an increase in Na^+ over time (**Fig. 5.1A**). This slow reversal, which can also be measured as an increase and decrease in extracellular potassium and sodium, respectively, is well documented and is mostly due to the inactivation by cold of the Na^+/K^+ pump, as transfusion units are kept at 4 °C.

In as little as three days, from day 4 to day 7 post-blood withdrawal, K^+ content decreases by 10.9 mmmol/l cell water, the largest drop in the whole 42-day period. Between day 21 and day 31 post-blood withdrawal the intracellular K^+ concentration plateaus at a mean value of 90.8 ± 0.6 mmol/l cell water. On Day 41, the efflux has taken the intracellular K^+ concentration to 83.1 mmol/l cell water, a 25.9% reduction compared to Day 4 (**Fig. 5.1A**). Intracellular sodium was 21.8 mmol/l cell water on Day 4 at the start of the follow-up, reaching 47.7 mmol l/cell water on Day 41, a 2.2-fold increase in concentration. Intracellular water increases from Day 4 to Day 28 by 5.3% only to swiftly decrease by 12.6% by Day 41. This is a decline of 8.0% comparing Day 4 and Day 41. This indicates moderate swelling during the first 4 weeks in storage followed by dehydration on the last two weeks of storage (**Fig. 5.1B**).

Gárdos activation via calcium ionophore

If cation imbalance occurs during storage, as it is evident in Figure 5.1, it is important to know how ion channels behave once they meet conditions known to trigger their activity. As for water, K^+, and Na^+ measurements, following experiments were performed on RBCs stored on SAGM on Days 4, 7, 10, 14, 17, 21, 24, 28, 31, 35, 38 and 41 post-withdrawal. For the sake of clarity, only a subset taken every seven days is shown. See the supplementary figures for the full data set.

Gárdos is maximally activated when the intracellular calcium concentration is raised above 2 µM [216]. This can be achieved with a calcium ionophore, such as A23187. As mentioned before Gárdos is the most powerful dissipative conductive pathway. Thus, in the first set of experiments, RBCs were subjected to Gárdos activation by the use of A23187, with or without G_{Cl^-} inhibition (NS3623, 10 µM) and enhanced NSC activity (NS3623,

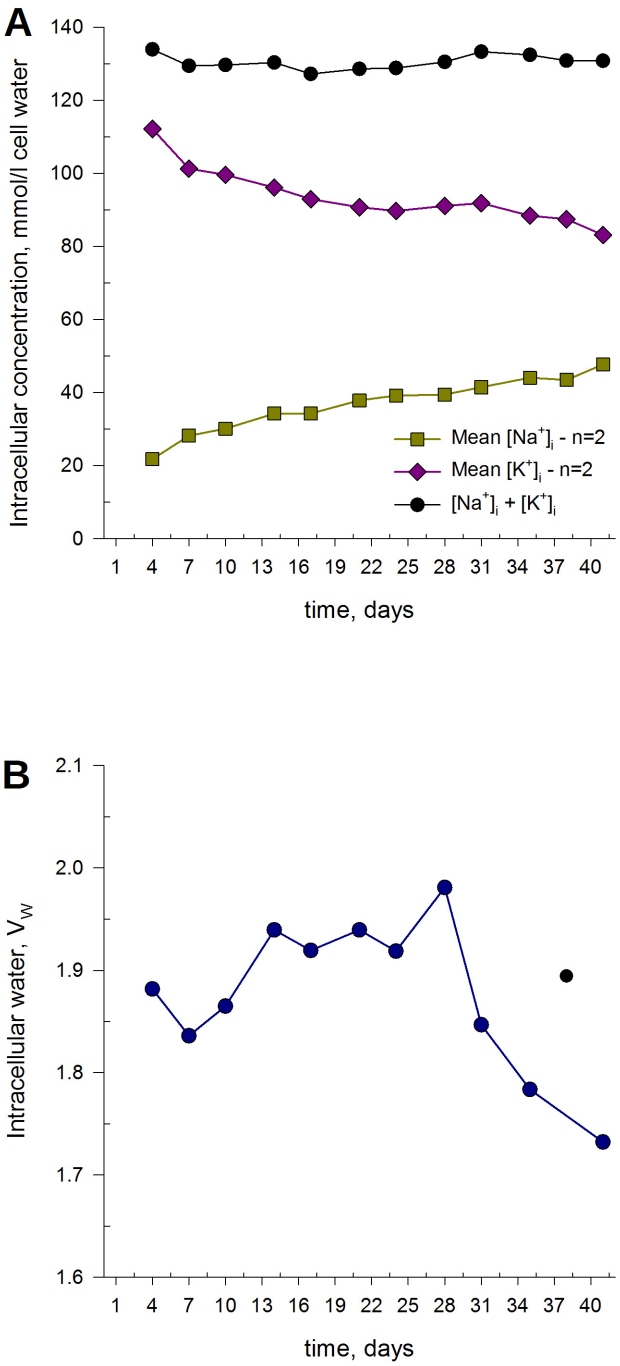

Figure 5.1: Intracellular water, sodium and potassium progression over time of stored RBCs.
Mean intracellular sodium (golden squares) and potassium (purple diamonds) concentration (**A**) (mmmol/l cell water) and mean intracellular water content (**B**) V_W, intracellular water ratio, (wet weight/dry weight) of RBCs from two red cell concentrate bags stored 42 days at 4 °C in CPD-SAGM. The sum of cations (Na^+ + K^+) is also plotted (dark blue circles). Each point is a mean of two independent measurements from two bags, except for Day 7 and Day 41 where n=1.

100 µM), a concentration for which G_{Cl^-} is still inhibited (Chapter 3 on page 69). Hence, a hyperpolarization occurs instantaneously upon A23187 addition. Maximum hyperpolarization of cells treated with A23187 was -42.8 mV on Day 7, and the equilibrium reached was quickly lost due to a gentle repolarization which develops until it arrives to a new equilibrium by 15 minutes of experiment (**Fig. 5.2A**). Red cells reach -46.8 mV following treatment with A23187 (10 µM) after 4 days of storage (**Fig. 5.3**). Maximum hyperpolarizations decrease over time until Day 17 with 24.91 mV where it plateaus for the remaining of the storage duration. Hence, the

mean between Day 17 and 41 is -26.81 ± 2.19 mV (n=8) (**Fig. 5.3A**, dark green circles).
Maximum hyperpolarizations are dependent on A23187-induced Gárdos activity but also on cytosolic K^+ levels, the countereffect of G_{Cl^-} and NSC activity. Hence NS3623, a known chloride inhibitor, that we have demonstrated it potentiates NSC activity at high concentrations, was used to assess cation conductances only after A23187 stimulation. On Day 7 the difference in maximum hyperpolarizations reached between 10 and 100 µM NS3623-pretreated cells was 31.87 mV (**Fig. 5.3A**, Δ between 10 and 100 µM NS3623-pretreated cells). If cells are pretreated with 10 µM NS3623 a membrane potential of -92.0 mV is attained after A23187 treatment and again a decrease in maximum hyperpolarizations is found over time until Day 21 with -62.9 mV where it plateaus to -64.0 ± 3.0 mV (n=7) up to the end of the storage duration (**Fig. 5.3**). On the storage period mid-point, there is a general decrease in the extent of hyperpolarizations. The hyperpolarization after A23187 treatment for red cells exposed to 100 µM NS3623 greatly diminished to -25.3 mV (**Fig. 5.2C**).

Considering Gárdos to be fully activated by A23187 exposure, whatever the conditions (0, 10 or 100 µM NS3623), these findings clearly indicate that NSC activity increases during storage. In this sense, depolarizations are found to develop immediately after NS3623 addition meaning that NSC activity is strong and becomes predominant once the chloride conductance is blocked. Very pronounced depolarizations are observed on Day 35 after addition of either 10 µM NS3623, with a maximum of 15.3 mV, or 100 µM NS3623, with a maximum of -22.5 (**Fig. 5.2E**). This phenomenon is indicative of a strengthened basal cationic conductance which is apparent only when the chloride conductance, which is dominant, is inhibited. In addition, 100 µM NS3623 is able to further enhance the activity of NSC, which boosts the rate of depolarization. Gárdos is, upon A23187 stimulation, immediately opened and hyperpolarization is swift to reach a new equilibrium in cells treated with 10 µM NS3623, but not for 100 µM NS3623-pretreated cells where a considerable delay is observed before the membrane potential starts to return to negative values and an equilibrium is far from reached by the end of the experiment.

Very positive membrane potential values are observed the last day of the storage period after exposing red cells to NS3623. 20.8 mV for 10 µM NS3623-treated cells and 24.9 mV for red cells treated with 100 µM NS3623 (**Fig. 5.2F**). However, whereas hyperpolarization is sudden and the V_M reaches -65.1 mV in seconds following A23187 addition for cells exposed to 10 µM NS3623, 100 µM NS3623-pretreated cells respond to A23187 with a brief and mild return towards 0 mV, before a depolarizing trend dominates again. These facts are telling of the enormous sodium uptake by red cells at this terminal point in unit storage if NSC activity is further magnified by 100 µM NS3623.

Interestingly, hyperpolarizations of 100 µM NS3623-pretreated cells as a result of Gárdos activity decrease the longer RBCs stay stored so that while erythrocytes reach -73.17 mV following A23187 exposure on Day 4, by Day 41 100 µM NS3623-pretreated RBCs do not hyperpolarize at all (**Fig. 5.3A**, upward red hexagon trend). Rather, the membrane potential attains very positive values, 29.6 mV, after a brief Gárdos activity (when the trace goes towards zero for a few seconds) is overcome by the dominant NSC activity (**Fig. 5.2F**, red and **Fig. 5.3B**, upward red hexagon trend).

10 µM NS3623-pretreated cells also increasingly depolarize over time before A23187 is added, with maximal membrane potential reaching 20.2 mV, a difference of 9.4 mV between 10 and 100 µM NS3623-pretreated cells (**Fig. 5.3**, cyan diamonds and Δwith last red hexagon). Compared to unchanged maximal values and slight repolarizations observed for red cells untreated with NS3623, these findings indicate that a strong chloride conductance masks the underlying increased activity of NSC (**Fig. 5.3B**).

The most striking observation is the difference found in membrane potential 5 minutes after treatment with 100 μM NS3623 followed by A23187 when comparing the beginning and the end of the storage period. It was -68.4 mV on Day 4 and went to 28.9 mV on Day 41, a difference of 97.3 mV (**Fig. 5.3C**, upward red hexagon trend).

Gárdos activation in the absence of Na^+

In physiological conditions, choline is an impermeant cation unable to cross the plasma membrane. Replacing sodium by choline in extracellular solutions allows for a reduction of available sodium able to pass through the membrane via a cationic pathway such as a NSC. The presence of choline instead of sodium was proven to preclude repolarizations and reduce the development of hyperpolarizations indicating that Na^+ entry through NSCs occurs in freshly drawn erythrocytes (See Chapter 3 on page 69) [286]. Red cells injected into solutions where 0 %, 25 %, 50% or 100% of Na^+ has been replaced by the impermeant cation choline, treated with 10 μM NS3623 followed by A23187 hyperpolarize to the same extent after 4 days in storage, -100.0 ± 1.8 mV (n=3), except cells in 50 % choline solutions which attain a slightly smaller V_M^{maxhyp}, at -90.5 mV (**Fig. 5.4A**). If cells are treated with 100 μM NS3623 plus A23187 (10 μM) then cells will hyperpolarize according to the availability of sodium, with cells in 25% choline solutions reaching 73.0 mV compared to -92.8 mV 100% 100 μM NS3623-pretreated cells. The latter quickly arrives to the equilibrium where no repolarization occurs. Moreover, all sodium-containing solutions, which have a maximal mean hyperpolarization of -74.7 ± 2.7 mV (n=3), have smaller hyperpolarizations compared to choline-only solution (-92.8 mV) (**Fig. 5.4A, B**).

These findings, for both 10 μM NS3623- and 100 μM NS3623-pretreated cells, are consistent with experiments performed with freshly drawn erythrocytes (See Chapter 3 on page 69 [286]. On Day 21, the overall hyperpolarization of 10 μM NS3623-pretreated cells was -58.7 ± 3.6 mV (n=4). Furthermore, a depolarization develops on NS3623 addition prior to A23187 treatment, already reaching positive membrane potential values. 100 μM NS3623-pretreated cells hyperpolarize according to sodium availability, although hyperpolarizations are diminished: -38.0 mV for cells in 25% choline solutions in contrast to -51.0 mV in a 100 % choline solution. In addition, there is a long delay until the maximum hyperpolarization is attained even for cells in 100% solutions suggesting a loss of the driving force (**Fig. 5.4D**). On Day 41, 10 μM NS3623-pretreated cells display a strong depolarization upon NS3623 addition and the mean hyperpolarization following A23187 treatment was -60.5 ± 1.3 mV (n=4) (**Fig. 5.4E**). Cells treated with 100 μM NS3623 showed an even greater depolarization, to the point that subsequent A23187 exposure did not suffice to bring the cells to negative membrane potentials and the depolarization took off again after a brief drop towards zero. To compound this striking observation, cells within 100% choline solutions reached similar values to other solutions, such as the control containing no choline. Thus, the possibility that choline crosses the plasma membrane in these conditions at the terminal stage of the storage period cannot be ruled out.

On Day 21 and 41, erythrocytes resuspended in 100% choline solutions and treated with 100 μM NS3623 and A23187 hyperpolarize to the same extent as 10 μM NS3623-pretreated cells showing that sodium is necessary for the enhancing effect of 100 μM NS3623 on NSC activity to become apparent. Even though on Day 21 100 μM NS3623-pretreated cells in 100% choline solutions hyperpolarize more strongly than solutions containing sodium, there is a reduction in the hyperpolarization difference due to the ongoing loss of potassium and gain of

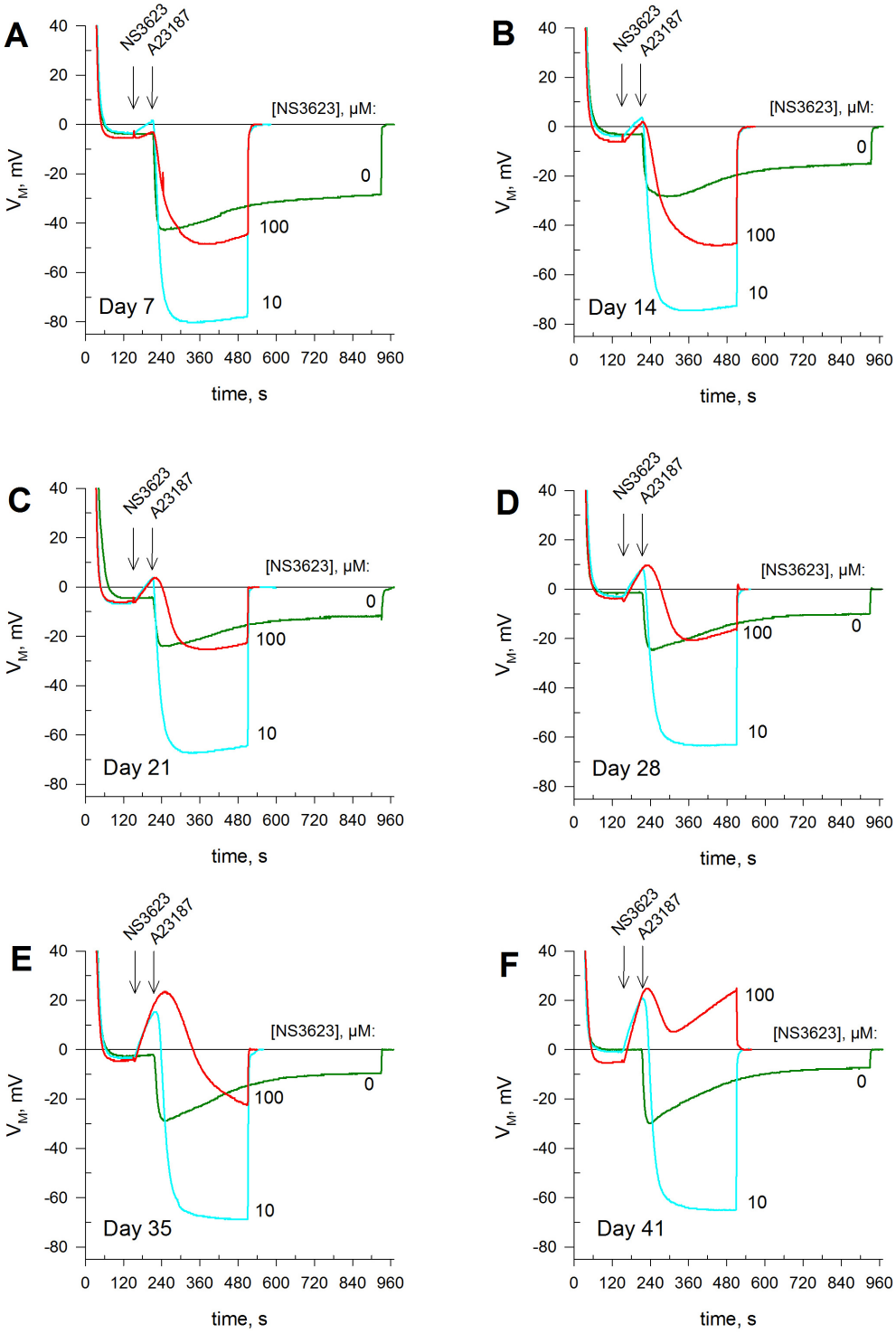

Figure 5.2: A23187-mediated Gárdos opening and emerging NSC activity at selected points of 42-day RBC storage.

Membrane potential development from cells injected into normal Ringer, treated with 0 µM (dark green), 10 µM (cyan) or 100 µM (red) of chloride conductance inhibitor NS3623 and hyperpolarized with calcium ionophore A23187 (10 µM). Membrane potential was determined by CCCP method. Measurements shown are from Days 7 (**A**), 14 (**B**), 21 (**C**), 28 (**D**), 35 (**E**) and 41 (**F**) after blood withdrawal. This is data from one red cell concentrate bag (n=1) out of two measured. Bag 2 of 2. See Fig. S5.10, S5.11, S5.12 for the full data.

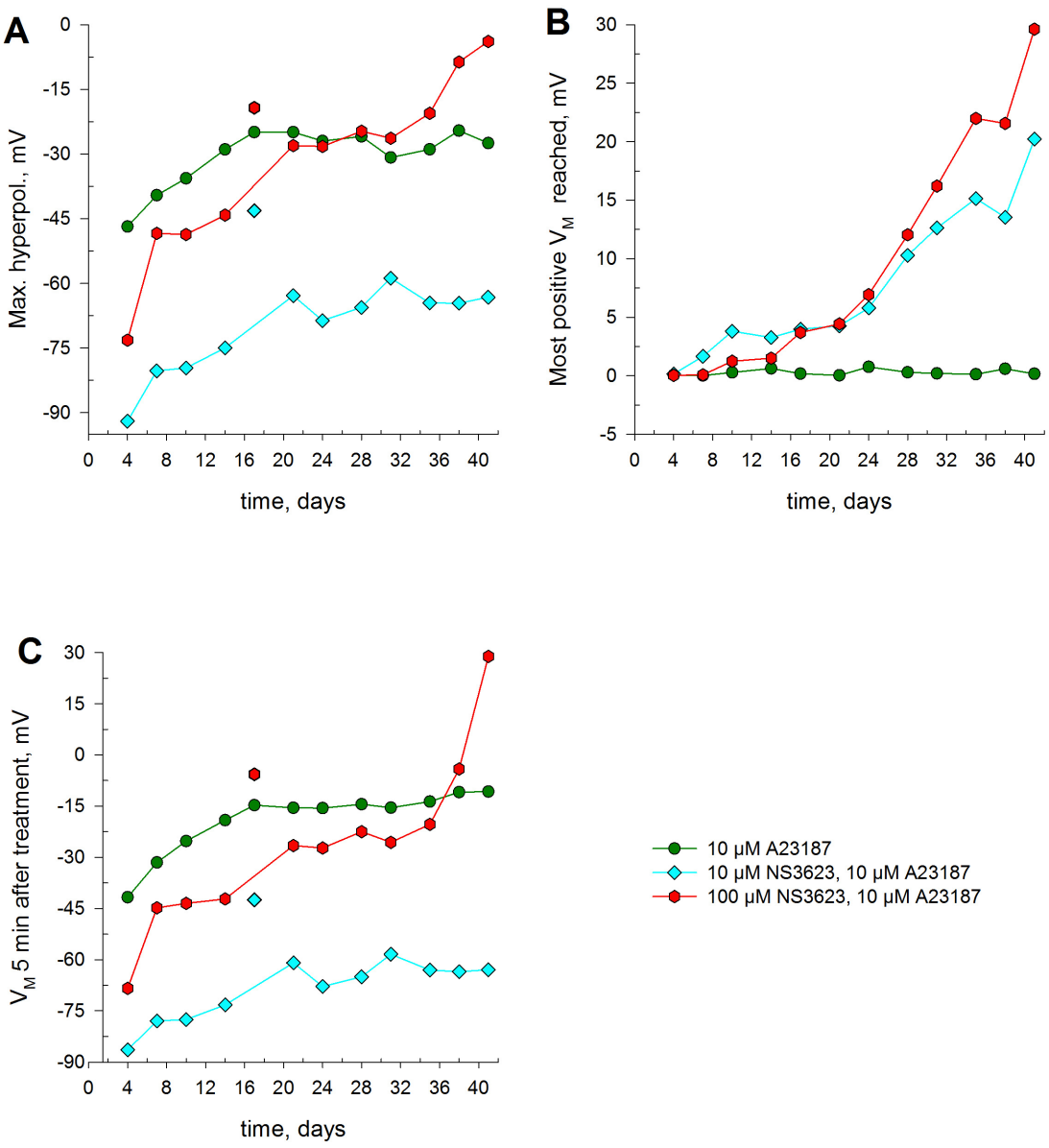

Figure 5.3: Evolution of A23187-mediated Gárdos activity and emerging NSC activity at selected points of 42-day RBC storage.

Evolution over 42 days of storage of most negative membrane potential (**A**), most positive membrane potential (**B**) and 5 minutes post-treatment membrane potentials (**C**) reached by red cells treated with 0 µM (dark green), 10 µM (cyan) or 100 µM (red) of NS3623 followed by Gárdos activation by A23187 (10 µM). Each point is a mean of two independent measurements from two bags except for Day 7 where n=1.

sodium happening in the bag (**Fig. 5.4C, D**). The fact that cells depolarize to very positive membrane potentials only on Day 41 when 100 µM NS3623-pretreated cells in 100% choline solutions reach similar values than cells in sodium-containing solutions at the end of the experiment, 31.05 ± 4.56 mV (n=4), is strongly indicative of choline passing through a cationic pathway and contributing to the depolarization as much as sodium does (**Fig. 5.4E-F**).

Impact of plasma proteins and metabolites on ion channel activity

Many studies have found a deterioration of metabolic parameters as the storage lesion progresses, especially during the last two weeks of storage. Moreover, SAGM lacks numerous physiological components which are

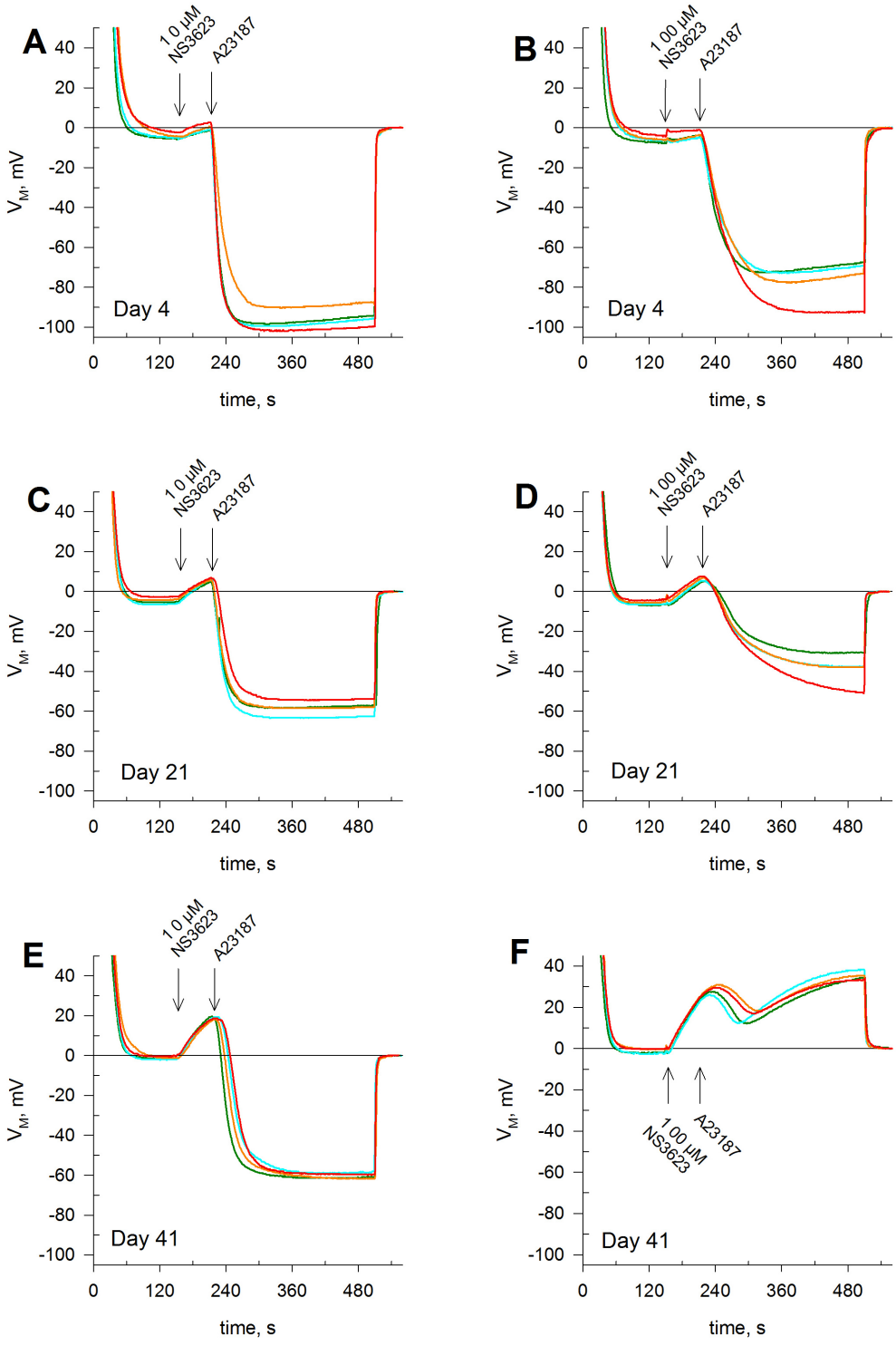

Figure 5.4: A23187-mediated Gárdos openings and emerging NSC activity when impermeant cation is in the experimental medium at selected points of 42-day RBC storage.

Membrane potential development from cells injected into 0 % (green), 25 % (cyan), 50% (orange) or 100% (red) Choline Chloride solutions, treated with 10 µM (**A**, **C** and **E**) or 100 µM (**B**, **D** and **F**) of chloride conductance inhibitor NS3623 and hyperpolarized with calcium ionophore A23187 (10 µM). Membrane potential was determined by CCCP method. Choline chloride substitution percentage was: 0 % Choline Chloride solution = normal Ringer = 154 mM NaCl, 2 mM KCl and 100 % Choline Chloride solution = 154 mM Choline Chloride, 2 mM KCl. Measurements shown are from Days 4 (**A** and **B**), 21 (**C** and **D**), and 41 (**E** and **F**) after blood withdrawal. This is data from one red cell concentrate bag (n=1) out of two measured. See Supplementary Figure S5.13 for the full data.

present in plasma and will be encountered by red cells upon transfusion, e.g. calcium, potassium and, notably, plasma proteins. To circumvent this state, red cells were incubated for about 3 hours in RPMI medium supplemented with 10% human serum before performing experiments to allow time for replenishment of metabolites, including ATP, and to allow interactions to take place between membrane and serum proteins. RPMI is often used on a variety of circulating cells including peripheral blood mononuclear cells and other leukocytes as well as *Plasmodium*-infected RBCs. It contains phosphate, vitamins and amino acids in similar concentrations as those of plasma.

Incubated RBCs were subsequently subjected to A23187 and compared to cells which were kept in SAGM at high hematocrit until use. Cells which were preincubated in RPMI before A23187-induced Gárdos activation achieved a stronger Gárdos activation reaching, on Day 28, -55.4 mV in contrast with -24.8 mV of cells which stayed in SAGM. Interestingly, repolarization quickly developed for RPMI-preincubated cells. Whereas the difference in hyperpolarization was 30.7 mV at the onset of Gárdos activation, by the end of the experiment this difference had shrunk to 9.79 mV between SAGM-kept cells and RBCs preincubated in RPMI (**Fig. 5.5A**). On Day 35, the maximum hyperpolarizations attained by red cells kept in SAGM was -28.9 mV compared to -49.7 mV of RPMI-preincubated erythrocytes (**Fig. 5.5B**). On Day 41, the difference in maximum hyperpolarization persists, yet it is reduced (**Fig. 5.5C**). **Figure 5.5E** shows the membrane potential right before the end of the experiment, 11.5 minutes after A23187 addition pointing to the repolarization which occurs during the experiment, although reduced hyperpolarizations have to be taken into account. Repolarization rates are greater the longer RBCs had stayed in SAGM, therefore the V_M at the end of the experiment decreases over time. Even though this trend is more pronounced for SAGM-kept RBCs it is also noticeable in RPMI-preincubated cells. The repolarization speeds up considerably at the end of the storage period, with RPMI-preincubated and unincubated RBCs finding a common equilibrium at the end of the experiment for both conditions (**Fig. 5.5C, E**)

Looking at mean maximum hyperpolarizations it is found that RPMI preincubated RBCs reach greater values than unincubated erythrocytes: -51.4 ± 1.7 mV (n=5) abd excluding Day 41, for which the maximum hyperpolarization is smaller, at -46.6 mV (**Fig. 5.5D**). Therefore, preincubation in complete RPMI restores the maximum hyperpolarization reached as late as Day 24 compared to Day 4 after storage. This reflects metabolic recovery, including importantly ion homeostasis, such as the potassium driving force required for strong Gárdos activation. Increasing repolarization rates over time point to sodium entry via an increase in NSC activity. The fact that maximum hyperpolarizations are restored upon Gárdos activation but repolarization are still observed in RPMI-preincubated indicate a restoration of sodium and potassium content, while NSC activity is not abrogated (**Fig. 5.5D, E**). These findings strongly suggest that the NSC channel activity which arises in SAGM storage conditions is independent from metabolic collapse, at least on Day 41, given that serum supplemented-RPMI does not prevent an enhanced repolarization observed on this late day.

Gárdos activation without artificially raising intracellular calcium levels

Gárdos activity can be measured by use of Gárdos activator NS309, which lowers the intracellular concentration threshold of Ca^{2+} necessary to open the channel, thus allowing activation at physiological levels of calcium, at the millimolar range. It should be noted that Gárdos activation is impossible in the bag as there is no calcium, as any residual amounts remaining are chelated by citrate and, moreover, there is no potassium in SAGM. Absence of potassium is known to inactivate the Gárdos channel [103].

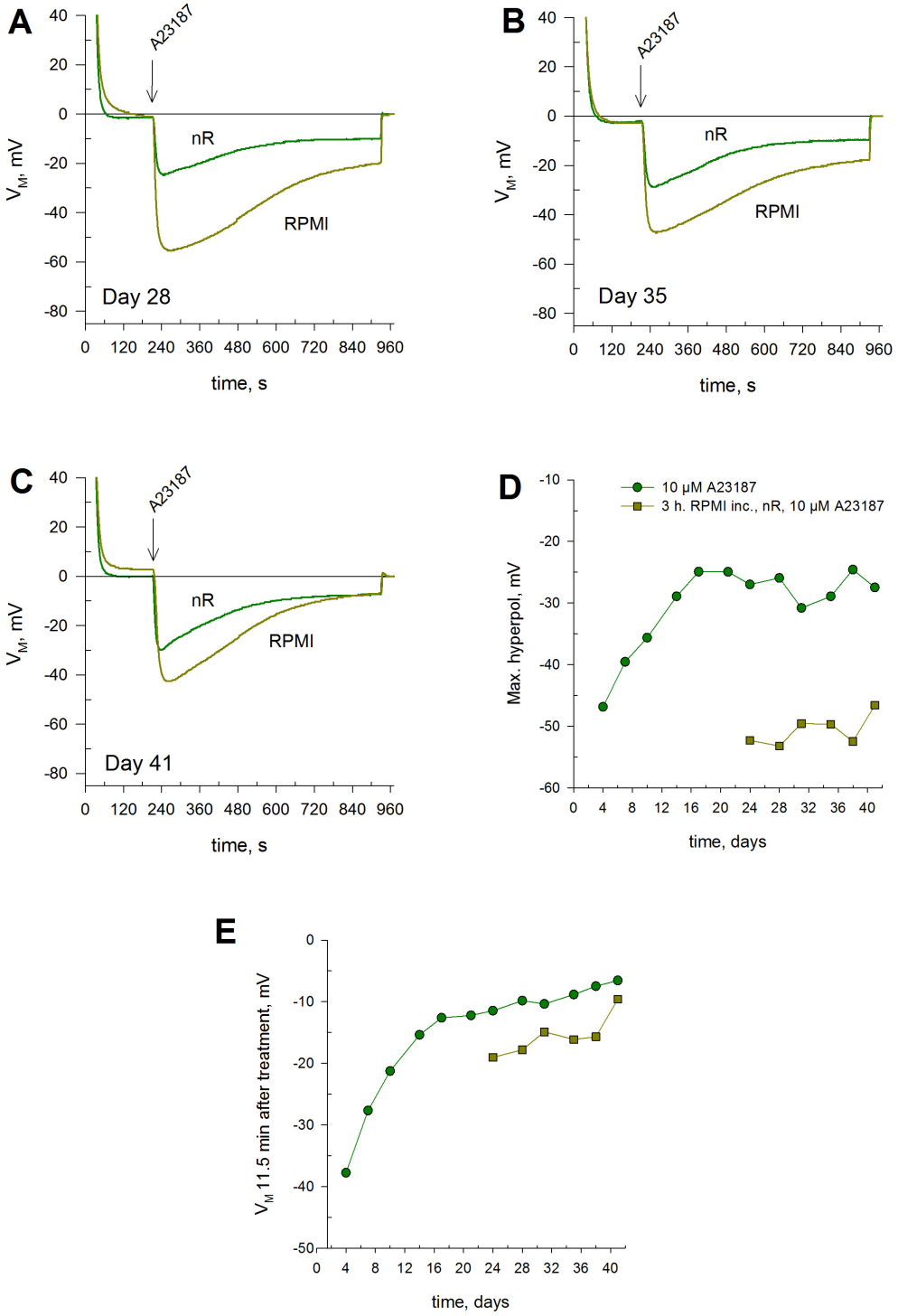

Figure 5.5: Effect of glucose and serum on A23187-mediated Gárdos openings and emerging NSC activity at selected points of 42-day RBC storage.

Membrane potential development from cells injected into normal Ringer, without (green) or with (golden) 3 hour-preincubation within serum-supplemented RPMI and hyperpolarized with calcium ionophore A23187 (10 µM). Membrane potential was determined by CCCP method. Measurements shown are from 28 (**A**), 35 (**B**) and 41 (**C**) after blood withdrawal. This is data from one red cell concentrate bag (n=1) out of two measured. Bag 2 of 2. See Fig. S5.10, S5.11, S5.12 for the full data. Evolution over 41 days or the last week of storage of maximum hyperpolarization (Max. hyperpol.) potential (**D**), most positive membrane potential (**E**) and 5 minutes post-treatment membrane potentials (**F**) reached by red cells treated with calcium ionophore A23187 (10 µM) without (green) or with (golden) 3 hour-preincubation within serum-supplemented RPMI. Each point is a mean of two independent measurements from two bags except for Day 7, 10 and 100 µM NS3623 pretreatment where n=1.

If nominally calcium-free solutions are employed, NS309 is still capable of opening the Gárdos channel due to the polluting amounts of calcium remaining in commercial salts, which are approximately 4 μM. However, when we treated stored red cells in this manner with either 50 or 100 μM NS309 we observed a small hyperpolarization throughout the entire 42-day period, resulting from weak Gárdos activation (not shown). This hints at severe calcium depletion and Gárdos inhibition taking place in the bag due to absence of Ca^{2+} and K^+ and residual citrate, so that even when cells are resuspended in normal Ringer, Gárdos is partially repressed.

Medium containing millimolar quantities of $CaCl_2$ emulates calcium levels in plasma, thereby allowing near-maximal Gárdos activations when NS309 is employed. In addition, the chloride conductance (G_{Cl^-}) can be inhibited by the use of inhibitors such as NS3623 (10 μM), revealing the full extent of Gárdos activity. Experiments were performed every three or four days during a 42-day storage period, with a pretreatment of 0, 10 or 100 μM NS3623 prior to NS309 application. NS3623 does not alter the resting membrane potential on freshly withdrawn cells (Chapter 3 on 69). Albeit there are some marginal differences between Bag 1 and 2, once cells are subjected to NS309 protocols, Gárdos and NSC channel activity trends are similar between both batches. During the first week membrane potential curves resemble those obtained from freshly drawn red cells except for repolarizations observed after NS3623 addition and a stronger hyperpolarization for 100 μM NS3623-pretreated cells. Nonetheless, the lag time between NS309 addition and hyperpolarization was significant for 100 μM NS3623-pretreated cells compared to the immediate activation seen on cells pretreated with 10 μM NS3623, a feature also found on freshly drawn cells. Maximum hyperpolarizations were thus on Day 7: -27.3 mV, -75.0 mV and -83.8 mV for 0, 10 and 100 μM NS3623-pretreated cells, respectively (**Fig. 5.6A**). A week after, on Day 14, maximum hyperpolarizations were reduced, especially for 100 μM NS3623-pretreated cells with a value of -26.6 mV for -72.4 mV of 10 μM NS3623-pretreated cells. At this point, blocking the chloride conductance entailed a delay in Gárdos activation, nevertheless a smaller delay still compared to 100 μM NS3623-pretreated cells. The difference in maximum hyperpolarization achieved was 43.8 mV between 10 and 100 μM NS3623 (**Fig. 5.6B**, blue and magenta traces).

Maximum hyperpolarizations are small on Day 21 for 0 μM and, especially for 10 μM NS3623-pretreated cells, suggesting an outlier if the trend for the storage period is considered altogether (**Fig. 5.6C** and **Fig. 5.7A**, blue diamonds). A key finding, by looking at V_M changes after Gárdos activation in 100 μM NS3623-pretreated RBCs, is that Gárdos and NSC relative strengths appear to be roughly equal during this week, with small preponderances of either conductances impacting the membrane potential in such a way that it goes towards positive values if NSC activity is stronger (such as on Day 21) or towards negative values if it is Gárdos (such as on Day 28) (**Fig. 5.6C, D**, magenta traces). As a consequence no hyperpolarization takes place on Day 21 upon Gárdos activation on 100 μM NS3623-pretreated cells, while it reaches a maximum of -16.2 mV on Day 28 (**Fig. 5.6C, D**, magenta traces). 10 μM NS3623-pretreated erythrocytes hyperpolarize, on the other hand, strongly with a maximum of -66.0 mV (**Fig. 5.6D**, blue trace).

On Day 35 of storage, 100 μM NS3623-pretreated cells strongly depolarize despite the addition of Gárdos activator, to the point where they seem to reach an equilibrium by the end of the experiment, with the maximum value attained being 41.3 mV (**Fig. 5.6E**). The evolution of Gárdos activation for 10 μM NS3623-pretreated cells resemble those of 100 μM NS3623-pretreated cells from Day 7 of storage showing the reduction of Gárdos activity over time. They reached -62.6 mV at this point (**Fig. 5.6E**). Strikingly, at the end of the storage duration, hyperpolarizations are stronger for cells untreated with NS3623 and those treated with 10 μM NS3623: -23.7 and -87.2 mV, respectively compared to Day 35. Moreover, Gárdos activation is not instantaneous for 10

μM NS3623-pretreated cells, contrary to first-week activations and there is an initial depolarization reaching 24.8 mV before hyperpolarization ensues. The kinetics after NS309 application show a strong delay before Gárdos activity is observed. 100 μM NS3623-pretreated cells also display Gárdos activity upon NS309 exposure, as assessed by the eventual fall of the membrane potential towards zero. However they reach such positive values, 54.7 mV, that Gárdos opening is not enough to bring the membrane potential to negative values in the time span of the experiment (**Fig. 5.6F**). At the end of the recording, they have attained 31.6 mV (**Fig. 5.6F**). A huge difference in V_M is observed by the end of the experiment compared to 10 μM NS3623-pretreated cells equal to 118.6 mV(**Fig. 5.6F**). Such values, far removed from physiological ones, point to the decay in ion homeostasis after long-term storage. The apparent renewed strength of Gárdos and cation reversal this late in storage may explain part of cell removal observed on reinfusion.

To summarize, calcium enters the cell through leak pathways and the action of NS309 on Gárdos, by lowering the calcium threshold for opening, entails maximal activations. Mean maximum hyperpolarization was -25.7 mV on Day 7, was reduced to -15.8 mV by Day 21 where it plateaus until a stronger activation is seen again on the last day with a value of -27.3 mV (**Fig. 5.7A**, green circles trend). 10 μM NS3623-pretreated cells strongly hyperpolarize upon NS309 treatment on Day 4, but weaker activations are seen up to Day 14 where it remains largely similar with slightly stronger activation over storage time until the last day, where maximum hyperpolarization is stronger than on Day 7 (**Fig. 5.7A**, blue diamonds trend). Compare this with the clear upward trend of 100 μM NS3623-pretreated cells, in red in **Figure 5.7A**, where maximal hyperpolarizations are similar to those of 10 μM NS3623-pretreated cells at the beginning of storage and are quickly diminished over time with no hyperpolarization taking place on the last week of storage. As 100 μM NS3623 enhances NSC activity, NSC activity becomes stronger than Gárdos. Cationic conductance almost matches already the chloride conductance as seen in **Figure 5.7B**, which point to the maximum point in V_M right after NS3623 addition. Both 10 and 100 μM NS3623 show an upward trend, in contrast to cells untreated with chloride conductance inhibitor. **Figure 5.7C** points to the fact that for 10 μM NS3623 RBCs (blue diamond trend) K^+ efflux through Gárdos is greater than Na^+ influx through NSC at least by the end of the experiment, during the last week of storage. V_M, thus, becomes more negative. 100 μM NS3623-pretreated cells, on the other hand, display positive V_M values as early as Day 31, which can only be explained by cation influx through a conductive pathway, doubly stimulated by 100 μM NS3623 and storage conditions (**Fig. 5.7C**, red hexagon trend).

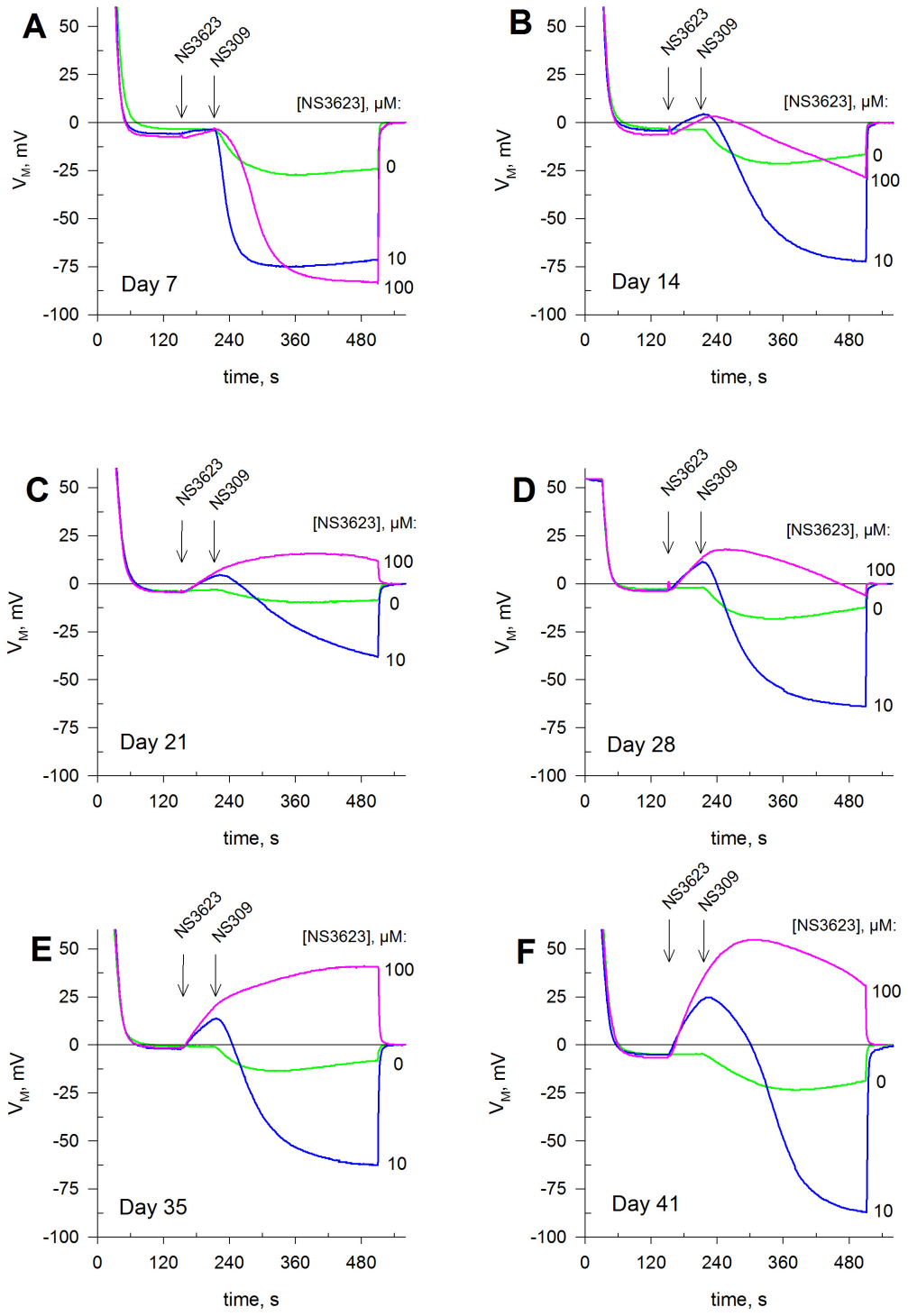

Figure 5.6: NS309-mediated Gárdos openings and emerging NSC activity, when extracellular calcium levels are at the physiological range, at selected points of 42-day RBC storage.

Membrane potential development from cells injected into calcium Ringer, treated with 0 µM (green), 10 µM (blue) or 100 µM (magenta) of chloride conductance inhibitor NS3623 and hyperpolarized with Gárdos activator NS309 (100 µM). Membrane potential was determined by CCCP method. Measurements shown are from Days 7 (**A**), 14 (**B**), 21 (**C**), 28 (**D**), 35 (**E**) and 41 (**F**) after blood withdrawal. This is data from one red cell concentrate bag (n=1) out of two measured. See Supplementary Figure S5.14, S5.15 and S5.16 for the full data.

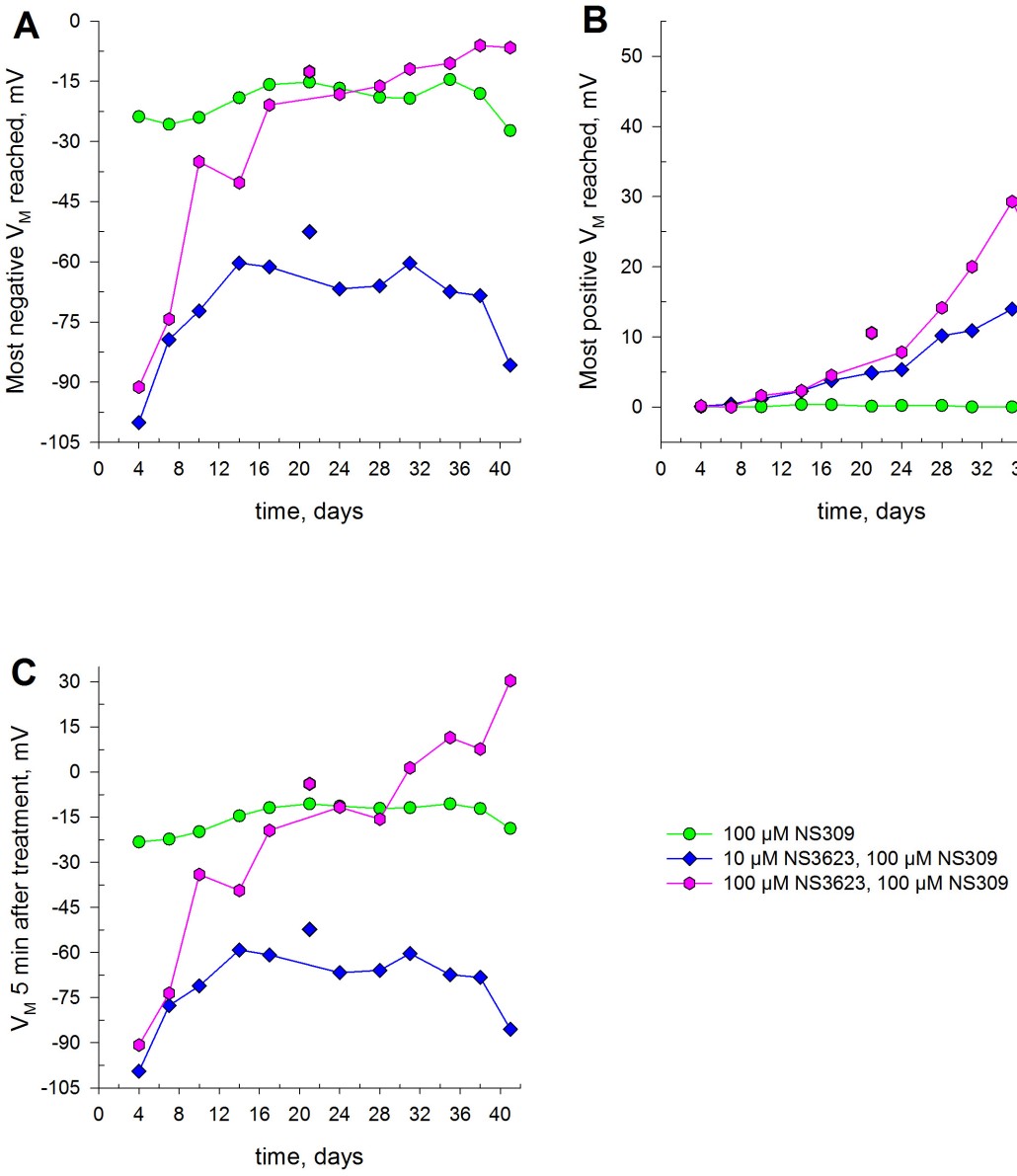

Figure 5.7: Evolution of NS309-mediated Gárdos activity and emerging NSC activity at selected points of 42-day RBC storage.

Evolution over 42 days of storage of most negative membrane potential (**A**), most positive membrane potential (**B**) and 5 minutes post-treatment membrane potentials (**C**) reached by red cells following Gárdos activation by NS309 upon treatment with 50 µM NS309 in normal Ringer (gray), 100 µM NS309 in normal Ringer (black), 100 µM in calcium Ringer (light green), 10 µM NS3623 and 100 µM NS309 in calcium Ringer (blue) and 100 µM NS3623 and 100 µM NS309 in calcium Ringer (magenta). 'Most negative membrane potential' refers to maximum hyperpolarization value reached by all treatments except 100 µM NS3623-pretreated cells. Each point is a mean of two independent measurements from two bags.

Piezo1 activation via Yoda1 and concomitant Gárdos activity

Piezo1 is a Non Selective cation Channel which opens in response to mechanical stimuli. It is therefore a pathway for Ca^{2+}, K^+ and Na^+. Upon activation cations move down their gradients: potassium flows out whereas sodium and calcium enter the cell. Calcium, in turn, opens Gárdos leading to a net potassium exit and concomitant dehydration. Piezo1 can be opened pharmacologically via agonist Yoda1. The use of this compound at small doses (625 nM) leads to a transient activation of the Gárdos channel, therefore to a brief hyperpolarization followed by a return close to resting membrane potential values. This is observed on Day 4, with erythrocytes exposed to Yoda1 (625 nM) hyperpolarizing to -56.1 mV (**Fig. 5.8A**). Yoda1 fails to hyperpolarize erythrocytes at this low concentration (625 nM) as early as the second week in storage. Given the trend in the lack of activation it was decided to use a very high concentration (20 μM) from then on to determine Piezo1 activity (via parallel Gárdos opening). Hence, on Day 17, 20 μM Yoda1-treated cells reached -22.5 mV already a 59.8% decrease in maximum hyperpolarization despite a 32-fold increase in Yoda1 concentration employed (**Fig. 5.8B**). The extent of Piezo1 activity remains stable the following weeks with a briefer hyperpolarization at the end, on Day 41 (**Fig. 5.8C-D**). Consequently, on average, Piezo1 activity, as measured by the action of the Gárdos channel, activated by Piezo1, decreased fast during the first week, being minimal the second week at levels of activation (625 nM Yoda1) thought to be close to physiological mechanically-induced activation. However, in spite of high concentrations used (20 μM Yoda1), Piezo1-Gárdos concerted activity plateaus during the remainder of the storage period, between Days 17 and 41, with a mean hyperpolarization of -21.7 ± 1.8 mV (n=8) (**Fig. 5.8E**).

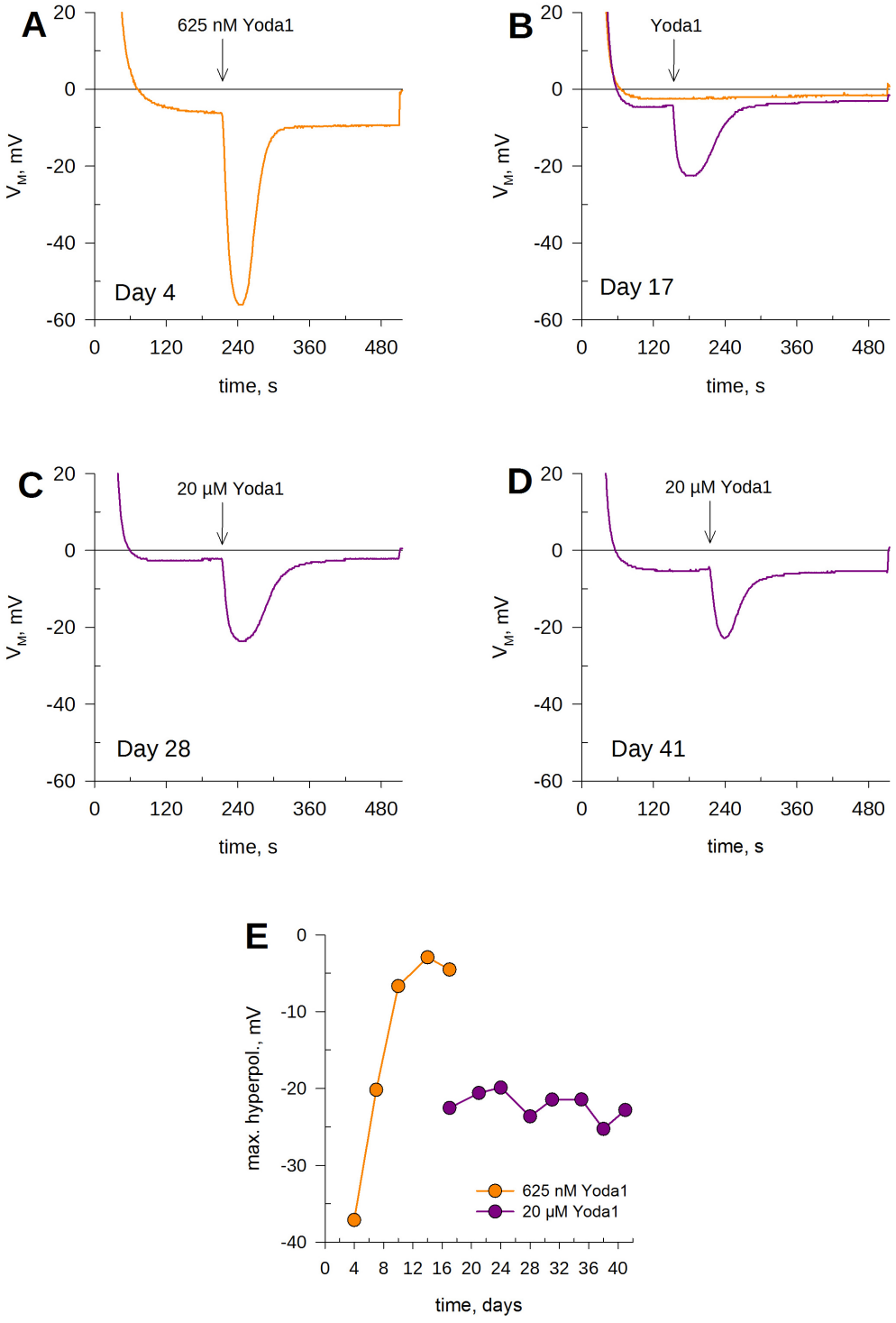

Figure 5.8: Piezo1-induced Gárdos activity via Yoda1 stimulation at selected points of 42-day RBC storage.
(**A-D**) Membrane potential development from cells injected into calcium Ringer, treated with 625 nM (orange) or 20 µM (dark purple) Yoda1. Membrane potential was determined by CCCP method. Measurements shown are from Days 4 (**A**), 17 (**B**), 28 (**C**) and 41 (**D**) after blood withdrawal. This is data from one red cell concentrate bag (n=1) out of two measured.
(**E**) Evolution over 42 days of storage of maximum hyperpolarizations (**E**) reached by red cells treated with 625 nM (orange) or 20 µM (dark purple) Yoda1. Each point is a mean of two independent measurements from two bags. See supplementary figure S5.17 for the full data.

Discussion

We have investigated ion channel activity every three or four days over a 42-day period corresponding to the legal maximum RBCCs can be kept stored in most parts of the world. This cutoff is not completely arbitrary but based on hemolysis and post-transfusion recovery data for red cells kept in SAGM. As quality control ensuring safety and efficacy of blood components, RBCCs must not surpass a hemolysis rate over 0.8 % according to European regulations [266, 323]. The American Food and Drug Administrations sets 1 % as the maximum allowable hemolysis but additionally conducts post-transfusion recovery trials where no less than 25 % of cells transfused should be removed from circulation after 24 hours. SAGM is inexpensive and allows storage up to six weeks, however cells must survive in a very artificial environment. They lack surrounding plasma proteins, save for those remaining after centrifugation as trapped plasma between cells, known to aid in the maintenance of proper morphology [24, 324]. SAGM does not contain calcium owing mainly to its pro-coagulating effect. Even though it would be partially chelated by trapped citrate from CPD during whole-blood processing, red cells are continually exposed and adapted *in vivo* to an environment, plasma, containing 1.9 mM $CaCl_2$. Whilst calcium-free solutions undoubtedly help long-term storage, there may be unintended effects such as cytoskeleton disorganization or a tendency for Gárdos activation following transfusion as the cell suddenly restores all intracellular calcium. Strikingly, potassium is also absent, creating a huge driving force for potassium efflux. The Gárdos channel is, however, irreversibly inhibited in the absence of extracellular potassium if Ca^{2+} is present. However Ca^{2+} is missing from the solution. Moreover, hemolysis occurs within the bag and is a source of K^+. If we assume the maximum legal hemolysis, 0.8% takes place and considering RBCs are at 80% hematocrit, with a RBCC volume of 300 ml, a simple calculation give a final $[K^+]_o$ of about 4 mM, a concentration largely sufficient to provide a driving force for Gárdos activation. Gárdos inhibition during storage should be beneficial because it prevents severe dehydration throughout the storage duration. These results establish that Gárdos is fully activable at physiological calcium levels.

Experiments with NS309 with 1 mM of extracellular Ca^{2+} display a strong hyperpolarization once Gárdos is opened (Fig. 5.8E). Nevertheless, a progressive decline of Gárdos-triggered hyperpolarizations, save for the last day, is observed throughout the storage period. In view of these findings, Gárdos may maximally activate upon cell recirculation and replenishment of intracellular calcium levels contributing to early cell removal from the bloodstream. Intracellular water measurements showed moderate water influx the second week of storage, a plateau phase between weeks two and four followed by moderate dehydration the last two weeks (**Fig. 5.8E**). Although the dehydration observed cannot be accounted for by Gárdos activation, as the channel is fully inhibited in SAGM, if we assume high rates of hemolysis towards the end of the storage period, the K^+ released would render Gárdos activable again and thereby it would explain the drop in intracellular water which occurs during the last week of storage. It is known that hemolysis increases over time and there is a progressive loss of discocytic morphology (**Fig. 5.8E**). Earlier reports display a slight dehydration between the first and third week and in following weeks there was barely no subsequent volume change measured as 'mean corpuscular volume' (MCV). Despite, a shift towards smaller, morphologically aberrant erythrocyte has been observed [325]. An important consideration is the fact that the way we measure water content (and thus cell volume) is totally independent on cell morphology though it is clear that moderate shrinking occurs during storage. Lack of plasma proteins, as in SAGM, is known to heavily alter red cell morphology and is likely largely responsible for causing microvesiculation reducing the surface-volume ratio. Trapped plasma between cells and the stabilizing

effect of DEHP on cell membranes would account for the limited scale of morphological alterations [24, 324, 326, 327]. The so-called glass effect by which erythrocytes undergo morphological changes due to contact with a surface was reported to happen with PVC [25]. Furthermore, intracellular K^+ and Na^+ decrease and increase over time, the overall cation concentration stays constant with a whole-period mean of 130.45 ± 1.97 mM (CV = 1.51 %, n = 12), which is consistent with Non Selective Cation Channel activity (**Fig. 5.8E**).

Regardless whether Gárdos activity is low or nonexistent, NSC basal contribution to the membrane conductance is clearly potentiated. Indeed, experiments conducted with NS3623 (10 or 100 µM) immediately triggers a depolarization as early as the second week postwithdrawal. The fact that the depolarization rate is identical for both NS3623 concentrations implies that the NSC conductance is close, at that time, to the nominal chloride conductance. Hence if the latter is blocked, a dominant NSC conductance is revealed. A23187-induced Gárdos activation in the absence of chloride conductance shows a moderate repolarization over 12 minutes consistent with what is observed in fresh blood (not shown). However, this repolarization becomes more pronounced during storage along with a reduction on overall hyperpolarizations pointing to a decreased driving force for Gárdos as a result of K^+ efflux. After the instantaneous hyperpolarization induced, cells repolarize owing to chloride and cationic currents. An increased sodium influx explains increasingly pronounced repolarizations over storage time. In order to mimic cell reinfusion into the circulation where calcium, nutrients and plasma proteins are plentiful, we incubated cells in RPMI medium supplemented with serum. Upon A23187 treatment, cells hyperpolarize to greater extents owing mainly to a restored potassium and calcium content. Nonetheless, marked repolarizations quickly develop, noticeable on Day 28, and evident by Day 41, where the hyperpolarization difference between RBCs incubated in SAGM and unincubated cells is lost within 10 min owing to membrane repolarization. Indeed, this sodium influx is apparent when cells are treated with 100 µM NS3623, which enhances NSC activity and which brings the membrane potential to very positive values unless Gárdos is activated with A23187 (**Fig. 5.2D,E**). A study found washing RBCs stored for six weeks in SAGM with 1% human serum albumin reverted echinocytic morphological changes, but not when they were washed, puzzlingly, with plasma (**Fig. 5.9**) [328]. The authors offer the hypothesis that albumin binds to many different plasma constituents, thereby reducing available binding sites for interaction with RBCs. Globulins found in plasma are echinocytogenic, contrary to albumin, which is stomatocytogenic, but the matter has to be further explored.

Interestingly, at late stages of the storage lesion, on Day 41, Gárdos cannot fully counter this sodium influx, compounded by reduced intracellular K^+, and the membrane potential resumes its upward trend following a brief A23187-induced hyperpolarization (**Fig. 5.2F**). The use of choline solutions allows to ascertain sodium permeability through conductive pathways as choline itself is an impermeant cation. This was the strategy presented in Chapter 3 (page 69) which enabled to clearly demonstrate that repolarization observed after Gárdos activation upon enhancement of NSC activity is due to sodium influx. On Day 4 cells immersed in choline-substituted solution and treated with NS3623 and A23187 respond as fresh cells (Chapter 3). On Day 21 we observe a deviation from both fresh and SAGM-stored cells for 4 days. A depolarization takes places with both 10 or 100 µM NS3623, as seen in A23187 experiments with sodium-containing solutions, pointing to strengthened NSC activity, which was very moderate on Day 4. Upon 100 µM NS3623 addition, NSC activity is further enhanced, thus delaying considerably the onset of Gárdos-induced hyperpolarization and explaining slope variation. On Day 41, 10 µM NS3623-pretreated cells hyperpolarize to the same extent regardless of the availability of sodium, albeit with reduced hyperpolarizations and apparent underlying cationic current ob-

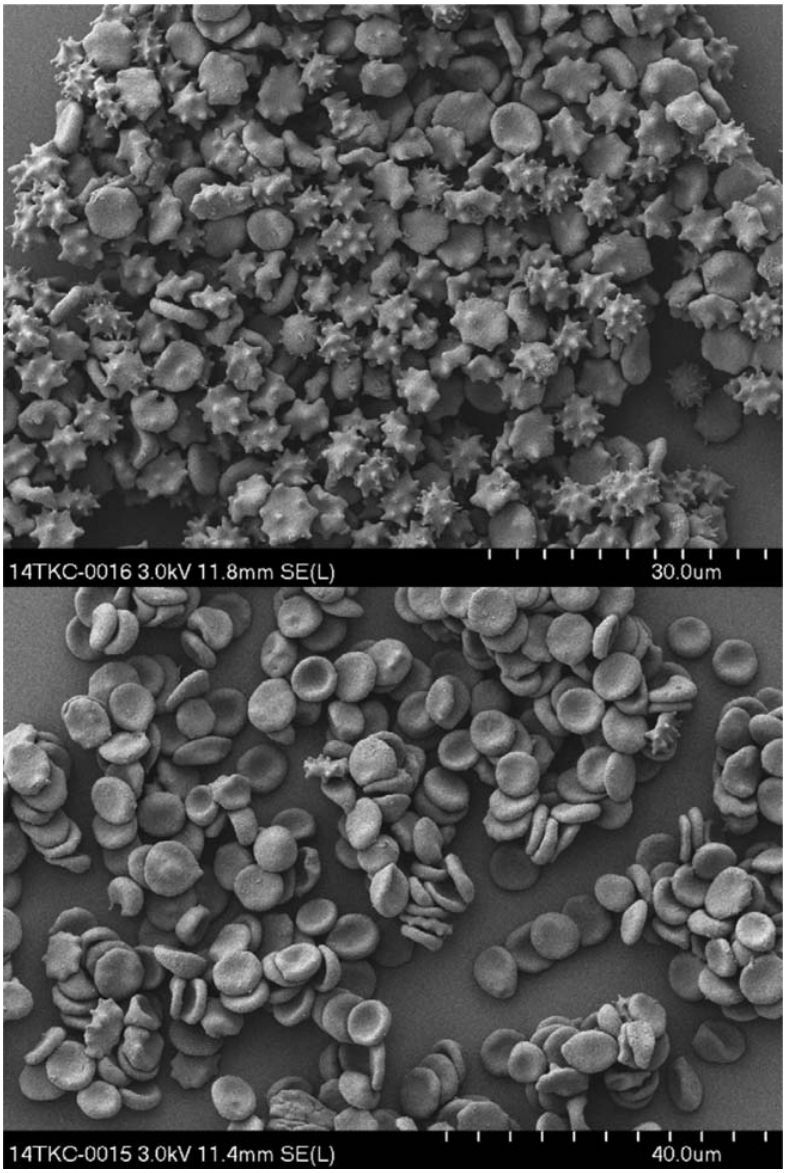

Figure 5.9: Top: RBCs stored in SAGM for 6 weeks. Bottom: The same stored RBCs as in the top panel washed in a 1% HSA solution. Scanning electron micrographs from [328].

served upon chloride conductance inhibitor exposure. However, 100 µM NS3623-pretreated cells are unable to hyperpolarize strongly by A23187 as cation conductance is dominant. Sodium is the cation going into the cell via a NSC. How are cells in 100 % choline solutions, devoid of sodium, able to depolarize? The only explanation is that choline must cross the plasma membrane. A transporter has been known to exist in the membrane, allegedly SLC44A1 and SLC44A2 [329] albeit those are expressed in mitochondria elsewhere. In a choline uptake study with *Plasmodium*-infected cells, uninfected controls took 0.2 µM per 10^{12} erythrocytes in 10 minutes with an extracellular choline concentration of 50 µM [330]. This transporter in healthy erythrocytes has a K_M of 10 µM and saturates at about 100 µM [330, 331]. Nevertheless, a transporter is not only incompatible with the speed at which the cell population depolarizes but it is electroneutral, therefore its activity would be invisible by means of membrane potential change. On Day 41, RBCs depolarize at a rate of 0.358 mV/s, which can only be achieved by a channel. Such hypothesis has been previously proposed by Lew et al. [251] suggesting that A23187-triggered P_{cat} activity is permeable to choline.

But, more importantly, research into New Permeation Pathways (NPPs), which are induced by *Plasmodium* infection, allowed to obtain information on VDAC, a pathway contributing to the NPPs and an endogenous NSC pore. NPPs are known to be permeant to choline [187], and although it is not known whether this is mediated by VDAC, the pore is permeable to choline in mitochondria. In fact, it was found in mitochondrial studies that VDAC can oligomerize in order to form a large pore able to let pass molecules as large as cytochrome *c* [332, 333]. VDAC forms dimers, trimers, tetramers, hexamers and even larger oligomers. VDAC is more permeable to cations in the closed state, yet it has been shown to be permeable to large cations such as acetylcholine in the fully open state [334]. Furthermore, the fact that Gárdos activity is insufficient to bring the membrane potential to negative values and repolarization quickly develops is proof a channel is responsible for the phenomenon observed, aided by the reduced K^+ driving force on Day 41.

Experiments where Gárdos activation was conducted at physiological calcium levels by the action of calcium sensitizer NS309 led to critical observations:

i Gárdos activation by NS309 in nominally calcium-free Ringers was minimal throughout the storage period indicating severe depletion of cytoplasmic calcium levels, far lower than in freshly withdrawn cells.

ii The chloride conductance remains mostly stable during storage despite the huge increase in cation permeability with only a slight effect on membrane potential at th resting state.

iii RBCs become so depleted in intracellular calcium that placing them in solution with millimolar levels of Ca^{2+}, levels they will encounter upon reinfusion into the circulation, entails a calcium loading above resting levels which favors subsequent Gárdos activations. Calcium depletion is almost immediate as judged by the strong Gárdos activation, stronger than with A23187, on Day 4. Gárdos activity is masked afterwards by the rise of NSC channel activity.

iv Gárdos-induced hyperpolarization are stronger on Day 41 after 10 µM NS3623 pretreatment despite the previous trend of decline. The observation may be explained by the nonlinear increase in NSC conductance observed on the last days of storage contrary to the moderate but steady climb in activity during the first weeks.

Yoda1 is an agonist of Piezo1 independent of mechanical stimuli or other cellular components than the trimeric channel itself [163]. Even though its use elicits an instantaneous Piezo1 opening, a Gárdos-induced hyperpolarization is what is actually observed in membrane potential recordings. Piezo1 is a NSC channel, therefore sodium influx and potassium efflux will be balanced in an almost 1:1 ratio. However, calcium will enter RBCs and activate Gárdos leading to a net K^+ efflux. On channel closure the membrane potential returns to values close to the original resting membrane potential. Hence, the study of Piezo1 in this manner has the caveat of relying on Gárdos activity. A strong chloride conductance may also mask full activation. By the end of the second week of storage, Piezo1 activity heavily declines requiring thereafter high doses of agonist Yoda1 to elicit weak hyperpolarizations. Nevertheless, an involvement of Piezo1 in the NSC activity that arises during storage cannot be ruled out, as it may be opened in storage conditions independently of mechanical or pharmacological stimulation.

We have presented herein a thorough analysis of channel activity during Red Blood Cell Concentrate storage for 42 days in CPD-SAGM. An impact on ion homeostasis is clear as early as the first two weeks of storage. Ion channel activity is altered, heavily towards the end of the storage duration with a strong cation conductance arising that is consistent with Non Selective Cation channel activity. These alterations have ramifications on cell hydration and morphology, which may ultimately jeopardize erythrocyte passage through narrow vessels and, thus, survival right after transfusion.

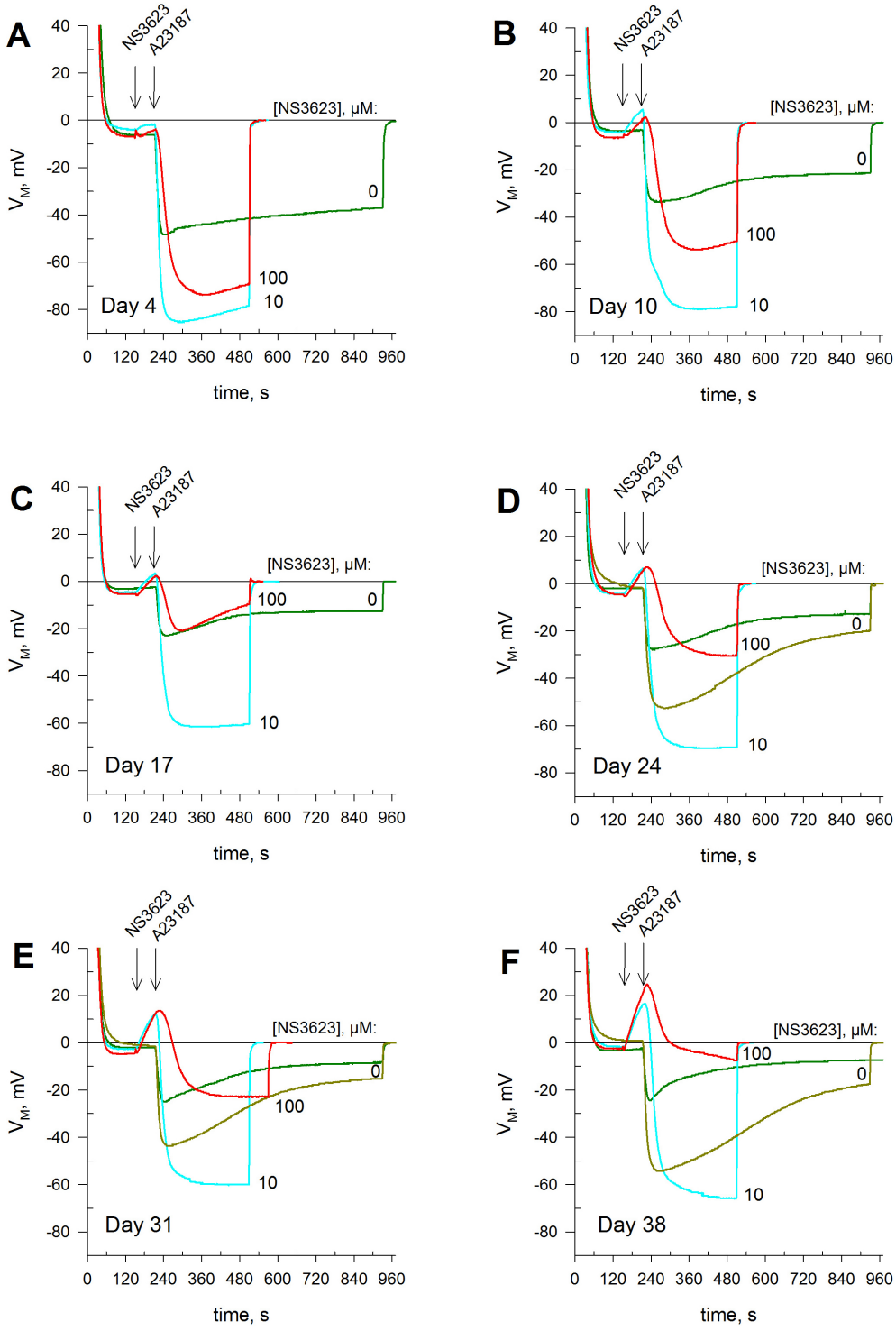

Supplementary Figure S5.10: A23187-mediated Gárdos openings and emerging NSC activity at selected points of 42-day RBC storage.

Membrane potential development from cells injected into normal Ringer, treated with 0 µM (dark green), 10 µM (cyan) or 100 µM (red) of NS3623 and hyperpolarized with A23187 (10 µM). Golden traces show cells preincubated in RPMI medium supplemented with serum for approximately three hours and then injected in normal Ringer and treated with 10 µM A23187. Membrane potential was determined by CCCP method. Measurements shown are from Days 4 (**A**), 10 (**B**), 17 (**C**), 24 (**D**), 31 (**E**) and 38 (**F**) after blood withdrawal. This is data from one red cell concentrate bag (n=1) out of two measured. Bag 2 of 2 See Fig. 5.2 for data from Days 7, 14, 21, 28, 35 and 41.

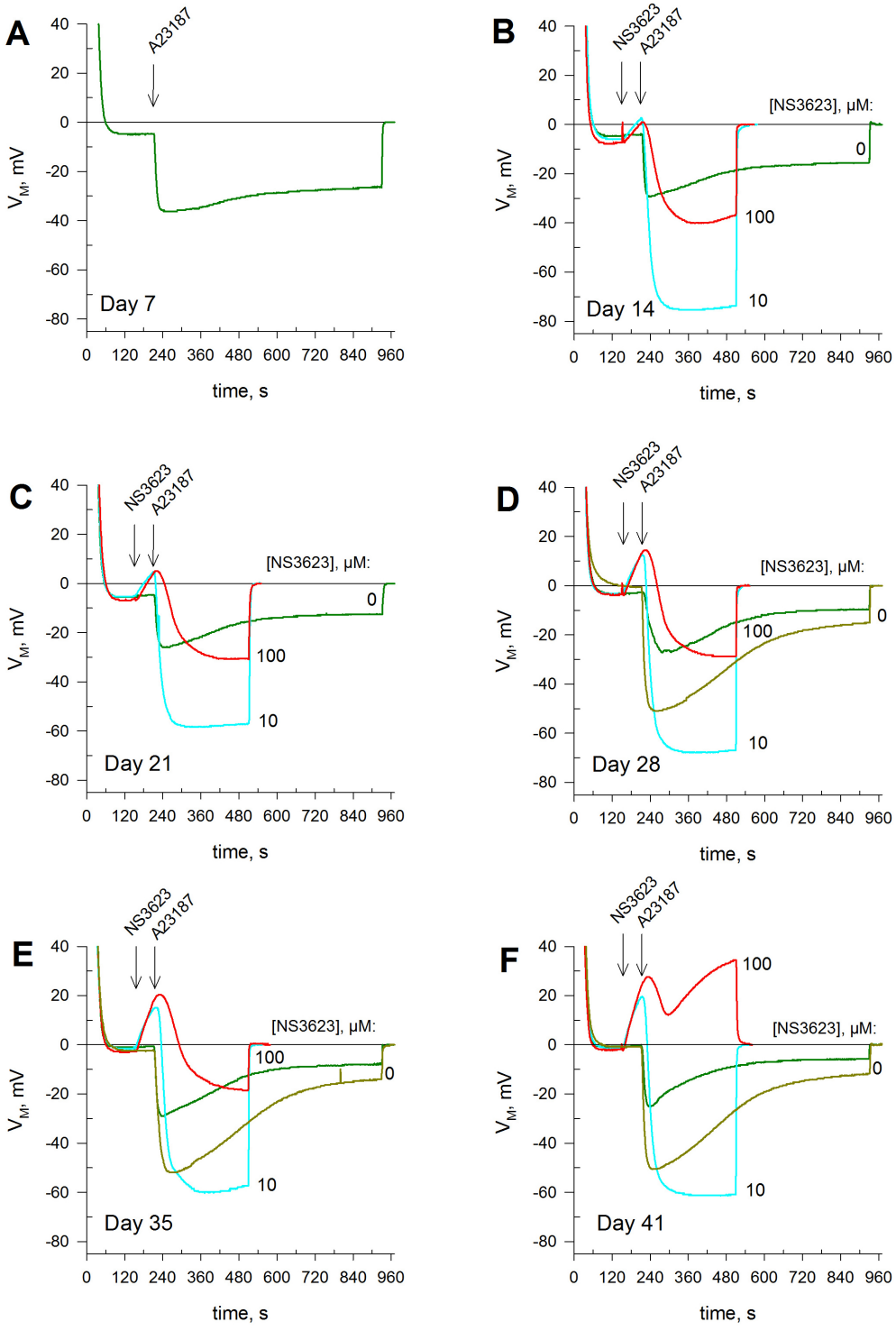

Supplementary Figure S5.11: A23187-mediated Gárdos openings and emerging NSC activity at selected points of 42-day RBC storage.

Membrane potential development from cells injected into normal Ringer, treated with 0 µM (dark green), 10 µM (cyan) or 100 µM (red) of NS3623 and hyperpolarized with A23187 (10 µM). Golden traces show cells preincubated in RPMI medium supplemented with serum for approximately three hours and then injected in normal Ringer and treated with 10 µM A23187. Membrane potential was determined by CCCP method. Measurements shown are from Days 7 (**A**), 14 (**B**), 21 (**C**), 28 (**D**), 35 (**E**) and 41 (**F**) after blood withdrawal. This is data from one red cell concentrate bag (n=1) out of two measured. Bag 1 of 2. See Fig. S5.12 for data from Days 4, 10, 17, 24, 31 and 38.

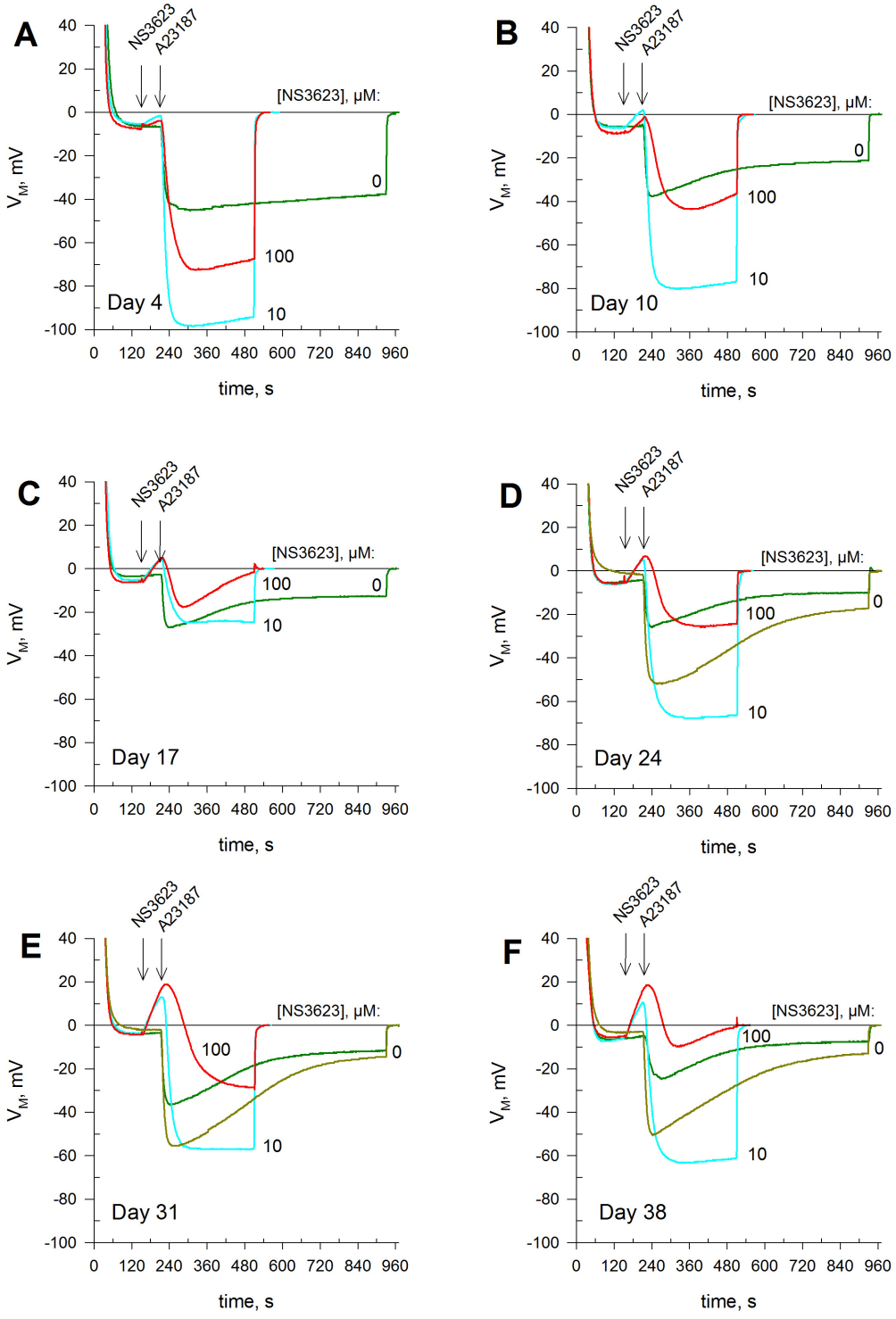

Supplementary Figure S5.12: A23187-mediated Gárdos openings and emerging NSC activity at selected points of 42-day RBC storage.

Membrane potential development from cells injected into normal Ringer, treated with 0 µM (dark green), 10 µM (cyan) or 100 µM (red) of NS3623 and hyperpolarized with A23187 (10 µM). Golden traces show cells preincubated in RPMI medium supplemented with serum for approximately three hours and then injected in normal Ringer and treated with 10 µM A23187. Membrane potential was determined by CCCP method. Measurements shown are from Days 4 (**A**), 10 (**B**), 17 (**C**), 24 (**D**), 31 (**E**) and 38 (**F**) after blood withdrawal. This is data from one red cell concentrate bag (n=1) out of two measured. Bag 1 of 2. See Fig. S5.11 for data from Days 7, 14, 21, 28, 35 and 41.

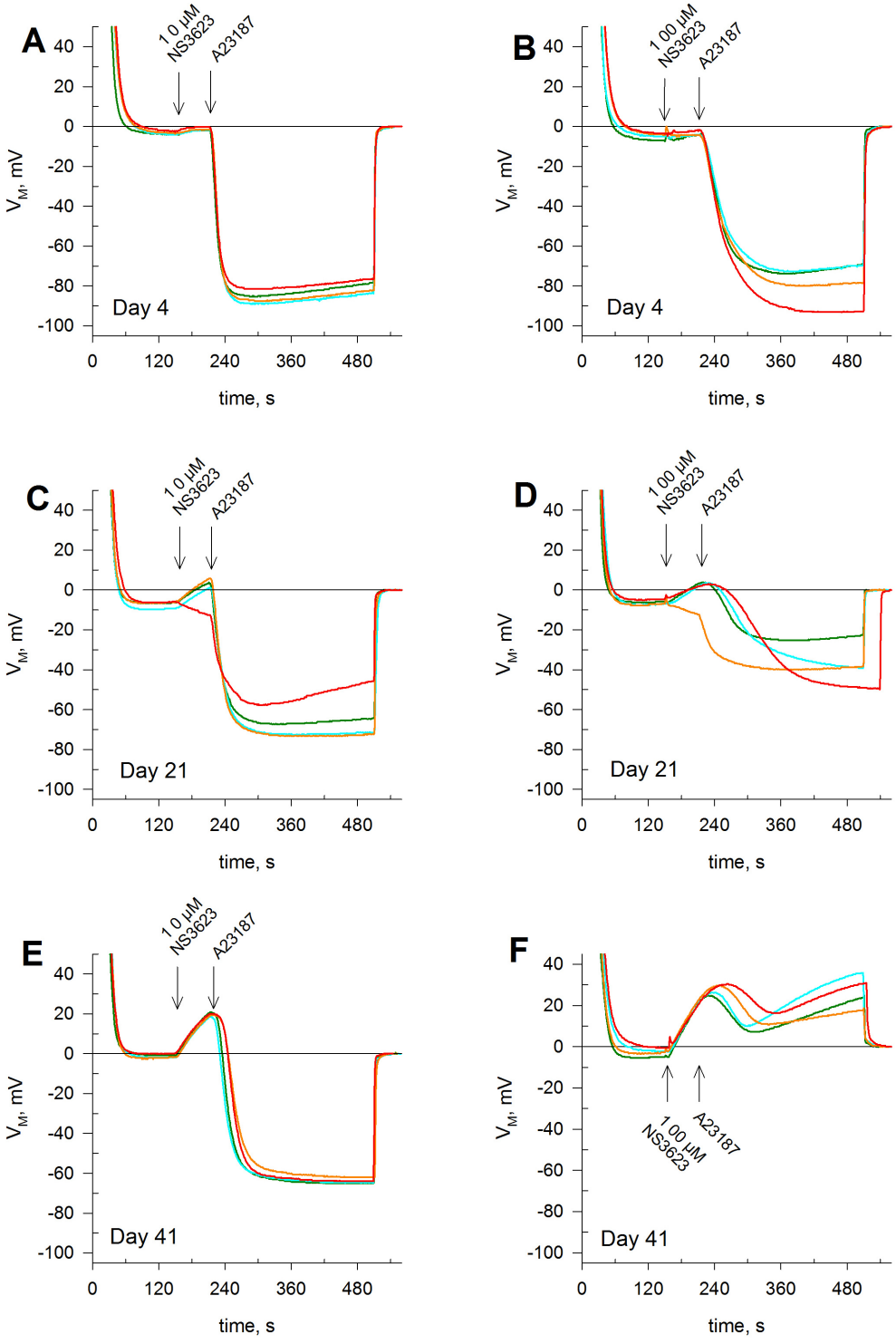

Supplementary Figure S5.13: A23187-mediated Gárdos openings and emerging NSC activity when impermeant cation is in the experimental medium at selected points of 42-day RBC storage.

Membrane potential development from cells injected into 0 % (green), 25 % (cyan), 50% (orange) or 100% (red) Choline Chloride solutions, treated with 10 µM (**A**, **C** and **E**) or 100 µM (**B**, **D** and **F**) of chloride conductance inhibitor NS3623 and hyperpolarized with calcium ionophore A23187 (10 µM). Membrane potential was determined by CCCP method. Choline chloride substitution percentage was: 0 % Choline Chloride solution = normal Ringer = 154 mM NaCl, 2 mM KCl and 100 % Choline Chloride solution = 154 mM Choline Chloride, 2 mM KCl. Measurements shown are from Days 4 (**A** and **B**), 21 (**C** and **D**), and 41 (**E** and **F**) after blood withdrawal. This is data from one red cell concentrate bag (n=1) out of two measured. Bag 2 out of of 2. See Figure 5.4 for the other dataset.

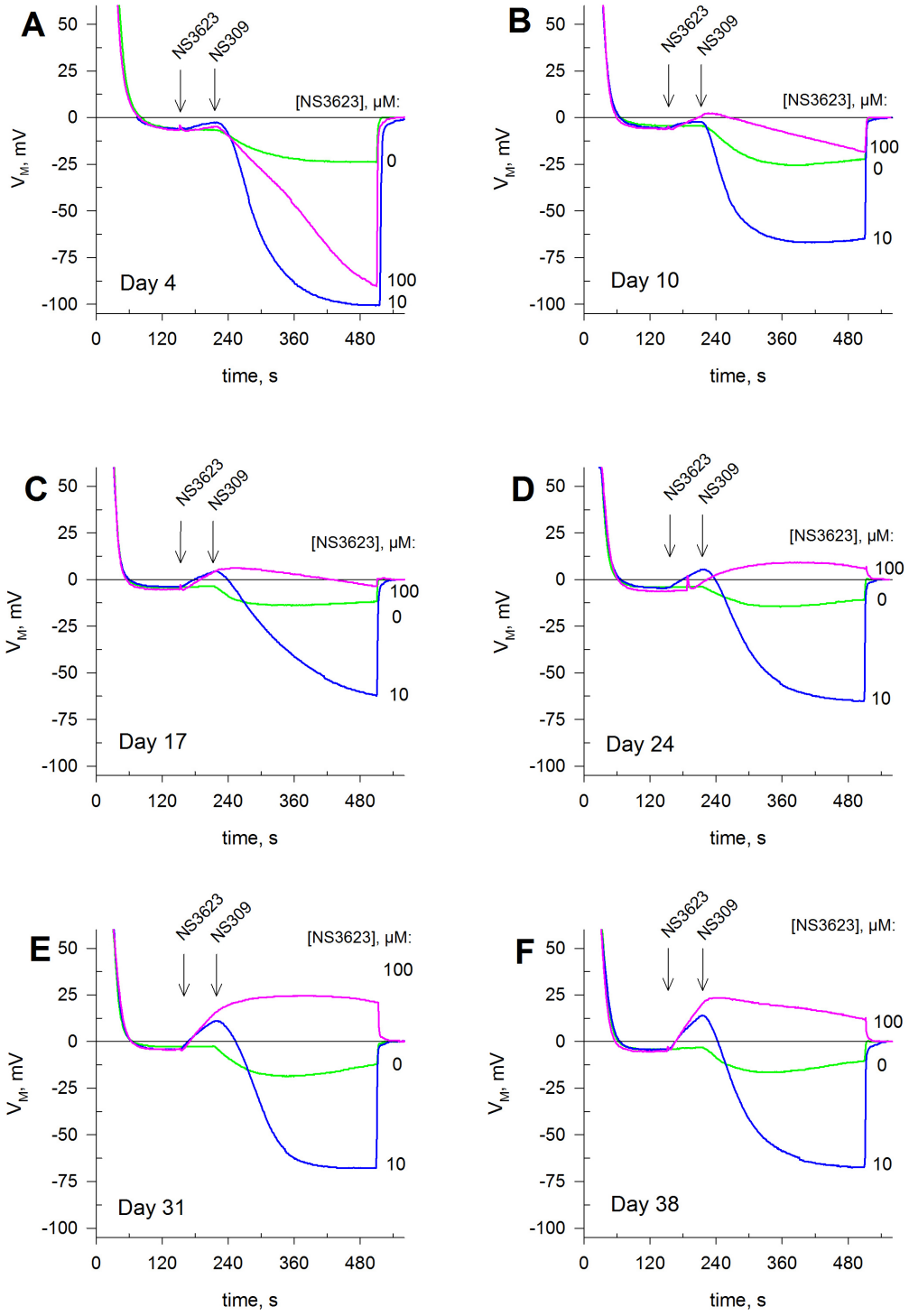

Supplementary Figure S5.14: NS309-mediated Gárdos openings and emerging NSC activity, when extracellular calcium levels are at the physiological range, at selected points of 42-day RBC storage.

Membrane potential development from cells injected into calcium Ringer, treated with 0 µM (green), 10 µM (blue) or 100 µM (magenta) of chloride conductance inhibitor NS3623 and hyperpolarized with Gárdos activator NS309 (100 µM). Measurements shown are from Days 4 (**A**), 10 (**B**), 17 (**C**), 24 (**D**), 31 (**E**) and 38 (**F**) after blood withdrawal. This is data from one red cell concentrate bag (n=1) out of two measured. Bag 1 of 2. See Fig. 5.6 for data from Days 7, 14, 21, 28, 35 and 41.

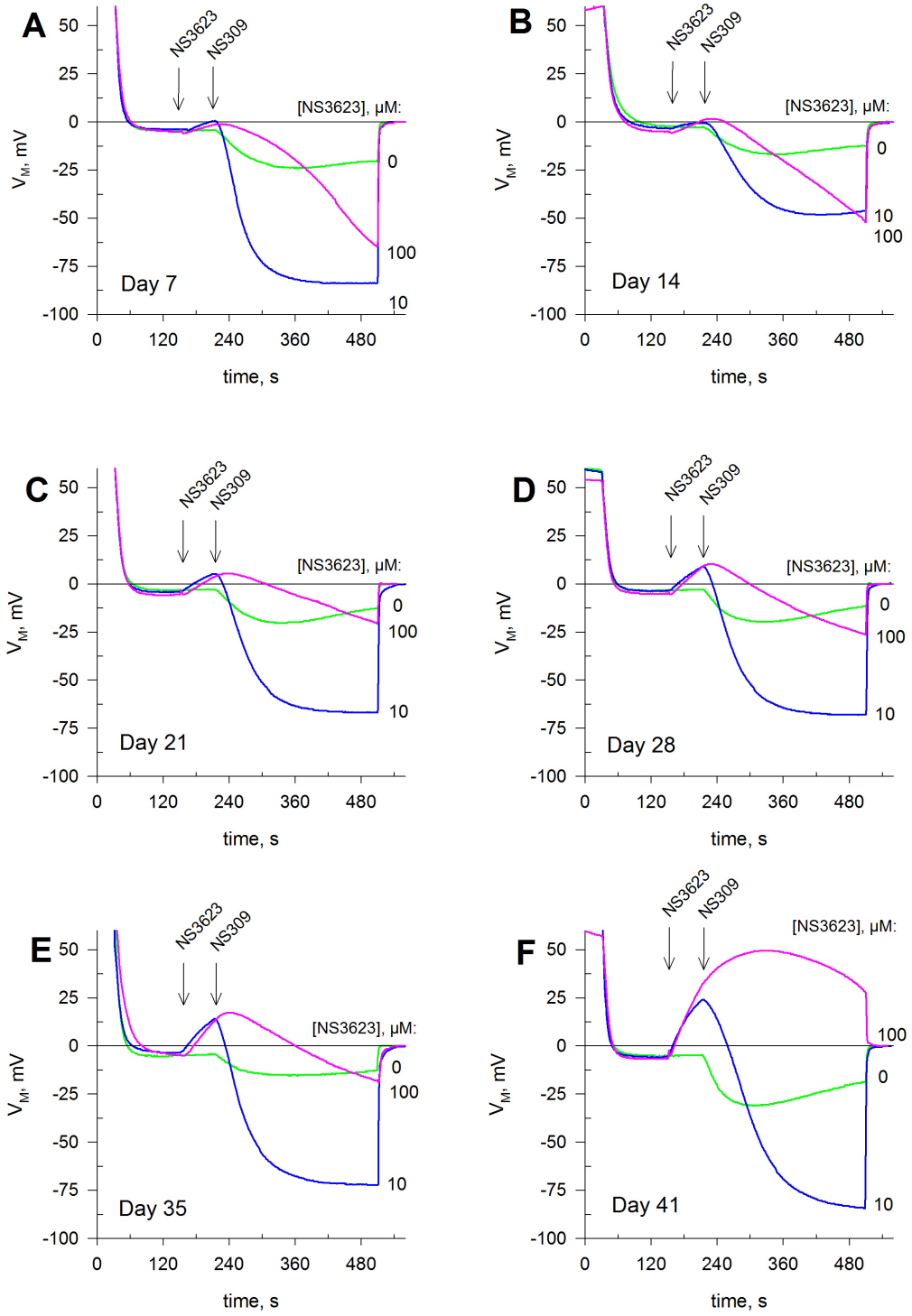

Supplementary Figure S5.15: NS309-mediated Gárdos openings and emerging NSC activity, when extracellular calcium levels are at the physiological range, at selected points of 42-day RBC storage.

Membrane potential development from cells injected into calcium Ringer, treated with 0 µM (green), 10 µM (blue) or 100 µM (magenta) of chloride conductance inhibitor NS3623 and hyperpolarized with Gárdos activator NS309 (100 µM). Measurements shown are from Days 7 (**A**), 14 (**B**), 21 (**C**), 28 (**D**), 35 (**E**) and 41 (**F**) after blood withdrawal. See Fig. 5.6 for the rest of the data. This is data from one red cell concentrate bag (n=1) out of two measured. Bag 2 of 2. See Fig. S5.16 for data from Days 4, 10, 17, 24, 31 and 38.

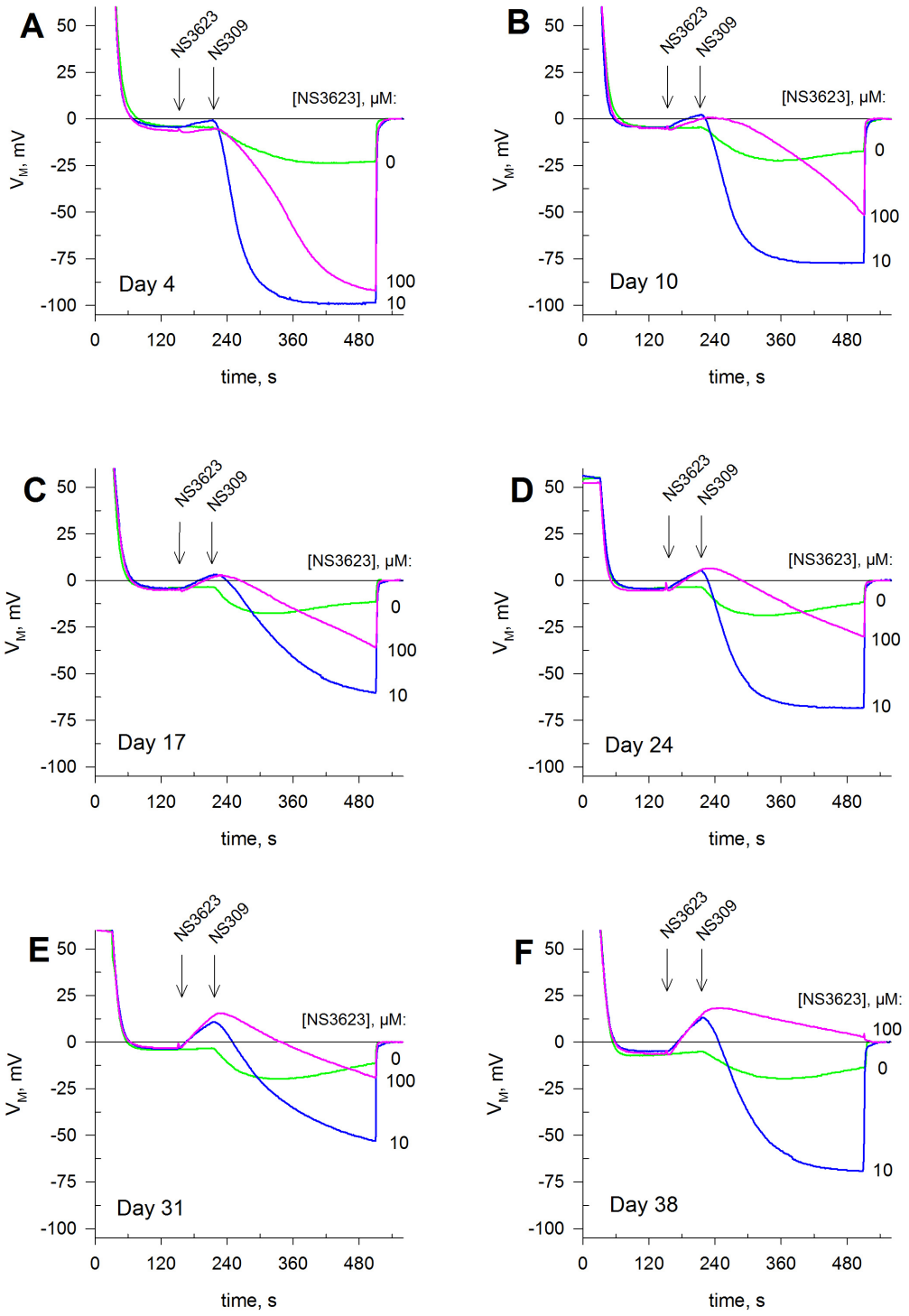

Supplementary Figure S5.16: NS309-mediated Gárdos openings and emerging NSC activity, when extracellular calcium levels are at the physiological range, at selected points of 42-day RBC storage.

Membrane potential development from cells injected into calcium Ringer, treated with 0 µM (green), 10 µM (blue) or 100 µM (magenta) of chloride conductance inhibitor NS3623 and hyperpolarized with Gárdos activator NS309 (100 µM). Measurements shown are from Days 4 (**A**), 10 (**B**), 17 (**C**), 24 (**D**), 31 (**E**) and 38 (**F**) after blood withdrawal. This is data from one red cell concentrate bag (n=1) out of two measured. Bag 2 of 2. See Fig. S5.15 for data from Days 7, 14, 21, 28, 35 and 41.

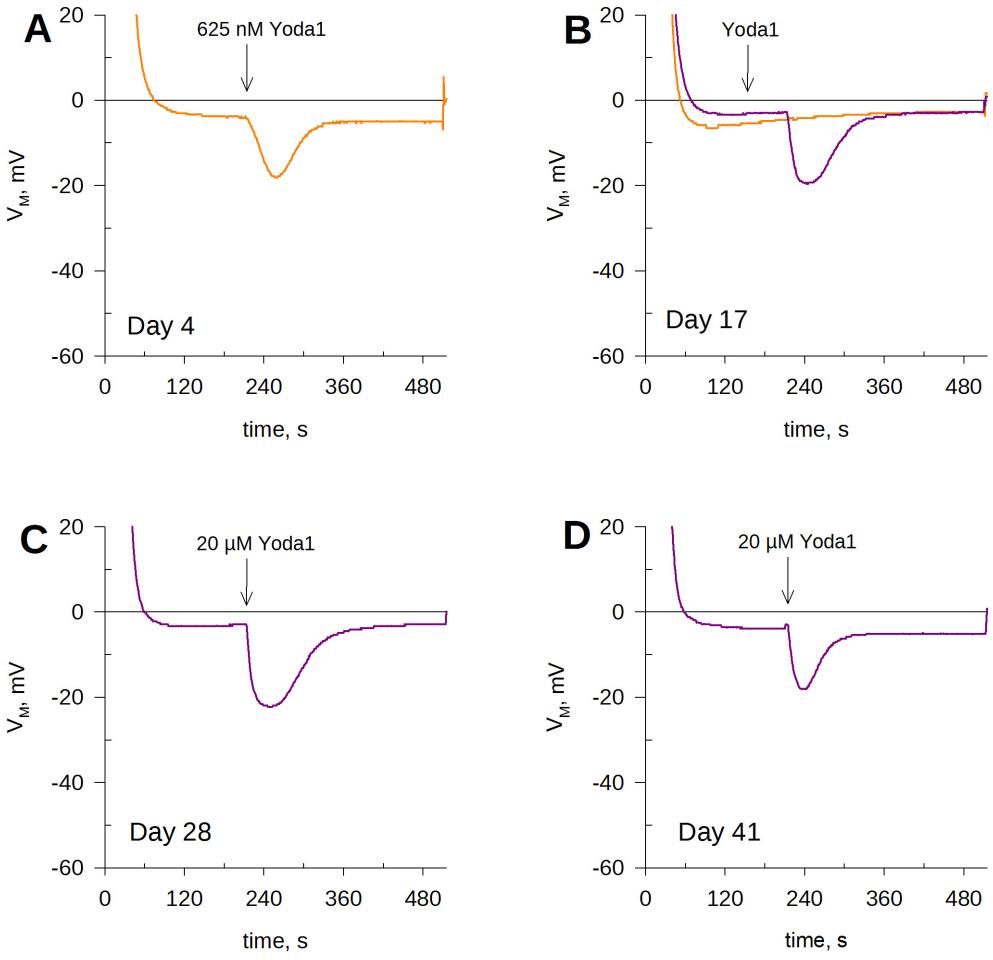

Supplementary Figure S5.17: Piezo1-induced Gárdos activity via Yoda1 stimulation at selected points of 42-day RBC storage.

(**A-D**) Membrane potential development from cells injected into calcium Ringer, treated with 625 nM (orange) or 20 µM (dark purple) Yoda1. Membrane potential was determined by CCCP method. Measurements shown are from Days 4 (**A**), 17 (**B**), 28 (**C**) and 41 (**D**) after blood withdrawal. This is data from one red cell concentrate bag (n=1) out of two measured.

General Discussion

Chapter 6

General Discussion

Human erythrocytes have a lifespan of 120 days within the bloodstream before removal. During this period, without any capacity for protein renewal, they have to survive and contend with many stresses related to their biological function. Among the challenges RBCs have to cope with, they must maintain a constant surface/volume ratio in order to provide the best gas delivery efficacy, being also essential to fulfill the need for deformability [335]. While evolution optimized these RBC functions, a counterpart is the huge hemoglobin content which tends to draw cations into the cells. RBC volume stability for such highly water-permeable cells depends on a key property: membrane permeability to cations is very low. However, erythrocytes are endowed with numerous membrane transporters for cations that may endanger this fragile equilibrium if they malfunction. Among them, cation channels are poorly described, though their dissipative effect has been reported in several situations. Thus, studying them in detail is essential for a better understanding of RBC homeostasis and cellular physiology.

The study of the RBC cation conductance is hindered by its magnitude being much lower than that of the chloride conductance. At rest, cation leak is tiny and is coupled to active transport carried out by ATPases resulting in no net cation movements [33]. However, even when cation channels, such as Gárdos, are activated, the strong chloride conductance masks the true extent of cation activity. It is especially cumbersome when ion channel activity is studied by the impact of conductance changes (i. e. channel opening) on the membrane potential [294]. It is noteworthy that K^+ efflux via Gárdos is rate-limited by Cl^- efflux via G_{Cl^-} [216], being also the case when NSC channels open, for electroneutrality purposes. Therefore, chloride conductance inhibitors are routinely employed in order to reveal the underlying cation channel activity. NS3623 is the best chloride conductance inhibitor available to date. Hence a thorough analysis of its activity was carried out uncovering an unexpected effect at high concentrations. NS3623 enhances NSC channel activity at high concentrations (100 μM) while retaining its chloride conductance inhibiting capabilities. As studying cation conductances requires the comparative study of several states of permeability in order to gauge NSC channel involvement, NS3623 has proven to be an excellent tool as NSC channel potentiation without background chloride conductance can be obtained with a single drug supplementation. The molecular nature of the NSC channel or channels enhanced by NS3623 are unknown. Na^+ influx was not prevented when RBCs were exposed to high concentrations of NS3623 during 30 min in the presence of inhibitor ruthenium red (RR) (not shown). RR is reported to inhibit Piezo1 and VDAC [151, 336]. It interacts with VDAC calcium binding sites, decreasing the open probability [195]. Despite, ruthenium red is fairly nonspecific and its molecular targets are unknown. No specific NSC channel inhibitors exist and due to the unknown molecular identity of some NSC channel activities, high-throughput screenings seems the only promising approach to obtain specific inhibitors against NSC channels.

Importantly, due to the nature of membrane potential estimation experiments only ion channel activity impact on the membrane potential can be assessed, excluding any other electroneutral transporter, which are dependent on chemical gradients. Moreover, ion channels are able to move tens of thousands of ions per second, contrary to passive transporters, where each ion has to bind the appropriate domain before a conformation change allows translocation to take place and the ion unbinds on the other side of the lipid bilayer. Thus, take a single ion

channel permeable to monovalent cation with a current of 1 pA when fully active, the ion flow rate through the pore is 6.25×10^6 ions/s! Thereby, should NSC channels play a role in the so-called leak, they ought to be the main contributors or actors so studying them in detail is essential to understand RBC homeostasis and cellular physiology.

Two possibilities exist regarding leak pathways:

Either leaks typically observed in tracer experiments are associated to symporter or antiporter activity and cation channels are active only in nonphysiological (e.g. LIS solutions) or paraphysiological (e.g. storage conditions) situations,

or leaks are caused mainly by ion channels due to very low but nonzero open probabilities which increase over time as erythrocytes age and cells lose protein functions and homeostatic balance due to oxidation.

The second hypothesis would explain the almost exponential increase in cation permeability seen during the last week of SAGM storage of RBCs akin to the $[Na^+]_i/[K^+]_i$ ratio reversal observed in the oldest cell fraction. Two NSC channels presumed with high certainty to be involved in the NSC activity reported in this thesis are:

1. NSVDC, considering it has been thoroughly characterized in Low Ionic Strength Solution and also via patch-clamp, but whose molecular identity is unknown [168].

2. Piezo1, as membrane potential repolarizations in LIS conditions are partially blocked by GsMTx4 also in freshly drawn wild-type RBCs (not shown). Nonetheless GsMTx4 is not fully specific to this channel, and as its effect comes from interactions with the lipid bilayer, it may act indirectly on other nonmechanosensitive channels. Piezo1 involvement in the potassium efflux occurring in LIS conditions is also supported by the finding of a voltage-gated mode, which prevents inactivation at positive membrane potentials with stronger currents at +60 mV compared to -60mV when pressure is exerted on the membrane (**Fig. 6.1A-C**) [160]. However, caution must be taken again in extrapolating these results, carried out in excised patches of Piezo1-overexpressing Neuro 2A cells, to erythrocytes.

Nevertheless, several reports have pointed out specific hypothesis regarding the origin and the molecular identity of NSC channels. Beside the well-described P_{sickle}, VDAC has been proposed as a potential route for cations at the RBC membrane, since when it oligomerizes it assembles as a large pore having an enhanced selectivity for cations [332, 333].

TRPC6 has also been described at least at the protein level by immunoblot [175]. Some pharmacological evidence exists supporting TRPC family involvement in cation movements upon PGE_2 [337].

Moreover, some other conditions lead to the description of permeability owing to the characteristics of Non Selective Cation channels. Among them, P_{cat} has been described in hyperpolarizing conditions after Gárdos activation by A23187 [251], a condition similar to the one I report on Chapter 3.

The contribution of some or all five ion channels even with tiny currents can have a huge impact over long timespans, such as RBC lifespan of 120 days, with cation movements decoupling from Na^+/K^+ pump activity as oxidation affects the pumps and glycolytic enzymes cutting off ATP supply. NSVDC and P_{cat} molecular identity may match that of a known existing channels under different modes of operation.

Cation conductance is critical to RBC physiology as its untimely or overdimensioned change leads to RBC demise via the impact of altered ion distribution on cell volume either by dehydration and loss of rheological

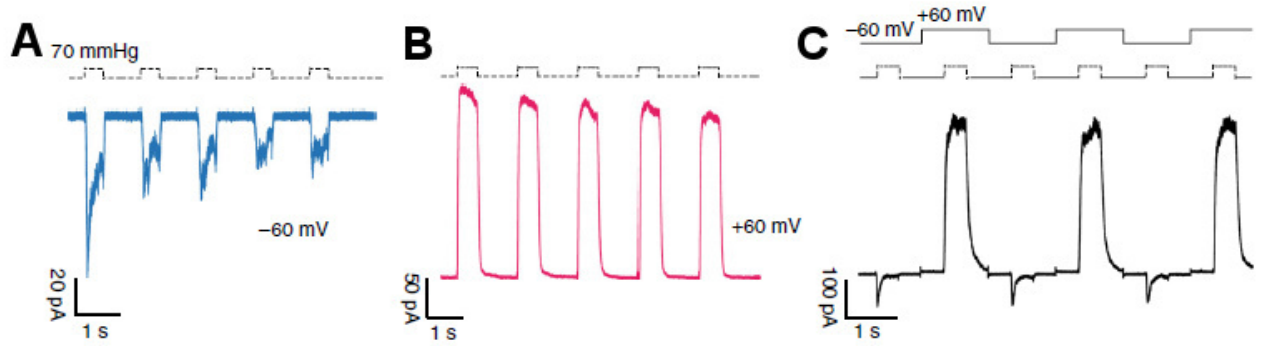

Figure 6.1: Wild-type Piezo1 displays voltage gating.
Inactivation and desensitization of Piezo1 can be reset by outward permeation. Repetitive pressure stimulations desensitize Piezo1 at −60 mV (**A**) but not at +60 mV (**B**). Note the decreased peak current and low peak/steady-state current ratio at −60 mV. (**C**) Alternating pressure pulses at −60 mV and +60 mV abolishes desensitization and prevents Piezo1 from entering a noninactivating state. Adapted from [160].

properties conducing to spleen or small vessel obstruction or by overhydration leading to the critical hemolytic volume and lysis. Red blood cell deformability is critical for optimal rheology and gas exchange functionality during capillary flow, best fulfilled when the volume of each human red blood cell is kept at a fraction of about 0.55–0.60 of the maximal spherical volume allowed by its membrane area, the optimal-volume-ratio range [338]. Ion distribution must be kept constant considering osmotic movements happen extremely fast. Cation leak can be considered, as cation movements through non-inhibitable pathways. Therefore the Na^+/K^+ pump ensures that there is no net movement of cations allowing Cl^- to stay at equilibrium which is essential for RBC gas transport. Therefore, some evidence is provided for NSC channel playing a role as a contributor if not main actor in pump-leak concept, which so elegantly summarizes RBC homeostasis.

Pump-leak homeostasis is disturbed as soon as RBCCs are refrigerated at 4 °C as the Na^+/K^+ pump is inhibited by cold. Cation leak will reverse slowly but steadily the Na^+/K^+ ratio of RBCs. This reversal is well known and largely attributed to a passive leak, which at 37 °C is easily compensated by the Na^+/K^+ pump. Cation imbalance is hence often dismissed as a consequence of Na^+/K^+ pump inhibition. Nevertheless cell volume changes and morphological alterations cannot be entirely accounted for by passive diffusion through the phospholipid bilayer according to the rate of this phenomenon, nor by microvesiculation. Our data reveals important ion channel susceptibility upon storage under experimental conditions. By the second week the emerging NSC activity is apparent as soon as G_{Cl^-} is inhibited and continues to rise over time with a further spurt of activity observed on the last day. Withholding calcium from SAGM solutions, though certainly preferable for the main aim of long-term storage and to prevent clots and worsen microvesiculation seems to cause unforeseen consequences upon reinfusion. Such a heavy calcium starvation may imply a sudden and large cation influx upon transfusion when cells encounter Ca^{2+}-containing plasma at the millimolar range. And indeed, there is evidence that Piezo1 aids in this process via mechano-induced opening during capillary passage [166, 302]. Given the enormous difference in Ca^{2+} concentration, very close to zero for CPD-SAGM-stored RBCs and 1.9 mM in plasma, a Piezo1-mediated increase in calcium permeability should entail strong Gárdos activation resulting in shrinkage and menacing removal from the circulation. Up to 25% of RBCs transfused are known to be removed upon reinfusion and this is accounted for by quality control criteria set by the American Food and Drug Administration (FDA) and European directives.

Oxidation: a link between senescence and the storage lesion Senescence begins with erythrocyte densification. Average pump-leak Ca^{2+} turnover is about 50 µmol $\cdot$ l_{cells}^{-1} $\cdot$ h^{-1} and although pump activity decreases with cell age, V_{max} is 10-15 mmol $\cdot$ l_{cells}^{-1} $\cdot$ h^{-1} ensuring adequate calcium levels for a longer time [34, 251, 339]. Furthermore, huge variation in PMCA activity among a RBC population, up to 50% of coefficient of variation, indicates that there is an erythrocyte subpopulation which ages faster, being unable to cope with calcium leak influx. Calcium entry triggers Gárdos leading to dehydration and an increase in cell density. A modest increase in calcium levels to 80 nM would be enough to induce low-level Gárdos activation [251]. RBC age can be measured via glycated hemoglobin fraction, HbA1c, because protein glycosylation is a nonenzymatic process proportional to glucose concentration and progressing over time [340]. Senescent RBCs with high Na^+ levels are known to circulate and they were shown to be the oldest among erythrocytes measured by HbA1c levels. This Na^+ permeability has been reported to be P_{cat} and it emerges in response to shrinking and, mainly, to raised intracellular calcium concentration [251]. P_{cat} was proven to be permeable to large cations such as NMDG and choline [251]. Nevertheless, another study showed such regain of sodium, and thus, cell water after prolonged exposure to high intracellular calcium levels to be minimal and barely detectable [280]. In any case, calcium is absent in storage conditions, hence P_{cat} is unlikely to be stimulated in such scenario.

Thereby, the observation reported here that choline is able to pass through a Non-Selective conductive pathway cannot be ascribed to a classical, α-helix-containing NSC channel. A true pore-forming β-barreled Non-Selective Cation channel changing its conformation, thus enlarging the pore and allowing larger ions to pass is the most likely explanation for that phenomenon. VDAC is a prime candidate in such scenario as it is known to facilitate the passage of large solutes, especially when forming large oligomers, thus requiring a structural change from a basal state. Lipid bilayer breakdown cannot account for the observation as it would alter proton equilibria, by which membrane potential changes are measured, bringing the membrane potential to zero. On the other hand, protein oxidation by Reactive Oxygen Species (ROS) is not restricted to pumps and is rather a pancellular process affecting lipids, transporters and ion channels. ROS indiscriminately oxidize protein sulfhydryl groups, inhibit membrane-bound regulatory proteins such as kinases and peroxidize membrane phospholipids [341]. Despite, Gárdos, for instance, has been found to become oxidized in some cell types but not others. Some proteins and, therefore, ion channels may be more resistant to ROS interaction, perhaps by displaying less labile groups, and their function persist under substantial oxidative stress. Therefore, oxidation may be essential to the understanding of the storage lesion as it is directly connected to the metabolic state of red cells.

Transfusion and the storage lesion. 4 million blood donations are performed every year worldwide according to the World Health Organization [342]. About 33% of all unit discards are due to passing the expiry date, set by national laws, mostly six weeks after collection [343]. Expiry dates have been put in place to guarantee the safety and quality of blood products, as they degrade over time upon storage. Hence, long-term effective preservation of erythrocytes intended for transfusion remains a critical problem in medicine [344].

Research into the storage lesion, the set of alterations appearing over the course of RBC refrigerated storage in additive solutions, such as SAGM, stems from the concern that cells stored for a long period may not properly perform their functions once back in the circulation, diminishing transfusion efficiency.

These alterations cover the whole RBC physiology: alteration of cation distribution, loss of key metabolites, microvesiculation, Band 3 crosslinking leading to loss of function [261], high phosphatidylserine exposure,

irreversible morphological changes, poor deformability, carbonyl modification of Band 4.1 [345] and hemolysis [344]. Diminished ATP levels, failing to provide energy, via NADPH, to reduce glutathione disulfide (among other antioxidant defenses) are thought to be primarily responsible in tipping over homeostasis and starting other cellular injures [345]. Hemoglobin can start an oxidation chain reaction if its iron, needed for O_2 binding in the ferrous state, oxidizes to the ferric state, as methemoglobin (Met-Hb) will then form. Met-Hb denatures if not readily converted by enzymes into Hb, forming hemichromes. Hemichromes can react with itself and other proteins forming adducts and releasing heme or free iron, which ultimately acts as a Fenton reagent catalyzing endless ROS-producing reactions [346]. RBCCs stored in anaerobic conditions extend storage by more than 50%, stressing how much oxidation damage hampers RBC preservation. Nevertheless, past the first 24 hours post-transfusion no difference in erythrocyte survival rate was found between aerobic and anaerobic conditions [346]. Moreover, phosphatidylserine exposure did not correlate with RBC survival and ensuring high intracellular ATP concentrations did not prevent RBC clearance upon reinfusion. Therefore, clearance is not entirely dependent on oxidation of glycolytic enzymes providing ATP or membrane lipids. Another mechanism ought to account for such huge (up to a quarter of all cells transfused) RBC removal.

In view of this and the data herein presented, the following hypothesis may explain phenomena related to the storage lesion and subsequent reinfusion into the circulation:

The so-called glass effect is the shape change RBCs undergo when in contact with glass. PVC has also been found to cause this, which along with lack of plasma proteins leads to membrane instability during storage. Morphological changes ensue with substantial microvesiculation causing a reduced surface to volume ratio. DHEP, a plasticizer used to polymerize PVC, strongly limits the effect by leaching from the bag and stabilizing plasma membrane lipids [267]. In spite of this, echinocyte and spheroechinocyte subpopulations arise within the stored RBC population and their relative proportions increase during storage, with respect to general stored RBC population, manifestly by the end of the storage period [325]. These cells show reduced filterability. Low-level Gárdos activation coming from hemolysis within the bag, which could provide 5 mM KCl during the last week of the storage period, might explain reduced cell volume. NSC activity steadily arises during storage, putting strain on the pumps, which will then require more ATP and its levels will begin to fall. Enzyme oxidation and failing adenosine pools will reduce ATP production, speeding up metabolic collapse. Exacerbated ion channel activity upon RBC reinfusion would lead to strong Gárdos activity as calcium influx via NSC channel would be massive and sodium entry would not be enough to compensate for K^+ loss and dehydration. Elevated calcium levels are known to diminish erythrocyte plasticity [347] which along with severe dehydration imposed by maximal Gárdos activation would result in retention in the splenic slits and removal by macrophages or, worse, to intravascular hemolysis or thrombotic events in splenectomized patients.

Extracellular potassium has been reported to increase during storage, reaching dramatic levels by the third week of storage: 20 mM [348]. However, this does not fit our observations, as such a high extracellular potassium concentration would reduce the driving force for Gárdos so reduced activation would be expected. Rather, strong activations are seen during the sixth week of storage in our experimental conditions. Moreover, extreme changes occur during the sixth week of storage, such as morphological changes producing irreversible echinocytes and vastly reduced filterability, were seen as potentially harmful, with procoagulating, poorly deformable cells risking thrombosis or premature hemolysis. Therefore, extensive research was focused on the question whether “fresher” cells, that is, those stored for less than three weeks, were more desirable for transfusion than older cells and whether there was any causative link between storage time and adverse transfusion

effects. Patients with a chronic illness requiring frequent transfusions are in principle at a higher risk for iron overload and spleen complications due to long-termed stored RBCs being cleared by the reticuloendothelial system. Many studies attempting to find a connection between storage duration and adverse transfusion reactions were inconclusive, but harmfulness of old stored cells could not be proven and clinical practice remains not to prioritize fresh RBCCs [318–321]. However, the effects of transfusing RBCCs stored for six weeks are poorly studied and none of the clinical trials covered by a large meta-review on transfusion outcomes looked into adverse effects from units stored longer than 35 days [322]. RBC oxygen delivery takes between 8 and 24 hours to reach full delivery capacity when stored in standard conditions (i.e. refrigerated SAGM or AS3) [346]. It seems puzzling then, that RBCs markedly altered from their typical metabolic and membrane properties would perform in the same manner to cells just recently stored, besides the fact that the most damaged cells (about 25% on the sixth week of storage) are immediately removed from circulation on transfusion.

Rejuvenation Several laboratories are currently exploring the viability of different rejuvenating solutions to be used before reinfusion to remedy at least some storage lesions displayed by RBCs especially after 21 days of storage. In fact, rejuvenating solutions containing inosine, sodium pyruvate and adenine are approved by the FDA for use between three days after withdrawal and three days after expiration [349]. Despite low temperatures slowing down cell metabolism, production of lactate by RBCs continues resulting in a decrease of medium pH during storage, further reducing glycolytic activity hence decreasing downstream ATP and 2,3-DPG turnover. Use of a rejuvenation solution increases 2,3-DPG and ATP cytosolic levels, up to 120 days of storage, with diminished amelioration over time [349]. Rejuvenating solutions have also been used on SAGM-stored cells with satisfactory replenishment of key metabolites [350]. However, it is performed at 37 °C during 3-4 hours and a metabolic reversal is seen within 24 h, hence the regulatory need for mandating reinfusing of rejuvenated RBCs within 72h. The rejuvenating solution currently used focus mainly (if not solely) on restoring cell energy, with the added benefit that during the rejuvenating procedure washing steps remove toxic by-products, microvesicules and, importantly, surplus extracellular potassium which may induce hyperkalemia if high enough, which could be potentially fatal. Shape maintenance requires protein interactions, but current rejuvenating solutions do not contain albumin or human serum. I incubated SAGM-stored RBCs with RPMI supplemented with serum akin to rejuvenation procedures: 3-4 hours at 37 °C followed by washing steps and measurement of membrane potential changes upon Gárdos activation by A23187 (See details in Chapter 5 on page 165). In this manner, in addition to metabolic recovery (not measured), erythrocytes can establish interaction between the plasma membrane and plasma proteins.

Marked Gárdos-induced hyperpolarizations were observed when RBCs where placed in experimental medium, containing low potassium and plenty of calcium, with restoration of channel activity compared to the start of the storage period. Even though high extracellular potassium may be present in the bag, it is certainly removed along with the supernatant and RBCs are subsequently resuspended, so that it cannot have a direct effect on our observations. Arguably, supernatant removal or washing of stored RBCs is beneficial for transfusion, to minimize adverse event risks, as mentioned above. On Day 41 of storage, NSC channel activity is pronounced despite serum-supplemented RPMI rejuvenation suggesting ion channel activity is at this point independent of metabolic and morphological restoration. The choice of serum-supplemented RPMI aims to mimic the environment of RBCs in circulation, that of plasma, which contains abundant amino acids, albeit unneeded by erythrocytes. It is obvious that such a rich medium is not cost-effective for large-scale rejuvenation in the clinic,

Components (mM)	SAGM$^{\alpha}$	PAGGSM$^{\beta}$	AS-1$^{\gamma}$	AS-3$^{\gamma}$	AS-5$^{\gamma}$	AS-7$^{\delta}$	E-Sol 5$^{\delta}$	PAG3M$^{\delta}$	Rejuvesol$^{\varphi}$
NaCl	150	72	154	70.1	150	—	—	—	—
Adenine	1.25	1.4	2	2.2	2.2	2	2	1.4	5
Glucose	45	47	111	55.5	45	80	111	47	—
Mannitol	30	55	41	—	45.4	55	41	55	—
Guanosine	—	1.4	—	—	—	—	—	1.4	—
Na-Gluconate	—	—	—	—	—	—	—	40	—
Citrate	—	—	—	12	—	—	25	—	—
Trisodium citrate	—	—	—	20	—	—	—	—	—
NaH_2PO_4	—	8	—	23	—	—	—	8	29
Na_2HPO_4	—	16	—	—	—	12	20	8	70.4
$NaHCO_3$	—	—	—	—	—	26	—	—	—
Na-Pyruvate	—	—	—	—	—	—	—	—	100
Inosine	—	—	—	—	—	—	—	—	100
Osmolality (mOsm/kg)	376	287	462	418	393	228	301	278	498
pH	5.7	6.0	5.5	5.8	5.5	8.5	8.4	8.2	6.7-7.4

Table 6.1: Additive solutions used for RBC storage.
Table indicating composition of a range of additive solutions currently used for storage of RBCs intended for transfusion or in research. Rejuvesol is used for RBC rejuvenation prior to transfusion. Adapted from [349, 352]
α Used in the European Union. β Licensed in Germany. γ Licensed by the FDA. δ Experimental solution. φ Licensed by the FDA for rejuvenation prior transfusion, not for storage.

hence why currently used solutions minimize the number of components to acceptable improvement outcomes.

Additive solutions Other storage or additive solutions (AS) have been tested in order to reduce storage lesions during storage focusing on one or more factors (Table 6.1). PAGGSM (Phosphate Adenosine Guanosine Glucose Saline Mannitol) differs from SAGM by including sodium phosphate and guanosine, with varied proportions of other components to achieve a lower, more isotonic medium. After 42 days of storage PAGGSM there was a mild reduction in hemolysis and osmotic fragility compared to SAGM, but all other parameters were similar [351]. Storage of RBC in other solutions such as PAG3M (also known as PAGGGM), E-Sol 5 and AS-7 has also been assessed [352]. All these have in common being hypo- or isotonic, chloride-free and containing phosphate buffers. The idea behind removing chloride is to raise the intracellular pH due to the chloride shift effect, due to replacement by OH^- as some chloride goes out of cells. Hypotonicity is thought, on the other hand, to prevent much vesiculation. ATP and 2,3-DPG levels stay at much higher values compared to SAGM or PAGGSM, especially after Day 35, when they plummet in SAGM. Hemolysis is similar until Day 35, where is much higher in SAGM compared to new AS. Morphology is better overall than in SAGM, though $\sim$35% of RBCS are echinocytes by Day 56 compared to $\sim$44% so hypotonicity and greater cytosolic pH do not prevent echinocytosis [352]. PAG3M was found to maintain metabolic activity, as measured by lactate production and impact on ATP and 2,3-DPG on another study [353]. Although a sharp decline in 2,3-DPG is found on Day 21, its levels remain higher than in SAGM.

Metabolomic studies corroborate these findings and identify PAG3M as the best overall solution out of SAGM, PAGGSM, E-Sol 5 and AS-7, with excellent preservation of glycolytic metabolites and GSH/GSSG ratio owing to guanosine providing supplementary nucleoside for ATP production. Although oxidative defenses are less affected with these hypotonic solutions, free fatty acids and oxidized forms mean lipid peroxidation still takes place [354]. Guanosine better preserves ATP levels due to the lack of adenosine utilization by RBCs after 18 days of storage [355], which may partially explain the good performance of guanosine-containing AS, such as PAG3M. There are many strategies available to target ROS with the aim of decreasing oxidation storage damage. Supplementation with a vitamin E analogue, a lipophilic antioxidant, was shown to prevent lipid peroxidation and GSH depletion compared to SAGM at the micromolar range, positively affecting morphology up to Day 42 of storage [356]. Peroxiredoxin 2 is an enzyme with catalase activity and a marker of oxidative stress in its oxidized form. This form increases in SAGM-stored RBCs starting from Day 21. Storage in chloride-free, buffered solution prevents this rise for about six weeks, but rejuvenation does not [357]. Use of antioxidant dihydrolipid acid (DHLA) precludes oxidation of this enzyme.

Although they are empirically proven to improve metabolic conditions, these solutions lack potassium, calcium, chloride and contain very high glucose concentrations and are, thus, far from being a physiological solution. It is concerning whether they induce extensive glycation and, given how essential cation balance is in RBC physiology, whether their absence affects ion channel activity. In particular, chloride removal is worrisome as the chloride conductance will be altered, which in turn will affect the resting membrane potential. NSC channel activity, which would otherwise be silent as seen in our study, is favored by heavily altered chloride conductance and voltage-dependent channels (such as NSVDC) exist in the RBC plasma membrane and will activate at positive membrane potentials [358]. Nevertheless, only hemolysis would be able to provide ions for ion channel activity in such circumstances and it is decreased compared to SAGM [352]. Enhanced ion channel activity, presumed to be catastrophic for cellular homeostasis when SAGM-stored cells are reinfused, would be expected to be worse with these hypotonic, chloride-free solutions. Contrarily, better survivability 24 hours post-transfusion is observed. There is a gap between empirical knowledge and the physiological mechanisms in play. Do these improvements stem from reduced oxidation? What triggers enhanced NSC channel activity in paraphysiological (SAGM) and nonphysiological (hypotonic, chloride-free solutions) media? Do RBCs quickly restore their normal ion homeostasis once in circulation or is cell volume impacted? What are the risks associated with protein glycation? Many questions remain unanswered and although a problem-solving approach to RBC storage has provided many advances in transfusion practice, a call for caution is understandably often put forth. A combination of a new additive solution with rejuvenation in a physiological solution seems the most sensible strategy to combine the benefits of long-term storage while minimizing loss of transfusion efficiency and adverse events. Unfortunately, it would be very costly. SAGM is still in use due to being inexpensive and the interoperability it provides to blood banks across the European Union. Its replacement would need an entire overhaul of the complex logistics involved in blood banking, so extensive research on additive solutions will continue until the best, most cost-effective candidate makes it to European blood banks.

Metabolic decay is notably important during the first three weeks of storage whereas oxidation seems to play a central role especially during the last three weeks, although a positive-feedback occurs between the two. Rejuvenation fails to address raising ion channel activity and antioxidant-supplemented additive solutions improve storage. The impact of ion channel activity in cellular damage during storage was until now ignored and though their activation may be largely suppressed in the bag due to lack of potassium and calcium, given

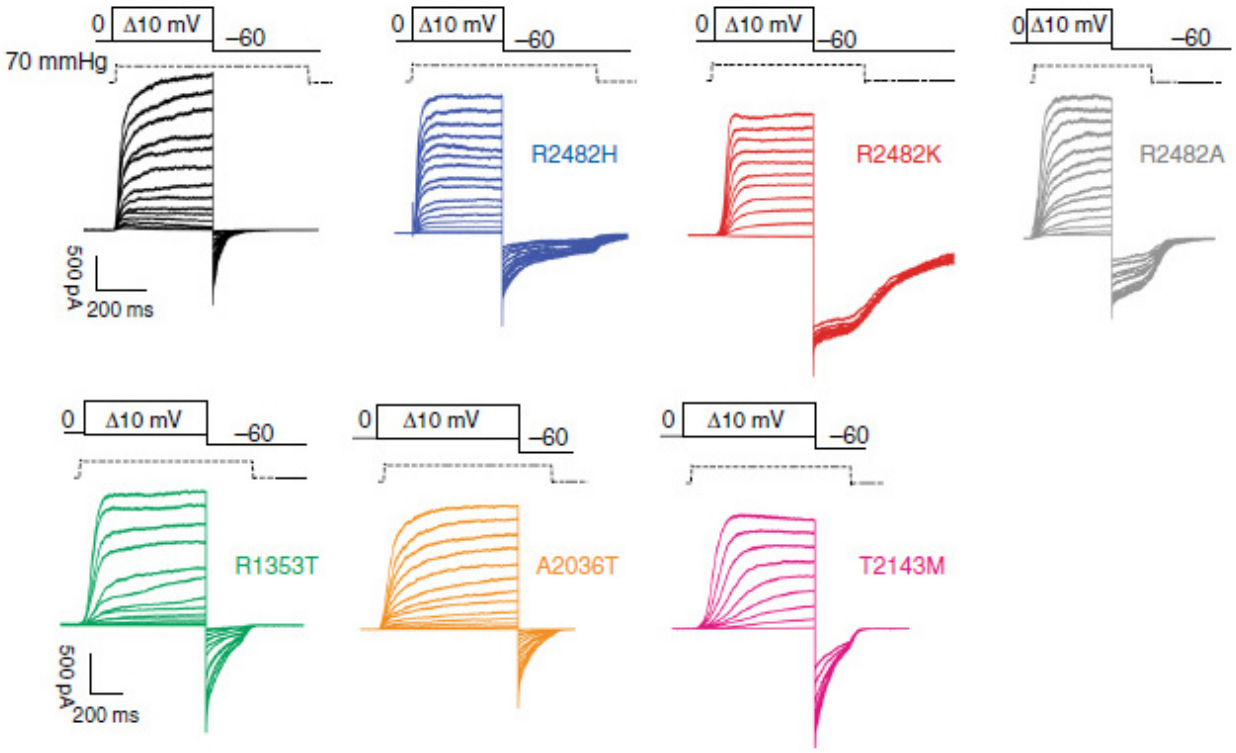

Figure 6.2: Mutant Piezo1 display altered voltage gating.
Current responses to a pressure stimulation of 70 mmHg during 300 ms voltage steps ranging from 0 to 150 mV, followed by a repolarization step to −60 mV to obtain tail currents for wild-type Piezo1 (black), R2482H (blue), R2482K (red), R1353T (green), A2036T (orange), T2143 (magenta), and R2482A (gray) mutants. The R2482K mutant shows decreased voltage modulation. Adapted from [160].

that Gárdos activation provides a driving force for NSC channels, it is not impossible as potassium is measured in the extracellular solution so enough calcium from lysed cells could lead to noticeable Gárdos activity. In turn, hyperpolarizing conditions enable NSC channel activation providing more calcium and therefore starting a feedback loop. If this does not seem to happen is because the chloride conductance remains dominant and is able to counteract increased cation leak. However, as soon as RBCs are transfused, ion channel activated may prove fatal for the most fragile subpopulation compounded by morphological and metabolic degradation. How does ion channel activity increase despite substantial oxidation? Possible explanations include: i) low copy numbers of these channels decrease the probability of redox reactions, ii) an innate resistance to oxidation due to amino acid composition and the most labile residues being buried in the lipid bilayer or iii) the most labile residues to oxidation promote the open state configuration of the channel or calcium-binding by Gárdos in their oxidized or adduct form, leading to enhanced open probabilities. A study did find positive modulation of NSC channel activity by oxidation. Exposure of RBCs to oxidizing agent *t*-butylhydroxyperoxide enhances the activity of NSC channel, which is additionally labile to changes in chloride concentration [358]. Future studies involving oxidants and antioxidants, focusing on ion channel activity in the context of RBCC storage, are still required to further address these hypotheses, although the unknown molecular identity of NSC channels will undoubtedly hinder the characterization of the underlying mechanisms.

Membrane potential estimation advantages for diagnosis I have described experimental approaches that allow to gather functional information about ion channel activity via membrane potential estimation in real

time. Patch-clamp remains the golden standard to characterize wild-type or mutant ion channels. **Figure 6.2** shows tail currents at negative membrane potentials of mutant Piezo1, clearly showing impaired inactivation. A recent study demonstrated that dietary fatty acids act on Piezo1 by modifying lipid properties thereby further proving that the force-from-lipids principle holds true for Piezo1 [304]. It was shown that after margaric acid incorporation in membranes of N2A or HMVEC cells more pressure was needed to be applied on the membrane for channel activation. Margaric acid rigidifies lipid bilayer by creating a more ordered lipid arrangement. Interestingly, use of eicosapentaenoic acid abolishes slow inactivation observed in several Piezo1-HX mutations, including R2456H [304]. Moreover, eicosapentaenoic acid together with margaric acid decrease the inactivation time constant and Piezo1 currents of both wild-type and R2456H RBCs. Patch-clamp studies in mature RBCs are scarce, especially in the context of mutant channel characterization. Patching small cells with such plasticity as RBCs is challenging and laborious as noise must be carefully minimized and gigaohms seals obtained before any pharmacological stimulation or inhibition may be attempted. An advantage of patch-clamp is that it provides single-cell analysis, however RBC populations can display wide variation, especially when composed of pathological cells. Automatic patch-clamp enables high-throughput analysis combining single-cell analysis with big sampling, so that the mean response of the whole population may be estimated. RBCs from a Piezo1-HX patient with R2110W mutation have been successfully studied with this approach showing higher currents than wild-type when the voltage was clamped at +80 mV and greater sensitivity to Yoda1 [359]. Nonetheless both manual and automatic patch-clamp impose some constraints such as sustained pressure on the membrane. Automatic patch-clamp may also apply shear stress and requires the use of nonphysiological solutions. Tracer experiments may be more precise, but need strict protocols in place due to involving radioactivity. Membrane potential estimation, while relying on pharmacology, allows the study of erythrocyte populations without disturbing the plasma membrane during recording and provides substantial information from a small fraction of the cost of setting-up manual patch-clamp (let alone automated patch-clamp). Only fast-responding electrodes, pH meter, simple saline solutions, appropriate drugs and a regular computer are needed. Such a minimal set-up is feasible in hospital laboratories, with several experiments demanding only a few milliliters of blood, so that ion channel activity analyses can be performed with freshly-drawn RBCs from the patients, removing any deleterious effect of shipping blood samples. Screenings of proband's relatives could provide a more detailed picture of ion channel involvement in anemia and identify the need for extra genetic tests to be carried out. This is particularly relevant for *de novo* mutations, which are often found in addition to an inherited mutation from the proband's parents.

Until very recently, the effects of calcium in RBC physiology have been underestimated, as the cation is a secondary messenger not only triggering Gárdos activation, but a score of changes in RBC homeostasis (**Fig. 6.3**). It causes relaxation of spectrin fibers, interacting directly to 4.2 and indirectly to adducin, ankyrin and many other proteins in these complexes via calpain [360]. Furthermore, most patients afflicted with hereditary anemia, including HX patients, have abnormal RBC calcium levels [283]. An elevated intracellular calcium concentration is evidently highly deleterious to erythrocytes by itself, while also masking Na^+/K^+ reversal in the context of NSC channel openings which in turn alters cell volume.

In conclusion, membrane potential recordings via CCCP method have proven that it can be helpful for fast and inexpensive determination of ion channel defects in RBCs. Next Generation Sequencing and, especially whole exome sequencing, remains expensive to be performed in a systematic manner and requires substantial

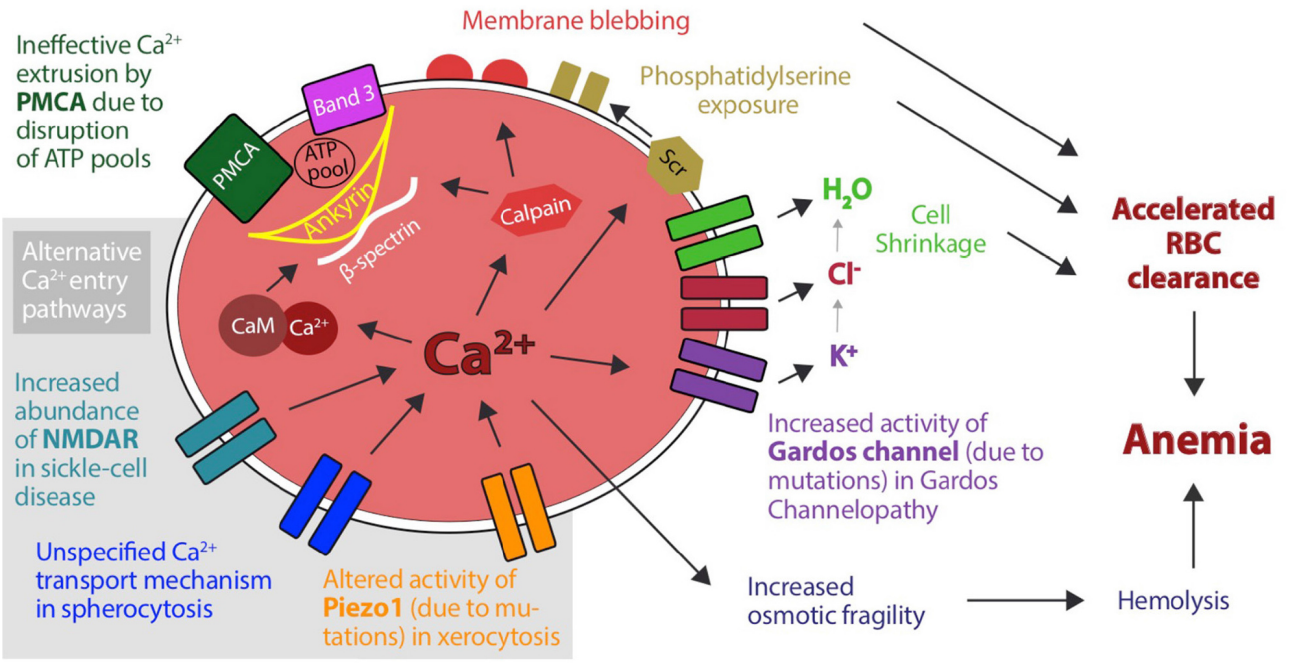

Figure 6.3: Schematic showing effects of elevated cytosolic calcium levels in human RBCs.
Proposed mechanisms leading to increased intracellular Ca^{2+} levels in diseased RBCs and accordingly to accelerated clearance of cells from the blood stream. Alternative or cumulating Ca^{2+} entry pathways are highlighted with gray background: increased abundance of NMDA-receptors (NMDAR), e.g., in sickle cell disease, altered activity of Piezo1, e.g., in hereditary xerocytosis, increased activity of Gárdos Channel, e.g., in Gárdos Channelopathy, or unspecified Ca^{2+} transport mechanisms. Additionally, ineffective extrusion of Ca^{2+} due to disruption of ATP pools fueling the plasma membrane Ca^{2+} ATPase (PMCA) can contribute. Several downstream processes follow Ca^{2+} overload in RBCs, e.g.: activation of calmodulin by formation of the Ca^{2+}-calmodulin complex (Ca-CaM) and activation of calpain, thereby loosening the cytoskeletal structure; activation of the scramblase (Scr) leading to exposure of phosphatidylserine on the outer leaflet of the membrane; activation of the Gárdos channel followed by the efflux of K^+, Cl^- and H_2O and consecutive cell shrinkage. Adapted from [283].

bioinformatic expertise and time-consuming analysis. At a time when personalized medicine is becoming a critical issue for European health services, the miniaturization of such technique could represent a major asset for diagnosis. Thus, a complete mapping ion channel mutations, chiefly Gárdos and Piezo1, is of high importance.

Importance of cation balance

RBCs have no strong cation conductance in resting conditions and the anion conductance is limited to the action of an electroneutral transporter, Band3, while anion channels operate at minimal activity at rest. The advent of patch-clamp revealed the complexity underlying channels in RBCs, with a maxi-anion channel identified and three main cation channels found in healthy cells: NSVDC, Gárdos and Piezo1. As I point the reader to activators, inhibitors or holding potentials the question arises: what is the physiological role of ion channels *in vivo*? After more than sixty years of research on ion channels, this question remains unsettled. Nonetheless, a hypothesis which must be considered is that ion channels in mature RBCs are a relic of erythropoiesis required for proliferation and differentiation and kept due to lack of specific targeting for destruction during or after enucleation. Most proteins are degraded during the transition to reticulocyte stage and, in fact, the system responsible for targeted protein degradation, ubiquitin-proteasome system, was discovered in reticulocytes due

to its frenetic activity [361]. However, little is known about the mechanisms which spare some proteins while marking the rest for removal. Protein remodeling is a complex matter far from elucidated in red cell physiology. We do know that the expression levels of known ion channels, such as Gárdos, and Piezo1 and all VDAC isoforms except VDAC3, which predominates in mature RBCs, decrease during erythroid differentiation [301]. An observation compatible with ion activity being essential for rapid proliferation and, in the case of Piezo1, for potentially aiding in spatial organization of progenitors. Conversely, morpholino knockout of Piezo1 in zebrafish has no impact on erythroid differentiation although it decreases the number of circulating erythrocytes, as a consequence of cell swelling and lysis [362]. Despite, not only reduced Piezo1 expression delays differentiation in human erythroid progenitors, but its activation delays differentiation of human erythroid cells [Toye, *pers. comm.*][363]. Hence, Piezo1 must play an essential role in erythropoiesis, likely in the context of cell-cell interactions in erythroblastic islands and its fine regulation shows it needs to be active only at very precise times, perhaps triggering then differentiation, with excessive activation leading to cell cycle arrest.

Yet, ion channels take part in many processes. Their involvement is known in a variety of disorders such as sickle cell disease, malaria and, recently, Gárdos-associated hereditary stomatocytosis (Gárdos-HSt) and Piezo1-associated xerocytosis (Piezo1-HX). All of them have in common an increase in ion channel activity leading to a worsening of the disease (SCD, malaria) or to the main phenotype (Gárdos-HSt, Piezo1-HX), to the point that channel inhibition has been proposed as a treatment strategy. Why have these normally dormant proteins been kept during evolution in mature cells if their malfunction is deleterious? In other words, why are they not lost during maturation? While it might be that they are not deleterious enough, given the wide array of functions they perform it may rather mean they are required for red cell homeostasis. This points out the potential role of channels in circulating physiology.

Gárdos and Piezo1 have been shown to support erythrocyte passage in small vessels. Piezo1 is a mechanosensor and opens when RBCs traverse a constriction in a vessel, as cations move down their gradients, calcium activates the Gárdos channel resulting in shrinkage and facilitating cell passage. Calcium entry is inhibited by MS channel blocker GsMTx4. Mouse RBCs loaded with calcium-sensitive fluorescent dye Fluo4 gained calcium after going into a vessel of smaller caliber compared to one of constant caliber [302]. Furthermore, RBC filterability is impaired by use of either GsMTx4 or Gárdos inhibitor Tram34. Piezo1 opening *in vivo* are likely very brief and given the inactivation kinetics of the channel, Piezo1 may only be open in a range of milliseconds. Hence, it is expected Gárdos activation will be just above its calcium activation threshold. Volume changes are slow in RBCs so it is difficult to picture erythrocytes dehydrating fast and regaining the volume immediately after thousands of times per minute. It must also be noted that Gárdos-induced dehydration relies on the simultaneous enhancement of a strong anion channel and any rehydration and restoration of the resting state must rely in the slow pumping process of the Na^+/K^+ ATPase. In fact, the Band 3-independent component of net anion efflux increases as much as the magnitude of Gárdos-evoked hyperpolarizations. It is thought this nonBand 3 chloride conductance activates at membrane potentials more negative than -40 mV [364, 365]. Therefore, the deformability improvement observed may have to do with another factor, such as the relationship between calcium and the cytoskeleton. Adducin and protein 4.1 interact with each other and calmodulin [302]. Adducin blocks elongation and depolymerization at the fast growing barbed ends and in the presence of calcium it is downregulated [366]. Both Gárdos and a Non Selective Cation Channel are said to be activated by prostaglandin E_2 [367, 368]. Gárdos- induced shrinking in the presence of prostaglandin E_2, which is released

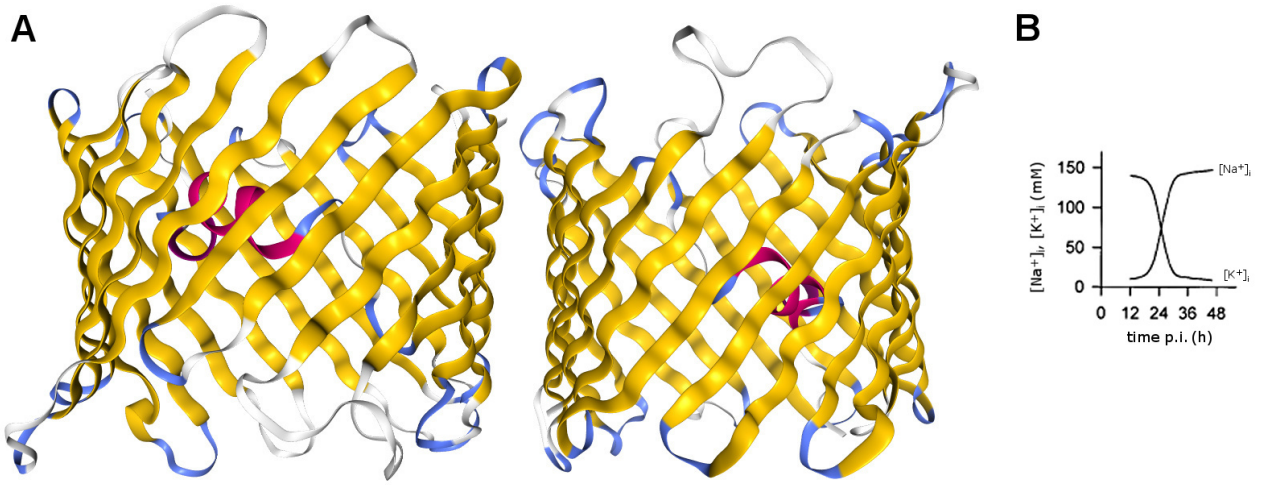

Figure 6.4: VDAC dimeric structure and Na^+/K^+ reversal in malaria
(**A**) Human VDAC1 oligomerized as a dimer. (**B**) Mathematical modeling of *Plasmodium*-induced changes in cytosolic Na^+ and K^+ concentrations. 'time p.i. (h)' : time post-invasion (hours). A.- Structure from the Protein Data Bank: 6g6u [369]. B.- Adapted from [184].

by platelets and leads to reduced filterability, suggests RBCs aid in the formation of blood clots [367]. A NSC may provide for higher calcium levels so that Gárdos reaches stronger activations. However, the sensitivity to prostaglandin E_2 was seen in a small subpopulation of RBCs.

Among ion channels, VDAC, as part of the PBR complex along TSPO and ANT, is an excellent candidate to explain ground permeabilities and inducible-increases in both anionic and cationic conductances (**Fig. 6.4**). Although its gating mechanisms are unknown and it is closed at the resting state, its maxi-anion channel capabilities would account for the rate-limiting trailing chloride conductance seen upon Gárdos activation, which is ultimately responsible for severe dehydration. At high voltages it displays low conductance levels of monovalent and divalent cations, thus operating as Non Selective Cation channel. Moreover, VDAC may oligomerize up to a hexamer arrangement which, along with complex regulation by ligands (such as reactive oxygen species), phosphorylation (such as GSK3, PKA and PKC) and interactions with other proteins forming the PBR complex and the cytoskeleton provides with the flexibility in ion channel activity and conductance operational modes required of ion flux phenomena observed in RBCs [370].

Ion channel activity increases during aging as gauged by the reduced K^+ and volume loss linked to Gárdos and anion channel activation as well as gain of sodium due to the opening of a Non Selective Cation Channel, be it VDAC, Piezo1, NSVDC or a yet unidentified channel. Channel activation may likely be due to a metabolic collapse of the RBC, caused by the oxidation of glycolytic enzymes and a failure to provide the Na^+/K^+ and the Ca^{2+} pump with ATP, magnifying the cation leak. However, Gárdos activation does occur and the rate at which Na^+ enters the cell, considering the large K^+ efflux of Gárdos openings must be due to Non Selective Cation channel involvement. Therefore, these channels may act as indirect sensors of protein oxidation and loss of protein function and on the breakdown of the pump-leak balance they increase their activity, further worsening the homeostasis of the cell and leading to RBCs being more easily retained at the spleen and recognized by macrophages, thus leading to timely removal and preventing underperforming RBCs to stay in circulation.

Given the wide range of functions NSC channels take part in, ion channels should be considered as actors in erythrocyte physiology. The origin of the true cation leak of RBCs has not been established. A case can

be made for NSC channels participating in the pump-leak, as their different conductance modes and complex kinetics leading to stochastic openings at resting conditions may provide a stable, minimal leak, which is required for proper operation of erythrocytes. In this sense, their role in pump-leak maintenance is their most important function. In the words of Poul Bennekou: "However, as part of a pump/leak system these cation conductances are crucial for the long term maintenance of the low red cell membrane potential (−12 mV), which with physiological ion gradients must be based on leak pathways for K^+ and Na^+ having a conductance ratio close to one" [171].

References

[1] E. Bianconi, A. Piovesan, F. Facchin, et al. “An estimation of the number of cells in the human body”. *Annals of human biology* 40.6 (2013), pp. 463–471.

[2] F. B. Jensen. “Red blood cell pH, the Bohr effect, and other oxygenation-linked phenomena in blood O2 and CO2 transport”. *Acta Physiologica Scandinavica* 182.3 (2004), pp. 215–27.

[3] H. Minasyan. “Erythrocyte and blood antibacterial defense”. *European Journal of Microbiology & Immunology* 4.2 (2014), pp. 138–43.

[4] H. Minasyan. “Mechanisms and pathways for the clearance of bacteria from blood circulation in health and disease”. *Pathophysiology* 23.2 (2016), pp. 61–6.

[5] J. Duhm and E. Gerlach. “On the mechanisms of the hypoxia-induced increase of 2,3-diphosphoglycerate in erythrocytes. Studies on rat erythrocytes in vivo and on human erythrocytes in vitro.” *Pflugers Archiv: European Journal of Physiology* 326 (1971), pp. 254–269.

[6] J. C. Ellory and I. Bernhardt, eds. *Red Cell Membrane Transport in Health and Disease*. Springer, 2003, p. 750.

[7] M. H. Jacobs and D. R. Stewart. “The role of carbonic anhydrase in certain ionic exchanges involving the erythrocyte”. *The Journal of General Physiology* 25.4 (1942), pp. 539–552.

[8] J. O. Wieth, O. S. Andersen, J. Brahm, et al. “Chloride-bicarbonate exchange in red blood cells: physiology of transport and chemical modification of binding sites”. *Philosophical Transactions of the Royal Society of London* 299.1097 (1982), pp. 383–399.

[9] S. Lahiri and R. E. Forster II. “CO2/H+ sensing: peripheral and central chemoreception”. *The International Journal of Biochemistry & Cell Biology* 35.10 (2003), pp. 1413–1435.

[10] G. G. Van Beek and S. H. De Bruin. “Identification of the residues involved in the oxygen-linked chloride-ion binding sites in human deoxyhemoglobin and oxyhemoglobin”. *European Journal of Biochemistry* 105.2 (1980), pp. 353–60.

[11] C. Bohr, K. Hasselbalch, and A. Krogh. “Ueber einen in biologischer Beziehung wichtigen Einfluss, den die Kohlensäurespannung des Blutes auf dessen Sauerstoffbindung übt 1”. *Skandinavisches Archiv für Physiologie* 16.2 (1904), pp. 402–412.

[12] J. Christiansen, C. G. Douglas, and J. S. Haldane. “The absorption and dissociation of carbon dioxide by human blood”. *The Journal of Physiology* 48.4 (1914), pp. 244–71.

[13] A. F. Riggs. “The Bohr effect”. *Annual review of physiology* 50 (1988), pp. 181–204.

[14] J. A. Lukin and C. Ho. “The structure–function relationship of hemoglobin in solution at atomic resolution”. *Chemical reviews* 104.3 (2004), pp. 1219–30.

[15] S. Lux. “Red Cell Membrane”. *Nathan and Oski’s Hematology and Oncology of Infancy and Childhood E-Book*. Ed. by S. H. Orkin. Elsevier Health Sciences, 2014. Chap. 15, pp. 455–514.

[16] J. E. Hall. *Guyton and Hall textbook of medical physiology e-Book*. Elsevier Health Sciences, 2015.

[17] T. J. Greenwalt. “The how and why of exocytic vesicles.” *Transfusion* 46 (2006), pp. 143–152.

[18] Y. Lange, H. B. Cutler, and T. L. Steck. “The effect of cholesterol and other intercalated amphipaths on the contour and stability of the isolated red cell membrane”. *The Journal of Biological Chemistry* 255.19 (1980), pp. 9331–7.

[19] M. P. Sheetz. “Integral membrane protein interaction with Triton cytoskeletons of erythrocytes”. *Biochimica et biophysica acta* 557.1 (1979), pp. 122–34.

[20] S. Lux. “Disorders of the Red Cell Membrane”. *Nathan and Oski’s Hematology and Oncology of Infancy and Childhood E-Book*. Ed. by S. H. Orkin. Elsevier Health Sciences, 2014. Chap. 15, pp. 515–579.

[21] M. Bessis. “Red-Cell Shapes - Illustrated Classification and Its Rationale”. *Nouvelle Revue Francaise D Hematologie* 12.6 (1972), pp. 721–746.

[22] E. H. Ponder. *Hemolysis and Related Phenomena*. Grune and Stratton, 1948, p. 104.

[23] W. D. Trotter. "The Slide-Coverslip Disc-Sphere Transformation in Mammalian Erythrocytes". *British Journal of Haematology* 2.1 (1956), pp. 65–74.

[24] N. G. Mehta. "Role of Membrane Integral Proteins in the Modulation of Red-Cell Shape by Albumin, Dinitrophenol and the Glass Effect". *Biochimica Et Biophysica Acta* 762.1 (1983), pp. 9–18.

[25] L. E. Eriksson. "On the shape of human red blood cells interacting with flat artificial surfaces–the 'glass effect'". *Biochimica et biophysica acta* 1036.3 (1990), pp. 193–201.

[26] J. S. Beck. "Relations between Membrane Monolayers in Some Red-Cell Shape Transformations". *Journal of Theoretical Biology* 75.4 (1978), pp. 487–501.

[27] J. S. Beck. "Echinocyte Formation - Test Case for Mechanisms of Cell-Shape Changes". *Journal of Theoretical Biology* 71.4 (1978), pp. 515–524.

[28] J. Ferrell J. E., K. J. Lee, and W. H. Huestis. "Membrane bilayer balance and erythrocyte shape: a quantitative assessment". *Biochemistry* 24.12 (1985), pp. 2849–57.

[29] J. Ford. "Red blood cell morphology". *International Journal of Laboratory Hematology* 35.3 (2013), pp. 351–357.

[30] G. Deplaine, I. Safeukui, F. Jeddi, et al. "The sensing of poorly deformable red blood cells by the human spleen can be mimicked in vitro." *Blood* 117 (2011), e88–e95.

[31] J. E. Harris. "The influence of the metabolism of human erythrocytes on their potassium content". *Journal of Biological Chemistry* 141.2 (1941), pp. 579–595.

[32] T. S. Danowski. "The transfer of potassium across the human blood cell membrane". *Journal of Biological Chemistry* 139.2 (1941), pp. 693–705.

[33] D. C. Tosteson and J. F. Hoffman. "Regulation of cell volume by active cation transport in high and low potassium sheep red cells". *The Journal of General Physiology* 44 (1960), pp. 169–94.

[34] V. L. Lew, R. Y. Tsien, C. Miner, et al. "Physiological [Ca2+]i level and pump-leak turnover in intact red cells measured using an incorporated Ca chelator". *Nature* 298.5873 (1982), pp. 478–81.

[35] S. A. Desai, P. H. Schlesinger, and D. J. Krogstad. "Physiologic rate of carrier-mediated Ca2+ entry matches active extrusion in human erythrocytes". *The Journal of General Physiology* 98.2 (1991), pp. 349–64.

[36] D. Sterling, B. V. Alvarez, and J. R. Casey. "The extracellular component of a transport metabolon. Extracellular loop 4 of the human AE1 Cl-/HCO3- exchanger binds carbonic anhydrase IV". *The Journal of Biological Chemistry* 277.28 (2002), pp. 25239–46.

[37] P. M. Piermarini, E. Y. Kim, and W. F. Boron. "Evidence against a direct interaction between intracellular carbonic anhydrase II and pure C-terminal domains of SLC4 bicarbonate transporters". *The Journal of Biological Chemistry* 282.2 (2007), pp. 1409–21.

[38] J. W. Vince and R. A. Reithmeier. "Carbonic anhydrase II binds to the carboxyl terminus of human band 3, the erythrocyte C1-/HCO3- exchanger". *The Journal of Biological Chemistry* 273.43 (1998), pp. 28430–7.

[39] J. W. Vince, U. Carlsson, and R. A. Reithmeier. "Localization of the Cl-/HCO3- anion exchanger binding site to the amino-terminal region of carbonic anhydrase II". *Biochemistry* 39.44 (2000), pp. 13344–9.

[40] H. Chu, E. Puchulu-Campanella, J. A. Galan, et al. "Identification of cytoskeletal elements enclosing the ATP pools that fuel human red blood cell membrane cation pumps". *Proceedings of the National Academy of Sciences of the United States of America* 109.31 (2012), pp. 12794–9.

[41] E. Puchulu-Campanella, H. Chu, D. J. Anstee, et al. “Identification of the components of a glycolytic enzyme metabolon on the human red blood cell membrane.” *The Journal of biological chemistry* 288 (2013), pp. 848–858.

[42] S. E. Lux. “Anatomy of the red cell membrane skeleton: unanswered questions”. *Blood* 127.2 (2016), pp. 187–199.

[43] M. Maizels. “Phosphate, base and haemoaelysis in stored blood”. *Quarterly Journal of Experimental Physiology and Cognate Medical Sciences: Translation and Integration* 32.2 (1943), pp. 143–181.

[44] F. Flynn and M. Maizels. “Cation control in human erythrocytes”. *The Journal of Physiology* 110.3-4 (1949), pp. 301–18.

[45] L. J. Mullins, W. O. Fenn, T. R. Noonan, et al. “Permeability of erythrocytes to radioactive potassium”. *American Journal of Physiology* 135.1 (1941), pp. 93–101.

[46] L. Hahn and G. Hevesy. “Rate of penetration of ions into erythrocytes”. *Acta Physiologica Scandinavica* 3.3 (1942), pp. 193–223.

[47] A. Krogh. “The active and passive exchanges of inorganic ions through the surfaces of living cells and through living membranes generally”. *Proceedings of the Royal Society of Medicine* 133 (1946), pp. 140–200.

[48] E. J. Harris and M. Maizels. “Distribution of ions in suspensions of human erythrocytes”. *The Journal of Physiology* 118.1 (1952), pp. 40–53.

[49] E. J. Harris. “Linkage of Na and K transport as a basis for the interpretation of the kinetics of movement of these ions between human erythrocytes and the suspension medium”. *The Biochemical Journal* 54.2 (1953), p. xiv.

[50] R. L. Post and P. C. Jolly. “The linkage of sodium, potassium, and ammonium active transport across the human erythrocyte membrane”. *Biochimica et biophysica acta* 25.1 (1957), pp. 118–28.

[51] J. R. Sachs. “Na+/K+ pump”. *Red Cell Membrane Transport in Health and Disease*. Springer, 2003. Chap. 5, pp. 111–137.

[52] L. Zylinska and M. Soszynski. “Plasma membrane Ca2+-ATPase in excitable and nonexcitable cells”. *Acta Biochimica Polonica* 47.3 (2000), pp. 529–39.

[53] T. Tiffert and V. L. Lew. “Apparent Ca2+ dissociation constant of Ca2+ chelators incorporated non-disruptively into intact human red cells”. *The Journal of Physiology* 505 (Pt 2) (1997), pp. 403–10.

[54] T. Tiffert and V. L. Lew. “Cytoplasmic calcium buffers in intact human red cells”. *The Journal of Physiology* 500 (Pt 1) (1997), pp. 139–54.

[55] G. Dagher and V. L. Lew. “Maximal calcium extrusion capacity and stoichiometry of the human red cell calcium pump”. *The Journal of Physiology* 407 (1988), pp. 569–86.

[56] T. Tiffert, N. Daw, D. Perdomo, et al. “A fast and simple screening test to search for specific inhibitors of the plasma membrane calcium pump”. *Journal of Laboratory and Clinical Medicine* 137.3 (2001), pp. 199–207.

[57] T. Tiffert and V. L. Lew. “Kinetics of inhibition of the plasma membrane calcium pump by vanadate in intact human red cells”. *Cell Calcium* 30.5 (2001), pp. 337–42.

[58] J. S. Wiley and R. A. Cooper. “A furosemide-sensitive cotransport of sodium plus potassium in the human red cell”. *The Journal of Clinical Investigation* 53.3 (1974), pp. 745–55.

[59] J. Duhm. “Furosemide-sensitive K+ (Rb+) transport in human erythrocytes: modes of operation, dependence on extracellular and intracellular Na+, kinetics, pH dependency and the effect of cell volume and N-ethylmaleimide”. *The Journal of Membrane Biology* 98.1 (1987), pp. 15–32.

[60] C. Lytle. “A volume-sensitive protein kinase regulates the Na-K-2Cl cotransporter in duck red blood cells”. *The American Journal of Physiology* 274.4 (1998), pp. C1002–10.

[61] C. Lytle. "Na^+-K^+-2Cl^-cotransport". *Red cell membrane transport in health and disease*. Springer, 2003, pp. 173–195.

[62] P. B. Dunham and J. C. Ellory. "Passive potassium transport in low potassium sheep red cells: dependence upon cell volume and chloride". *The Journal of Physiology* 318 (1981), pp. 511–30.

[63] P. K. Lauf and B. E. Theg. "A chloride dependent K+ flux induced by N-ethylmaleimide in genetically low K+ sheep and goat erythrocytes". *Biochemical and biophysical research communications* 92.4 (1980), pp. 1422–8.

[64] C. M. Gillen, S. Brill, J. A. Payne, et al. "Molecular cloning and functional expression of the K-Cl cotransporter from rabbit, rat, and human. A new member of the cation-chloride cotransporter family". *The Journal of Biological Chemistry* 271.27 (1996), pp. 16237–44.

[65] J. S. Gibson, P. F. Speake, and J. C. Ellory. "Differential oxygen sensitivity of the K+-Cl- cotransporter in normal and sickle human red blood cells". *Journal of Physiology* 511.Pt 1 (1998), pp. 225–34.

[66] A. R. Cossins and J. S. Gibson. "Volume-sensitive transport systems and volume homeostasis in vertebrate red blood cells". *The Journal of Experimental Biology* 200.Pt 2 (1997), pp. 343–52.

[67] M. Apovo, Y. Beuzard, F. Galacteros, et al. "The involvement of the Ca-dependent K channel and of the KCl cotransport in sickle cell dehydration during cyclic deoxygenation". *Biochimica et biophysica acta* 1225.3 (1994), pp. 255–8.

[68] J. S. Gibson, A. Khan, P. F. Speake, et al. "O2 dependence of K+ transport in sickle cells: the effect of different cell populations and the substituted benzaldehyde 12C79". *FASEB journal* 15.3 (2001), pp. 823–32.

[69] J. C. Ellory, A. C. Hall, S. O. Ody, et al. "Selective inhibitors of KCl cotransport in human red cells". *FEBS Letters* 262.2 (1990), pp. 215–218.

[70] O. Olivieri, D. Vitoux, D. Bachir, et al. "K+ efflux in deoxygenated sickle cells in the presence or absence of DIOA, a specific inhibitor of the [K+, Cl-] cotransport system". *British journal of haematology* 77.1 (1991), pp. 117–20.

[71] H. Guizouarn, F. Borgese, B. Pellissier, et al. "Role of protein phosphorylation and dephosphorylation in activation and desensitization of the cAMP-dependent Na+/H+ antiport". *Journal of Biological Chemistry* 268.12 (1993), pp. 8632–9.

[72] H. Guizouarn, F. Borgese, B. Pellissier, et al. "Regulation of Na+/H+ exchange activity by recruitment of new Na+/H+ antiporters: effect of calyculin A". *American Journal Physiology* 268.2 Pt 1 (1995), pp. C434–41.

[73] E. K. Hoffmann and P. B. Dunham. "Membrane mechanisms and intracellular signalling in cell volume regulation". *International Review Cytology* 161 (1995), pp. 173–262.

[74] I. Cicha, Y. Suzuki, N. Tateishi, et al. "Changes of RBC aggregation in oxygenation-deoxygenation: pH dependency and cell morphology". *American Journal of Physiology* 284.6 (2003), pp. 2335–42.

[75] J. L. Kinsella and P. S. Aronson. "Interaction of NH4+ and Li+ with the renal microvillus membrane Na+-H+ exchanger". *American Journal of Physiology-Cell Physiology* 241.5 (1981), pp. C220–C226.

[76] W. Scholz, U. Albus, H. J. Lang, et al. "Hoe 694, a new Na+/H+ exchange inhibitor and its effects in cardiac ischaemia." *British journal of pharmacology* 109 (1993), pp. 562–568.

[77] C. Harris and L. Fliegel. "Amiloride and the Na(+)/H(+) exchanger protein: mechanism and significance of inhibition of the Na(+)/H(+) exchanger (review)." *International journal of molecular medicine* 3 (1999), pp. 315–321.

[78] B. Masereel, L. Pochet, and D. Laeckmann. "An overview of inhibitors of Na(+)/H(+) exchanger." *European Journal of Medicinal Chemistry* 38 (2003), pp. 547–554.

[79] S. N. Orlov, N. C. Adragna, V. A. Adarichev, et al. “Genetic and biochemical determinants of abnormal monovalent ion transport in primary hypertension”. *American Journal of Physiology* 276.3 (1999), pp. C511–36.

[80] O. Giampietro, E. Matteucci, and R. Pedrinelli. “Erythrocyte sodium-hydrogen exchange and microalbuminuria in type I diabetes”. *Diabetes Care* 19.9 (1996), pp. 995–7.

[81] M. Canessa, M. E. Fabry, S. M. Suzuka, et al. “Na+/H+ exchange is increased in sickle cell anemia and young normal red cells”. *The Journal of Membrane Biology* 116.2 (1990), pp. 107–15.

[82] S. F. Pedersen and P. M. Cala. “Comparative biology of the ubiquitous Na+/H+ exchanger, NHE1: lessons from erythrocytes”. *Journal of experimental zoology. Part A, Comparative experimental biology* 301.7 (2004), pp. 569–78.

[83] K. Alleva, O. Chara, and G. Amodeo. “Aquaporins: another piece in the osmotic puzzle.” *FEBS letters* 586 (2012), pp. 2991–2999.

[84] G. M. Preston and P. Agre. “Isolation of the cDNA for erythrocyte integral membrane protein of 28 kilodaltons: member of an ancient channel family”. *Proceedings of the National Academy of Sciences of the United States of America* 88.24 (1991), pp. 11110–11114.

[85] G. M. Preston, T. P. Carroll, W. B. Guggino, et al. “Appearance of water channels in Xenopus oocytes expressing red cell CHIP28 protein”. *Science* 256.5055 (1992), pp. 385–7.

[86] B. Yang, T. Ma, and A. S. Verkman. “Erythrocyte water permeability and renal function in double knockout mice lacking aquaporin-1 and aquaporin-3”. *The Journal of Biological Chemistry* 276.1 (2001), pp. 624–8.

[87] G. M. Preston, B. L. Smith, M. L. Zeidel, et al. “Mutations in aquaporin-1 in phenotypically normal humans without functional CHIP water channels”. *Science* 265.5178 (1994), pp. 1585–7.

[88] G. J. Cooper and W. F. Boron. “Effect of PCMBS on CO2 permeability of Xenopus oocytes expressing aquaporin 1 or its C189S mutant”. *American Journal of Physiology* 275.6 Pt 1 (1998), pp. C1481–6.

[89] V. Endeward, J.-P. Cartron, P. Ripoche, et al. “RhAG protein of the Rhesus complex is a CO2 channel in the human red cell membrane.” *FASEB journal* 22 (2008), pp. 64–73.

[90] E. Neher and B. Sakmann. “Single-channel currents recorded from membrane of denervated frog muscle fibres”. *Nature* 260.5554 (1976), pp. 799–802.

[91] E. Neher, B. Sakmann, and J. H. Steinbach. “The extracellular patch clamp: a method for resolving currents through individual open channels in biological membranes”. *Pflugers Archiv: European Journal of Physiology* 375.2 (1978), pp. 219–28.

[92] B. Sakmann and E. Neher. “Patch clamp techniques for studying ionic channels in excitable membranes”. *Annual review of physiology* 46 (1984), pp. 455–72.

[93] E. Neher and B. Sakmann. “The patch clamp technique”. *Scientific American* 266.3 (1992), pp. 44–51.

[94] O. P. Hamill. “Potassium channel currents in human red blood cells”. *The Journal of Physiology* 319 (1981), pp. 97–98.

[95] G. Gardos. “The function of calcium in the potassium permeability of human erythrocytes.” *Biochimica et biophysica acta* 30.3 (1958), p. 653.

[96] P. A. Knauf, J. R. Riordan, B. Schuhmann, et al. “Calcium-potassium-stimulated net potassium efflux from human erythrocyte ghosts”. *The Journal of Membrane Biology* 25.1-2 (1975), pp. 1–22.

[97] D. R. Yingst and J. F. Hoffman. “Ca-induced K transport in human red blood cell ghosts containing arsenazo III. Transmembrane interactions of Na, K, and Ca and the relationship to the functioning Na-K pump”. *The Journal of General Physiology* 83.1 (1984), pp. 19–45.

[98] J. R. Riordan and H. Passow. “Effects of calcium and lead on potassium permeability of human erythrocyte ghosts”. *Biochimica et Biophysica Acta (BBA)-Biomembranes* 249.2 (1971), pp. 601–605.

[99] R. M. Blum and J. F. Hoffman. “Ca-induced K transport in human red cells: localization of the Ca-sensitive site to the inside of the membrane”. *Biochemical and biophysical research communications* 46.3 (1972), pp. 1146–1152.

[100] U. V. Lassen, L. Pape, B. Vestergaard-Bogind, et al. “Calcium-related hyperpolarization of the Amphiuma red cell membrane following micropuncture”. *The Journal of Membrane Biology* 18.2 (1974), pp. 125–44.

[101] U. V. Lassen, L. Pape, and B. Vestergaard-Bogind. “Effect of calcium on the membrane potential of Amphiuma red cells”. *The Journal of Membrane Biology* 26.1 (1976), pp. 51–70.

[102] J. F. Hoffman and P. C. Laris. “Determination of membrane potentials in human and Amphiuma red blood cells by means of fluorescent probe”. *The Journal of Physiology* 239.3 (1974), pp. 519–52.

[103] A. Heinz and H. Passow. “Role of external potassium in the calcium-induced potassium efflux from human red blood cell ghosts”. *The Journal of Membrane Biology* 57.2 (1980), pp. 119–31.

[104] S. Lepke, M. Shields, and H. Passow. “Irreversible inhibition of Ca2+ activated K+ channels in the red blood cell membrane by Ca2+.” *Biological Chemistry Hoppe-Seyler* 368.10 (1987), pp. 1262–1262.

[105] E. Reichstein and A. Rothstein. “Effects of quinine on Ca++-induced K+ efflux from human red blood cells”. *The Journal of Membrane Biology* 59.1 (1981), pp. 57–63.

[106] O. P. Hamill. “Potassium and Chloride Channels in Red Blood Cells”. *Single-Channel Recording*. Ed. by B. Sakmann and E. Neher. Boston, MA: Springer US, 1983, pp. 451–471.

[107] B. Vestergaard-Bogind and P. Bennekou. “Calcium-induced oscillations in K+ conductance and membrane potential of human erythrocytes mediated by the ionophore A23187”. *Biochimica et Biophysica Acta* 688.1 (1982), pp. 37–44.

[108] B. Vestergaard-Bogind, P. Stampe, and P. Christophersen. “Single-file diffusion through the Ca2+-activated K+ channel of human red cells”. *The Journal of Membrane Biology* 88.1 (1985), pp. 67–75.

[109] R. Grygorczyk and W. Schwarz. “Properties of the CA2+-activated K+ conductance of human red cells as revealed by the patch-clamp technique”. *Cell Calcium* 4.5-6 (1983), pp. 499–510.

[110] P. G. Wood and H. Mueller. “Modification of the cation selectivity filter and the calcium receptor of the Ca-stimulated K channel in resealed ghosts of human red blood cells by low levels of incorporated trypsin”. *European Journal of Biochemistry* 141.1 (1984), pp. 91–95.

[111] R. Grygorczyk. “Temperature dependence of Ca2+-activated K+ currents in the membrane of human erythrocytes”. *Biochimica et Biophysica Acta* 902.2 (1987), pp. 159–68.

[112] P. G. Wood. “The spontaneous activation of a potassium channel during the preparation of resealed human erythrocyte ghosts”. *Biochimica et Biophysica Acta* 774.1 (1984), pp. 103–109.

[113] L. R. Berkowitz and E. P. Orringer. “An analysis of the mechanism by which cetiedil inhibits the Gardos phenomenon”. *American Journal of Hematology* 17.3 (1984), pp. 217–23.

[114] J. Alvarez, M. Montero, and J. Garcia-Sancho. “High affinity inhibition of Ca(2+)-dependent K+ channels by cytochrome P-450 inhibitors”. *The Journal of Biological Chemistry* 267.17 (1992), pp. 11789–93.

[115] N. A. Castle and P. N. Strong. “Identification of two toxins from scorpion (Leiurus quinquestriatus) venom which block distinct classes of calcium-activated potassium channel”. *FEBS Letters* 209.1 (1986), pp. 117–21.

[116] D. Wolff, X. Cecchi, A. Spalvins, et al. “Charybdotoxin blocks with high affinity the Ca-activated K+ channel of Hb A and Hb S red cells: individual differences in the number of channels”. *The Journal of Membrane Biology* 106.3 (1988), pp. 243–52.

[117] H. Wulff, M. J. Miller, W. Hansel, et al. “Design of a potent and selective inhibitor of the intermediate-conductance Ca2+-activated K+ channel, IKCa1: A potential immunosuppressant”. *Proceedings of the National Academy of Sciences of the United States of America* 97.14 (2000), pp. 8151–8156.

[118] A. Ekman, V. Manninen, and S. Salminen. “Ion movements in red cells treated with propranolol”. *Acta Physiologica Scandinavica* 75.3 (1969), pp. 333–44.

[119] D. C. Devor, A. K. Singh, R. A. Frizzell, et al. “Modulation of Cl- secretion by benzimidazolones. I. Direct activation of a Ca(2+)-dependent K+ channel”. *American Journal of Physiology* 271.5 Pt 1 (1996), pp. L775–84.

[120] D. Strobaek, L. Teuber, T. D. Jorgensen, et al. “Activation of human IK and SK Ca2+ -activated K+ channels by NS309 (6,7-dichloro-1H-indole-2,3-dione 3-oxime)”. *Biochimica et biophysica acta* 1665.1-2 (2004), pp. 1–5.

[121] H. L. Meltzer and S. Kassir. “Inhibition of calmodulin-activated Ca2+-ATPase by propranolol and nadolol”. *Biochimica et biophysica acta* 755.3 (1983), pp. 452–6.

[122] W. Schwarz, H. Keim, R. Fehlau, et al. “Modulation of the Ca2+- or Pb2+-activated K+-selective channels in human red cells. I. Effects of propranolol”. *Biochimica et biophysica acta* 978.1 (1989), pp. 32–6.

[123] P. Bennekou. “The feasibility of pharmacological volume control of sickle cells is dependent on the quantization of the transport pathways. A model study”. *Journal of theoretical biology* 196.1 (1999), pp. 129–37.

[124] M. Baunbaek and P. Bennekou. “Evidence for a random entry of Ca2+ into human red cells”. *Bioelectrochemistry* 73.2 (2008), pp. 145–50.

[125] M. Pellegrino and M. Pellegrini. “Modulation of Ca2+-activated K+ channels of human erythrocytes by endogenous cAMP-dependent protein kinase”. *Pflugers Archiv: European Journal of Physiology* 436.5 (1998), pp. 749–56.

[126] R. L. Schroder, B. S. Jensen, D. Strobaek, et al. “Activation of the human, intermediate-conductance, Ca2+-activated K+ channel by methylxanthines”. *Pflugers Archiv: European Journal of Physiology* 440.6 (2000), pp. 809–18.

[127] R. B. Moore, G. A. Plishker, and S. K. Shriver. “Purification and measurement of calpromotin, the cytoplasmic protein which activates calcium-dependent potassium transport”. *Biochemical and Biophysical Research Communications* 166.1 (1990), pp. 146–53.

[128] P. Kristensen, D. E. Rasmussen, and B. I. Kristensen. “Properties of thiol-specific anti-oxidant protein or calpromotin in solution”. *Biochemical and biophysical research communications* 262.1 (1999), pp. 127–31.

[129] C. Brugnara, L. De Franceschi, and S. L. Alper. “Ca(2+)-activated K+ transport in erythrocytes. Comparison of binding and transport inhibition by scorpion toxins”. *The Journal of Biological Chemistry* 268.12 (1993), pp. 8760–8.

[130] P. Christophersen and P. Bennekou. “Evidence for a voltage-gated, non-selective cation channel in the human red cell membrane”. *Biochimica et Biophysica Acta* 1065.1 (1991), pp. 103–6.

[131] P. Stampe and B. Vestergaard-Bogind. “Ca2+-activated K+ conductance of the human red cell membrane: voltage-dependent Na+ block of outward-going currents”. *The Journal of Membrane Biology* 112.1 (1989), pp. 9–14.

[132] P. Bennekou, O. Pedersen, A. Moller, et al. “Volume control in sickle cells is facilitated by the novel anion conductance inhibitor NS1652”. *Blood* 95.5 (2000), pp. 1842–8.

[133] E. F. Gautier, M. Leduc, S. Cochet, et al. “Absolute proteome quantification of highly purified populations of circulating reticulocytes and mature erythrocytes”. *Blood Advances* 2.20 (2018), pp. 2646–2657.

[134] W. J. Joiner, L. Y. Wang, M. D. Tang, et al. “hSK4, a member of a novel subfamily of calcium-activated potassium channels”. *Proceedings of the National Academy of Sciences of the United States of America* 94.20 (1997), pp. 11013–8.

[135] T. M. Ishii, C. Silvia, B. Hirschberg, et al. “A human intermediate conductance calcium-activated potassium channel”. *Proceedings of the National Academy of Sciences of the United States of America* 94.21 (1997), pp. 11651–6.

[136] B. S. Jensen, D. Strobaek, P. Christophersen, et al. “Characterization of the cloned human intermediate-conductance Ca2+- activated K+ channel”. *American Journal Physiology* 275.3 Pt 1 (1998), pp. C848–56.

[137] J. Alvarez, J. Garcia-Sancho, and B. Herreros. “The role of calmodulin on Ca2+ -dependent K+ transport regulation in the human red cell”. *Biochimica et biophysica acta* 860.1 (1986), pp. 25–34.

[138] C. M. Fanger, S. Ghanshani, N. J. Logsdon, et al. “Calmodulin mediates calcium-dependent activation of the intermediate conductance KCa channel, IKCa1”. *The Journal of Biological Chemistry* 274.9 (1999), pp. 5746–54.

[139] C. H. Lee and R. MacKinnon. “Activation mechanism of a human SK-calmodulin channel complex elucidated by cryo-EM structures”. *Science* 360.6388 (2018), pp. 508–513.

[140] A. Dyrda, U. Cytlak, A. Ciuraszkiewicz, et al. “Local membrane deformations activate Ca2+-dependent K+ and anionic currents in intact human red blood cells”. *PLoS One* 5.2 (2010), e9447.

[141] B. Coste, J. Mathur, M. Schmidt, et al. “Piezo1 and Piezo2 are essential components of distinct mechanically activated cation channels”. *Science* 330.6000 (2010), pp. 55–60.

[142] K. Satoh, M. Hata, S. Takahara, et al. “A novel membrane protein, encoded by the gene covering KIAA0233, is transcriptionally induced in senile plaque-associated astrocytes”. *Brain research* 1108.1 (2006), pp. 19–27.

[143] J. Geng, Q. Zhao, T. Zhang, et al. “In touch with the mechanosensitive Piezo channels: structure, ion permeation, and mechanotransduction”. *Current topics in membranes*. Vol. 79. Elsevier, 2017. Chap. 6, pp. 159–195.

[144] O. P. Hamill and B. Martinac. “Molecular basis of mechanotransduction in living cells”. *Physiological reviews* 81.2 (2001), pp. 685–740.

[145] C. D. Cox, N. Bavi, and B. Martinac. “Origin of the force: the force-from-lipids principle applied to piezo channels”. *Current topics in membranes*. Ed. by P. A. Gottlieb. Vol. 79. Elsevier, 2017. Chap. 3, pp. 59–96.

[146] F. Maingret, A. J. Patel, F. Lesage, et al. “Lysophospholipids open the two-pore domain mechano-gated K+ channels TREK-1 and TRAAK”. *Journal of Biological Chemistry* 275.14 (2000), pp. 10128–10133.

[147] C. Berrier, A. Pozza, A. de Lacroix de Lavalette, et al. “The purified mechanosensitive channel TREK-1 is directly sensitive to membrane tension”. *The Journal of Biological Chemistry* 288.38 (2013), pp. 27307–14.

[148] A. H. Lewis and J. Grandl. “Mechanical sensitivity of Piezo1 ion channels can be tuned by cellular membrane tension”. *eLife* 4 (2015).

[149] C. D. Cox, C. Bae, L. Ziegler, et al. “Removal of the mechanoprotective influence of the cytoskeleton reveals PIEZO1 is gated by bilayer tension”. *Nature Communications* 7 (2016).

[150] Y. Qi, L. Andolfi, F. Frattini, et al. “Membrane stiffening by STOML3 facilitates mechanosensation in sensory neurons”. *Nature communications* 6 (2015), p. 8512.

[151] B. Coste, B. Xiao, J. S. Santos, et al. “Piezo proteins are pore-forming subunits of mechanically activated channels”. *Nature* 483.7388 (2012), pp. 176–181.

[152] A. Kurrle, P. Rieber, and E. Sackmann. “Reconstitution of transferrin receptor in mixed lipid vesicles. An example of the role of elastic and electrostatic forces for protein/lipid assembly”. *Biochemistry* 29.36 (1990), pp. 8274–8282.

[153] D. R. Fattal and A. Ben-Shaul. “A molecular model for lipid-protein interaction in membranes: the role of hydrophobic mismatch”. *Biophysical Journal* 65.5 (1993), pp. 1795–1809.

[154] S. Leikin, M. M. Kozlov, N. L. Fuller, et al. “Measured effects of diacylglycerol on structural and elastic properties of phospholipid membranes”. *Biophysical Journal* 71.5 (1996), pp. 2623–2632.

[155] R. Gnanasambandam, P. A. Gottlieb, and F. Sachs. “The Kinetics and the Permeation Properties of Piezo Channels”. *Current topics in membranes*. Ed. by P. A. Gottlieb. Vol. 79. Academic Press, 2017. Chap. 11, p. 275307.

[156] Y. R. Guo and R. MacKinnon. “Structure-based membrane dome mechanism for Piezo mechanosensitivity”. *eLife* 6 (2017), e33660.

[157] J. Ge, W. Li, Q. Zhao, et al. “Architecture of the mammalian mechanosensitive Piezo1 channel”. *Nature* 527.7576 (2015), pp. 64–9.

[158] B. Coste, S. E. Murthy, J. Mathur, et al. “Piezo1 ion channel pore properties are dictated by C-terminal region”. *Nature communications* 6 (2015), p. 7223.

[159] R. Gnanasambandam, C. Bae, P. A. Gottlieb, et al. “Ionic Selectivity and Permeation Properties of Human PIEZO1 Channels”. *PloS one* 10.5 (2015), e0125503.

[160] M. Moroni, M. R. Servin-Vences, R. Fleischer, et al. “Voltage gating of mechano-sensitive PIEZO channels.” *Nature communications* 9 (2018), p. 1096.

[161] C. Bae, F. Sachs, and P. A. Gottlieb. “The mechanosensitive ion channel Piezo1 is inhibited by the peptide GsMTx4”. *Biochemistry* 50.29 (2011), pp. 6295–300.

[162] Y. O. Posokhov, P. A. Gottlieb, M. J. Morales, et al. “Is lipid bilayer binding a common property of inhibitor cysteine knot ion-channel blockers?” *Biophysical journal* 93.4 (2007), pp. L20–2.

[163] R. Syeda, J. Xu, A. E. Dubin, et al. “Chemical activation of the mechanotransduction channel Piezo1”. *eLife* 4 (2015).

[164] Y. Wang, S. Chi, H. Guo, et al. “A lever-like transduction pathway for long-distance chemical- and mechano-gating of the mechanosensitive Piezo1 channel”. *Nature communications* 9.1 (2018), p. 1300.

[165] E. L. Evans, K. Cuthbertson, N. Endesh, et al. “Yoda1 analogue (Dooku1) which antagonizes Yoda1-evoked activation of Piezo1 and aortic relaxation”. *British journal of pharmacology* 175.10 (2018), pp. 1744–1759.

[166] E. Cinar, S. Zhou, J. DeCourcey, et al. “Piezo1 regulates mechanotransductive release of ATP from human RBCs”. *Proceedings of the National Academy of Sciences of the United States of America* 112 (2015), pp. 11783–11788.

[167] S. M. Cahalan, V. Lukacs, S. S. Ranade, et al. “Piezo1 links mechanical forces to red blood cell volume”. *eLife* 4 (2015).

[168] J. A. Halperin, C. Brugnara, M. T. Tosteson, et al. “Voltage-activated cation transport in human erythrocytes”. *The American Journal of Physiology* 257.5 Pt 1 (1989), pp. C986–96.

[169] P. Bennekou and P. Christophersen. “Ion channels”. *Red Cell Membrane Transport in Health and Disease*. Ed. by J. C. Ellory and I. Bernhardt. Springer, 2003. Chap. 6, pp. 139–152.

[170] H. Davson. “Studies on the permeability of erythrocytes: The effect of reducing the salt content of the medium surrounding the cell”. *The Biochemical Journal* 33.3 (1939), pp. 389–401.

[171] P. Bennekou. “The voltage-gated non-selective cation channel from human red cells is sensitive to acetylcholine”. *Biochimica et Biophysica Acta* 1147.1 (1993), pp. 165–7.

[172] L. Kaestner, P. Christophersen, I. Bernhardt, et al. “The non-selective voltage-activated cation channel in the human red blood cell membrane: reconciliation between two conflicting reports and further characterisation”. *Bioelectrochemistry* 52.2 (2000), pp. 117–25.

[173] A. Makhro, P. Hänggi, J. S. Goede, et al. “N-methyl-D-aspartate receptors in human erythroid precursor cells and in circulating red blood cells contribute to the intracellular calcium regulation.” *American journal of physiology. Cell physiology* 305 (2013), pp. C1123–C1138.

[174] P. Hanggi, A. Makhro, M. Gassmann, et al. “Red blood cells of sickle cell disease patients exhibit abnormally high abundance of N-methyl D-aspartate receptors mediating excessive calcium uptake”. *British Journal of Haematology* 167.2 (2014), pp. 252–264.

[175] M. Foller, R. S. Kasinathan, S. Koka, et al. “TRPC6 contributes to the Ca(2+) leak of human erythrocytes”. *Cellular Physiology and Biochemistry* 21.1-3 (2008), pp. 183–92.

[176] T. Lange, P. Jungmann, J. Haberle, et al. “Reduced number of CFTR molecules in erythrocyte plasma membrane of cystic fibrosis patients.” *Molecular membrane biology* 23 (2006), pp. 317–323.

[177] R. S. Sprague, M. L. Ellsworth, A. H. Stephenson, et al. “Deformation-induced ATP release from red blood cells requires CFTR activity.” *The American journal of physiology* 275 (1998), H1726–H1732.

[178] S. M. Huber, C. Duranton, G. Henke, et al. “Plasmodium induces swelling-activated ClC-2 anion channels in the host erythrocyte.” *The Journal of biological chemistry* 279 (2004), pp. 41444–41452.

[179] J. Roth E. “Plasmodium falciparum carbohydrate metabolism: a connection between host cell and parasite”. *Blood cells* 16.2-3 (1990), pp. 453–66.

[180] H. Ginsburg, S. Kutner, M. Krugliak, et al. “Characterization of permeation pathways appearing in the host membrane of Plasmodium falciparum infected red blood cells”. *Molecular Biochemical Parasitology* 14.3 (1985), pp. 313–22.

[181] K. Kirk, H. A. Horner, B. C. Elford, et al. “Transport of diverse substrates into malaria-infected erythrocytes via a pathway showing functional characteristics of a chloride channel”. *Journal of Biological Chemistry* 269.5 (1994), pp. 3339–47.

[182] S. L. Cranmer, A. R. Conant, W. E. Gutteridge, et al. “Characterization of the enhanced transport of L- and D-lactate into human red blood cells infected with Plasmodium falciparum suggests the presence of a novel saturable lactate proton cotransporter”. *The Journal of Biological Chemistry* 270.25 (1995), pp. 15045–52.

[183] K. Kirk, H. A. Horner, and J. Kirk. “Glucose uptake in Plasmodium falciparum-infected erythrocytes is an equilibrative not an active process”. *Molecular Biochemical Parasitology* 82.2 (1996), pp. 195–205.

[184] H. M. Staines, J. C. Ellory, and K. Kirk. “Perturbation of the pump-leak balance for Na+ and K+ in malaria-infected erythrocytes”. *American Journal of Physiology-Cell Physiology* 280.6 (2001), pp. C1576–C1587.

[185] K. Kirk, H. A. Horner, D. J. Spillett, et al. “Glibenclamide and meglitinide block the transport of low molecular weight solutes into malaria-infected erythrocytes”. *FEBS Letters* 323.1-2 (1993), pp. 123–8.

[186] K. Kirk and H. A. Horner. “In search of a selective inhibitor of the induced transport of small solutes in Plasmodium falciparum-infected erythrocytes: effects of arylaminobenzoates”. *Biochemical Journal* 311.Pt 3 (1995), pp. 761–8.

[187] H. M. Staines, C. Rae, and K. Kirk. “Increased permeability of the malaria-infected erythrocyte to organic cations”. *Biochimica et Biophysica Acta* 1463.1 (2000), pp. 88–98.

[188] R. E. Martin, R. I. Henry, J. L. Abbey, et al. “The ’permeome’ of the malaria parasite: an overview of the membrane transport proteins of Plasmodium falciparum”. *Genome biology* 6.3 (2005), R26.

[189] R. E. Martin, H. Ginsburg, and K. Kirk. “Membrane transport proteins of the malaria parasite”. *Molecular microbiology* 74.3 (2009), pp. 519–28.

[190] A. Gupta, P. Balabaskaran-Nina, W. Nguitragool, et al. “CLAG3 Self-Associates in Malaria Parasites and Quantitatively Determines Nutrient Uptake Channels at the Host Membrane.” *mBio* 9 (2018).

[191] S. A. Desai. “Ion and nutrient uptake by malaria parasite-infected erythrocytes.” *Cellular microbiology* 14 (2012), pp. 1003–1009.

[192] S. Egee, F. Lapaix, G. Decherf, et al. “A stretch-activated anion channel is up-regulated by the malaria parasite Plasmodium falciparum”. *Journal of Physiology* 542.Pt 3 (2002), pp. 795–801.

[193] S. M. Huber, A.-C. Uhlemann, N. L. Gamper, et al. “Plasmodium falciparum activates endogenous Cl(-) channels of human erythrocytes by membrane oxidation.” *The EMBO journal* 21 (2002), pp. 22–30.

[194] G. Bouyer, A. Cueff, S. Egee, et al. “Erythrocyte peripheral type benzodiazepine receptor/voltage-dependent anion channels are upregulated by Plasmodium falciparum”. *Blood* 118.8 (2011), pp. 2305–12.

[195] V. Shoshan-Barmatz, V. De Pinto, M. Zweckstetter, et al. “VDAC, a multi-functional mitochondrial protein regulating cell life and death.” *Molecular aspects of medicine* 31 (2010), pp. 227–285.

[196] G. W. Stewart, J. C. Ellory, and R. A. Klein. “Increased human red cell cation passive permeability below 12 degrees C.” *Nature* 286 (1980), pp. 403–404.

[197] J. F. Flatt and L. J. Bruce. “The Molecular Basis for Altered Cation Permeability in Hereditary Stomatocytic Human Red Blood Cells.” *Frontiers in Physiology* 9 (2018), p. 367.

[198] S. E. Coles and G. W. Stewart. “Temperature effects on cation transport in hereditary stomatocytosis and allied disorders.” *International Journal of Experimental Pathology* 80 (1999), pp. 251–258.

[199] H. S. Jacob and J. H. Jandl. “Increased cell membrane permeability in the pathogenesis of Hereditary Spherocytosis.” *The Journal of clinical investigation* 43 (1964), pp. 1704–1720.

[200] H. Guizouarn, S. Martial, N. Gabillat, et al. “Point mutations involved in red cell stomatocytosis convert the electroneutral anion exchanger 1 to a nonselective cation conductance.” *Blood* 110 (2007), pp. 2158–2165.

[201] L. J. Bruce, H. Guizouarn, N. M. Burton, et al. “The monovalent cation leak in overhydrated stomatocytic red blood cells results from amino acid substitutions in the Rh-associated glycoprotein.” *Blood* 113 (2009), pp. 1350–1357.

[202] D. Darghouth, B. Koehl, J. F. Heilier, et al. “Alterations of red blood cell metabolome in overhydrated hereditary stomatocytosis.” *Haematologica* 96 (2011), pp. 1861–1865.

[203] M. J. Tanner, L. Bruce, P. G. Martin, et al. “Melanesian hereditary ovalocytes have a deletion in red cell band 3.” *Blood* 78 (1991), pp. 2785–2786.

[204] H. Kuma, Y. Abe, D. Askin, et al. “Molecular basis and functional consequences of the dominant effects of the mutant band 3 on the structure of normal band 3 in Southeast Asian ovalocytosis.” *Biochemistry* 41 (2002), pp. 3311–3320.

[205] L. J. Bruce, S. M. Ring, K. Ridgwell, et al. “South-east asian ovalocytic (SAO) erythrocytes have a cold sensitive cation leak: implications for in vitro studies on stored SAO red cells.” *Biochimica et biophysica acta* 1416 (1999), pp. 258–270.

[206] H. Guizouarn, F. Borgese, N. Gabillat, et al. “South-east Asian ovalocytosis and the cryohydrocytosis form of hereditary stomatocytosis show virtually indistinguishable cation permeability defects.” *British Journal of Haematology* 152 (2011), pp. 655–664.

[207] I. Andolfo, S. L. Alper, J. Delaunay, et al. “Missense mutations in the ABCB6 transporter cause dominant familial pseudohyperkalemia.” *American Journal of Hematology* 88 (2013), pp. 66–72.

[208] I. Andolfo, S. L. Alper, L. De Franceschi, et al. “Multiple clinical forms of dehydrated hereditary stomatocytosis arise from mutations in PIEZO1.” *Blood* 121 (2013), 3925–35, S1–12.

[209] D. C. Tosteson, E. Shea, and R. C. Darling. “Potassium and sodium of red blood cells in sickle cell anemia”. *The Journal of clinical investigation* 31 (1952), pp. 406–411.

[210] A. C. Hall and J. C. Ellory. “Evidence for the presence of volume-sensitive KCl transport in ’young’ human red cells.” *Biochimica et biophysica acta* 858 (1986), pp. 317–320.

[211] P. K. Lauf, J. Bauer, N. C. Adragna, et al. “Erythrocyte K-Cl cotransport: properties and regulation.” *The American journal of physiology* 263 (1992), pp. C917–C932.

[212] P. K. Lauf and G. Valet. “Na+ K+ pump and passive K+ transport in large and small red cell populations of anemic high and low K+ sheep.” *Journal of cellular physiology* 116 (1983), pp. 35–44.

[213] N. Mohandas, M. E. Rossi, and M. R. Clark. “Association between morphologic distortion of sickle cells and deoxygenation-induced cation permeability increase.” *Blood* 68 (1986), pp. 450–454.

[214] C. R. Beddell, P. J. Goodford, G. Kneen, et al. “Substituted benzaldehydes designed to increase the oxygen affinity of human haemoglobin and inhibit the sickling of sickle erythrocytes.” *British journal of pharmacology* 82 (1984), pp. 397–407.

[215] B. H. Lubin, V. Pena, W. C. Mentzer, et al. “Dimethyl adipimidate: a new antisickling agent.” *Proceedings of the National Academy of Sciences of the United States of America* 72 (1975), pp. 43–46.

[216] V. L. Lew and R. M. Bookchin. “Ion transport pathology in the mechanism of sickle cell dehydration.” *Physiological reviews* 85 (2005), pp. 179–200.

[217] J. F. Bertles and P. F. Milner. “Irreversibly sickled erythrocytes: a consequence of the heterogeneous distribution of hemoglobin types in sickle-cell anemia.” *The Journal of clinical investigation* 47 (1968), pp. 1731–1741.

[218] L. Lorand, L. B. Weissmann, D. L. Epel, et al. “Role of the intrinsic transglutaminase in the Ca2+-mediated crosslinking of erythrocyte proteins.” *Proceedings of the National Academy of Sciences of the United States of America* 73 (1976), pp. 4479–4481.

[219] C. H. Joiner. “Deoxygenation-induced cation fluxes in sickle cells: II. Inhibition by stilbene disulfonates.” *Blood* 76 (1990), pp. 212–220.

[220] V. L. Lew, O. E. Ortiz, and R. M. Bookchin. “Stochastic nature and red cell population distribution of the sickling-induced Ca2+ permeability.” *The Journal of clinical investigation* 99 (1997), pp. 2727–2735.

[221] Y. L. Ma, D. C. Rees, J. S. Gibson, et al. “The conductance of red blood cells from sickle cell patients: ion selectivity and inhibitors.” *The Journal of physiology* 590.9 (2012), pp. 2095–2105.

[222] J. A. Browning, H. M. Staines, H. C. Robinson, et al. “The effect of deoxygenation on whole-cell conductance of red blood cells from healthy individuals and patients with sickle cell disease.” *Blood* 109 (2007), pp. 2622–2629.

[223] C. H. Joiner, M. Jiang, W. J. Claussen, et al. “Dipyridamole inhibits sickling-induced cation fluxes in sickle red blood cells.” *Blood* 97 (2001), pp. 3976–3983.

[224] H. Chaplin, N. Alkjaersig, A. P. Fletcher, et al. “Aspirin-dipyridamole prophylaxis of sickle cell disease pain crises.” *Thrombosis and haemostasis* 43 (1980), pp. 218–221.

[225] A. Brovelli and G. Minetti. “Red Cell Ageing”. *Red Cell Membrane Transport in Health and Disease*. Ed. by I. Bernhardt and J. C. Ellory. Berlin, Heidelberg: Springer Berlin Heidelberg, 2003. Chap. 29, pp. 673–690.

[226] W. Ashby. “The Determination of the Length of Life of Transfused Blood Corpuscles in Man”. *The Journal of Experimental Medicine* 29.3 (1919), pp. 267–81.

[227] W. Ashby. “Study of Transfused Blood : I. The Periodicity in Eliminative Activity Shown by the Organism”. *The Journal of Experimental Medicine* 34.2 (1921), pp. 127–46.

[228] S. T. Callender, E. O. Powell, and L. J. Witts. “Normal red-cell survival in men and women”. *The Journal of Pathology and Bacteriology* 59.4 (1947), pp. 519–32.

[229] D. Shemin and D. Rittenberg. “The life span of the human red blood cell”. *The Journal of Biological Chemistry* 166.2 (1946), pp. 627–36.

[230] N. I. Berlin, B. M. Tolbert, and J. H. Lawrence. “Studies in glycine-2-C14 metabolism in man. I. The pulmonary excretion of C14O2”. *The Journal of Clinical Investigation* 30.1 (1951), pp. 73–6.

[231] N. I. Berlin, C. Reynafarje, and J. H. Lawrence. “Red cell life span in the polycythemia of high altitude”. *Journal of applied physiology* 7.3 (1954), pp. 271–2.

[232] P. L. Mollison and N. Veall. “The use of the isotope 51Cr as a label for red cells”. *British journal of haematology* 1.1 (1955), pp. 62–74.

[233] P. L. Mollison. “Further observations on the normal survival curve of 51 Cr-labelled red cells”. *Clinical science* 21 (1961), pp. 21–36.

[234] I. Cavill. “Red cell lifespan estimation by (51)Cr labelling”. *British journal of haematology* 117.4 (2002), p. 998.

[235] International Committe for Standardization in Hematology. “Recommended methods for radioisotope red cell survival studies”. *Blood* 38.3 (1971), pp. 378–386.

[236] C. Roussel, P. A. Buffet, and P. Amireault. “Measuring Post-transfusion Recovery and Survival of Red Blood Cells: Strengths and Weaknesses of Chromium-51 Labeling and Alternative Methods”. *Frontiers in Medicine* 5.130 (2018).

[237] W. C. Peacock, R. D. Evans, J. W. Irvine, et al. “The Use of Two Radioactive Isotopes of Iron in Tracer Studies of Erythrocytes”. *The Journal of Clinical Investigation* 25.4 (1946), pp. 605–15.

[238] C. A. Finch, J. G. Gibson, and et al. “Iron metabolism; utilization of intravenous radioactive iron”. *Blood* 4.8 (1949), pp. 905–27.

[239] G. S. Eadie and J. Brown I. W. “Red blood cell survival studies”. *Blood* 8.12 (1953), pp. 1110–36.

[240] A. Strocchi, S. Schwartz, M. Ellefson, et al. “A simple carbon monoxide breath test to estimate erythrocyte turnover”. *The Journal of Laboratory and Clinical Medicine* 120.3 (1992), pp. 392–9.

[241] J. K. Furne, J. R. Springfield, S. B. Ho, et al. “Simplification of the end-alveolar carbon monoxide technique to assess erythrocyte survival”. *The Journal of Laboratory and Clinical Medicine* 142.1 (2003), pp. 52–7.

[242] T. Suzuki and G. L. Dale. “Biotinylated erythrocytes: in vivo survival and in vitro recovery”. *Blood* 70.3 (1987), pp. 791–5.

[243] W. H. Crosby. “Normal functions of the spleen relative to red blood cells: a review”. *Blood* 14.4 (1959), pp. 399–408.

[244] E. R. Borun, W. G. Figueroa, and S. M. Perry. “The distribution of Fe59 tagged human erythrocytes in centrifuged specimens as a function of cell age”. *The Journal of Clinical Investigation* 36.5 (1957), pp. 676–9.

[245] V. L. Lew, J. E. Raftos, M. Sorette, et al. “Generation of normal human red cell volume, hemoglobin content, and membrane area distributions by” birth” or regulation?” *Blood* 86.1 (1995), pp. 334–341.

[246] F. L. Willekens, B. Roerdinkholder-Stoelwinder, Y. A. Groenen-Dopp, et al. “Hemoglobin loss from erythrocytes in vivo results from spleen-facilitated vesiculation”. *Blood* 101.2 (2003), pp. 747–51.

[247] A. R. Williams and D. R. Morris. “The internal viscosity of the human erythrocyte may determine its lifespan in vivo”. *Scandinavian journal of haematology* 24.1 (1980), pp. 57–62.

[248] R. M. Bookchin, Z. Etzion, M. Sorette, et al. “Identification and characterization of a newly recognized population of high-Na+, low-K+, low-density sickle and normal red cells”. *Proceedings of the National Academy of Sciences of the United States of America* 97.14 (2000), pp. 8045–8050.

[249] V. L. Lew and T. Tiffert. “The terminal density reversal phenomenon of aging human red blood cells.” *Frontiers in Physiology* 4 (2013), p. 171.

[250] L. M. Crespo, T. S. Novak, and J. C. Freedman. “Calcium, cell shrinkage, and prolytic state of human red blood cells.” *The American journal of physiology* 252.2 Pt 1 (1987), pp. C138–C152.

[251] V. L. Lew, N. Daw, Z. Etzion, et al. “Effects of age-dependent membrane transport changes on the homeostasis of senescent human red blood cells”. *Blood* 110.4 (2007), pp. 1334–42.

[252] M. Inaba and Y. Maede. “Correlation between protein 4.1a/4.1b ratio and erythrocyte life span”. *Biochimica et biophysica acta* 944.2 (1988), pp. 256–64.

[253] M. M. Kay. “Mechanism of removal of senescent cells by human macrophages in situ”. *Proceedings of the National Academy of Sciences of the United States of America* 72.9 (1975), pp. 3521–5.

[254] E. M. Alderman, H. H. Fudenberg, and R. E. Lovins. “Binding of immunoglobulin classes to subpopulations of human red blood cells separated by density-gradient centrifugation”. *Blood* 55.5 (1980), pp. 817–22.

[255] A. Ensinck, C. S. Biondi, A. Marini, et al. “Effect of membrane-bound IgG and desialysation in the interaction of monocytes with senescent erythrocytes”. *Clinical and experimental medicine* 6.3 (2006), pp. 138–42.

[256] A. G. Morell, G. Gregoriadis, I. H. Scheinberg, et al. “The role of sialic acid in determining the survival of glycoproteins in the circulation”. *The Journal of Biological Chemistry* 246.5 (1971), pp. 1461–7.

[257] M. M. Kay. “Localization of senescent cell antigen on band 3”. *Proceedings of the National Academy of Sciences of the United States of America* 81.18 (1984), pp. 5753–7.

[258] M. M. Kay. “Molecular mapping of human band 3 aging antigenic sites and active amino acids using synthetic peptides”. *Journal of protein chemistry* 11.6 (1992), pp. 595–602.

[259] K. E. Badior and J. R. Casey. “Molecular mechanism for the red blood cell senescence clock”. *IUBMB life* 70.1 (2018), pp. 32–40.

[260] J. Freedman. “Membrane-bound immunoglobulins and complement components on young and old red cells”. *Transfusion* 24.6 (1984), pp. 477–81.

[261] E. M. Welbourn, M. T. Wilson, A. Yusof, et al. “The mechanism of formation, structure and physiological relevance of covalent hemoglobin attachment to the erythrocyte membrane”. *Free Radical Biology & Medicine* 103 (2017), pp. 95–106.

[262] K. S. Lang, P. A. Lang, C. Bauer, et al. “Mechanisms of suicidal erythrocyte death”. *Cellular Physiology and Biochemistry* 15.5 (2005), pp. 195–202.

[263] R. S. Franco, M. E. Puchulu-Campanella, L. A. Barber, et al. “Changes in the properties of normal human red blood cells during in vivo aging”. *American Journal of Hematology* 88.1 (2012), pp. 44–51.

[264] P. Arese, F. Turrini, and E. Schwarzer. “Band 3/complement-mediated recognition and removal of normally senescent and pathological human erythrocytes.” *Cellular Physiology and Biochemistry* 16 (2005), pp. 133–146.

[265] L. J. Dumont and J. P. AuBuchon. “Evaluation of proposed FDA criteria for the evaluation of radiolabeled red cell recovery trials”. *Transfusion* 48.6 (2008), pp. 1053–60.

[266] European Drectorate for the Quality of Medicines and Healthcare of the Council of Europe. *Guide to the preparation, use and quality assurance of Blood Components. Recommendation No. R (95) 15*. 19th ed. 2017.

[267] T. N. Estep, R. A. Pedersen, T. J. Miller, et al. “Characterization of erythrocyte quality during the refrigerated storage of whole blood containing di-(2-ethylhexyl) phthalate”. *Blood* 64.6 (1984), pp. 1270–6.

[268] J. R. Hess. “An update on solutions for red cell storage”. *Vox sanguinis* 91.1 (2006), pp. 13–9.

[269] B. Horowitz, M. H. Stryker, A. A. Waldman, et al. “Stabilization of red blood cells by the plasticizer, diethylhexylphthalate”. *Vox sanguinis* 48.3 (1985), pp. 150–5.

[270] R. I. Macey, J. S. Adorante, and F. W. Orme. “Erythrocyte-Membrane Potentials Determined by Hydrogen-Ion Distribution”. *Biochimica Et Biophysica Acta* 512.2 (1978), pp. 284–295.

[271] R. Rapetti-Mauss, C. Lacoste, V. Picard, et al. “A mutation in the Gardos channel is associated with hereditary xerocytosis”. *Blood* 126.11 (2015), pp. 1273–80.

[272] I. Andolfo, R. Russo, F. Manna, et al. “Novel Gardos channel mutations linked to dehydrated hereditary stomatocytosis (xerocytosis)”. *American Journal of Hematology* 90.10 (2015), pp. 921–6.

[273] E. Glogowska and P. G. Gallagher. "Disorders of erythrocyte volume homeostasis". *International Journal of Laboratory Hematology* 37 Suppl 1 (2015), pp. 85–91.

[274] R. Zarychanski, V. P. Schulz, B. L. Houston, et al. "Mutations in the mechanotransduction protein PIEZO1 are associated with hereditary xerocytosis". *Blood* 120.9 (2012), pp. 1908–15.

[275] C. Bae, R. Gnanasambandam, C. Nicolai, et al. "Xerocytosis is caused by mutations that alter the kinetics of the mechanosensitive channel PIEZO1". *Proceedings of the National Academy of Sciences of the United States of America* 110.12 (2013), E1162–8.

[276] I. Andolfo, R. Russo, A. Gambale, et al. "New insights on hereditary erythrocyte membrane defects". *Haematologica* 101.11 (2016), pp. 1284–1294.

[277] R. Del Orbe Barreto, B. Arrizabalaga, A. B. De la Hoz Rastrollo, et al. "Hereditary xerocytosis, a misleading anemia." *Annals of hematology* 95 (2016), pp. 1545–1546.

[278] I. Andolfo, F. Manna, G. De Rosa, et al. "PIEZO1-R1864H rare variant accounts for a genetic phenotype-modifier role in dehydrated hereditary stomatocytosis". *Haematologica* 103.3 (2018), e94–e97.

[279] H. W. Kaufman, J. K. Niles, D. R. Gallagher, et al. "Revised prevalence estimate of possible Hereditary Xerocytosis as derived from a large US Laboratory database". *American Journal of Hematology* 93.1 (2018), E9–E12.

[280] A. Cueff, R. Seear, A. Dyrda, et al. "Effects of elevated intracellular calcium on the osmotic fragility of human red blood cells". *Cell Calcium* 47.1 (2010), pp. 29–36.

[281] L. Conforti. "Patch-Clamp Techniques". *Cell physiology source book: essentials of membrane biophysics*. Ed. by N. Sperelakis. Elsevier, 2012.

[282] E. Fermo, A. Bogdanova, P. Petkova-Kirova, et al. "'Gardos Channelopathy': a variant of hereditary Stomatocytosis with complex molecular regulation". *Scientific Reports* 7.1 (2017), p. 1744.

[283] L. Hertz, R. Huisjes, E. Llaudet-Planas, et al. "Is increased intracellular calcium in red blood cells a common component in the molecular mechanism causing anemia?" *Frontiers in Physiology* 8 (2017), p. 673.

[284] A. Makhro, R. Huisjes, L. P. Verhagen, et al. "Red Cell Properties after Different Modes of Blood Transportation." *Frontiers in Physiology* 7 (2016), p. 288.

[285] P. Morales, L. Garneau, H. Klein, et al. "Contribution of the KCa3. 1 channel–calmodulin interactions to the regulation of the KCa3. 1 gating process". *The Journal of General Physiology* 142.1 (2013), pp. 37–60.

[286] D. Monedero-Alonso, L. Peres, G. Bouyer, et al. "NS3623 enhances the activity of a Non Selective Cation Channel in hyperpolarizing conditions". 2019.

[287] J. Delaunay. "The hereditary stomatocytoses: genetic disorders of the red cell membrane permeability to monovalent cations". *Seminars in Hematology* 41.2 (2004), pp. 165–172.

[288] J. W. Stocker, L. De Franceschi, G. A. McNaughton-Smith, et al. "ICA-17043, a novel Gardos channel blocker, prevents sickled red blood cell dehydration in vitro and in vivo in SAD mice". *Blood* 101.6 (2003), pp. 2412–2418.

[289] K. I. Ataga, W. R. Smith, L. M. De Castro, et al. "Efficacy and safety of the Gardos channel blocker, senicapoc (ICA-17043), in patients with sickle cell anemia". *Blood* 111.8 (2008), pp. 3991–3997.

[290] R. Rapetti-Mauss, O. Soriani, H. Vinti, et al. "Senicapoc: a potent candidate for the treatment of a subset of hereditary xerocytosis caused by mutations in the Gardos channel". *Haematologica* 101.11 (2016), e431–e435.

[291] V. Picard, C. Guitton, I. Thuret, et al. "Clinical and biological features in PIEZO1-hereditary xerocytosis and Gardos-channelopathy: A retrospective series of 126 patients". *Haematologica* 104 (2019), pp. 1554–1564.

[292] Q. Zhao, H. Zhou, S. Chi, et al. "Structure and mechanogating mechanism of the Piezo1 channel." *Nature* 554 (2018), pp. 487–492.

[293] S. E. Murthy, A. E. Dubin, and A. Patapoutian. “Piezos thrive under pressure: mechanically activated ion channels in health and disease.” *Nature reviews. Molecular cell biology* 18 (2017), pp. 771–783.

[294] P. Bennekou, B. I. Kristensen, and P. Christophersen. “The human red cell voltage-regulated cation channel. The interplay with the chloride conductance, the Ca(2+)-activated K(+) channel and the Ca(2+) pump.” *The Journal of membrane biology* 195 (2003), pp. 1–8.

[295] P. Bennekou, T. L. Barksmann, L. R. Jensen, et al. “Voltage activation and hysteresis of the non-selective voltage-dependent channel in the intact human red cell”. *Bioelectrochemistry* 62.2 (2004), pp. 181–5.

[296] G. W. Stewart, J. A. L. Amess, S. W. Eber, et al. “Thrombo-embolic disease after splenectomy for hereditary stomatocytosis”. *British Journal of Haematology* 93.2 (1996), pp. 303–310.

[297] X. Jaïs, S. J. Till, T. Cynober, et al. “An Extreme Consequence of Splenectomy in Dehydrated Hereditary Stomatocytosis: Gradual Thrombo-embolic Pulmonary Hypertension and Lung–Heart Transplantation”. *Hemoglobin* 27.3 (2003), pp. 139–147.

[298] J. Albuisson, S. E. Murthy, M. Bandell, et al. “Dehydrated hereditary stomatocytosis linked to gain-of-function mutations in mechanically activated PIEZO1 ion channels”. *Nature communications* 4 (2013), p. 1884.

[299] J. Wu, M. Young, A. H. Lewis, et al. “Inactivation of mechanically activated Piezo1 ion channels is determined by the C-terminal extracellular domain and the inner pore helix”. *Cell reports* 21.9 (2017), pp. 2357–2366.

[300] R. Rapetti-Mauss, V. Picard, C. Guitton, et al. “Red blood cell Gardos channel (KCNN4): the essential determinant of erythrocyte dehydration in hereditary xerocytosis.” *Haematologica* 102 (2017), e415–e418.

[301] P. D. Kingsley, E. Greenfest-Allen, J. M. Frame, et al. “Ontogeny of erythroid gene expression.” *Blood* 121 (2013), e5–e13.

[302] J. G. Danielczok, E. Terriac, L. Hertz, et al. “Red Blood Cell Passage of Small Capillaries Is Associated with Transient Ca2+-mediated Adaptations”. *Frontiers in Physiology* 8.979 (2017).

[303] P. L. Moura, M. A. Lizarralde Iragorri, O. Français, et al. “Reticulocyte and red blood cell deformation triggers specific phosphorylation events.” *Blood Advances* 3 (2019), pp. 2653–2663.

[304] L. O. Romero, A. E. Massey, A. D. Mata-Daboin, et al. “Dietary fatty acids fine-tune Piezo1 mechanical response.” *Nature Communications* 10 (2019), p. 1200.

[305] E. Honoré, J. R. Martins, D. Penton, et al. “The Piezo Mechanosensitive Ion Channels: May the Force Be with You!” *Reviews of physiology, biochemistry and pharmacology* 169 (2015), pp. 25–41.

[306] P. Bennekou, L. de Franceschi, O. Pedersen, et al. “Treatment with NS3623, a novel Cl-conductance blocker, ameliorates erythrocyte dehydration in transgenic SAD mice: a possible new therapeutic approach for sickle cell disease”. *Blood* 97.5 (2001), pp. 1451–7.

[307] R. Weil. “Sodium citrate in the transfusion of blood”. *Journal of the American Medical Association* 64 (1915), pp. 425–426.

[308] C. W. Walter. “Invention and development of the blood bag”. *Vox sanguinis* 47.4 (1984), pp. 318–24.

[309] C. F. Hogman, L. Eriksson, A. Ericson, et al. “Storage of saline-adenine-glucose-mannitol-suspended red cells in a new plastic container: polyvinylchloride plasticized with butyryl-n-trihexyl-citrate”. *Transfusion* 31.1 (1991), pp. 26–9.

[310] J. Delobel, O. Garraud, S. Barelli, et al. “Storage lesion: History and perspectives”. *World Journal of Hematology* 4.4 (2015), pp. 54–68.

[311] G. M. D’Amici, C. Mirasole, A. D’Alessandro, et al. “Red blood cell storage in SAGM and AS3: a comparison through the membrane two-dimensional electrophoresis proteome”. *Blood Transfusion* 10 Suppl 2 (2012), s46–54.

[312] M. Nakao, T. Nakao, H. Yoshikawa, et al. “A new preservative medium containing adenine and inosine”. *Bibliotheca haematologica* 13 (1962), pp. 455–61.

[313] C. F. Hogman, K. Hedlund, and H. Zetterstrom. “Clinical usefulness of red cells preserved in protein-poor mediums”. *The New England Journal of Medicine* 299.25 (1978), pp. 1377–82.

[314] C. F. Hogman, K. Hedlund, and Y. Sahlestrom. “Red cell preservation in protein-poor media. III. Protection against in vitro hemolysis”. *Vox sanguinis* 41.5-6 (1981), pp. 274–81.

[315] C. F. Hogman. “Preparation and preservation of red cells”. *Vox sanguinis* 74 Suppl 2 (1998), pp. 177–87.

[316] T. Burnouf, M. L. Chou, H. Goubran, et al. “An overview of the role of microparticles/microvesicles in blood components: Are they clinically beneficial or harmful?” *Transfusion and Apheresis Science* 53.2 (2015), pp. 137–45.

[317] M. García-Roa, M. del Carmen Vicente-Ayuso, A. M. Bobes, et al. “Red blood cell storage time and transfusion: current practice, concerns and future perspectives”. *Blood Transfusion* 15.3 (2017), pp. 222–231.

[318] D. Belpulsi, S. L. Spitalnik, and E. A. Hod. “The controversy over the age of blood: what do the clinical trials really teach us?” *Blood Transfusion* 15.2 (2017), pp. 112–115.

[319] C. Lelubre, M. Piagnerelli, and J. L. Vincent. “Association between duration of storage of transfused red blood cells and morbidity and mortality in adult patients: myth or reality?” *Transfusion* 49.7 (2009), pp. 1384–94.

[320] C. Chai-Adisaksopha, P. E. Alexander, G. Guyatt, et al. “Mortality outcomes in patients transfused with fresher versus older red blood cells: a meta-analysis”. *Vox sanguinis* 112.3 (2017), pp. 268–278.

[321] C. Lelubre and J. L. Vincent. “Relationship between red cell storage duration and outcomes in adults receiving red cell transfusions: a systematic review”. *Critical care* 17.2 (2013), R66.

[322] Z. K. McQuilten, C. J. French, A. Nichol, et al. “Effect of age of red cells for transfusion on patient outcomes: a systematic review and meta-analysis”. *Transfusion medicine reviews* 32.2 (2018), pp. 77–88.

[323] Parliament and Council of the European Union. *Directive 2002/98/EC setting standards of quality and safety for the collection, testing, processing, storage and distribution of human blood and blood components and amending Directive 2001/83/EC*. 2003.

[324] I. Talstad, P. Scheie, H. Dalen, et al. “Influence of plasma proteins on erythrocyte morphology and sedimentation”. *Scandinavian Journal of Haematology* 31.5 (1983), pp. 478–84.

[325] C. Roussel, M. Dussiot, M. Marin, et al. “Spherocytic shift of red blood cells during storage provides a quantitative whole cell-based marker of the storage lesion”. *Transfusion* 57.4 (2017), pp. 1007–1018.

[326] R. Lovrien, W. Tisel, and P. Pesheck. “Stoichiometry of compounds bound to human erythrocytes in relation to morphology”. *The Journal of biological chemistry* 250.8 (1975), pp. 3136–41.

[327] D. Y. Hui and J. A. Harmony. “Interaction of plasma lipoproteins with erythrocytes. I. Alteration of erythrocyte morphology”. *Biochimica et biophysica acta* 550.3 (1979), pp. 407–24.

[328] W. H. Reinhart, N. Z. Piety, J. W. Deuel, et al. “Washing stored red blood cells in an albumin solution improves their morphologic and hemorheologic properties.” *Transfusion* 55 (2015), pp. 1872–1881.

[329] A. H. Bryk and J. R. Wisniewski. “Quantitative Analysis of Human Red Blood Cell Proteome”. *Journal of proteome research* 16.8 (2017), pp. 2752–2761.

[330] K. Kirk, H. Y. Wong, B. C. Elford, et al. “Enhanced choline and Rb+ transport in human erythrocytes infected with the malaria parasite Plasmodium falciparum”. *Biochemical Journal* 278.Pt 2 (1991), pp. 521–5.

[331] K. Kirk. “Membrane transport in the malaria-infected erythrocyte”. *Physiological Reviews* 81.2 (2001), pp. 495–537.

[332] R. Zalk, A. Israelson, E. S. Garty, et al. “Oligomeric states of the voltage-dependent anion channel and cytochrome c release from mitochondria.” *The Biochemical journal* 386 (2005), pp. 73–83.

[333] B. W. Hoogenboom, K. Suda, A. Engel, et al. “The supramolecular assemblies of voltage-dependent anion channels in the native membrane.” *Journal of Molecular Biology* 370 (2007), pp. 246–255.

[334] V. Shoshan-Barmatz, D. Mizrachi, and N. Keinan. “Oligomerization of the mitochondrial protein VDAC1: from structure to function and cancer therapy.” *Progress in Molecular Biology and Translational Science* 117 (2013), pp. 303–334.

[335] L. Kaestner and A. Bogdanova. “Regulation of red cell life-span, erythropoiesis, senescence, and clearance.” *Frontiers in Physiology* 5 (2014), p. 269.

[336] A. Israelson, H. Zaid, S. Abu-Hamad, et al. “Mapping the ruthenium red-binding site of the voltage-dependent anion channel-1.” *Cell calcium* 43 (2008), pp. 196–204.

[337] J. Danielczok, L. Hertz, S. Ruppenthal, et al. “Does Erythropoietin Regulate TRPC Channels in Red Blood Cells?” *Cellular physiology and biochemistry : international journal of experimental cellular physiology, biochemistry, and pharmacology* 41 (2017), pp. 1219–1228.

[338] V. L. Lew and T. Tiffert. “On the Mechanism of Human Red Blood Cell Longevity: Roles of Calcium, the Sodium Pump, PIEZO1, and Gardos Channels.” *Frontiers in Physiology* 8 (2017), p. 977.

[339] H. G. Ferreira and V. L. Lew. “Use of ionophore A23187 to measure cytoplasmic Ca buffering and activation of the Ca pump by internal Ca.” *Nature* 259 (1976), pp. 47–49.

[340] H. F. Bunn, D. N. Haney, S. Kamin, et al. “The biosynthesis of human hemoglobin A1c. Slow glycosylation of hemoglobin in vivo.” *The Journal of clinical investigation* 57 (1976), pp. 1652–1659.

[341] J. I. Kourie. “Interaction of reactive oxygen species with ion transport mechanisms.” *The American journal of physiology* 275 (1998), pp. C1–24.

[342] World Health Organization. 2019. URL: https://www.who.int/news-room/fact-sheets/detail/blood-safety-and-availability.

[343] *Global status report on blood safety and availability 2016*. World Health Organization, 2017.

[344] Y. V. Kucherenko and I. Bernhardt. “Natural antioxidants improve red blood cell ”survival” in non-leukoreduced blood samples.” *Cellular physiology and biochemistry* 35 (2015), pp. 2055–2068.

[345] U. J. Dumaswala, L. Zhuo, D. W. Jacobsen, et al. “Protein and lipid oxidation of banked human erythrocytes: role of glutathione.” *Free radical biology & medicine* 27 (1999), pp. 1041–1049.

[346] T. Yoshida and S. S. Shevkoplyas. “Anaerobic storage of red blood cells.” *Blood transfusion* 8 (2010), pp. 220–236.

[347] J. W. Eaton, T. D. Skelton, H. S. Swofford, et al. “Elevated erythrocyte calcium in sickle cell disease.” *Nature* 246 (1973), pp. 105–106.

[348] E. Bennett-Guerrero, T. H. Veldman, A. Doctor, et al. “Evolution of adverse changes in stored RBCs.” *Proceedings of the National Academy of Sciences of the United States of America* 104 (2007), pp. 17063–17068.

[349] E. K. Meyer, D. F. Dumont, S. Baker, et al. “Rejuvenation capacity of red blood cells in additive solutions over long-term storage.” *Transfusion* 51 (2011), pp. 1574–1579.

[350] P. A. Smethurst, J. Jolley, R. Braund, et al. “Rejuvenation of RBCs: validation of a manufacturing method suitable for clinical use.” *Transfusion* 59 (2019), pp. 2952–2963.

[351] L. Zehnder, T. Schulzki, J. S. Goede, et al. “Erythrocyte storage in hypertonic (SAGM) or isotonic (PAGGSM) conservation medium: influence on cell properties.” *Vox sanguinis* 95 (2008), pp. 280–287.

[352] J. W. Lagerberg, H. Korsten, P. F. Van Der Meer, et al. "Prevention of red cell storage lesion: a comparison of five different additive solutions." *Blood transfusion* 15 (2017), pp. 456–462.

[353] P. Burger, H. Korsten, D. De Korte, et al. "An improved red blood cell additive solution maintains 2,3-diphosphoglycerate and adenosine triphosphate levels by an enhancing effect on phosphofructokinase activity during cold storage." *Transfusion* 50 (2010), pp. 2386–2392.

[354] A. D'Alessandro, J. A. Reisz, R. Culp-Hill, et al. "Metabolic effect of alkaline additives and guanosine/gluconate in storage solutions for red blood cells." *Transfusion* 58 (2018), pp. 1992–2002.

[355] G. Paglia, Ó. E. Sigurjónsson, A. Bordbar, et al. "Metabolic fate of adenine in red blood cells during storage in SAGM solution." *Transfusion* 56 (2016), pp. 2538–2547.

[356] A. Antosik, K. Czubak, N. Cichon, et al. "Vitamin E Analogue Protects Red Blood Cells against Storage-Induced Oxidative Damage." *Transfusion Medicine and Hemotherapy* 45 (2018), pp. 347–354.

[357] S. B. Bayer, M. B. Hampton, and C. C. Winterbourn. "Accumulation of oxidized peroxiredoxin 2 in red blood cells and its prevention." *Transfusion* 55 (2015), pp. 1909–1918.

[358] C. Duranton, S. M. Huber, and F. Lang. "Oxidation induces a Cl(-)-dependent cation conductance in human red blood cells". *Journal of Physiology* 539.Pt 3 (2002), pp. 847–55.

[359] M. G. Rotordam, E. Fermo, N. Becker, et al. "A novel gain-of-function mutation of Piezo1 is functionally affirmed in red blood cells by high-throughput patch clamp." *Haematologica* 104 (2019), e179–e183.

[360] A. Bogdanova, A. Makhro, J. Wang, et al. "Calcium in red blood cells-a perilous balance." *International Journal of Molecular Sciences* 14 (2013), pp. 9848–9872.

[361] A. Ciechanover. "The unravelling of the ubiquitin system." *Nature reviews. Molecular cell biology* 16 (2015), pp. 322–324.

[362] A. Faucherre, K. Kissa, J. Nargeot, et al. "Piezo1 plays a role in erythrocyte volume homeostasis." *Haematologica* 99.1 (2014), pp. 70–75.

[363] A. Caulier, N. Jankovsky, Y. Demont, et al. "PIEZO1 activation delays erythroid differentiation of normal and Hereditary Xerocytosis-derived human progenitors." *Haematologica* (2019).

[364] J. C. Freedman, T. S. Novak, J. D. Bisognano, et al. "Voltage dependence of DIDS-insensitive chloride conductance in human red blood cells treated with valinomycin or gramicidin." *The Journal of General Physiology* 104 (1994), pp. 961–983.

[365] J. C. Freedman and T. S. Novak. "Electrodiffusion, barrier, and gating analysis of DIDS-insensitive chloride conductance in human red blood cells treated with valinomycin or gramicidin." *The Journal of General Physiology* 109 (1997), pp. 201–216.

[366] P. A. Kuhlman, C. A. Hughes, V. Bennett, et al. "A new function for adducin. Calcium/calmodulin-regulated capping of the barbed ends of actin filaments." *The Journal of biological chemistry* 271 (1996), pp. 7986–7991.

[367] Q. Li, V. Jungmann, A. Kiyatkin, et al. "Prostaglandin E2 stimulates a Ca2+-dependent K+ channel in human erythrocytes and alters cell volume and filterability." *The Journal of biological chemistry* 271 (1996), pp. 18651–18656.

[368] L. Kaestner and I. Bernhardt. "Ion channels in the human red blood cell membrane: their further investigation and physiological relevance." *Bioelectrochemistry* 55 (2002), pp. 71–74.

[369] A. Razeto, P. Gribbon, and C. Loew. "The dynamic nature of the VDAC1 channels in bilayers as revealed by two crystal structures of the human isoform in bicelles at 2.7 and 3.3 Angstrom resolution: implications for VDAC1 voltage-dependent mechanism and for its oligomerization".

[370] S. L. Thomas, G. Bouyer, A. Cueff, et al. “Ion channels in human red blood cell membrane: actors or relics?” *Blood Cells, Molecules and Diseases* 46.4 (2011), pp. 261–5.

Acknowledgments

I have been very fortunate to come to Roscoff, the number of good people I have found here and, thanks to the PhD, elsewhere, is amazing.

Je voudrais d'abord remercier à l'équipe qui m'a accueilli très chaleureusement depuis le début. Guillaume, patient et toujours prêt à arriver au secours, notamment lors du patch-clampling. Laurent, qui m'appris les techniques fondamentales de cette thèse, toujours avec la bonne humeur. À Stéphane, qui quand il me dit qu'il arrive dans 5 minutes je peux m'organiser pour 45 minutes, mais qui a fait, en grand partie, cette thèse possible, grâce à son enthousiasme, générosité, bienveillance et des discussions passionnantes de science fondamentale. Un grand merci, tu es formidable tant au niveau scientifique qu'au niveau personnel. À tous mes amis francophones que je n'aurais pas pu rencontrer sans la langue française, donc je suis très content de l'avoir appris. Merci à Dung, Omid, Benoît, Harold, Maria, Hajar, Lucile, Damien, Mathilde, Jeremy, Eugénie, Élie et beaucoup d'autres.

To my English-speaking friends, thanks a lot. To the Relevance brethren, whom I was always looking forward to see at every relevant event. Giustina, Ralfs for awesome reciprocal secondments, Jill an excellent host for a great Amsterdam trip, Greta and Asena for their seemingly endless energy, Pedro and Francesca for the true American experience, Ario, Virginia, Niamh, Valeria, Anjali and Ankie. Also to the PIs involved: Richard van Wijk, Anna Bogdanova and especially Ash Toye, Marieke von Lindern and those who welcomed me in their labs: Lars Kästner, Wassim El Nemer, Markus Rapedius and Nadine Becker for wonderful secondments. Many others, who left Roscoff too soon: Niels, Lulu, Joseph, Wei Ting, Orestis and Baso. Plus others who are in for Finistère for longer: Catherine, Mariana, Marieke, Lydia, Joost and Ioannis. Plus others found on the path like Linda, and Max. Some names may be missing, but considering I was a disaster at remembering any name only three years ago I'd say it is good progress.

I would like to thank once more to our collaborators, which contributed samples: the groups of Paola Bianchi, Richard van Wijk and Lamisse Mansour-Hemdili and, of course, the patients themselves.

I would like to give my deepest thanks to Hélène Guizouarn and Mariano Ostuni for having accepted to be referees of this thesis manuscript, considering their busy schedules. Their goodwill was to me apparent during our brief encounters at a congress or during my secondments. I thank the members of the jury: Lars Kästner and Paola Bianchi who generously accepted to come from afar and to François Lallier for finding time for this thesis.

Y por supuesto, gracias a mis amigos hispanohablantes con los que he podido volver a la lengua de Cervantes de vez en cuando. Peche, María, Mahmoud, Aída, Meri, Vincent, Marina, Laura y algunos más. Momentos geniales en los que el humor fluye más fácilmente en la lengua materna.

Para terminar, a toda mi familia y en especial a mis padres, mi hermana Lucía y mi tía Estrella que no dudaron en apoyarme desde el principio cuando decidí empezar Biotecnología allá por el año 2010. Muchísimas gracias por todo el cariño que me habéis dado, ¡puedo decir que ha llegado hasta Roscoff!

Merci !

Thank you!

¡Gracias!